HARMONIC MODELLING OF TRANSMISSION SYSTEMS CONTAINING SYNCHRONOUS MACHINES AND STATIC CONVERTORS

A thesis

presented for the degree of

Doctor of Philosophy in Electrical Engineering

in the

University of Canterbury

by

J. F. Eggleston, B.E. (Hons)

1985

NGINEERING
LIBRARY
THESIS
TK
3091
E29
985

CONTENTS

LIST OF FIGURES

LIST OF TABLES

LIST OF PRINCIPLE SYMBOLS

SYMBOL	
A_h	h^{th} harmonic diagonal block of Y_{abc}
B'_h, B''_h	h^{th} harmonic off-diagonal block of Y_{abc}
C_{nm}	integration constant
$d_{1,2,3}$	feeder system line lengths
E_c	commutating voltage
$E1_n$	iterative zero crossing error
G_{-h}^{h+2} $G_{+h}^{-(h-2)}$	open circuit voltage ratios
h	harmonic order
$H_{+h}^{-(h-2)}$, H_{-h}^{h+2}	short circuit current ratios
$i,[I]$	current vector in the harmonic space
i_c	commutation current
I_d	convertor d.c. current
$[I_d]$	vector of convertors d.c. currents
I_{dh}	h^{th} harmonic component of direct axis current
$I_{dNorton}$, $I_{qNorton}$	Norton current in d and q quantities
$I_{f,fil}$	feeder system filter currents
I_{fil}	filter current
I_{gh}	current injection to take into account harmonic conversion
I_{gh}^i	I_{gh} at i^{th} iteration
I_h	h^{th} harmonic component of injected current
$[I_{inj}]$	current injection
I_{lt}	left termination filter current
I_o	synchronous machine Norton current
I_{pfi}	i^{th} locomotive power factor current
I_{qh}	h^{th} harmonic component of quadrature axis current
I_{rec}	current in feed line, towards terminations
I_{rt}	right termination filter current

SYMBOL

I_{send}	current in feeder line, towards substation
I_{sys}	system harmonic current
I_{ti}	i^{th} locomotive current
I_{ts}	substation transformer current
$I_{1,2,3}$	currents in phases 1, 2 and 3
I_+ V_+	positive sequence component of harmonic space current or voltage
I_{+h}	positive sequence current or voltage of order h
I_{-h}	negative sequence current or voltage of order h
j	no. trains left of substation
L_d	direct axis inductance
L_f R_f	field winding inductance and resistance
L_q	quadrature axis inductance
L_s R_s	direct axis damper inductance and resistance
L_t R_t	quadrature axis damper inductance and resistance
L_t	locomotive convertor commutating inductance
$L_{1,2,3}$	inductance in phases 1,2 and 3
M_{df}	mutual inductance between direct axis and field winding
M_{ds}	mutual inductance between direct axis and direct axis damper winding
M_{fs}	mutual inductance between field and direct axis damper windings
M_{qt}	mutual inductance between quadrature axis and quadrature axis damper winding
NCONV	number of convertors
NHARM	maximum harmonic to be considered
NSAMPL	number of sample points
Nt	number of trains
NTERM	number of terminal busbars
p	the valve commutating in
R	stator resitance d,q quantities

SYMBOL	
$R_{1,2,3}$	resistance in phases 1,2 and 3
SCALE	harmonic voltage scale factor
T	matrix to extract positive sequence fundamental
T	connection matrix from phase to $\alpha\beta o$ components
TCS	Transient Convertor Simulation
U	identify matrix
v,[V]	voltage vector in the harmonic space
$V_{a,b,c}$	voltage on phases a, b and c
V_d	convertor d.c. voltage
V_d, I_d	direct axis voltage and current
V_{dh}	h^{th} harmonic component of d.c. voltage
V_{dh}	h^{th} harmonic of direct axis voltage
V_{dq} I_{dq}	dq components of stator harmonic voltages and currents
V_f, I_f	field winding voltage and current
$[V_h]$	vector of the 3 phase voltages at harmonic h
V_{hm}	is the peak magnitude of the h^{th} harmonic of the outgoing phase
V_{hn}	is the peak magnitude of the h^{th} harmonic of the incoming phase
$[V_{inj}]$	voltage at point of injection
V_q,I_q	quadrature axis voltage and current
V_{qh}	h^{th} harmonic at quadrature axis voltage
V_{rec}	voltage at the terminations end of the feeder line
V_s, I_s	direct axis damper voltage and current
V_{send}	voltage at the substation and of feeder line
V_{sys}	system voltage
V_t	terminal voltage
V_t, I_t	quadrature axis damper voltage and current
V_x	secondary voltage on a commutating phase
$V_{1,2,3}$	voltage on phases 1,2 and 3

SYMBOL	
$V_{\alpha\beta}$, $I_{\alpha\beta}$	αβ components of stator harmonic voltages and currents
$V_{\alpha h}$, $V_{\alpha h}$	h^{th} harmonic of stator voltage in α and β quantities
X_c	commutating reactance
X''_d, X''_q	direct and quadrature axis sub-transient reactance
X_g	conventional generator harmonic reactance
X_{sys}	equivalent system reactance
X_1, X_2	leakage reactances
X_{-1}	negative sequence reactance
[Y]	harmonic space nodal admittancd matrix
Y_{abc}	synchronous machine admittance matrix in the three phase harmonic space
$[Y_{ac}]$	a.c. system admittance matrix for iterative algorithm
$[Y_d]$	d.c. system admittance matrix
Y_{dq}	Synchronous machine d-q axis admittance
Y_{dqh}	h^{th} harmonic admittance in d-q quantities
$[Y_f]$	harmonic admittance matrix of the filters
$[Y_{feeder}]$	feeder system admittance matrix
Y_{gen}	equivalent to Y_{abc}
$[Y_h]$	system nodal admittance matirx at harmonic h
$[Y_{red}]$	$[Y_h]$ reduced to the point of injection
$[Y_{sys}]$	equivalent of $[Y_{red}]$
$[Y_t]$	harmonic admittance matrix of the convertors' transformers
Y_{o+-}	sequence component admittance matrix
$Y_{\alpha\beta}$	synchronous machine αβ admittance
$Y_{\alpha\beta o}$	$Y_{\alpha\beta}$ augmented to include zero sequence
$Y_{1,2,3,m}$	shunt admittance of the feeder lines
Z_h	harmonic impedance at harmonic h
Z_f	filter impedance
Z_{pf}	impedance of the power factor capacitor and choke

SYMBOL	
Z_s	transmission system impedance
Z_{sys}	harmonic impedance of the system
Z_t	locomotive's transformer impedance
Z_{tf}	termination filter impedance
Z_{ts}	substation transformer impedance
Z^{th}_{+h}, Z^{-h}_{-h}	open circuit harmonic impedance
Z^{+h+2}_{-h} $Z^{-(h-2)}_{+h}$	open circuit conversion impedance
$Z_{1,2,3,m}$	series impedance of the feeder lines
ZC_n	zero crossing of the commutating voltage at iteration n
α	delay angle
ε	permittivity of insulation
θ_p	firing instant of valve p
μ	permeability of insulation
μ	commutation angle
μ_p	p^{th} commutation angle
σ_f	excitation constant
σ_μ	standard deviation of the commutation angles
ϕ_{dh}	phase of the h^{th} harmonic component of the d.c. voltage
ϕ_h	rotor flux at harmonic h
ϕ_{hm}	is the phase of the h^{th} harmonic of the outgoing phase
ϕ_{hn}	is the phase of the h^{th} harmonic of the incoming phase
ω	fundamental angular frequency

ABSTRACT

This thesis describes the modelling of the major sources of harmonic distortion in electrical transmission systems, especially those of relevance to the New Zealand power system.

The harmonics generated by the operation of a.c./d.c. convertors are modelled using an interactive algorithm. The algorithm is applied to a number of test systems and verified using a transient convertor simulation program.

A harmonic admittance matrix model of a single phase traction system is derived and used to assess the effect of propossed harmonic filters. In this case the three phase iterative algorithm had to be modified to be able to model the locomotive's single phase convertors.

Synchronous machines are modelled using a harmonic Norton equivalent, derived from the d-q axes differential equations. The case of this model yields harmonic impedances consistent with existing models and demonstrates the well known, but greatly ignored, phenomenon of harmonic conversion. The modelling of harmonic conversion is shown to significantly modify the harmonic flows under certain system conditions.

ACKNOWLEDGEMENTS

I would like to thank my supervisor, Professor J. Arrillaga, for his advice, assistance, friendship and patience during the course of my study.

The financial support of the New Zealand Energy Research and Development Committee was most appreciated.

Special thanks are due to J. Baird, Professor H. Dommel and particularly Professor A. Semlyem for their guidance and technical assistance. Also, the encouragement and help of the staff and postgraduate students, especially T.J. Densem, N.R. Watson and C.D. Callaghan, is gratefully acknowledged.

Thank you to Mary Kinnaird for her excellent typing.

Particular thanks for my family and friends' patience and interest.

CHAPTER 1

INTRODUCTION

In recent years there has been a trend towards the use of power electronic devices in electric power transmission systems. In New Zealand this trend has been strong in the past with an aluminium smelter at Tiwai and one of the world's first h.v.d.c. links. In the future this trend is expected to continue with possible expansions to the existing h.v.d.c. link, the possibility of a second link and the electrification of part of the North Island main truck line. Also many alternative energy sources (micro-hydro, solar, wind and wave power) are electrically orientated and rely on power electronics for their control.

Thus much of the apparatus used for the generation, transmission and utilisation of electrical energy in the future will result in considerable waveform distortion due to the non-linear nature of power electronic devices. This is a form of electrical enviromental pollution which, like any other form of pollution, affects all the system users and is expensive to eliminate. In New Zealand the problems associated with harmonics are becoming larger. As a result, New Zealand was one of the first countries in the world to introduce Harmonic Standards (New Zealand Electricity 1983).

The aim of this thesis, therefore, is to examine the major sources of harmonic distortion in transmission systems and develop techniques to predict their impact.

In Chapter 2 harmonic distortion is introduced as a steady state phenomenon. The existing techniques for modelling power systems in the steady state, and in particular at harmonics frequencies are examined and their shortcomings discussed.

Chapter 3 develops an iterative algorithm for the modelling of converter operation and its associated harmonic current injections. The algorithm is based on previous work by Harker (1980) and Yacamini and de Oliveira (1980a and 1980b), with improvements as required.

In Chapter 4 various test systems are used to establish the usefulness of the iterative algorithm described in chapter 3. Firstly, a six busbar a.c. system supplying a 6-pulse convertor is considered, followed by a more simple system consisting of a single generator and transformer feeding a transmission line which supplies a 6-pulse convertor. Finally, the results of the iterative algorithm are verified by comparing them with those produced by a transient convertor simulation program.

The case of a single phase traction system is examined in chapter 5. This is of particular interest in New Zealand as part of the North Island main trunk line is to be electrified. The chapter is divided into two parts. The first part describes the modelling of the feeder system and analyses the performance of harmonic filters. The second part describes how the iterative algorithm of chapters 3 and 4 is modified to analyse the operation of the single phase convertors used in modern locomotives. The results are presented in appendix A7.

A less important, and hitherto ignored, source of harmonic distortion is the harmonic conversion inherent in synchronous machines, and in particular, hydro generators. A harmonic model including this effect, developed in chapter 6, is used to examine the harmonic characteristics of the synchronous machine. The results are compared to the existing synchronous machine harmonic models to assess the relative importance of harmonic conversion.

Chapter 7 examines the effect of synchronous machine harmonic conversion in simple test systems to assess its significance. These

systems include unbalanced loads, such as transmission lines, and h.v.d.c. converter installations. Further applications of the proposed machine model are discussed and possible problems examined.

Finally in chapter 8 the main conclusions and contributions of the work in this thesis are discussed.

CHAPTER 2

AN OVERVIEW OF POWER SYSTEM HARMONICS AND THEIR MODELLING

2.1 Steady State Modelling of Electrical Transmission Systems

In the steady state an ideal three phase transmission system would have uniform magnitude, perfectly balanced and purely sinusoidal voltages at each system busbar. However, these three ideals are not met in an actual system.

Because of voltage drop across system components due to the flow of real and reactive power in a system, the voltage magnitudes throughout an actual transmission system are not uniform. Various methods can be used to control the problem including series and shunt reactors and capacitors on long transmission lines, variable excitation of synchronous genrators and synchronous compensators and more recently, static Var controllers. The single phase power flow algorithm was developed to help system designers and operators maintain the system voltage magnitudes within specified limits.

Also in an actual transmission system the voltages are not perfectly balanced. There are several sources of unbalance (Roper and Leedham 1974), including untransposed lines, three phase transformers, unequal phase sharing by single phase distributed loads and large single phase loads such as arc furnaces and traction systems (Winthrop 1983). Because the effect of unbalance on generators and some critical loads can be important, the established single phase power flow algorithm was extended to model three phase systems.

Because h.v.d.c. links and other large convertors are at present in many transmission systems,and can dominate some like the South Island of New Zealand, a detailed representation of convertors was integrated into both single phase and three phase power flows.

Convertors need to be considered specifically, rather than as fixed loads, because their reactive power requirements depend both on the terminal busbar voltage and the control strategy, as well as the d.c. power. Significant interaction exists between the unbalanced operation of the a.c. and d.c. systems. To investigate the nature of the interaction requires a three phase a.c./d.c. power flow.

A detailed description of both single phase and three phase power flows, with and without the specific representation of convertors, is given by Arrillaga et al (1983a).

The third ideal not met in an actual transmission system is that of purely sinusoidal voltages. It is well known that any non-linear devices will generate harmonic voltages and currents. Common examples of such devices are power transformers and d.c. power conversion equipment.

2.2 HARMONICS IN THE POWER SYSTEM

In recent years power system harmonics have attracted significant attention. A conference specifically about power system harmonics was held in UMIST (1981) to examine the problem. Several other conferences have also made contributions in the area of harmonics (IEE Conf. Nos. 22, 107, 110, 197, 205, 210, 234 and IEEE (1984a). The IEEE have produced an overview (IEEE 1983) and a bibliography (IEEE 1984b). Much of the existing literature has been collated in Arrillaga et al (1985a) in a recent book.

The problems caused by power system harmonics are well documented (Kimbark 1971 and Arrillaga et al 1985a). In the New Zealand high voltage transmission system the most significant problems are interference with post office communications and ripple control equipment (Harker 1980). At the distribution level the significant problems are dielectric breakdown of power factor correction capacitors and

the masking of ripple control signals (Ross 1972).

The traditional sources of harmonics in transmission systems are transformers and synchronous machines. The non-linearity of the iron core of power transformers results in magnetizing currents containing odd harmonic orders. However, because the magnetizing current is relatively small, transformer related harmonics are generally insignificant. Similarly, the emf of a synchronous machine stator caused by a non-sinusoidal distribution of rotor flux is insignificant with good machine design. In more recent years, h.v.d.c. convertors for d.c. power transmission or metal smelting have become more common. This trend is expected to continue, or even accelerate, in the immediate future.

It is expected that, with the increased use of semiconductor controllers for drives, light dimmers, etc., and the large scale use of fluorescent lighting, many of the future harmonic problems will be found in distribution systems. This is expected to get worse if electric vehicles gain popularity, as they would be charged at night when the system is least damped, due to light night loading. Also the increased use of power factor correction capacitors may cause local resonances which exaggerate local harmonic problems.

Other sources of harmonic problems are electrified railway traction systems. This is of particular interest in the North Island of New Zealand where a large section of the main trunk line is being electrified. Apart from the normal problems when the harmonic currents enter the transmission system at the substation, the main area of concern with such systems is the local interference between the single phase reticulation wires to the locomotive and local communication circuits.

2.3 POWER SYSTEM MODELLING OF HARMONICS

To understand existing power system harmonic problems, and in order to predict future difficulties with system expansion, it is essential to be able to perform reliable simulations.

2.3.1 Early Models

Early insight with power system harmonics in New Zealand was gained when the h.v.d.c. link was being commissioned (Robinson 1966a). Another study was carried out by modelling the French end of the cross channel link on a simulator (Laurent et al 1962). Both studies found it difficult to match simulated results with those measured. A considerable level of harmonic voltage unbalance was reported with the measured results. The main problem with physical simulators is the difficulty of modelling the strong frequency dependencies of the various power system components by means of discrete RLC components. Also a transmission system may have hundreds of busbars, each of which may need to be considered. With the limitations of simulators and the developments in modern digital computers, most of the present power system harmonic studies are performed in software.

2.3.2 Harmonic Penetration

Harmonic penetration can be defined as the analysis of the propagation of harmonic currents in an a.c. system from their source. Generally all system components are assumed to be passive and linear, and therefore, each frequency has to be treated separately.

Initial harmonic penetration studies used balanced models for each system component (Ross and Smith 1948, Northcote-Green et al 1973 and Breuer et al 1982) to give a single phase positive sequence equivalent system representation. The results of Breuer et al (1982) show poor matching of measured and calculated results near system

resonances, as well as significant unbalance. Also the effect of coupling between the positive and zero sequences, reported by Whitehead and Radley (1949), could not be detected with a balanced line model. Because of the poor results obtained when modelling system resonances, and the importance of modelling system unbalance, it was concluded (Densem 1983) that a realistic analysis of harmonic levels requires a three phase representation of the power system. As the harmonic regulations normally refer to the phase to neutral voltages and line currents, the phase frame of reference was preserved. The use of sequence components provide no computational advantage in an unbalanced system but can be useful for the interpretation of results.

The basis of a harmonic penetration algorithm is the system nodal admittance matrix $[Y_h]$, calculated at each harmonic h. For a three phase study each element is a 3 x 3 block, consisting of self and mutual admittances between the three phases and ground. Details of the formation of the $[Y_h]$ from the nodal admittances are given by Arrillaga et al (1985a), and are based on the techniques used in power flow analysis.

Individual nodal admittance matrix models for the various system component at harmonic frequencies have been collated by Arrillaga et al (1985a).

Once $[Y_h]$ has been evaluated, the relationship between the busbar voltages and the injected currents are related by equation 2.1,

$$[I_h] = [Y_h][V_h] \qquad 2.1$$

where $[I_h]$ and $[V_h]$ are vectors of the three phase currents and voltages at each busbar respectively. Equation 2.1 is repeated at each harmonic of interest.

The obvious use for equation 2.1 is to specify a current injection at one or more busbars and, using Gaussian elimination, solve for the system voltages $[V_h]$. If the individual system element

admittances are preserved, the currents in each element can be calculated. With the propagation of harmonic currents clearly defined, potential harmonic overvoltages and potential communication interference problems can be identified.

Similarly, the same method can be used to determine the propagation of non-integer harmonic currents such as ripple control signals (Ross 1972 and Densem 1983). The results of such a study determine whether or not the ripple signals will be strong enough throughout the system to operate the ripple relays and to test for spillover of the ripple signal into other supply authority systems, via the transmission system.

The $[Y_h]$ matrix can be used to evaluate the admittance of an a.c. system at harmonic frequencies, as seen from the point of injection. If I_h is zero at all the busbars except one, the $[Y_h]$ can be reduced by Gaussian elimination to a single 3 x 3 block (Densem 1983), such that

$$[I_{inj}] = [Y_{red}][V_{inj}] \qquad 2.2$$

$[Y_{red}]$ can be inverted to derive the harmonic impedance loci (Densem 1983) which are often used to characterise the a.c. system at harmonic frequencies. $[Y_{red}]$ can also be used directly in the design of harmonic filters (Arrillaga 1983). For two or more points of injection $[Y_{red}]$ is of dimension 3n x 3n, where n is the number of points of injection.

Transmission lines are the major source of unbalance in power systems and are strongly frequency dependent. They therefore dominate the propagation of harmonic currents in the power system and must be modelled accurately. Details of the techniques used in the modelling of transmission lines are given by Arrillaga et al (1985a).

Standing wave effects are observed in both power and communication systems whenever the transmission distance is greater

than about 1/12th of a wavelength, for 1.2% accuracy (Arrillaga et al 1985a). In power systems this corresponds to 500 km at fundamental frequency, but only 10 km at 50th harmonic. Standing wave effects are accounted for by the use of an equivalent-π model of each line at each harmonic (Arrillaga et al 1985a).

With a three phase line three modes of propagation exist which can be found by modal analysis (Densem 1983). Each mode propagates in a different combination of conductors, including the earth, and will in general have slightly different propagation velocities. The effect of these slightly different velocities is most significant near resonance, with each mode resonating at different frequencies (Densem 1983), causing system unbalance.

The frequency dependence of the series impedance is an important aspect of transmission line modelling. Skin effect increases the a.c. resistance of a conductor and decreases the internal inductance. However, the effect on the internal inductance is usually ignored (Kimbark 1950). Carson's earth return correction terms increase both the series resistance and the inductance of a line. The variation of the series impedance with frequency will alter the resonant frequencies of the various propagation modes and the value of system impedance at resonance (Demsem 1983).

2.3.3 Dynamic Simulation of Harmonic Interaction

Convertor operation, and hence the uncharacteristic current injections produced, is modified by the presence of voltage distortion on the convertor bus. This phenomenon is discussed more fully in section 3.1.

Similarly, equation 2.2 shows that the injected harmonic currents will modify the voltage distortion on the convertor busbar. This interdependence of the voltage and current distortions is

discussed here as harmonic interaction.

It has been reported by several authors (Ainsworth 1967 and Kauferle et al 1970) that convertor operation may be unstable, if the background level of distortion is reinforced by the action of the convertor control on the a.c. current injections. This problem, often called harmonic instability, is discussed in detail in section 4.1.2.

One method of modelling the harmonic interaction of a converter is to simulate the convertor in the time domain (Reeve and Subba Rao 1974 and Kitchen 1981). After a period of simulation, about six cycles (Reeve and Subba Rao 1974), successive cycles are expected to be sufficiently similar to be regarded as the steady state solution. The time required will depend on the accuracy of the initial conditions and the degree of interaction.

In section 4.4 the use of the time domain algorithm TCS (Heffernan 1980), developed for the study of convertor faults, is discussed.

2.3.4 Limitations of Conventional Models

The present harmonic penetration techniques have several shortcomings. Firstly, more detailed models of the sources of harmonic current are needed to determine more accurately the size of the injected a.c. current injections and hence the distortion in the system. Dynamic modelling can be used but requires large amounts of CPU time. Also the complex nature of the a.c. system response has to be ignored or simplified to a balanced RLC network (Hingorani and Burbery 1970) when represented in the time domain. As the system impedances are a major factor contributing to harmonic interaction any degradation of their representation reduces the effectiveness of a dynamic simulation. Converter modelling is discussed in section 2.4

and the use of an alternative iterative algorithm to model convertor interaction is discussed in section 2.5 and chapter 3.

There is also a lack of agreement as to the most appropriate representation of some system components (Densem 1983). This is especially true of loads, transformers and synchronous machines. Synchronous machines are discussed more fully in chapter 6, while loads and transformers require future work.

Normally the system components are considered passive and linear with each frequency treated separately. The converter is an exception, being treated as a fixed injection. However, coupling between frequencies can exist and will be discussed in section 2.6 and in chapters 6 and 7.

2.4 HARMONIC MODELLING OF CONVERTORS

With increased understanding of non-ideal convertor operations and its associated problems, convertor modelling techniques have improved since those developed for ideal operation (Read 1945).

An important aspect of convertor modelling is the representation of the commutation process. Normally the commutating impedance is assumed to be a linear inductance. However, this was extended to include a series resistance (de Oliveira 1978). Some authors, including Phadke and Harlow (1968) and Harker (1980), use only the fundamental component of the terminal voltage to evaluate the commutating current and voltage waveforms.

The most detailed representation of the commutation process, provided by de Oliveira (1978) and Yacamini and de Oliveira (1980a and 1980b), includes series resistance in the commutating impedance and the effect of the full spectrum of commutating voltage harmonics. Yacamini and de Oliveira (1980a) also provide for any transformer connection with the use of zig-zag connected transformers. However,

there are limitations in the use of zig-zag transformers and these are discussed in section 3.3.1.

Earlier studies, including Ainsworth (1967), Reeve and Krishnayya (1968), Phadke and Harlow (1968) and Yacamini and de Oliveria (1980a), did not include d.c. current ripple. This is generally a reasonable assumption in the presence of a large smoothing reactor. Later studies have used a series inductor and resistor to represent the d.c. system (Reeve and Subba Rao 1971 and Yacomini and Smith 1983). Discrete RLC components have also been used to represent h.v.d.c. lines and cable combinations (Yacamini and de Olivera 1980b and Yacamini and Smith 1983). An area for improvement is the inclusion of standing wave and frequency dependency effects for the d.c. system lines and cables. This is discussed in section 3.5.

The method of representing the a.c. system is also important. Yacamini and de Oliveira (1980a and 1980b) generally use a series resistor and inductor combinations, based on the short circuit ratio. A similar representation (Rowles 1970) is generally used in dynamic studies (Reeve and Subba Rao 1974). However, the consensus of opinion (Kauferle et al 1970, Reeve and Baron 1971 and Harker 1980) is that individual impedances at each harmonic are required for an accurate harmonic analysis of converter operation because the system impedance, including the filters, is a major factor in harmonic stability (Ainsworth 1967). As discussed in sections 2.3.2 and 3.4, the harmonic penetration algorithm of Densem (1983) can be used to calculate the admittance matrix $[Y_{red}]$ at each harmonic. Each $[Y_{red}]$ contains all the information of frequency dependence and unbalance which can effect the operation of the convertor.

Many studies of the operation of convertors include accurate models of the convertor plant but simply specify arbitrary levels of

fundamental voltage unbalance and control variables. As these parameters dictate the convertors operation, the results of such studies are not representative of the actual convertor. Harker (1980) evaluated the fundamental terminal voltages, including unbalance, the d.c. current, the transformer tap ratios and the delay angles of the convertor for the actual system configuration present using an a.c./d.c. fundamental power flow.

The unbalanced operation of convertors and details of the iterative algorithm proposed in this thesis are discussed in chapter 3.

2.5 ITERATIVE ALGORITHM FOR MODELLING HARMONIC INTERACTION

The alternative to dynamic modelling is an iterative process adopted by several authors (Reeve and Baron 1971, Yacamini and de Oliveria 1980a and 1980b and Harker 1980). Normally the voltages at the convertors is initially assumed to be sinusoidal (Harker 1980) and the resulting a.c. current injections calculated. Then at each harmonic successively, the currents are injected into the a.c. system and the terminal voltage updated. The controller strategy is implemented by updating the firing instants from the distorted terminal voltage waveform zero crossings at each iteration. The later studies of Yacamini and de Oliveira (1980b) and Yacamini and Smith (1983) include a d.c. system. At each iteration the d.c. side voltage harmonics are calculated and the d.c. current ripple updated. The main advantages of the iterative approach are a reduction in CPU time and the ease of representing the complex harmonic behaviours of the a.c. and d.c. systems. Because the a.c. and d.c. systems are represented by admittance matrices at each harmonic, any frequency dependence of mutual couplings between phases can be modelled. However, the disadvantage of an iterative algorithm is that convergence is not guaranteed and divergence may not necessarily mean the actual

convertor is unstable. This problem is discussed in section 4.1.3.

In chapter 3 the iterative algorithm has been further developed with an enhanced representation of a.c. and d.c. systems. The problem of harmonic instability is further examined in chapter 4.

2.6 INTRODUCTION TO MODELLING IN THE HARMONIC SPACE

Throughout harmonic penetration studies it has been assumed that the a.c. system components are linear and passive. This has meant that each harmonic can be treated separately. Because a.c./d.c. convertors are not passive and linear they are not included in harmonic penetration studies, hence the need for the iterative algorithm.

However, synchronous machines and power transformers also produce coupling between harmonics. In the case of synchronous machines, the coupling is due to the salient nature of the rotor flux, while the power transformer's coupling is due to the magnetic non-linearity of the iron core. Therefore, with existing harmonic penetration algorithms, it is not possible to fully model all the harmonic phenomena associated with either synchronous machines or power transformers.

The problem of coupling between harmonics can be solved by introducing the concept of the harmonic space. This is defined as a set of 3nk phasors describing a quantity of voltage and currents, in each phase of the n busbar system at each of the k harmonics being considered. All the voltage phasors in each phase, busbar and frequency are combined to form a single vector [V], and similarly, all the currents combined to form [I].

The conventional harmonic penetration relationships of the harmonic currents and voltages, described at each harmonic by equation 2.1, can be combined to an equivalent representation in the harmonic

space. This is described in equation 2.3

$$[I] = \begin{vmatrix} I_1 \\ I_2 \\ \vdots \\ I_h \\ \vdots \\ I_k \end{vmatrix} = \begin{vmatrix} Y_1 & & & & \\ & Y_2 & & & \\ & & & Y_h & \\ & & & & Y_k \end{vmatrix} \begin{vmatrix} V_1 \\ V_2 \\ \\ V_h \\ \\ \end{vmatrix} \qquad 2.3$$

or

$$[I] = [Y][V] \qquad 2.4$$

The block diagonal nature of the [Y] matrix is indicative of the lack of coupling between harmonics.

However, where an a.c. system component exhibits coupling between harmonics, the inclusion of its full representation will introduce off diagonal elements. Therefore, any system component can be included directly into equation 2.1 if it can be represented by a harmonic Norton equivalent. That is, a fixed current injection and linear admittance matrix in the hamonic space.

CHAPTER 3

HARMONIC MODELLING OF CONVERTOR OPERATION

3.1 INTRODUCTION

Under the ideal conditions of a flat d.c. current, balanced fundamental terminal busbar voltage and commutating impedances, convertors produce only characteristic harmonics. In the a.c. system the characteristic harmonic currents are the negative sequence pk-1 and positive sequence pk+1 orders, where p is the pulse number of the convertor and k is an integer. Similarly, the characteristic voltage harmonics on the d.c. side of the convertor are of order pk. A summary of the characteristic harmonics was given by Read (1945).

However, convertor operation is susceptible to non-ideal system behaviour and will generate uncharacteristic a.c. and d.c. currents. Because the uncharacteristic harmonics are generally not filtered, the mechanisms for their generation need to be examined.

One of the major causes of non-ideal operation of convertors is an unbalanced fundamental terminal voltage (Reeve and Krishnayya 1968 and Phadke and Harlow 1968). Unbalanced voltages give rise to unequally spaced zero crossings. With a conventional constant delay angle controller the conduction periods in each phase are unequal, resulting in all the odd harmonics generated on the a.c. system and all the even harmonics generated on the d.c. side. A smaller modification to the current and voltage waveforms is due to the unequal commutation angles resulting from the unbalanced commutations voltages. Even with an equidistant controller giving firing pulses every 60 degrees (Ainsworth 1968), all the a.c. system odd harmonics and the d.c. side even harmonics will be produced due to the resulting unequal commutation angles. Appendix A1 shows the relationship between

third harmonic current and unequal commutation angles for an equidistant controller.

A similar effect to that of unbalanced terminal voltage is produced by unequal commutating reactances in each phase of the convertor transformer (Subbarao and Reeve 1976). The unbalanced reactances produce unequal commutation angles which cause the odd uncharacteristic a.c. harmonic currents and even uncharacteristic d.c. harmonic voltages.

Any voltage distortion on the convertor terminal busbar can cause the convertor to produce uncharacteristic harmonic currents (Ainsworth 1967, Phadke and Harlow 1968 and Reeve et al 1969). As for unbalanced terminal voltages, harmonic voltages shift the zero crossings which cause a variety of harmonic currents, depending on the nature of the distortion. When only a single disturbing harmonic voltage is considered at any time, it was found (Reeve et al 1969) that odd harmonic voltages produce odd harmonic currents only while even harmonic voltages produce harmonic currents of all orders. For both even and odd harmonic voltages which are balanced no triplen harmonics are produced. The effect of convertor terminal voltage distortion can be reduced by control system filters or an equidistant controller (Ainsworth 1967). The advantages of an equidistant controller over control system filters is discussed in section 4.1.2.

It has been shown by Dobinson (1975) that the presence of d.c. current ripple can dramatically modify the magnitudes of the characteristic harmonics. In the presence of convertor unbalance, and a finite smoothing inductor, uncharacteristic currents will flow in the d.c. system resulting in modified uncharacteristic a.c. currents. This has been observed by Giesner and Arrillaga (1972) and later by Yacamini and Smith (1983) for the case of second harmonic ripple producing third harmonic currents on the a.c. side.

The other source of uncharacteristic harmonics in the literature are controller errors (Reeve and Krishnayya 1968 and Reeve et al 1969). These errors produce unequal conduction periods in each phase, including half-wave asymmetry, and therefore all a.c. harmonic currents and d.c. side harmonic voltages are generated in a random fashion. This includes a d.c. current in the converter transformer which can produce saturation of the core and additional harmonics (Yacamini and de Oliveira 1978).

The iterative algorithm described in this chapter includes the effects of unbalanced terminal voltage and commutating reactance, as well as distortion on the a.c. terminal busbar voltage and d.c. current. Control system errors were ignored, as they are either due to a steady state disturbance already included in the algorithm or, only a random error not sustained in the steady state.

3.2 AN OUTLINE OF THE ITERATIVE ALGORITHM

It is clear that the operation of a convertor, and hence its associated a.c. current injections and d.c. voltage waveform, is dependent on the voltage on its terminal and the d.c. current ripple. At the same time however, the voltage distortion on the convertor's terminal is due to the a.c. current injected into the combined admittance of the a.c. system and the harmonic filters. Similarly, the ripple on the d.c. current is related to the d.c. voltage by the admittance of the d.c. system.

The proposed iterative algorithm, the structure of which is given in figure 3.1, is needed to assess the harmonic interaction that occurs between transmission systems and static convertors.

Firstly, the execution parameters, filter data and admittance matrices for the a.c. and d.c. systems are entered. A preliminary power flow must be carried out to provide an approximate estimate of

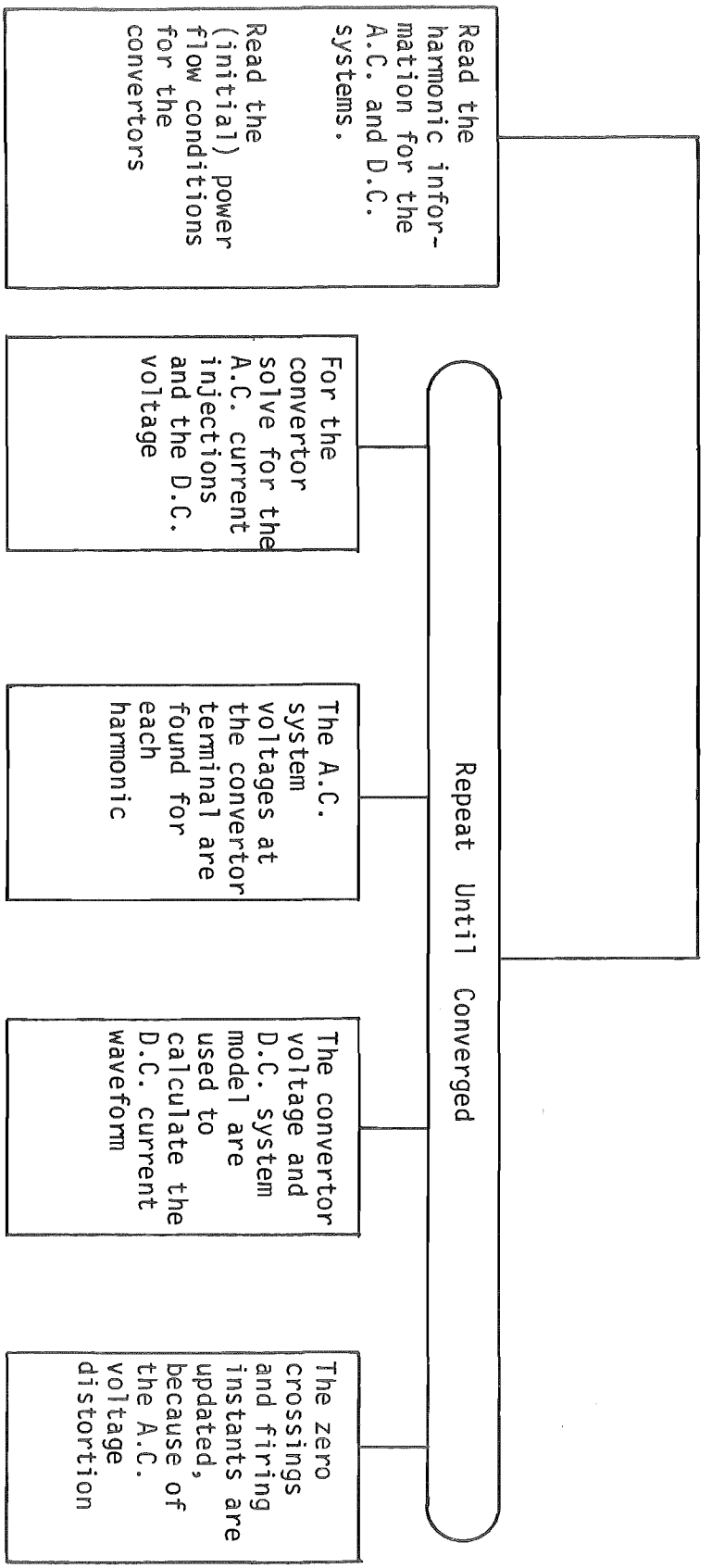

Figure 3.1 : Structure Diagram of the Iterative Algorithm

the fundamental frequency voltages and currents at the converter a.c. and d.c. terminals. In the presence of transmission line unbalance, the a.c./d.c. power flow must be three phase (Harker and Arrillaga 1979). The a.c./d.c. power flow contains the necessary information to derive the three-phase fundamental voltage and current waveforms at the convertor terminal, used to calculate the first estimates of the three-phase harmonic current injections and the d.c. side voltage waveform.

The iterative loop is divided into four blocks. Firstly the convertor operation is solved for its a.c. current injections and d.c. voltage waveform. This process is discussed in section 3.3. With the a.c. current injections calculated, the a.c. system is solved for the terminal voltage distortion. Similarly, the d.c. voltage waveform is used to derive the d.c. system current ripple. The solution of the a.c. and d.c. systems is examined in sections 3.4 and 3.5 respectively. Finally, from the firing strategy and the voltage distortion, control is implemented in the fourth block, as described in section 3.6.

The iterative loop is terminated by either convergence or divergence being detected. The solution has converged when the voltage and current distortions do not change significantly between successive iterations. However, instead of checking each individual voltage and current component, the iterative changes of the commutating voltage zero crossings are used to test for convergence. If all the zero crossings change by less than 0.0001 radians a flag is set and one more iteration performed.

Divergence of the algorithm is indicated when the maximum number of iterations is exceeded, multiple zero crossings are detected or the controller specifies a negative delay angle. An excessive number of iterations implies a marginally stable solution while either multiple zero crossings or negative delay angles point to large uncharacteristic voltage distortion.

3.3 SOLVING THE OPERATION OF THE CONVERTOR

Each convertor is solved for the a.c. harmonic current injections and the d.c. voltage harmonics. To achieve this, the convertor commutating voltages, the d.c. current waveform and firing instants are needed at each iteration. The commutating impedances, the transformer connection and tap ratios must also be specified.

The commutating voltages and impedances are defined in terms of a Thevenin equivalent for the secondary of the convertor transformer, as described in figure 3.2

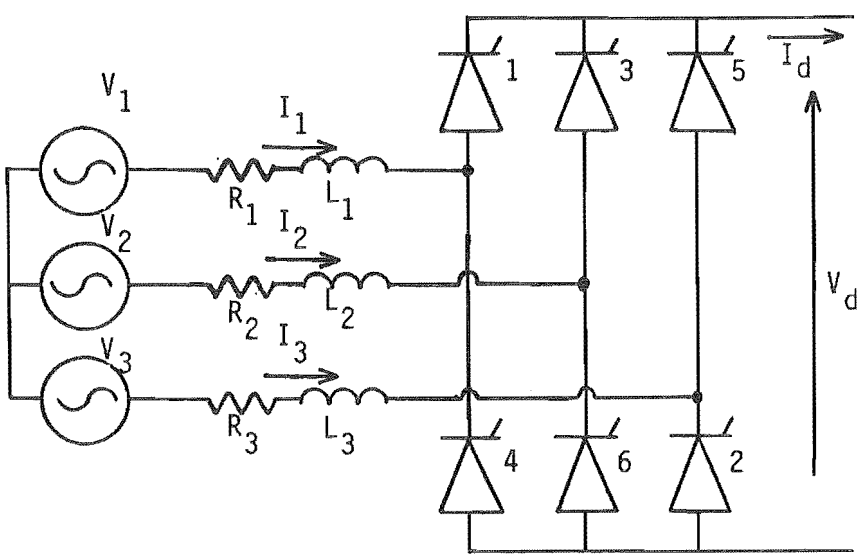

Figure 3.2 : The Convertor and the Thevenin Equivalent of its Transformer

The commutating voltages are the transformer primary voltages, including distortion, referred to the secondary with the transformer connection and tap ratios taken into account. The commutating impedances are the transformer's leakage inductance per phase with a series resistance. If data is available the three commutating impedances can be unbalanced.

The d.c. current waveform, I_d, contains ripple and is at any instant of time

$$I_d(t) = I_{do} + \sqrt{2} \sum_{j=1}^{NHARM} I_{dh} \sin(h\omega t + \phi_{dh}) \qquad 3.1$$

where I_{do} is the d.c. current specified by the power flow and I_{dh} and ϕ_{dh} are the rms magnitude and phase of the h^{th} harmonic component of ripple respectively. NHARM is the maximum harmonic order to be considered. The convertor firing instants are calculated at each previous iteration. The process of evaluating the firing instants is described in section 3.6.

3.3.1 Calculating the Commutation Current

The commutation is the period of time taken to turn off an outgoing valve when an incoming valve is fired. The incoming valve is fired after it is forward biased and cannot turn on instantaneously because the energy stored in the commutating reactance of the outgoing phase needs to be transferred to the incoming phase. The situation of valve 3 turning valve 1 off is described in figure 3.3.

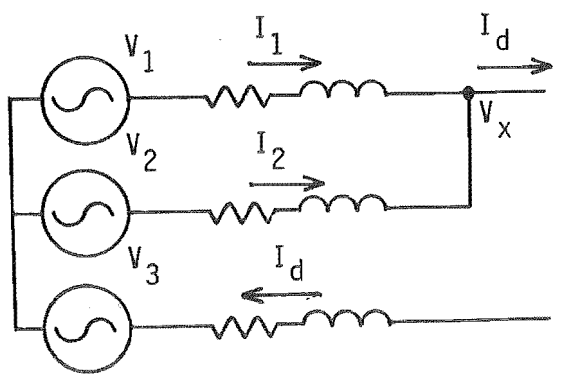

Figure 3.3 : Commutation of Valve 3

At the instant valve 3 is fired $I_1 = I_d$ and $I_2 = 0$. However, because V_2 is more positive than V_1, the commutation current I_2 grows, thus reducing the current I_1. When I_1 reaches zero, $I_2 = I_d$, valve 1 turns off and valve 3 is fully conducting. A generalised equation to describe any commutation, developed by Yacamini and de Oliveira (1980a), and is

$$i_n(t) = \sum_{h=1}^{NHARM} \frac{B_h}{L_{nm}}\left[\left(\frac{H_h + {}^{1}/_{T_{nm}}}{h^2\omega^2 + {}^{1}/_{T_{nm}^2}}\right) e^{-+/T_{nm}} + \frac{1}{h\omega}\left(\frac{H_h^2 + h^2\omega^2}{h^2\omega^2 + {}^{1}/_{T_{mn}^2}}\right) \sin(h\omega t+\phi_h)\right]$$

$$+\frac{R_m I_d}{R_{nm}}\left(1 - e^{-t/T_{nm}}\right) + C_{nm}$$

3.2

where P is the valve commutating in

θ_p is the firing instant of valve P

m is the outgoing phase

n is the incoming phase

$$R_{nm} = R_n + R_m \qquad 3.3$$

$$L_{nm} = L_n + L_m \qquad 3.4$$

$$T_{nm} = L_{nm}/R_{nm} \qquad 3.5$$

$$A_h = \hat{V}_{hn} \cos(h\theta_p + \phi_{hn}) - \hat{V}_{hm} \cos(h\theta_p + \phi_{hm}) \qquad 3.6$$

$$B_h = \hat{V}_{hn} \sin(h\theta_p + \phi_{hn}) - \hat{V}_{hm} \sin(h\theta_p + \phi_{hm}) \qquad 3.7$$

$$H_h = h\omega A_h/B_h \qquad 3.8$$

$$\phi_h = \tan^{-1}({}^{1}/_{h\omega\, T_{nm}}) - \tan^{-1}\left(\frac{H_h}{h\omega}\right) \qquad 3.9$$

$\hat{V}_{hn}$ is the peak magnitude of the h^{th} harmonic of the incoming phase

$\hat{V}_{hm}$ is the peak magnitude of the h^{th} harmonic of the outgoing phase

ϕ_{hn} is the phase of the h^{th} harmonic of the incoming phase

ϕ_{hm} is the phase of the h^{th} harmonic of the outgoing phase

C_{nm} an integration constant such that $i_n(0) = 0$.

Equation 3.2 can be simplified to

$$i_n(t) = \sum_{h=1}^{NHARM} (X_h e^{-t/T_{nm}} + S_h \sin(h\omega t + \phi_h) \qquad 3.10$$

$$+ Y(1-e^{-t/T_{nm}}) + C_{nm}$$

where

$$x_h = \frac{B_h}{L_{nm}} \left(\frac{H_h - 1/T_{nm}}{h^2\omega^2 + 1/T_{nm}^2}\right) \qquad 3.11$$

$$S_h = \frac{B_h}{h\omega L_{nm}} \frac{H_h^2 + 1/T_{nm}^2}{h^2\omega^2 + 1/T_{nm}^2} \qquad 3.12$$

$$Y = R_m I_d / R_{nm} \qquad 3.13$$

C_{nm} is evaluated by setting t and $i_n(0)$ equal to zero in equation 3.10. This yields

$$C_{nm} = - \sum_{h=1}^{NHARM} \left(X_h + S_h \sin(\phi_h)\right) \qquad 3.14$$

If equation 3.14 is substituted into 3.10

$$i_n(t) = \sum_{h=1}^{NHARM} \left[X_h(e^{-t/T_{nm}} -1) + S_h(\sin(h\omega t + \phi_h) - \sin\phi_h)\right] + Y\left(1-e^{-t/T_{nm}}\right) \qquad 3.15$$

To calculate V_1, V_2 and V_3 for the convertor transformer secondary, Yacamini and de Oliveira (1980a) used a zig-zag representation of the convertor transformer connection. This has the advantage of being able to represent any phase shift of the transformer and is therefore useful for modelling convertors of large pulse number. While the zig-zag connection is perfectly accurate for the star-g/star connection, it is not for the star-g/delta connection in the presence of zero sequence voltage at the convertor terminal. Because of the unbalance of transformers and transmission lines, and the fact that the star-g/delta connection is not a perfect short circuit to zero sequence (Chen and Dillon 1974), a finite level of zero sequence voltage can exist on the convertor's terminal busbar. This

zero sequence voltage cannot exist on the secondary of a star-g/delta transformer but is referred to the secondary of an equivalent zig-zag. This is demonstrated in Appendix A2 for a transformer with a DY11 connection.

The need for a zig-zag equivalent and its associated inaccuracies can be overcome by calculating the secondary phase to phase voltages directly from the primary voltages rather than solving for V_1, V_2 and V_3 explicitly. Thus, if V_a, V_b and V_c are the primary phase voltages, the secondary phase to phase voltages for a star-g/star transformer are

$$V_{21}(t) = V_b(t) - V_a(t) \qquad 3.16$$

$$V_{32}(t) = V_c(t) - V_b(t) \qquad 3.17$$

$$V_{13}(t) = V_a(t) - V_c(t) \qquad 3.18$$

and for a star-g/delta (DY11) transformer

$$V_{21}(t) = -\sqrt{3}V_a(t) \qquad 3.19$$

$$V_{32}(t) = -\sqrt{3}V_b(t) \qquad 3.20$$

$$V_{13}(t) = -\sqrt{3}V_c(t) \qquad 3.21$$

where the $\sqrt{3}$ is due to the P.U. system.

3.3.2 Sampling the A.C. Current Injections

To calculate the a.c. current injections in the frequency domain, each of the three phases are sampled at NSAMPL equally spaced points in the time domain over one cycle and a Fast Fourier Transform performed. The method of sampling is preferable to the equation form used by Yacamini and de Oliveira (1980a) because of its generality and ease of adding new features (Harker 1980).

The three current waveforms can be divided into 12 sections. For six of the sections normal conduction by one valve on each side of the bridge occurs. This situation is described in figure 3.4 for

valves 1 and 2 conducting.

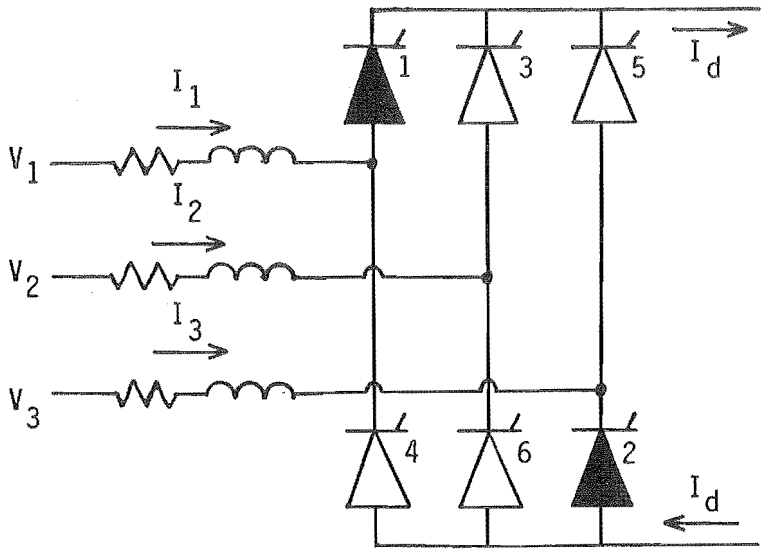

Figure 3.4 : Normal Conduction of Valves 1 and 2

At any instant of time t during this section the three phase current samples are

$$I_{ac} = \begin{bmatrix} I_1 \\ I_2 \\ I_3 \end{bmatrix} \quad \begin{bmatrix} I_d \\ 0 \\ -I_d \end{bmatrix} \qquad 3.22$$

The other six sections correspond to each of the commutations that occur each cycle. The example of valve 3 commutating valve 1 out with normal conduction of valve 2 is given in figure 3.5.

The commutating current, i_c, is calculated by equation 3.15. The corresponding current samples are therefore

$$I_{ac} = \begin{bmatrix} I_1 \\ I_2 \\ I_3 \end{bmatrix} = \begin{bmatrix} I_d - i_c \\ i_c \\ -I_d \end{bmatrix} \qquad 3.23$$

For simplicity the possibility of simultaneous commutations has been ignored. This is not a limitation as simultaneous commutations do not occur under normal steady-state operation.

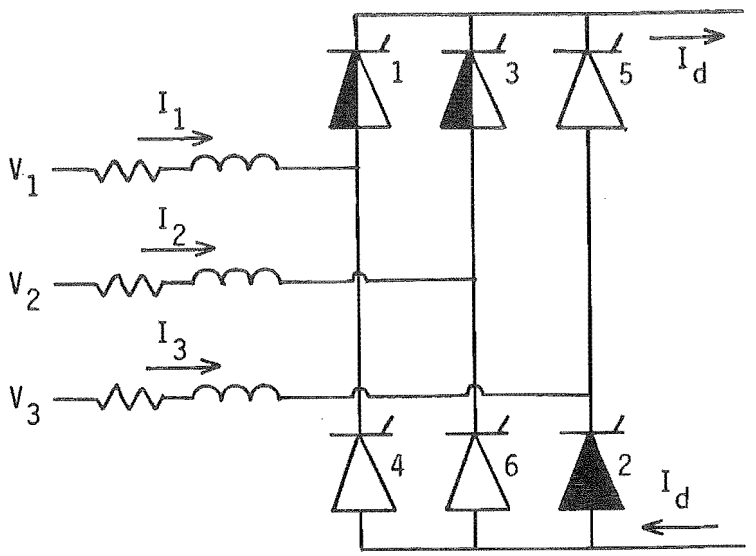

Figure 3.5 : Commutation from Valve 1 to Valve 3 with Valve 2 Conducting

The first sample point, and the time reference, is taken as the firing instant of valve 1. For each conduction and commutating section, equivalent equations to 3.22 and 3.23 are derived to describe a complete cycle of each phase. Figure 3.6 shows the three phase current waveform for a cycle. Similarly, table 3.1 defines the current in each phase for each section.

At the beginning of the iteration each phase to phase voltage pair $V_{nm}(t)$ is calculated such that

$$V_{nm}(t) = \sum_h A_h^{(nm)} \sin(h\omega t) + B_h^{(nm)} \cos(h\omega t) \qquad 3.24$$

where t is referenced to θ_1. For a star-g/star transformer equations 3.6 and 3.7 are used to calculate the A_h and B_h respectively where, $V_1 = V_a$, $V_2 = V_b$ and $V_3 = V_c$. For a star-g/delta transformer

$$V_{nm}(t) = -\sqrt{3} V_q(t) \qquad 3.25$$

$$= -\sqrt{3} \sum_h \hat{V}_q \sin(h\omega t + \phi_{qh} + h\theta_1)$$

$$= -\sqrt{3} \sum_h A_h^{(nm)} \sin(h\omega t) + B_h^{(nm)} \cos(h\omega t) \qquad 3.26$$

where n,m and q are defined by equations 3.19, 3.20 and 3.21, and

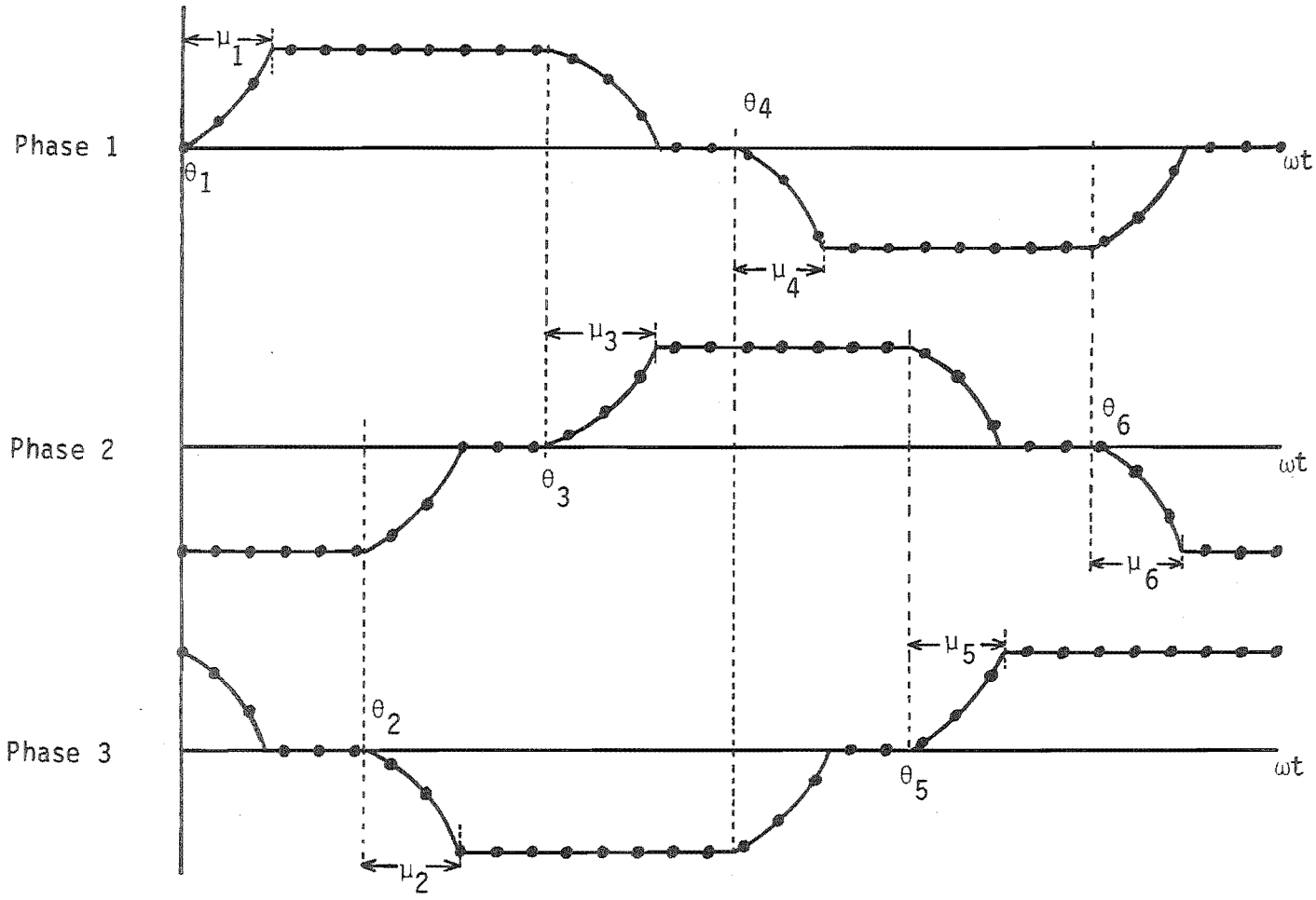

Figure 3.6 : The 12 Sections of the Convertor's A.C. Currents

Table 3.1 : The three phase currents in each phase and section

Section	Phase 1	Phase 2	Phase 3	Limits, reference to θ_1		
1	i_c	$-I_d$	$I_d - i_c$	0	$< \omega t <$	μ_1
2	I_d	$-I_d$	0	μ_1	$< \omega t <$	$\theta_2 - \theta_1$
3	I_d	$-I_d - i_c$	i_c*	$\theta_2 - \theta_1$	$< \omega t <$	$\theta_2 - \theta_1 + \mu_2$
4	I_d	0	$-I_d$	$\theta_2 - \theta_1 + \mu_2$	$< \omega t <$	$\theta_3 - \theta_1$
5	$I_d - i_c$	i_c	$-I_d$	$\theta_3 - \theta_1$	$< \omega t <$	$\theta_3 - \theta_1 + \mu_3$
6	0	I_d	$-I_d$	$\theta_3 - \theta_1 + \mu_3$	$< \omega t <$	$\theta_1 - \theta_1$
7	i_c*	I_d	$-I_d - i_c$	$\theta_1 - \theta_1$	$< \omega t <$	$\theta_1 - \theta_1 + \mu_1$
8	$-I_d$	I_d	0	$\theta_1 - \theta_1 + \mu_1$	$< \omega t <$	$\theta_5 - \theta_1$
9	$-I_d$	$I_d - i_c$	i_c	$\theta_5 - \theta_1$	$< \omega t <$	$\theta_5 - \theta_1 + \mu_5$
10	$-I_d$	0	I_d	$\theta_5 - \theta_1 + \mu_5$	$< \omega t <$	$\theta_6 - \theta_1$
11	$-I_d - i_c$	i_c*	I_d	$\theta_6 - \theta_1$	$< \omega t <$	$\theta_6 - \theta_1 + \mu_6$
12	0	$-I_d$	I_d	$\theta_6 - \theta_1 + \mu_6$	$< \omega t <$	2π

* the commutation currents on the common anode have negative values.

$$A_h^{(nm)} = \hat{V}_q \cos(\phi_{qh} + h\theta_1) \qquad 3.27$$

$$B_h^{(nm)} = V_q \sin(\phi_{qh} + h\theta_1) \qquad 3.28$$

Because during the p^{th} commutation the time t of the commutation equation 3.15 is referenced to θ_p, the $A_h^{(nm)}$ and $B_h^{(nm)}$ are modified to A_h and B_h such that

$$A_h = \hat{V}_{hn} \cos(h\theta_p + \phi_{hm}) - V_{hm} \cos(h\theta_p + \phi_{hm}) \qquad 3.29$$

$$= A_h^{(nm)} \cos(h\theta_p - h\theta_1) - B_h^{(nm)} \sin(h\theta_p - h\theta_1) \qquad 3.30$$

and

$$B_h = A_h^{(nm)} \sin(h\theta_p - h\theta_1) + B_h^{(nm)} \cos(h\theta_p - h\theta_1) \qquad 3.31$$

Note that equations 3.30 and 3.31 also hold for star-g/delta transformers, even though V_n and V_m are not explicitly formed.

The end of the commutation is detected when the magnitude of the current in the incoming phase exceeds the instantaneous value of I_d. Figure 3.7 shows the current samples for a typical commutation on the common cathode.

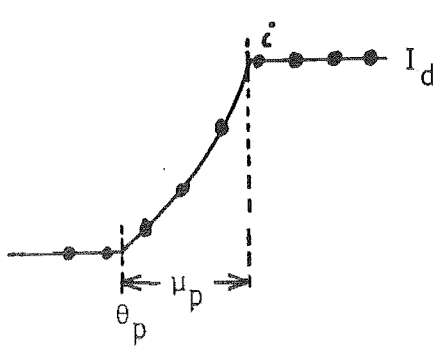

Figure 3.7 : Calculating the Commutation Angle

The commutation angle can be approximated by the angle from θ_p to half way between the $(i-1)^{th}$ and i^{th} samples, either side of the end of the commutation. At the i^{th} sample the angle from the θ_1 reference is

$$\theta_i = (i-1) \cdot 2\pi/NSAMPL \qquad 3.32$$

and therefore the p^{th} commutation angle can be approximated by

$$\mu_p = (i-1.5)\cdot 2\pi/NSAMPL - (\theta_p-\theta_1) \qquad 3.33$$

Because the actual commutation angle is only required as information to the user, and not used in later calculations, the approximation of 3.33 is sufficient. With 1024 samples per cycle the maximum error would be 0.2 degrees.

3.3.3 Sampling the D.C. Voltage Waveform

Sampling the d.c. voltage waveform is a similar process to sampling the a.c. currents, using the same sample points and 12 sections. Because the same commutation circuits, d.c. current waveforms and firing instants are also common to both calculations, both the convertor's a.c. current and d.c. voltage samples are evaluated simultaneously.

During the six sections of normal conduction the d.c. voltage, V_d, is equal to the appropriate phase to phase voltage. For example, when valves 1 and 2 are conducting, $V_d = V_{13}$. This assumes that the voltage drop across the commutation impedance is negligible and is valid for a small convertor transformer resistance and a small d.c. current ripple.

However, during the commutation process two of the secondary phases are shorted together resulting in a large voltage drop across the commutating impedance. For a commutation from valves 1 to 3, as described in figure 3.3,

$$V_d = V_{23} + V_x \qquad 3.34$$

where

$$V_x = - L_2\, di_2/d_t - R_2 i_2 \qquad 3.35$$

and i_2 is the commutation current of equation 3.15. Therefore

$$V_x = W\, e^{-t/T_{nm}} + \sum_h M_h \cos(h\omega t) + N_h \sin(h\omega t) + K_n$$

where $M_h = -(h\omega L_n S_h \cos(\phi_h) + R_n S_h \sin(\phi_h))$ 3.37

$N_h = (h\omega L_n S_h \sin(\phi h) - R_n S_h \cos(\phi_h))$ 3.38

$W = (L_n/T_{nm} - R_n)(X_h - Y)$ 3.39

$K_n = -R_n(Y + C_{nm})$ 3.40

The d.c. voltage waveform over one cycle is shown in figure 3.8, while the value of d.c. voltage is defined in table 3.2.

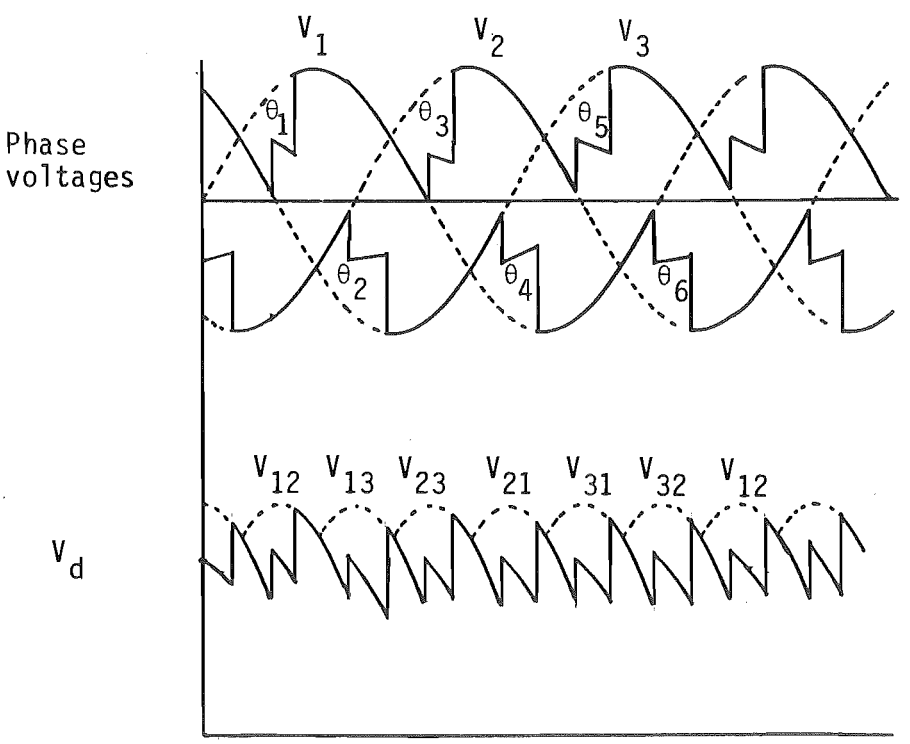

Figure 3.8 : The 12 Sections of the Convertor D.C. Voltage

Table 3.2 : The d.c. voltage in each section

Section	d.c. voltage	Limits, reference to θ_1
1	$V_{12} + V_x$	$0 < \omega t < \mu_1$
2	V_{12}	$\mu_1 < \omega t < \theta_2 - \theta_1$
3	$V_{13} - V_x$	$\theta_2 - \theta_1 < \omega t < \theta_2 - \theta_1 + \mu_2$
4	V_{13}	$\theta_2 - \theta_1 + \mu_2 < \omega t < \theta_3 - \theta_1$
5	$V_{23} + V_x$	$\theta_3 - \theta_1 < \omega t < \theta_3 - \theta_1 + \mu_3$
6	V_{23}	$\theta_3 - \theta_1 + \mu_3 < \omega t < \theta_1 - \theta_1$
7	$V_{21} - V_x$	$\theta_1 - \theta_1 < \omega t < \theta_1 - \theta_1 + \mu_4$
8	V_{21}	$\theta_4 - \theta_1 + \mu_4 < \omega t < \theta_5 - \theta_1$
9	$V_{31} + V_x$	$\theta_5 - \theta_1 < \omega t < \theta_5 - \theta_1 + \mu_5$
10	V_{31}	$\theta_5 - \theta_1 + \mu_5 < \omega t < \theta_6 - \theta_1$
11	$V_{32} - V_x$	$\theta_6 - \theta_1 < \omega t < \theta_6 - \theta_1 + \mu_6$
12	V_{32}	$\theta_6 - \theta_1 + \mu_6 < \omega t < 2\pi$

3.3.4 Conversion from the Time Domain to the Frequency Domain

With information of the d.c. current injections and d.c. voltage for the convertor described for one cycle in the time domain, an FFT is performed on each waveform to calculate their harmonic components.

The output of the FFT is an exponential series with time reference θ_1. However, during the rest of the iterative algorithm a sinewave series is assumed. Also the a.c. currents are in the form of an injection and need their sign reversed. Therefore the a.c. current phasors become

$$I_h = -2/\sqrt{2}\, I_h(\cos(\tfrac{\pi}{2} - h\theta_1) + j \sin(\tfrac{\pi}{2} - h\theta_1)) \qquad 3.41$$

and the d.c. voltage phasors

$$V_{dh} = 2/\sqrt{2}\, V_h(\cos(\tfrac{\pi}{2} - h\theta_1) + j \sin(\tfrac{\pi}{2} - h\theta_1) \qquad 3.42$$

where the 2 is due to the nature of the FFT and the $\sqrt{2}$ is to convert to rms quantities.

3.4 SOLVING THE A.C. SYSTEM

At each iteration the a.c. system is solved for the voltage distortion on the convertor terminals from the harmonic current injections into the secondary of the convertor transformers. Instead of referring the a.c. current injections to the primary, the convertor transformer secondaries are preserved to include any frequency dependence of the transformer. This means the total number of three phase busbars is NTERM plus NCONV, where NTERM and NCONV are the number of terminal busbars and convertors respectively. The busbar numbering is started with the terminal busbars.

The a.c. system is modelled as an admittance matrix $[Y_{ac}]$ at each harmonic. At each frequency the matrices have the same structure being made up of three components; an equivalent of the rest of the a.c. system $[Y_{sys}]$, the convertor transformers $[Y_t]$ and the harmonic filters $[Y_f]$. Figure 3.9 is an example of an a.c. system with convertors at more than one busbar used to illustrate the formation of the $[Y_{ac}]$ matrices.

The equavalent admittance of the a.c. system $[Y_{sys}]$, as seen from the convertor terminal can be measured (Breuer 1982) or calculated using a computer (Densem 1983). The use of a computer to form an equivalent admittance is discussed in section 2.3.2. From equation 2.2 $[Y_{red}]$ is substituted into $[Y_{sys}]$. In the example of figure 3.9

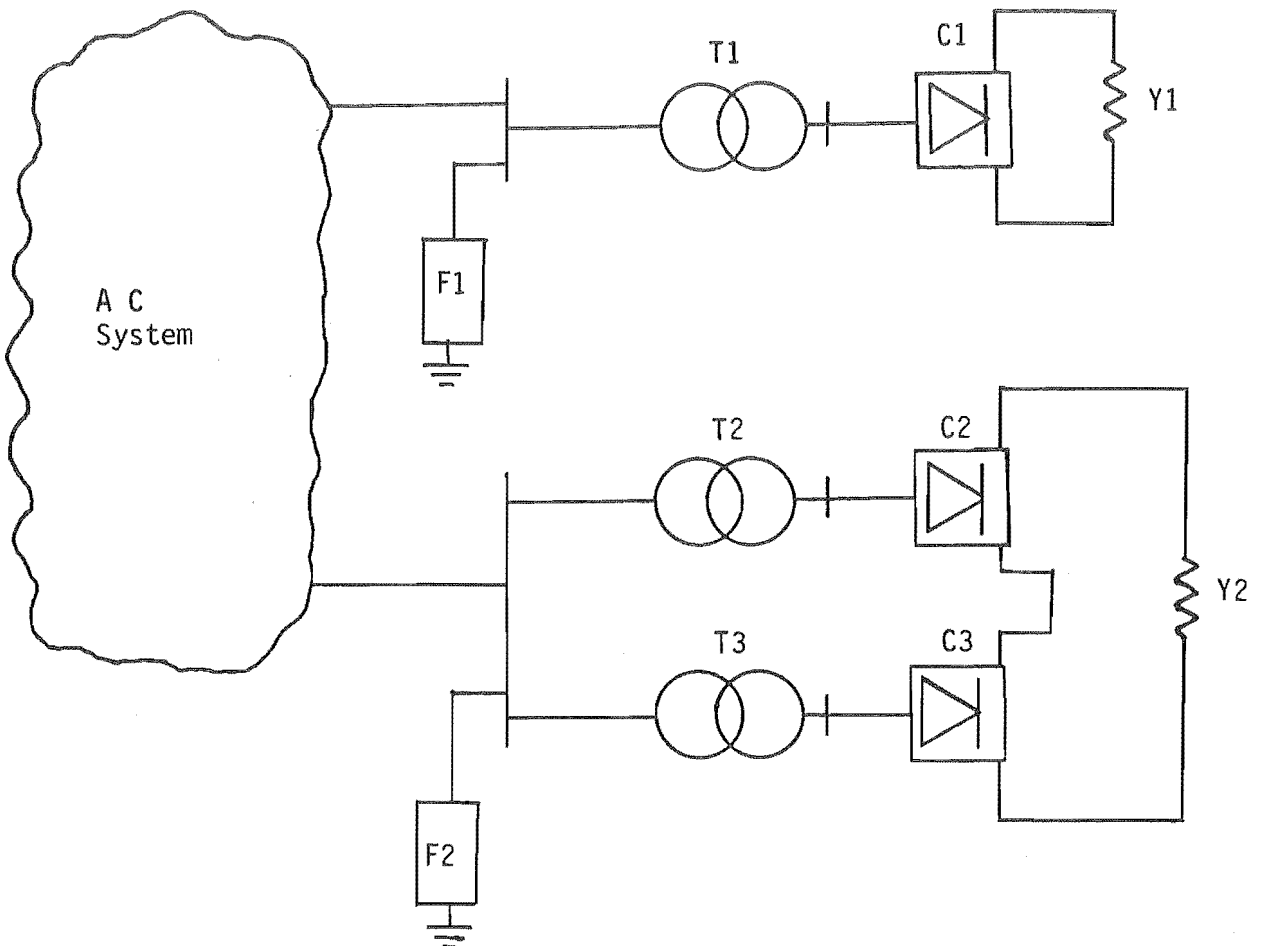

Figure 3.9 : An Illustrative Example of an A.C. System with A.C./D.C. Convertors

$$[Y_{sys}] = \begin{bmatrix} Y_{sys11} & Y_{sys12} & 0 & 0 & 0 \\ Y_{sys21} & Y_{sys22} & 0 & 0 & 0 \\ 0 & 0 & 0 & 0 & 0 \\ 0 & 0 & 0 & 0 & 0 \\ 0 & 0 & 0 & 0 & 0 \end{bmatrix} \begin{matrix} \} \text{NTERM} \\ \\ \} \text{NCONV} \end{matrix} \qquad 3.43$$

where Y_{sys11} and Y_{sys22} are the self admittances of the terminal busbars. Similarly, Y_{sys12} and Y_{sys21} represent the mutual couplings of the system between the busbars.

An individual transformer has an admittance matrix of the form

$$[Y_t] = \begin{bmatrix} Y_{pp} & Y_{ps} \\ Y_{sp} & Y_{ss} \end{bmatrix} \qquad 3.44$$

where each block is a 3 x 3 sub-matrix and the p and s refer to the primary and secondary respectively. The calculation of each block is based on the leakage reactance in parallel with a resistance equal to 80 times the leakage at fundamental frequency. Details of the formation of the admittance matrix for a transformer are given by Harker (1980) and Densem (1983). For the example of figure 3.9

$$[Y_t] = \begin{bmatrix} Y_{pp1} & 0 & Y_{ps1} & 0 & 0 \\ 0 & Y_{pp2} + Y_{pp3} & 0 & Y_{ps2} & Y_{ps3} \\ Y_{sp1} & 0 & Y_{ss1} & 0 & 0 \\ 0 & Y_{sp2} & 0 & Y_{ss2} & 0 \\ 0 & Y_{sp3} & 0 & 0 & Y_{ss3} \end{bmatrix} \qquad 3.45$$

Harmonic filters are used at most convertor terminals to limit the voltage distortion. Such filters can be included directly into the calculation of $[Y_{sys}]$ but, if connected directly to the convertor terminal busbar, can be modelled separately. The two commonly used filter configurations, second order band pass and third order high pass, can be modelled although other types could easily be included. At each harmonic and each terminal busbar, the admittance of each filter branch is calculated then summed to be included in $[Y_f]$. For the example of figure 3.9

$$[Y_f] = \begin{bmatrix} Y_{f1} & 0 & 0 & 0 & 0 \\ 0 & Y_{f2} & 0 & 0 & 0 \\ 0 & 0 & 0 & 0 & 0 \\ 0 & 0 & 0 & 0 & 0 \\ 0 & 0 & 0 & 0 & 0 \end{bmatrix} \qquad 3.46$$

The total admittance matrix $[Y_{ac}]$ is the sum of $[Y_{sys}]$, $[Y_t]$ and $[Y_f]$. At each iteration, the harmonic equation

$$\begin{bmatrix} 0 \\ I_c \end{bmatrix} = [Y_{ac}] \begin{bmatrix} V_t \\ V_c \end{bmatrix} \qquad 3.47$$

is solved where I_c are the NCONV current injections at the convertor and V_t and V_c are the NTERM and NCONV voltage components at the convertor terminals and transformer secondaries, respectively.

3.5 SOLVING THE D.C. SYSTEM

In a similar way to the a.c. system, at each iteration the d.c. system is solved for the ripple on the d.c. current from the d.c. voltage generated on the convertors d.c. terminal. As for the a.c. system, the most convenient representation of the d.c. system is an admittance matrix. At each harmonic the vector of d.c. terminal voltages is multiplied by the d.c. admittance matrix to give the current ripple at that frequency. That is

$$[I_d] = [Y_d] [V_d] \qquad 3.48$$

For the example of figure 3.9 the structure of $[Y_d]$ is

$$\begin{bmatrix} I_{d1} \\ I_{d2} \\ I_{d3} \end{bmatrix} = \begin{bmatrix} Y_1 & 0 & 0 \\ 0 & Y_2 & Y_2 \\ 0 & Y_2 & Y_2 \end{bmatrix} \begin{bmatrix} V_{d1} \\ V_{d2} \\ V_{d2} \end{bmatrix} \qquad 3.49$$

where Y_1 and Y_2 are the harmonic admittance of each of the loads. Note that Y_1 and Y_2 are single elements rather than 3 x 3 blocks in the case of the a.c. system.

In chapter 4 the following representations of the d.c. system have been used.

1. An infinite system with no ripple
2. RL series d.c. system.
3. D.C. motors using the series RL and Ewing (1968) models.
4. D.C. transmission systems including overhead lines and smoothing inductors. The algorithm used to derive $[Y_d]$ in this case is described in Appendix A3.

3.6 IMPLEMENTING CONTROL

The presence of harmonic voltages on the convertor terminal busbar will cause the actual zero crossings of the commutating voltages to be shifted from those of the fundamental alone. With the zero crossings modified, the control strategy is used at each iteration to recalculate the firing instants and delay angles.

3.6.1 Calculating the Zero Crossings

The zero crossings are the instant in time when the transformer secondary phase to phase voltages pass through zero and the next valve can be fired.

Because of the difficulty in calculating the zero crossings analytically, the regula falsi (Kreyzig 1979) iterative method is used. With an initial estimate of the most recent values, the six zero crossings are updated at each iteration.

If the zero crossing fail to converge in 100 iterations multiple zero crossings are assumed, indicating a divergent solution due to excessive distortion.

3.6.2 Calculating the Delay Angles

The delay angle refers to the angle between the actual zero crossing and the instant of firing for a particular valve. Given the set of zero crossings, the control strategy is implemented to

calculate the individual delay angles.

The two types of control strategies specified by the power flow are constant delay angle and equidistant control. Constant delay angle control maintains equal delay angles for each valve. An equidistant controller produces valve firings every 60 degrees. This is achieved within the algorithm by fixing the delay angle on valve one and adjusting the other delay angles to maintain equal conduction periods.

In many h.v.d.c. controllers filters are included in the control loop. The effect of these can be included into the iterative algorithm by calculating the delay angles such that the firing instants are unaltered by the presence of voltage distortion. This applies to either a constant delay angle or equidistant controller.

3.7 CONCLUSIONS

In this chapter an iterative algorithm has been developed to calculate the harmonic iteraction that occurs at a.c./d.c. convertors.

While the algorithm accurately models the convertor's operation and the a.c. and d.c. systems, the algorithm is susceptible to numerical instability. This problem is analysed in chapter 4. Furthermore, the iterative algorithm developed to model three phase convertors, is modified in chapter 5 to analyse the operation of single phase convertors.

CHAPTER 4

HARMONIC INTERACTION BETWEEN A.C., D.C. AND CONVERTOR SYSTEMS

4.1 INTRODUCTION

When considering the interaction between a.c. and d.c. systems in the steady state two main areas of investigation are evident. The first, and in general the most important area, is that of fundamental voltage and power interactions which are solved by the use of an integrated a.c./d.c. power flow (Harker and Arrillaga 1979). The other area is that of harmonics.

4.1.1. The Effect of Interactions on the Harmonic Currents Produced

The harmonic currents produced by the converter depend not only on the fundamental voltage conditions at the convertor terminals and the d.c. power being transmitted, both being calculated in the power flow, but also on the presence of a.c. voltage distortion on the terminal busbar and d.c. current distortion.

The iterative algorithm described in chapter 3 can be used to analyse the harmonic interactions between the convertor, a.c. and d.c. systems. A large 6-pulse convertor at Tiwai, in the system of the South Island of New Zealand, is used in this chapter together with various a.c. system and filter configurations as well as constant delay angle and equidistant control. Also the effect of the d.c. system was examined. The results are examined in sections 4.2 and 4.3.

At the distribution system level, three phase d.c. convertor drives have been examined and discussed in Appendix A6 in the form of a paper (Arrillaga et al 1985b).

Single phase traction convertor d.c. drives have been examined in a similar fashion to three phase d.c. drives. This is discussed in chapter 5.

4.1.2 Harmonic Instability

A problem associated with some h.v.d.c. schemes is harmonic magnification and/or instability. A harmonic instability can be characterised by excessive voltage distortion on the convertor terminal busbar (Kauferle et al 1970), which can make the link inoperable.

At the IEE conference No. 22, entitled High Voltage D.C. Transmission, several examples of harmonic magnification and instability were reported. A third harmonic instability at the Cross-Channel link (Holmborn and Martenssen 1966) often developed under some a.c. system configurations. This caused the link to be inoperable. The problem was removed by the inclusion of a third harmonic filter. Because of the Cross-Channel link experience, a third harmonic filter was included at the design stage of the Sardinian h.v.d.c. terminal to prevent a potential instability (Natale et al 1966 and Holmborn and Martenssen 1966).

Similarly, a problem was found during tests of the Kingsnorth Scheme (Last et al 1966). Excessive second harmonic voltage distortion under some system conditions was able to trigger the generator protection circuits and cause errors in the over-voltage protection of the filters.

At the Benmore terminal of the New Zealand d.c. link excessive ninth harmonic voltage was reported (Robinson 1966b). This was solved by the inclusion of a ninth harmonic filter.

A harmonic instability can, therefore, be defined as the generation and/or magnification of non-characteristic frequencies by a

d.c. system containing, initially, no unbalance asymmetry (Ainsworth 1981 and Arrillaga 1983).

At the convertor a positive feedback loop can exist such that distortion of either the a.c. or d.c. systems reaches the control system causing firing pulse irregularities which, in turn, can produce harmonic magnification or instability. Note that this is a waveform distortion rather than an ordinary low frequency instability (Ainsworth 1967).

The relative size of the converter currents and the a.c. system is an important factor contributing to a harmonic magnification and/or instability. The short circuit ratio, which is the ratio of the short circuit MVA at the terminal a.c. busbar to the total nominal d.c. power of the covertor station (Arrillaga 1983), is used as a practical criterion of convertor behaviour. However, since the combination of a.c. system and harmonic filters will have a low parallel resonance frequency, normally lower than fifth harmonic, the short circuit ratio does not define the impedance or system strength at these harmonic orders. The resulting resonance is normally the determining factor in the development of harmonic instabilities (Kauferle et al 1970). As a temporary measure, a harmonic instability can be removed because the effective size of a convertor can be reduced by decreasing the d.c. current (Ainsworth 1967).

The convertor controller is an important part of any harmonic instability positive feedback loop. The control strategy determines the firing pulses and therefore the extent the original disturbance is reinforced. Control system filters can be added to a conventional constant delay angle controller to attenuate the loop gain to harmonics and hence reduce the probability of instability. However, control system filters have several disadvantages (Ainsworth 1967). A filter introduces a variable phase shift to the control signal which

depends on the system frequency. Similarly, filters cannot filter the negative sequence fundamental which is itself a cause of irregular firing pulses. Repeated commutation failures with inverters can also occur as the valves respond to the actual system voltages, including harmonics, and the controller to the fundamental voltages only.

An alternative to the conventional constant delay angle controller is the equidistant controller (Ainsworth 1968). A phase locked oscillator produces six firing pulses per cycle with the frequency adjusted to maintain the delay angle which gives the specified d.c. current. The firing pulses are independent of the a.c. system voltages and, therefore, immune to conventional harmonic magnification and instabilities. However, the phase locked oscillator can be susceptible to d.c. current ripple entering the controller and modulating the firing pulses (Yacamini and de Oliveira 1980b).

4.1.3 Can the Iterative Algorithm be Used to Examine Harmonic Instabilities?

The problem with using the iterative algorithm of chapter 3 to analyse convertor harmonic interaction is the possibility of numerical instability. It was claimed by Yacamini and de Oliveira (1980a) that their harmonic interaction program did not involve problems of numerical stability, that is, in each case the program had been tried it converged when the actual system was stable and a harmonic instability of an actual system was characterised by divergence of the iterative algorithm. However, no mathematical proof has been given to substantiate that divergence of the algorithm is always due to a harmonic instability of the corresponding system.

A more cautious claim was made of a simpler algorithm by Reeve and Baron (1971). That is, that failure of their algorithm to converge is considered to be either indicative of a system harmonic instability

or at least a vulnerability of the system to be unstable. Examining the harmonic voltages and currents at the final iteration would expose the weaknesses of the system.

Harmonic instability with particular reference to the iterative algorithm of chapter 3 will be examined in sections 4.2 and 4.3. A comparison of the iterative algorithm of chapter 3 and a Transient Convertor Simulation algorithm (Heffernan 1980) is made in section 4.4. Future work is discussed in section 4.5.

4.2 SIX PULSE CONVERTOR AT TIWAI : SIX BUSBAR A.C. SYSTEM REPRESENTATION

The iterative program was first used with the data in chapter 8 of Harker's (1980) thesis of a six busbar representation of the South Island of New Zealand's 220 kV transmission system around the Tiwai smelter. The system is illustrated in figure 4.1 and the fundamental operating conditions were specified by a three phase power flow.

The solution involved the first 25 odd harmonics. At these frequencies the system is represented by the set of harmonic impedance data given in table 4.1.

The a.c. system is assumed to be perfectly balanced and its admittance matrix is

$$[Y_{sys}] = \begin{bmatrix} 1/Z_h & 0 & 0 \\ 0 & 1/Z_h & 0 \\ 0 & 0 & 1/Z_h \end{bmatrix}$$

The harmonic filters were those used at Benmore end of the New Zealand h.v.d.c. link. These consist of tuned branches connected to the 220 kV convertor terminal for the fifth, seventh, ninth, eleventh and thirteenth harmonics and a third order high pass filter.

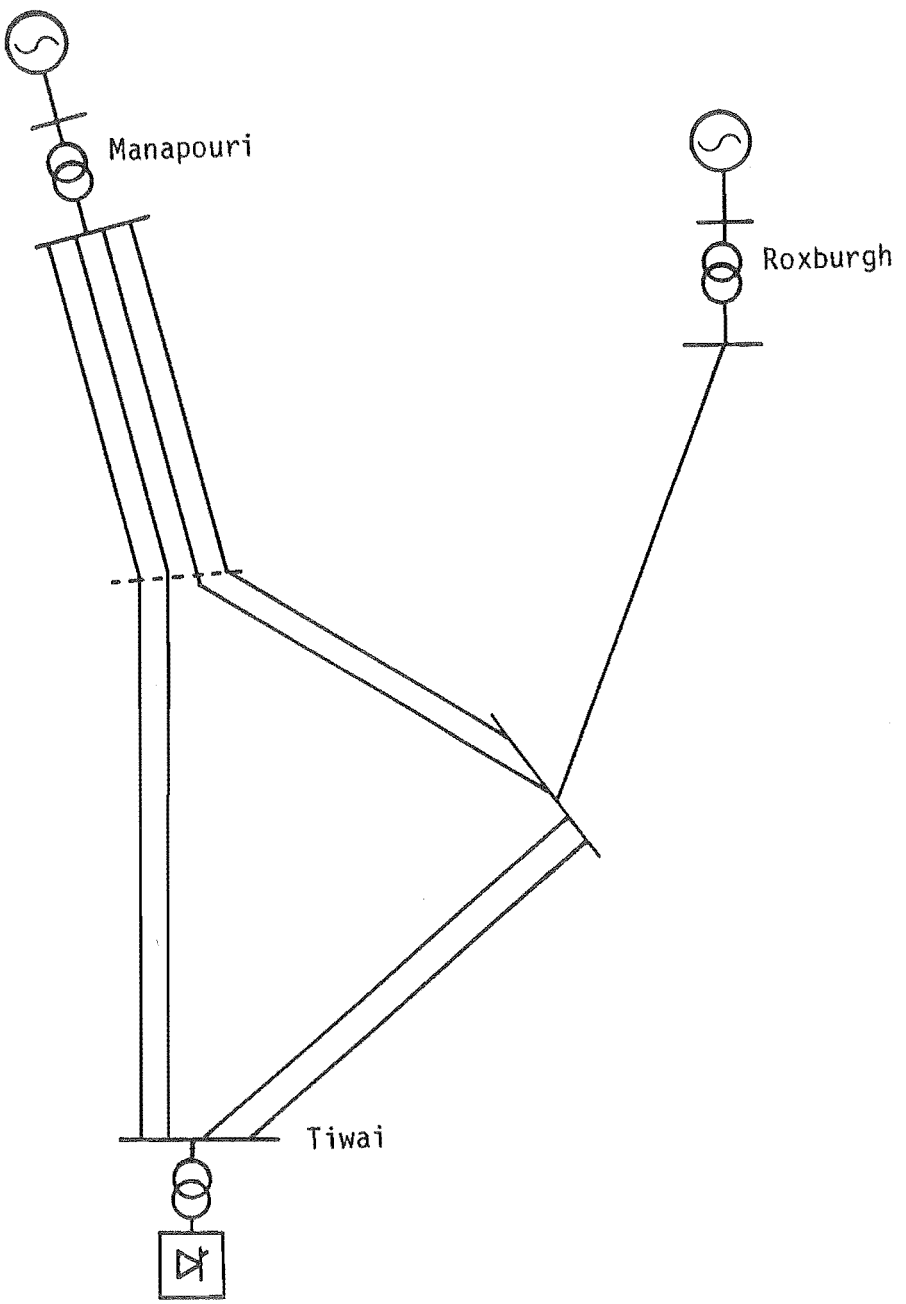

Figure 4.1 : Six Busbar Representation of the Southern Part of the South Island

Table 4.1 : Harmonic Impedance Data for the Tiwai Busbar

Harmonic Order	A.C. System Harmonic Impedance Z_h (Ohms at 220 kV)
3	27.6 + j 84.0
5	200.3 + j 8.6
7	54.4 - j 59.7
9	11.7 - j 40.2
11	2.5 - j 3.8
13	2.2 + j 23.2
15	6.2 + j 57.6
17	28.1 + j 122.3
19	79.7 - j 77.2
21	65.2 + j 66.6
23	111.3 - j 29.5
25	51.5 - j 100.5

The component values are given in table 4.2 and specified with a voltage base of 33 kV.

Table 4.2 : Harmonic Filter Data

Filter	R (Ohms)	L (mH)	C1 (uF)	C2 (uF)
5	0.412	13.1	30.9	--
7	0.454	10.3	20.0	--
9	0.56	10.0	12.1	--
11	0.249	3.6	23.2	--
13	0.305	3.75	16.1	--
h.p.	9.0	0.6	45.0	45.0

In the analysis the filters are connected to the convertor terminal busbar and the filter component values converted into per unit quantities.

The convertor transformer has a star-g/delta connection with a total leakage reactance of 0.05 p.u. and nominal tap ratios. The convertor controller was of the equidistant firing type with a minimum delay angle of 5.0 degrees. For the iterative process a flat d.c. current was also assumed and, with a d.c. power of 373.4 MW, convergence was reached in 10 iterations.

4.2.1 Instability with Improved Representation of the A.C. System

With the three phase harmonic penetration software now available in the department (Densem 1983), a full three phase system admittance matrix $[Y_{sys}]$ was formed for the Tiwai busbar taking into account any unbalance of system components and standing wave effects on transmission lines. To be consistent with the new harmonic

regulations in New Zealand (New Zealand Electricity 1983), $[Y_{sys}]$ was obtained for the first 50 harmonics, including both the odd and even orders.

However, with the new a.c. system representation the Harmonic Interaction program did not converge to a steady-state solution. The problem was to decide if the instability was numerical, i.e., within the computer, or due to a genuine instability (Yacamini and de Oliveira 1980b). A 373.3 MW 6-pulse convertor at Tiwai is potentially unstable as the actual smelter at Tiwai operates at 450 MW and uses a 48-pulse convertor configuration.

Under balanced conditions a convertor does not produce any third harmonic current, but when the a.c. system is unbalanced third harmonic current is produced (Phadke and Harlow 1968 and Reeve and Krishnayya 1968). As a result the levels of third harmonic current of the second run, and therefore the third harmonic voltage, were high and a potential cause of the instability. The magnitude of the third harmonic voltage for each phase at each iteration was plotted in figure 4.2.

It can be seen that the level of third harmonic voltage was high and unstable. The degree of instability is more clearly shown when the third harmonic is compared to the 5th. The level of the fifth harmonic is about 3% and does not vary more than 20% between iterations.

To confirm that the instability with the improved a.c. system representation is due to the third harmonic voltage, the ninth harmonic filter was replaced by a third harmonic filter. The Q was chosen to be 50, the same as the other filters, and a resistance value equal to that used in the fifth harmonic filter (0.412 ohms at 33 kV). With the new filter configuration the level of third harmonic voltage was reduced and the solution converged on the fourth iteration.

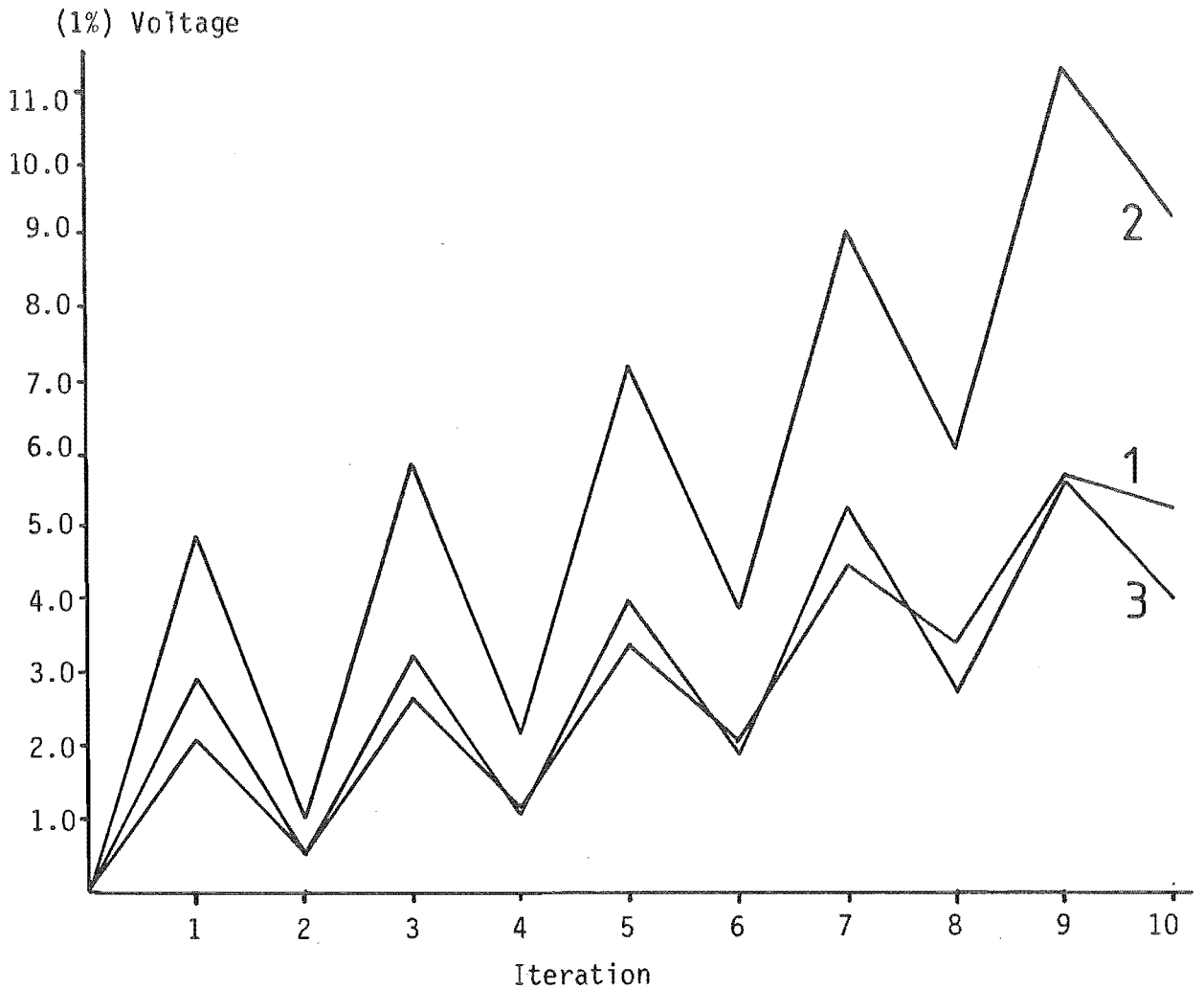

Figure 4.2 : Third Harmonic Voltage at each Iteration of the Unstable Second Run.

4.2.2 Further Investigation of the Instability

Further investigation of the problem was needed and various approaches were tried. A summary of the results obtained is now discussed with reference to the same system under two different filter configurations. The A series of runs refers to the case with the standard filters including a ninth harmonic filter (the Benmore arrangement). The B series refers to the stable case with the ninth harmonic filter replaced by a third harmonic filter.

4.2.2.1 Reduced current

A harmonic instability can occur when the size of the convertor is large compared to the short-circuit MVA of the terminal busbar. Therefore, the first approach used to determine the unstable condition was to repeat the study under gradually increasing convertor d.c. current. Convergence was obtained for values of current of 1.0, 2.0, 3.0 and 4.0 p.u. compared to the unstable 5.29 p.u. nominal case. The larger the current the more iterations were required to obtain a solution. Table 4.3 below shows the d.c. current, the d.c. power, the short-circuit ratio and the number of iterations for each of the 5 levels of d.c. current.

Table 4.3 : A Series Convergence

Run	I_d (p.u.)	Power (MW)	Short circuit ratio	No. iterations
A1	1.0	70.6	28.3	5
A2	2.0	141.2	14.2	8
A3	3.0	211.8	9.1	12
A4	4.0	282.3	7.1	37
A5	5.29	373.4	5.4	-

Looking at the number of iterations to convergence it can be seen that as the current increases the solution becomes less stable.

A set of corresponding runs were performed with the third harmonic filter. Table 4.4 shows that convergence was reached in less iterations in each case.

Table 4.4 : B Series Convergence

Run	I_d (p.u.)	Power (MW)	Short circuit ratio	No. iterations
B1	1.0	70.6	28.3	4
B2	2.0	141.2	14.2	4
B3	3.0	211.8	9.1	4
B4	4.0	282.3	7.1	5
B5	5.29	373.4	5.4	4

The increased rate of convergence is obviously due to the reduced level of third harmonic voltage distortion, although the actual injections of third harmonic current were slightly higher. Table 4.5 shows the magnitude of third harmonic voltage and current for each of the runs A1 - A5 and B1 - B5. The values of the table are the average of three phases.

Table 4.5 : Third Harmonic Voltage and Current at Each D.C. Current Level

	Runs A1 - A5		Runs B1 - B5	
I_d (p.u.)	voltage (p.u.)	current (p.u.)	voltage (p.u.)	current (p.u.)
1.0	.002552	.00517	.000201	.00535
2.0	.005568	.01094	.000522	.01398
3.0	.007669	.01503	.000880	.02304
4.0	.009309	.01806	.001214	.03151
5.29	--	--	.001584	.04032

From figure 4.2, the third harmonic voltage for the unstable A5 run was the cause of the instability. When the third harmonic voltage was reduced by the inclusion of a third harmonic filter the level of third harmonic voltages was reduced and stability restored.

In an actual system the stability is dependent on the relative size of the convertor and the strength of the a.c. system. When the load was reduced to about 75%, run A4 compared to run A5, the instability disappeared.

The level of third harmonic voltage is, therefore, critical. The worse the distortion the less equally spaced the zero-crossings become causing distortion in the a.c. current injections.

For each iteration the convertor is modelled as a current generator at harmonic frequencies. Therefore, the current injection into the secondary of the convertor transformers, I_h, causes a current to flow into the a.c. system, I_{sys} and the harmonic filters, I_{fil}. The ratio I_{sys}/I_h is dependent on the relative size and phase of $[Y_{sys}]$ and $[Y_f]$. Under normal conditions the ratio is less than 1 but at resonance can be greater than 1. In the run B5 the ratio is small. The result of this is that the B series of runs can produce a smaller level of third harmonic voltage distortion even though they produce larger levels of third harmonic current, i.e., there is only a small harmonic current injection into the a.c. system.

Because of the relatively large change in d.c. current between runs A4 and A5, another run (A4.5) was performed with the d.c. current set at 4.5 p.u. After initial settling down the solution started to converge, but after 100 iterations the execution was stopped as the solution had reached a limit cycle. Therefore, this run did not add any further information to the investigation.

There was also an attempt to make a B series to diverge. This was done by increasing the d.c. current from the nominal value of 5.29 p.u. to 10.0 and 14.0 p.u. Both these runs were stable and gave acceptable levels of harmonics. The level of 14.0 p.u. could not be exceeded as this gave commutation angles of 55.9, 54.3 and 56.1 degrees, with the sampling routine used in the harmonic interaction

program not able to cope with simultaneous commutations.

4.2.2.2 Diagonalizing the A.C. system

The instability of run A5 could have possibly been due to off-diagonal elements included in the improved representation of the a.c. system. To check this without changing the basic characteristics or resonances of the system, $[Y_{sys}]$ was modified at each harmonic from

$$[Y_{sys}] = \begin{bmatrix} Y_{11} & Y_{12} & Y_{13} \\ Y_{21} & Y_{22} & Y_{23} \\ Y_{31} & Y_{32} & Y_{33} \end{bmatrix}$$

to

$$[Y'_{sys}] = \begin{bmatrix} Y & 0 & 0 \\ 0 & Y & 0 \\ 0 & 0 & Y \end{bmatrix}$$

$$\text{where } Y = (Y_{11} + Y_{22} + Y_{33})/3$$

The modified version of run A5, with the ninth harmonic filter and diagonalized a.c. system, was unstable and diverged at a faster rate than the unmodified A5 run. In the case of the modified run B5, with the third harmonic filter and diagonalized a.c. system, the solution converged but to slightly higher values for the harmonic voltage distortions than for the unmodified B5 run.

Although the improved representation of the a.c. system did include a full admittance matrix the results did not change markedly when the matrix was diagonalized. Therefore, the instability of run A5 was not directly caused by the off-diagonal elements. However, it should be noted that the inclusion of the off-diagonal elements improves the accuracy of a stable solution.

4.2.2.3 Strengthening the A.C. system

Because the relative strength of the a.c. system plays an important part in convertor stability the next approach was to scale,

or strengthen, the a.c. syste, i.e.,

$$[Y'_{sys}] = [Y_{sys}] \cdot \text{scale factor}$$

Strengthening the a.c. system had a similar effect to decreasing the current and only a small increase in system strength was requried for stability. The results could be summarised as follows:

1. As the scale factor decreases the number of iterations required increases.

2. As the scale factor decreases the delay angles (and zero-crossings) move further from their power-flow values.

3. As the scale factor decreases the level of non-characteristic harmonic currents increase.

4. The voltage distortion is approximately inversely proportional to the scale factor.

These observations are consistent with a genuine instability caused by excessive third harmonic voltage. It is also important to realise that, as the scale factor changes, the resonance is modified and the susceptibility to harmonic instability affected.

4.2.2.4 Further linking of the instability to the third harmonic

The relationship between the instability and third harmonic voltage distortion was further emphasised by two additional runs.

The first run was with the maximum harmonic order present being the third. This left the fundamental, the second harmonic which was essentially zero, and the problem third harmonic. That is, all the higher order harmonic voltages had a value zero and the corresponding harmonic current injections were not calculated. Even though only the third harmonic was present, the solution was still unstable.

The second run included all harmonic orders except the third, which was set to zero at each iteration in the routine which solves for the a.c. harmonic voltages. This run proved to be stable.

Therefore the instability is definitely due to the third harmonic voltage being either genuinely or at least numerically unstable.

4.2.2.5 Improved initial conditions

Numerical instabilities are often avoided by a better set of initial conditions, and, therefore, the next strategy to try and achieve convergence aimed at improving the initial conditions.

One way of achieving this is by initially eliminating the third harmonic, or in general any other troublesome harmonic, from the problem. After reaching an intermediate point of convergence the harmonic is introduced gradually. With the use of a scale factor which starts at zero and is incremented at each intermediate solution, the program is reconverged until the scale factor equals one. This is demonstrated in figure 4.3.

The algorithm was tested on the stable B5 case and was found to be reliable in that it gave the same solution independently of the rate at which the scale factor was increased.

However, when the algorithm of figure 4.3 was applied to the unstable case convergence was still unobtainable. Different strategies for increasing the scale factor were tried. Some results and conclusions are given below:

1. When the increment was 0.2 a solution was reached at scale factors of 0, 0.2, 0.4 and 0.6. However no solution was reached with a value of 0.8.

2. When more than one strategy was used to reach the same scale factor, essentially the same solution was reached at that value of scale factor.

3. Starting from the converged state with a scale factor of 0.0 was of no advantage over starting directly from a value of scale factor of 0.6. This was because the third harmonic was the harmonic which caused the problems and therefore ignoring it (scale factor of 0.0) gave no useful interaction and hence did not help convergence.

4. Increasing the scale factor slowly only gave a solution marginally closer to that of the scale factor of 1.0 as compared to cases of more rapid increases.

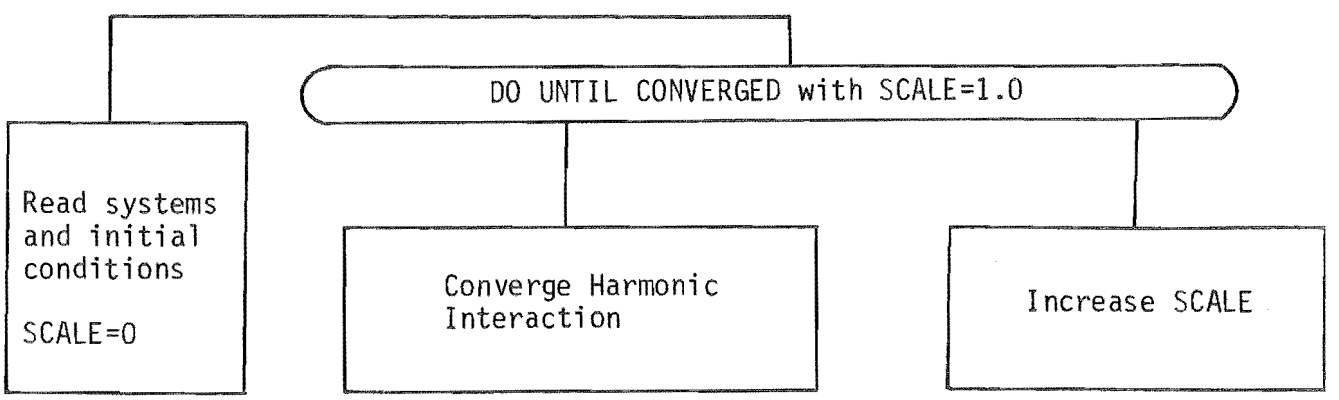

Figure 4.3 : Improved Initial Conditions

4.2.2.6 The use of an acceleration factor

At present, the derived iterative errors in the commutating voltage zero-crossings are used to modify the zero-crossings at each iteration. That is:

$$ZC_{n+1} = ZC_n + E1_n$$

where n is iteration number, ZC_n is the value of the zero-crossings at the n^{th} iteration and $E1_n$ is the iterative error or difference in the zero-crossing at the n^{th} iteration.

The rate of convergence may be increased, or decreased, by the use of an acceleration factor. When the acceleration factor operates on the iterative errors,

$$ZC_{n+1} = ZC_n + ACCF \cdot E1_n$$

where ACCF is the acceleration factor. An acceleration factor usually has a value in the range from 0 to 2. If the solution is monotonic a value of ACCF greater than 1.0 should improve convergence. However, if the solution is oscillatory then a value of ACCF less than 1.0 should improve convergence.

The stable run B5 was repeated for a variety of different acceleration factors in the range 0.5 to 1.3. Figure 4.4 shows the number of iterations required versus the value of the acceleration factor.

It can be seen from graph 4.4 that the best value of ACCF was in fact 1.0, or at least in the range of 0.95 to 1.05. Therefore, the inclusion of an acceleration factor gave no advantage in terms of increased rate of convergence. However, the acceleration factor did not change the final solution, just the rate of convergence, and may be of use in other cases.

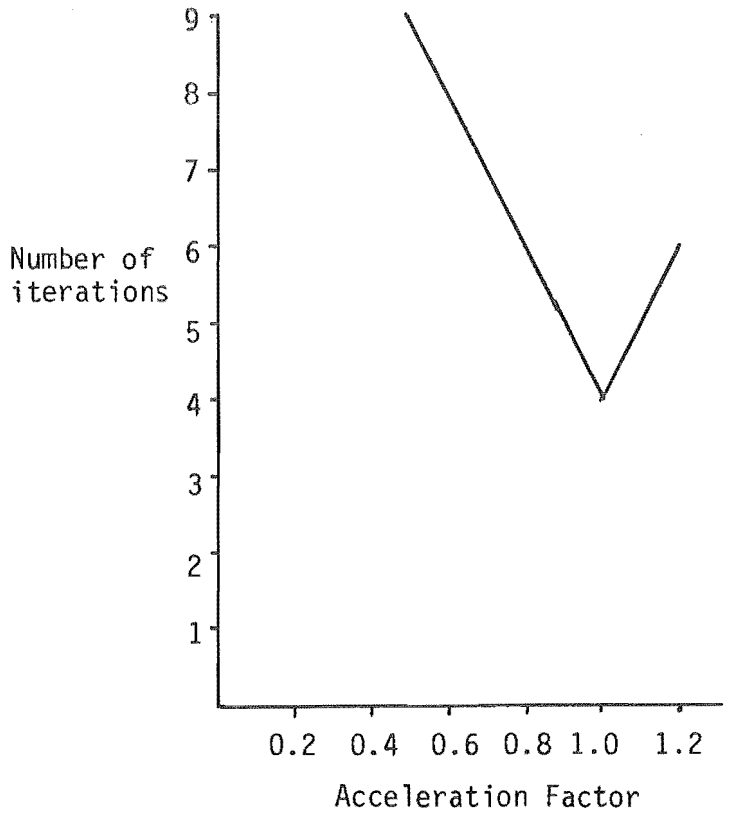

Figure 4.4 : Effect of Acceleration Factor on Stable Run

For the unstable case of run A5 two acceleration factors of 0.2 and 0.1 were initially tried. In both cases a large amount of third harmonic voltage was generated and divergence occurred. It is improbable that an acceleration factor of 0.1 is too large but to test this a value of 0.01 was tried. The solution was still divergent and levels of third harmonic voltage distortion soon went well outside the New Zealand harmonic regulations (New Zealand Electricity 1983).

Therefore the use of acceleration factors on both the stable run, to try and improve the rate of convergence, and on the unstable run, to try and improve reliability, both proved to be of no value.

4.2.3 The Effect of Harmonic Voltage During Commutation

4.2.3.1 A stable case

In the previous work of Harker (1980) only the fundamental terminal voltage and a purely inductive commutating impedance were used to calculate the current samples during commutation. However, all the runs so far have been sampled using an equation based on the equation of Yacamini and de Oliveira (1980a). This includes the voltage harmonic distortion on the terminal busbar and a series resistance in the commutating impedance.

The effect of including all the voltage information during the commutation was first tested on the stable B5 run. The first run was carried out with full harmonic information, as normal. During the second run, at each iteration only the fundamental voltages were used during the sampling routine. That is, only the sampling was affected. A third run was performed which took the solution of the second run as initial conditions, then continued with all subsequent iterations including full harmonic voltage during the sampling. A summary of results is given in table 4.6.

Because the harmonic voltages did not directly affect the commutation the solution of the second run took three iterations. The third run, which took two extra iterations, produced essentially the same solution as the first run as it is the same physical problem solved via a different path.

4.2.3.2 An unstable case

The effect of including, or not including, the harmonic voltage information when calculating the commutation current for the unstable case was very interesting. A total of 8 runs were performed to investigate different aspects of the phenomenon.

Table 4.6 : Comparison of the 3 Stable Runs

	First run			Second run			Third run		
	phase 1	phase 2	phase 3	phase 1	phase 2	phase 3	phase 1	phase 2	phase 3
No. of iterations		4			3			3 + 2 = 5	
Control angle	.08727	.11918	.09941	.08727	.12016	.09991	.08727	.11918	.09941
μ (rad)	.55837	.52974	.56246	.57064	.52974	.56246	.55837	.52974	.56246
μ (deg)	32.0	30.4	32.2	32.7	30.4	32.2	32.0	30.1	32.2
σ_μ		.0146			.0177			.0146	
% third harmonic									
voltage	.1008	.2375	.1367	.1107	.2617	.1508	.1008	.2375	.1367
current	0.114	1.032	1.142	0.124	1.136	1.260	0.114	1.032	1.142

First run : Normal B5 run.

Second run : B5 run without harmonic voltage information used during commutation

Third run : Same as second run except allowed to converge with full harmonic information

1. Only the fundamental voltages were used to calculate the commutation currents, with 512 samples per cycle. Convergence took only 5 iterations.

2. The second run took the solution of the first run and then added the full harmonic voltage information in an unsuccessful attempt to reconverge the unstable A5 run.

3. The full harmonic voltage information excluding the third harmonic, the third harmonic being manually set to zero at each iteration, was used to calculate the commutation samples. Convergence took 5 iterations.

4. Because it was thought that 512 sample points may not be enough, the third run was repeated with 2048 sample points. Again it took 5 iterations to converge.

5. Also the original unstable A5 run was repeated with 2048 sample points and diverged.

6. In an attempt to isolate the instability the fifth run was repeated with only the fundamental, second and third harmonic voltages being used for the entire program run. Again convergence failed.

7. For the sake of completeness the first run was repeated with 2048 sample points instead of the previous 512. Convergence was obtained but the results not analysed.

8. To test whether the off-diagonal elements of the a.c. system admittance matrix played an important part in the instability of the sixth run it was repeated with the diagonalized form of the a.c. system. Convergence failed.

The first, third, fourth and seventh runs converged. Table 4.7 shows the final solution for the first, third and fourth runs. There were also four unstable runs, the second, fifth, sixth and eighth.

Table 4.7 : Comparison of the Three Variations of the Unstable Run that Converged

	First run			Third run			Fourth run		
	phase 1	phase 2	phase 3	phase 1	phase 2	phase 3	phase 1	phase 2	phase 3
No. of -iterations		5			3 + 2 = 5			3 + 3 = 5	
-sample points		512			512			2018	
Control angle	.08727	.08574	.09632	.08727	.08560	.09624	.08727	.08562	.09597
μ (rad)	.58291	.54201	.57473	.57064	.52974	.57473	.57831	.54354	.57933
μ (deg)	33.4	31.1	32.9	32.7	30.4	32.9	33.1	31.1	33.2
σ_μ		.0177			.0203			.0166	
% third harmonic									
voltage	1.551	3.602	2.097	1.529	3.600	2.074	1.505	3.525	2.067
current	0.136	1.168	1.303	0.139	1.152	1.288	0.142	1.110	1.179

First run : Only fundamental voltage during commutation

Third run : Third harmonic voltage excluded during commutation

Fourth run : Same as third run except 2048 sample points

By removing the harmonic voltage information from the commutation a solution was reached in 5 iterations. However, when the solution of the first run was used as initial conditions for a normal full harmonic run a stable solution was not reached. These two runs show the potential importance of including the full harmonic voltage information during the commutation process.

The third run shows that the primary cause of the instability is the effect of the third harmonic voltage during commutation. With all the harmonic voltages with the exception of the third present a solution was obtained. Table 4.7 shows that including the other harmonics does not have a significant great effect on the level of distortion. In the fourth run the number of samples was increased to 2048 points but the difference between the third and fourth runs were small, with only minor discrepancies in the commutation angle. This was because with more sample points the fourth run could measure the commutation angles more accurately.

Because the commutation circuit is mainly inductive, the lower order harmonic voltages have the greatest effect on the commutation current. Therefore, the third harmonic, if it is not filtered, is very important, especially if the system has a resonance near the third harmonic.

Figure 4.5 shows the configuration used for our example

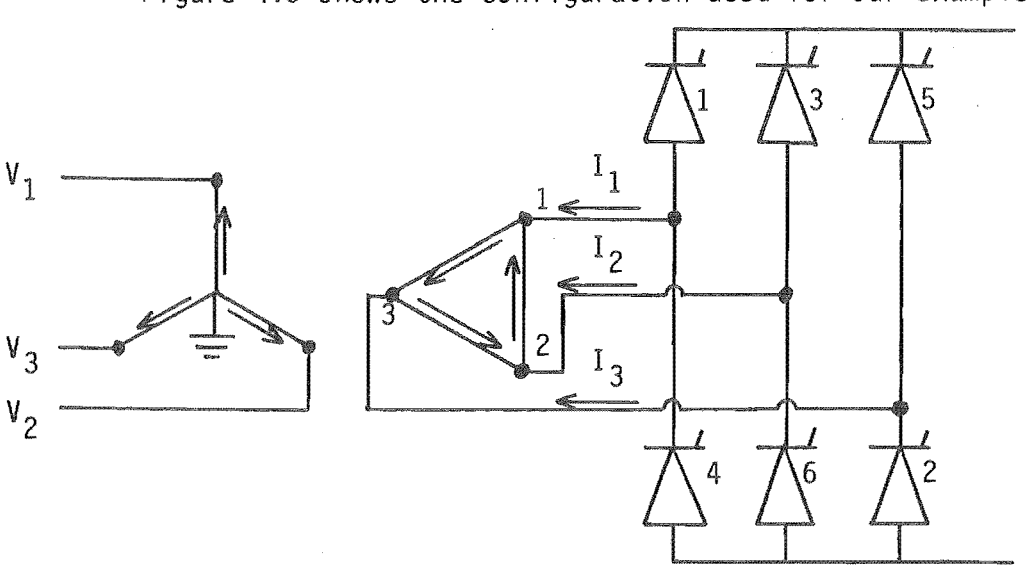

Figure 4.5 : Convertor Configuration

Figure 4.6 shows the effect of the third harmonic voltage on the commutations when equidistant firings are assumed with zero delay angle.

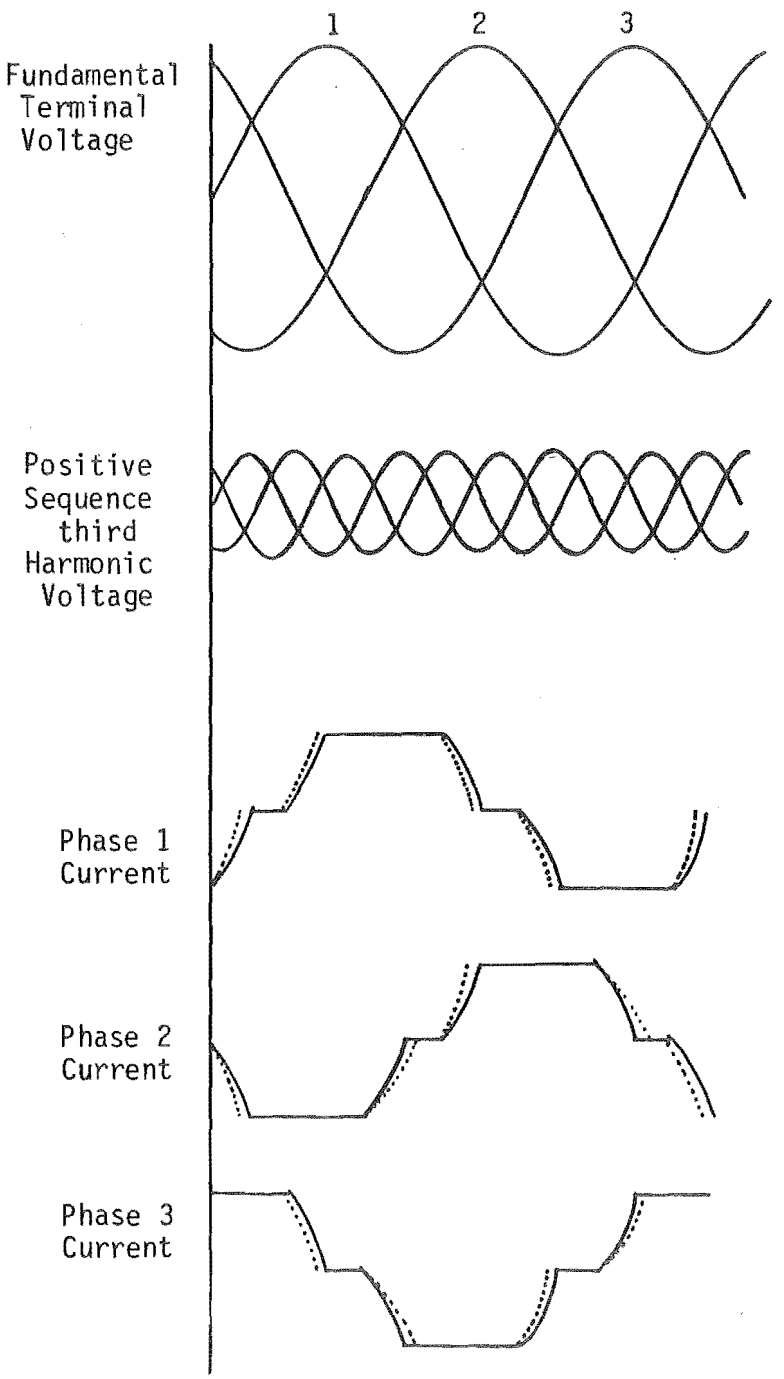

Figure 4.6 : Effect of the Third Harmonic Voltage on the Commutation

From figures 4.5 and 4.6, commutations 1 and 4 are driven by voltage V_3. Similarly, commutations 2 and 5 are driven by V_2 while commutations 3 and 6 are driven by V_1. Also, the current I_1 is

affected by μ_1 and μ_3, while I_2 is affected by μ_2 and μ_3 and I_3 is affected by μ_1 and μ_3. In our case the even harmonics were negligible making it safe to assume that $\mu_1=\mu_4$, $\mu_2=\mu_5$ and $\mu_3=\mu_6$.

The third harmonic voltage shown is that of the open circuit secondary voltage and the current is the line current in phases 1, 2 and 3. A positive sequence third harmonic with the phase relationship as shown would accelerate the first and third commutations and retard the second commutation, as demonstrated. In phase 1 both the commutations are accelerated causing very little effect on the third harmonic current. However, in phases 2 and 3 one commutation is accelerated and the other retarded having an effect on the magnitude of the third harmonic.

The effect of a component of negative sequence third harmonic voltage is similar to that of the positive sequence. The first commutation is retarded and the second and third commutations are accelerated.

To simplify the problem a sixth run was performed with just the third harmonic voltage used. Again it was unstable. However, when the sixth run was repeated with only a fundamental voltage used during the commutation (the seventh run) the solution was stable. Again this clearly shows that the presence of third harmonic during the commutation process is the primary cause of the instability. This was further emphasised by the last run which was a repeat of the sixth run except with the diagonalized form of the a.c. system. The diagonalized form of the a.c. system did not change the nature of the instability.

For the sixth run the commutation angles and the level of third harmonic voltage distortion are plotted for each iteration in figures 4.7 and 4.8 respectively.

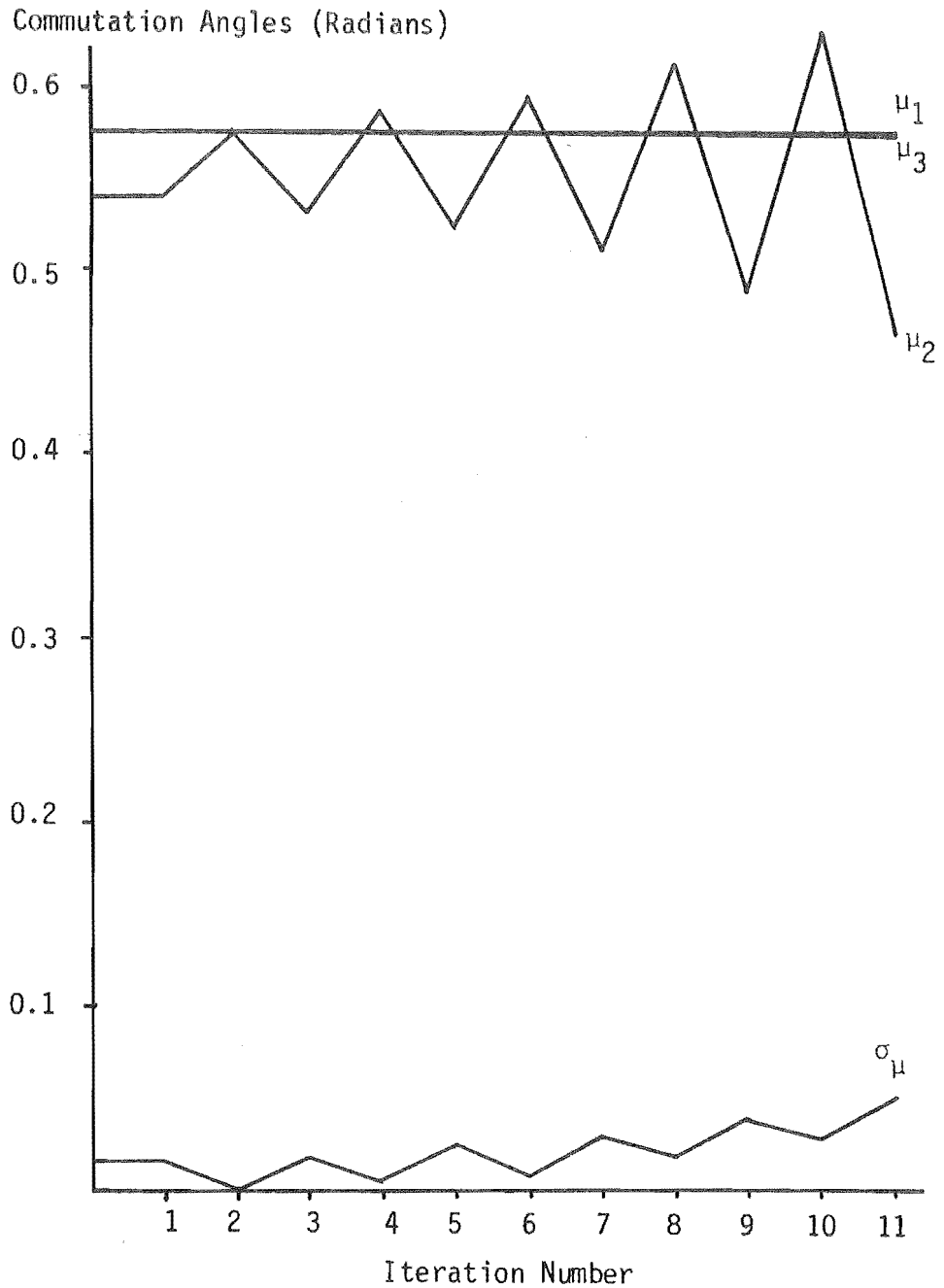

Figure 4.7 : Commutation Angles at Each Iteration (6^{th} run)

Similarly a plot of the magnitude of the third harmonic voltage distortion against the standard deviation of the commutation angles is included in figure 4.9

On comparing these graphs several trends can be seen.

1. Odd iterations of the solution have a peak in the standard deviation of the commutation angles. This corresponds to a peak in the level of third harmonic voltage.

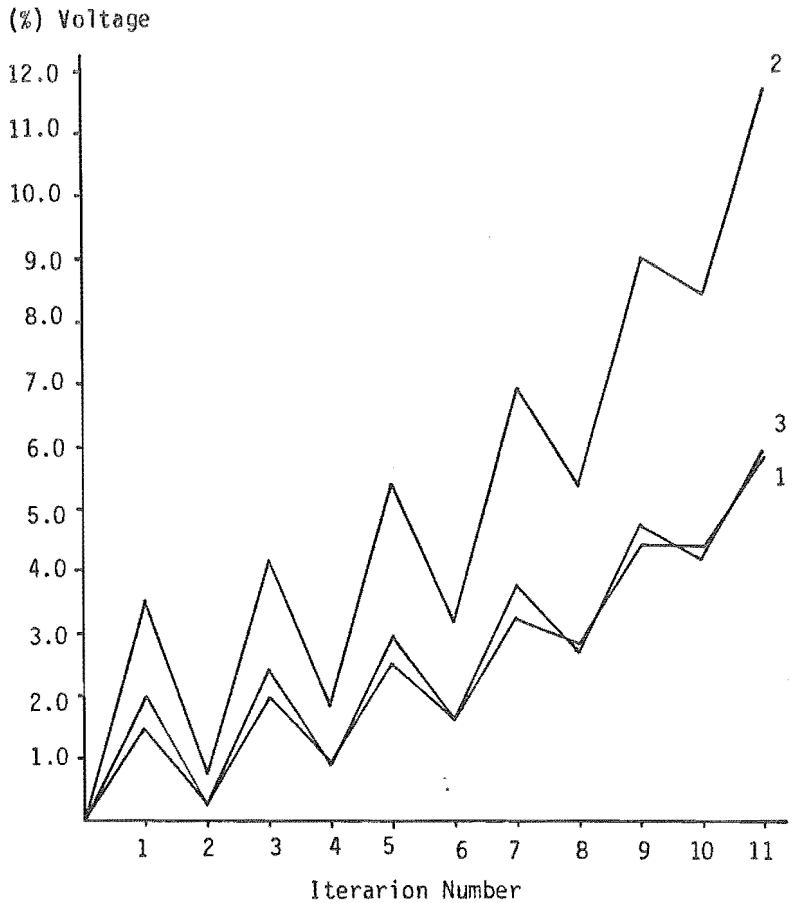

Figure 4.8 : Third Harmonic Voltage at Each Iteration (6^{th} run)

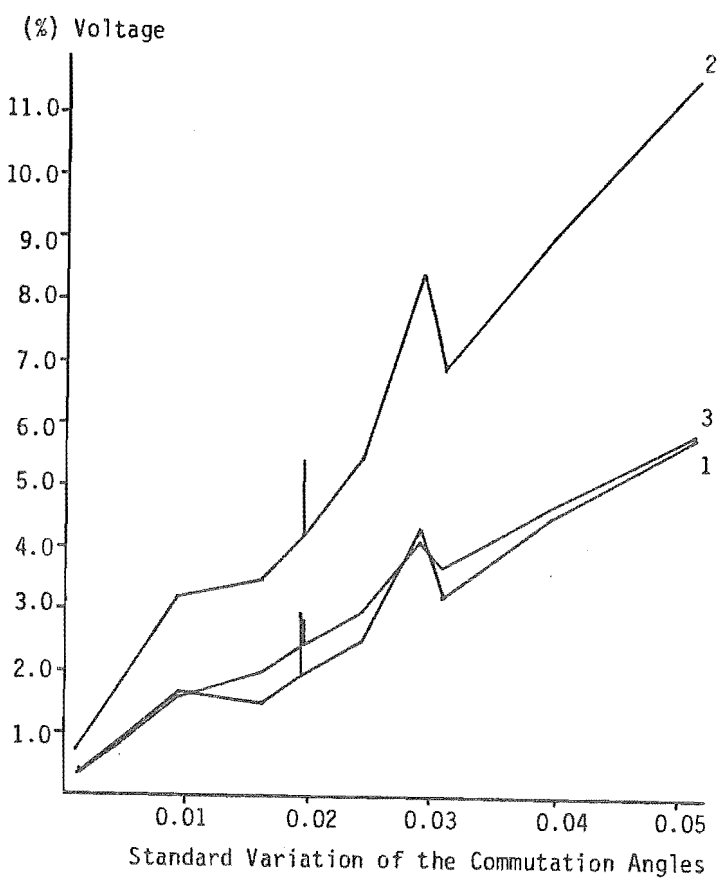

Figure 4.9 : Third Harmonic Voltage Versus the Standard Deviation of the Commutation Angles (6^{th} run)

2. Peak in third harmonic voltage magnitude, occurring on an odd iteration, producing an extension in μ_2 decreasing the standard deviation for the next iteration (an even iteration).

3. Because the standard deviation is smaller during the even iterations the level of third harmonic is a minimum.

4. A minimum in third harmonic voltage magnitude, occurring on even iterations, produces a shortening of μ_2 increasing the standard deviation for the next iteration (an odd iteration).

Figure 4.9 shows that there is a distinct correlation between unsymmetrical commutation angles and the level of third harmonic distortion.

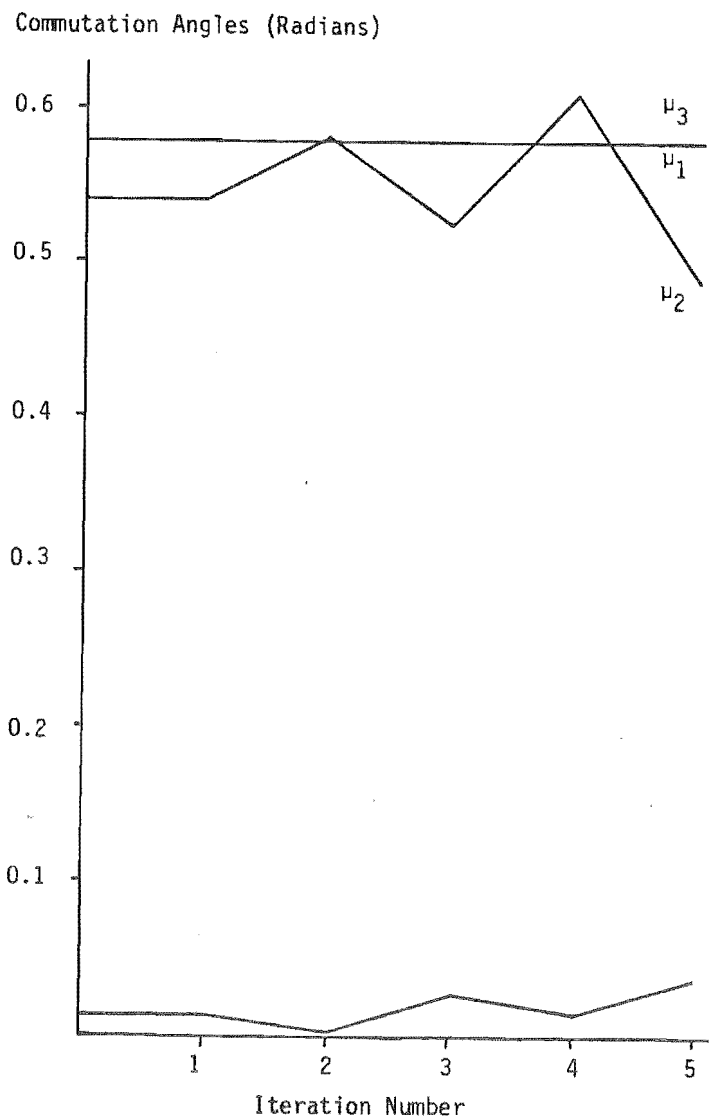

Figure 4.10 : Commutation Angles at Each Iteration (8^{th} run)

Similarly, run eight was included to reduce the complexity of the full three phase representation of the a.c. system present in the fifth and sixth runs. The commutation angles and the level of third harmonic voltage distortion are plotted for each iteration in figures 4.10 and 4.11 respectively.

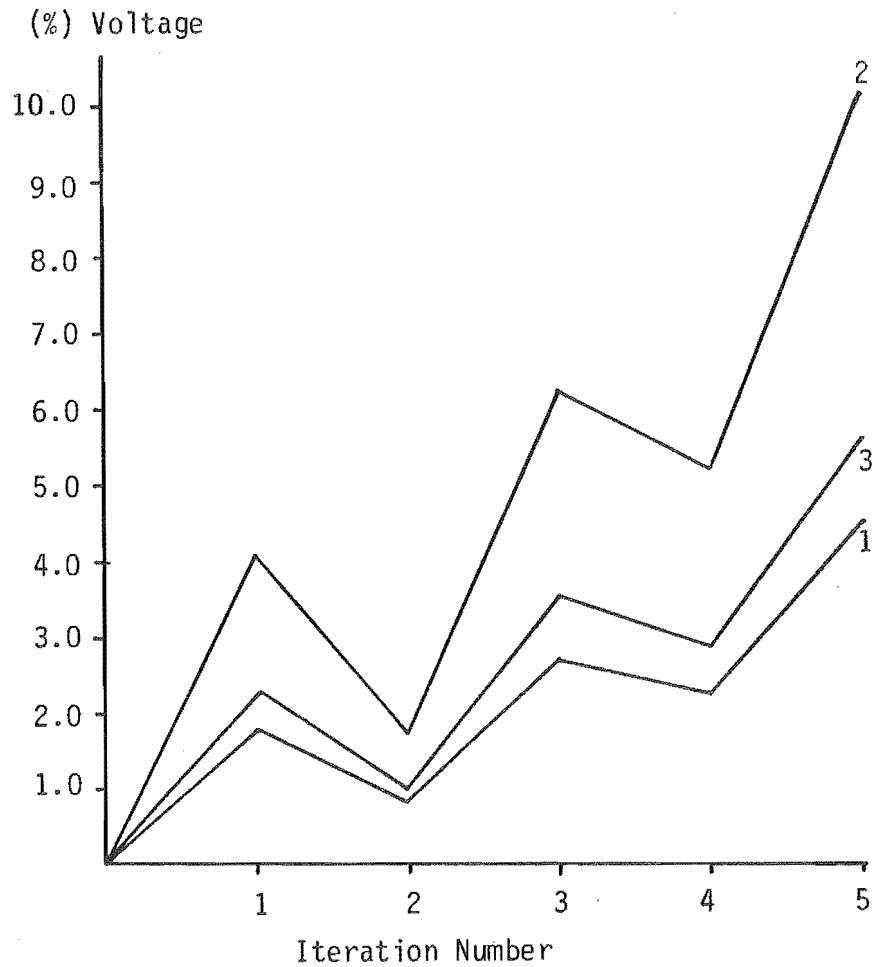

Figure 4.11 : Third Harmonic Voltage at Each Iteration (6^{th} run)

Also, a plot of the magnitude of the third harmonic voltage distortion against the standard deviation of the commutation angles is included in figure 4.12.

These graphs show the same trends as figures 4.7 and 4.8 for the 6th run. That is, a maximum in standard deviation leading to a maximum in the third harmonic distortion. This in turn leads to a reduction in standard deviation of the commutation angles.

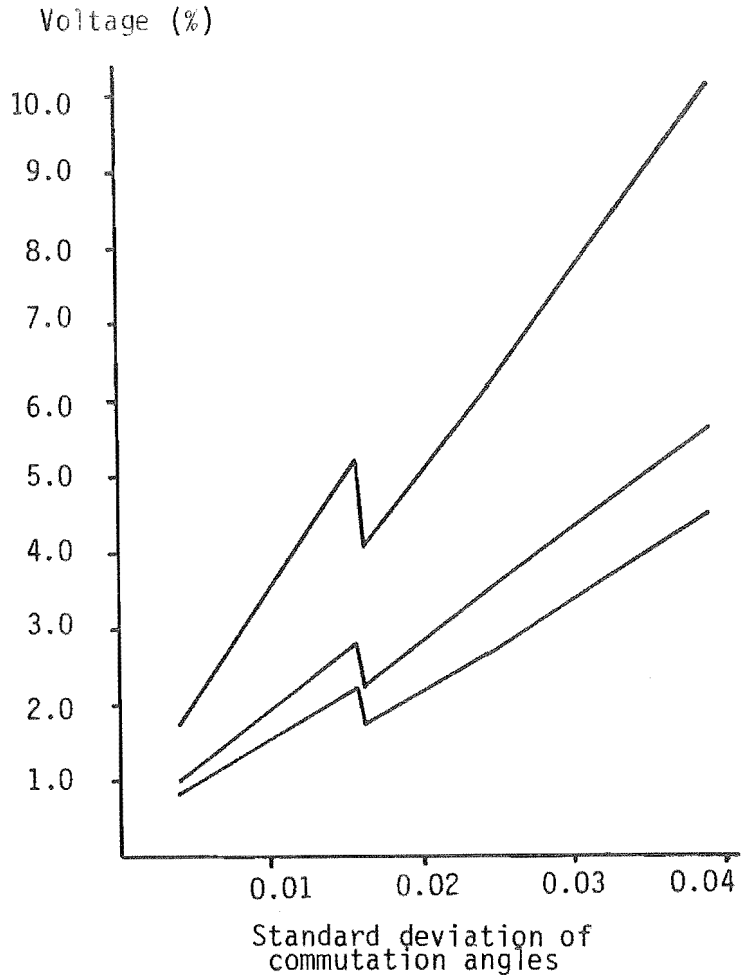

Figure 4.12 : Third Harmonic Voltage Versus the Standard Deviation of the Commutation Angles (8^{th} run)

To help understand the oscillatory nature of the solution, a graph of the phase angle of the third harmonic voltage at each iteration is illustrated in figure 4.13.

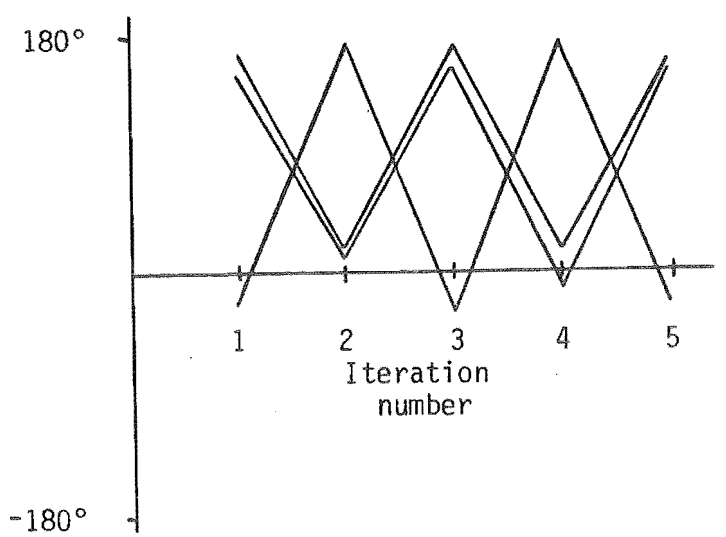

Figure 4.13 : Phase Angle of the Third Harmonic

To express the phase in terms of the third harmonic, firstly the phase angles of the third harmonic voltages were multiplied by 3 and then put into the range -180 to +180 degrees. In each case the phase angles of the third harmonic voltages alternated by 180 degrees between consecutive iterations. This means that the effect of the third harmonic is opposite at each consecutive iteration. This would produce the oscillatory nature of the graphs in figures 4.10 and 4.11 for the eighth run and explain the oscillatory nature of the sixth run with the full three phase a.c. system representation.

4.2.3.3 Further investigation of third harmonic during commutation

Further investigation of the effect of third harmonic voltage during the commutation process should be concentrated on the eighth run. This represents the most simple situation as only the third harmonic voltage is present and the a.c. system representation is purely diagonal. The approach used was to change the phase angle of the a.c. system third harmonic admittance and give a different phase relationship between the current injected into the a.c. system and the resulting voltage produced on the terminal busbar.

This was done by keeping the admittance constant and the angle varied from -90 to +90 degrees. As a comparison the process was repeated for the same case but without filters in order to avoid possible parallel resonances. Therefore, any variation of stability will be due to the change of system angle at third harmonic and not due to resonance effects.

At the third harmonic Y_{sys} = 0.0026 - j0.0063 siemens,

therefore $Z_{sys} = 1/Y_{sys}$

= 55.97 + j135.63 ohms

= 146.72 angle 67.57 ohms.

The actual system angle is approximately 67.5 degrees. Therefore a useful range of system impedance angles would be -90 to +90 degrees with steps of 22.5 degrees. The a.c. system admittance, and impedance, from table 4.8 were used in the eight run of the previous section with and without filters.

Table 4.8 : A Set of Third Harmonic A.C. Admittances and Impedances with Angles from -90 to +90 degrees

Angle of Z_{sys}	$Z_{sys}(\Omega)$	$Y_{sys}(s)$
-90.0	- j146.72	+ j.0068
-67.5	56.15 - j135.55	.0026 + j.0063
-15.0	103.75 - j103.75	.0048 + j.0048
-22.5	135.55 - j 56.15	.0063 + j.0026
0.0	146.72	.0068
22.5	135.55 + j 56.15	.0063 - j.0026
45.0	103.75 + j103.75	.0048 - j.0048
67.5	56.15 + j135.55	.0026 - j.0063
90.0	+ j146.72	- j.0068

The results are summarized in figure 4.14 which shows the number of iterations for each of the 18 runs.

With filters the problem of resonance may occur. That is at a particular system angle the total system admittance can become purely conductive, when the susceptance of the filters cancels the susceptance of the a.c. system.

The system admittance = 0.0068 /-Impedance angle siemens @ 220 kV

= 3.2987 /-Impedance angle p.u. @ PBASE 100 MVA

The filter admittance = 0.0154 + j1.7906 p.u.

With these parameters, a resonance occurs at 32.87 degrees.

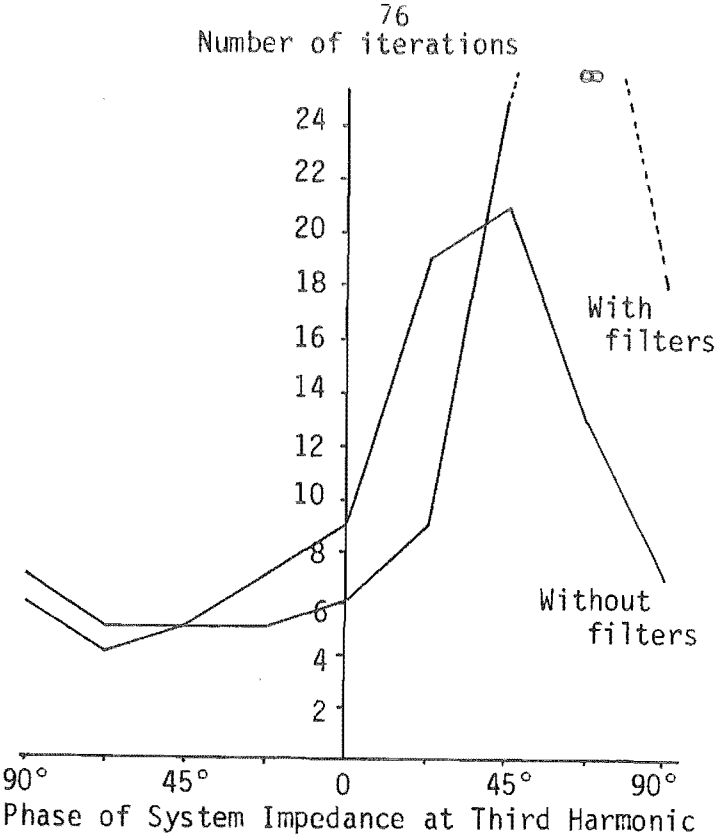

Figure 4.14 : Number of Iterations Versus Impedance Angle

While figure 4.15 is a plot of the percentage third harmonic distortion in each of the runs.

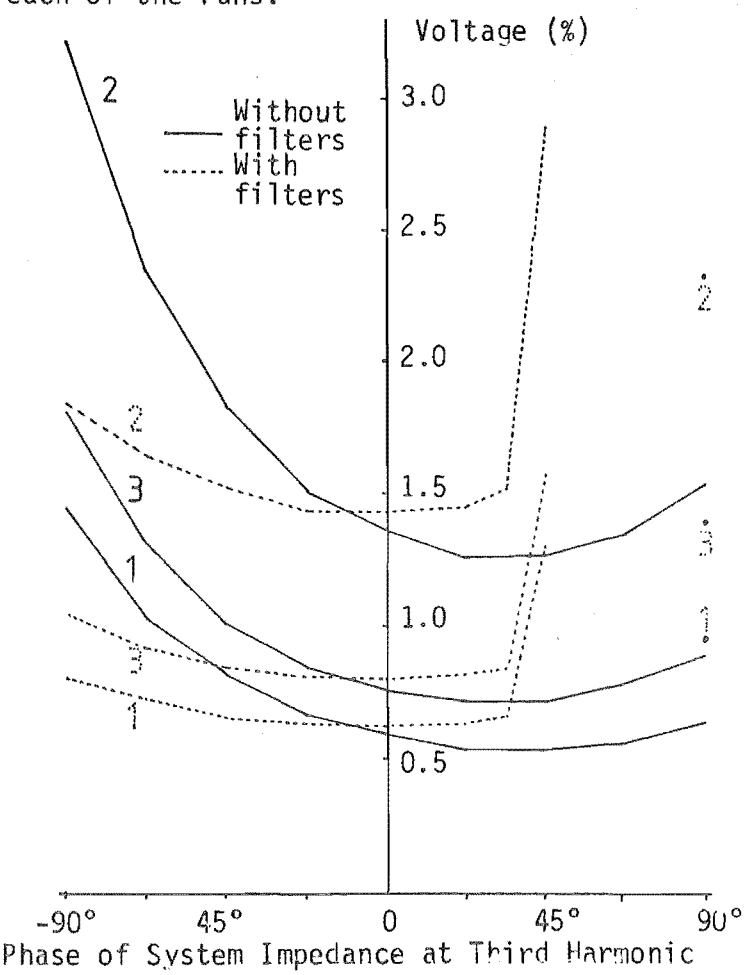

Figure 4.15 : Third Harmonic Voltage Versus Impedance Angle

The total a.c. system admittances (filters plus a.c. system) for the nine cases investigated are given in table 4.9 and figure 4.16 shows the admittance locus indicating the total, system and filter, admittances.

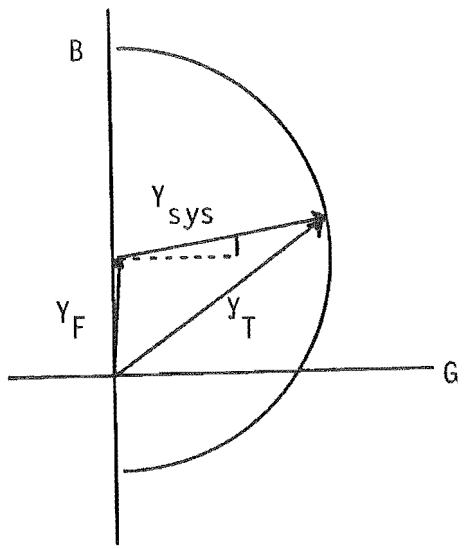

Figure 4.16 : Total Admittance Loci Including Filters for Variable Impedance Angle

Table 4.9 : Total A.C. Admittance with Filters

Impedance Angle	Total admittance (angle)		Conductance	Susceptance
-90.0	5.0893	89.8	0.0154	5.0983
-67.5	5.0041	75.2	1.2778	4.8382
-45.0	4.7448	60.3	2.3479	4.1231
-22.5	4.3246	43.8	3.0630	3.0530
0.0	3.7669	28.4	3.3141	1.7906
22.5	3.1082	9.8	3.0630	0.5282
45.0	2.4097	-13.0	2.3479	-0.5419
67.5	1.7924	-44.5	1.2778	-1.2570
90.0	1.5082	-89.3	0.0154	-1.5081

If table 4.9 is compared with the results of figures 4.14 and 4.15, some interesting facts emerge.

The case with an impedance angle of 67.5°was stopped after 5 iterations, because the third harmonic distortion was large enough to force the delay angle to attempt to go negative. Similarly, the case with an impedance angle of 45.0° was stopped at the 202nd iteration with a negative delay angle.

For the cases with negative values of third harmonic system angle the number of iterations required was reasonably constant, as was the level of third harmonic voltage.

However for values of system angle 45.0°and 67.5°no solution could be reached. Also for a small change in system angle near the instability, a large change in third harmonic voltage occurred.

Table 4.10 shows the total a.c. system admittance for the nine impedance angles in the absence of filters.

Table 4.10 : Total A.C. Admittance Without Filters

Impedance Angle	Total admittance	(angle)	Conductance	Susceptance
-90.0	3.2912	90.0	0.0000	3.2912
-67.5	3.2987	67.6	1.2584	3.0492
-45.0	3.2855	45.0	2.3232	2.3232
-22.5	3.2987	22.4	3.0492	1.2584
0.0	3.2912	0.0	3.2912	0.0000
22.5	3.2987	-22.4	3.0492	-1.2584
45.0	2.4097	-45.0	2.3232	-2.3232
67.5	3.2987	-67.6	1.2582	-3.0492
90.0	3.2912	-90.0	0.0000	-3.2912

In this case the effect of varying the system angle can be investigated more accurately and any changes in percentage distortion or the number of iterations can be better assessed.

For capacitive systems figure 4.14 shows that convergence was rapidly achieved. As the a.c. system goes inductive the convergence

slows down, the number of iterations reaching a peak at an impedance angle of 45 degrees. With a purely inductive system the rate of convergence was fast.

In contrast the curves for % third harmonic voltage distortion follow the opposite trend. The impedance angle of 45.0° gave a minimum value whereas it required the most iterations.

Table 4.11 shows the actual levels of third harmonic distortion for -67.5°, 0.0° and 67.5° degrees at each iteration. For the first iteration the values are essentially the same because the currents are identical and the magnitude of the system impedance constant. But after subsequent iterations three different solutions were produced. The greater the difference between the final solution and the first, in terms of the zero-crossings, the more iterations required.

Table 4.11 : Level of Third Harmonic Voltage (%) at Each Iteration

No filters and constant magnitude of a.c. system impedance.

	Impedance Angle = -67.5			Impedance Angle = 0.0			Impedance Angle = 67.5		
1	0.952	2.214	1.263	0.954	2.219	1.266	0.952	2.214	1.263
2	1.077	2.420	1.345	0.352	0.782	0.434	0.336	0.827	0.495
3	1.058	2.368	1.311	0.735	1.698	0.961	0.716	1.673	0.959
4	1.052	2.357	1.306	0.492	1.116	0.626	0.486	1.167	0.683
5	1.053	2.358	1.306	0.647	1.487	0.841	0.625	1.472	0.848
6				0.550	1.252	0.705	0.541	1.288	0.750
7				0.612	1.402	0.792	0.592	1.400	0.809
8				0.572	1.306	0.736	0.561	1.333	0.774
9				0.597	1.366	0.771	0.580	1.373	0.795
10							0.569	1.349	0.783
11							0.575	1.363	0.790
12							0.571	1.355	0.786
13							0.574	1.360	0.788

4.2.4 Conclusions

The nature of the instability was examined using a variety of methods. These included reducing the load and strengthening the a.c. system. Both these gave results consistent with a genuine instability caused by excessive third harmonic voltage distortion due to the relative size of the convertor. Similarly, when the a.c. system was diagonalized in section 4.2.2.2 the stability did not change which is consistent with an actual instability.

Two numerical analysis approaches were also tried. Neither improving the initial conditions nor introducing an acceleration factor made any real improvement to the solution. This is consistent with the presence of a genuine instability rather than purely a numerical problem.

An attempt was made to isolate the problem. It was clear that the instability was due to the third harmonic and in particular the presence of third harmonic voltage distortion during the commutation process. The problem was still further simplified by the removal of all the other harmonics except the third, but still the instability remained.

Another interesting aspect is the effect of varying the system impedance angle at third harmonic on the stability and the level of distortion. For simplicity this was done with only the third harmonic present. This investigation clearly shows that both the stability of the solution and the level of distortion depend on the system angle as well as the magnitude of the system impedance. That is, the angle between the current injections and the voltage distortion play an important part in the harmonic interaction. The impedance angle at harmonics is not indicated by the S.C.R. concept, making the SCR a poor indication of system strength.

The stable B series of runs also provided useful information. As in the case of the operation of a stable convertor small disturbances should not affect its steady state operation. Similarly, the stability and final solution of the B series are not affected by the path chosen. That is, whether a scale factor for the harmonic voltages (section 4.2.2.5), an acceleration factor for the zero crossings (section 4.2.2.6) or a scale factor for the harmonic voltages only during the commutation process (section 4.2.3.1) is used or simply the unmodified algorithm is used, the final solution is unaltered.

At this stage it should be emphasised that instability of the iterative algorithm cannot necessarily be attributed to a genuine instability.

4.3 SINGLE GENERATOR AND LINE A.C. SYSTEM SUPPLYING A 6-PULSE CONVERTOR AT TIWAI

To try and isolate the root of the problem, the a.c. system was simplified to a single generator and transformer and two parallel double circuit lines to transfer the power to the convertor. Figure 4.17 shows the simplified a.c./d.c. system.

Figure 4.17 : Convertor Supplied by a Single Generator/Transformer and Line A.C. System

While the system is not a realistic representation of the actual South Island transmission system (Densem 1983), it does include line

unbalance and series and parallel resonances typical of a.c. systems which are important in the operation of convertor loads.

The generator is a single equivalent generator representing the seven machines at Manapouri power station giving the total generation of 690 MW. The equivalent generator has a positive sequence reactance of 0.04 p.u., a zero sequence reactance of 0.02 p.u. and a negative sequence reactance of 0.004 p.u. at a power base of 100 MVA. For simplicity the machine's sequence resistances were neglected. The generator transformer has 0.0164 p.u. leakage reactance, 0.006 p.u. resistance and a star-g/delta connection. The transmission system consists of two 166.6 Km double circuit lines as described in Appendix A4. An earth resistivity of 100 ohm-metres was used when modelling the earth return.

The star-g/delta connected convertor transformer has a leakage reactance of 0.05 p.u. The convertor was operated with either a constant delay angle or equidistant firing control with the delay angle on valve one specified as 5.0 degrees. The d.c. system consists of a resistance, specified to vary the d.c. power, and an infinite smoothing inductor to give a flat d.c. current.

The harmonic filters are the same as those used in section 4.2 except that no uncharacteristic third or ninth harmonic filters have been included. This gives a fundamental filter susceptance of 0.043 siemens, or 0.46933 p.u., and provides 46.9 MVars of reactive compensation.

4.3.1 Initial Conditions

As for the previous case, the initial conditions have been calculated using the three phase a.c./d.c. power flow. The power flow requires six control specifications to define the convertor's operation (Harker 1980). The delay angle on valve one and the three tap ratios

are fixed, with the other two specifications being supplied by the control strategy. Finally, with the voltage at the generator's phase 'a' terminal fixed at 1.045 p.u. and the d.c. system resistance specified, the power flow can be run to produce the required initial conditions.

4.3.2 The Harmonic Impedances

4.3.2.1 The system without the filters

The impedance looking back into the Tiwai busbar, not including the harmonic filters, is made up of the three system components, i.e., the line, the transformer and the generator, with the line being the most dominant.

Using the three phase harmonic penetration software of Densem (1983), a full three phase system admittance matrix $[Y_{sys}]$, and the corresponding equivalent impedance information, was formed for the Tiwai busbar.

The large level of harmonic impedance unbalance can be seen in figure 4.18 which shows the three phase impedance up to the sixth harmonic. Because the impedances are calculated assuming a positive sequence current injection, a negative resistance is observed in phase 'a' near the sixth harmonic.

4.3.2.2 The effect of filters

As the a.c. system impedance is inductive below the fifth harmonic and the filters capacitive, a parallel resonance may occur which would affect any harmonic interaction.

Because a convertor can only produce positive and negative sequence injections, and because the a.c. system and filter impedances to the positive and negative sequences are equal, the effect of the filters was analysed in the positive sequence only.

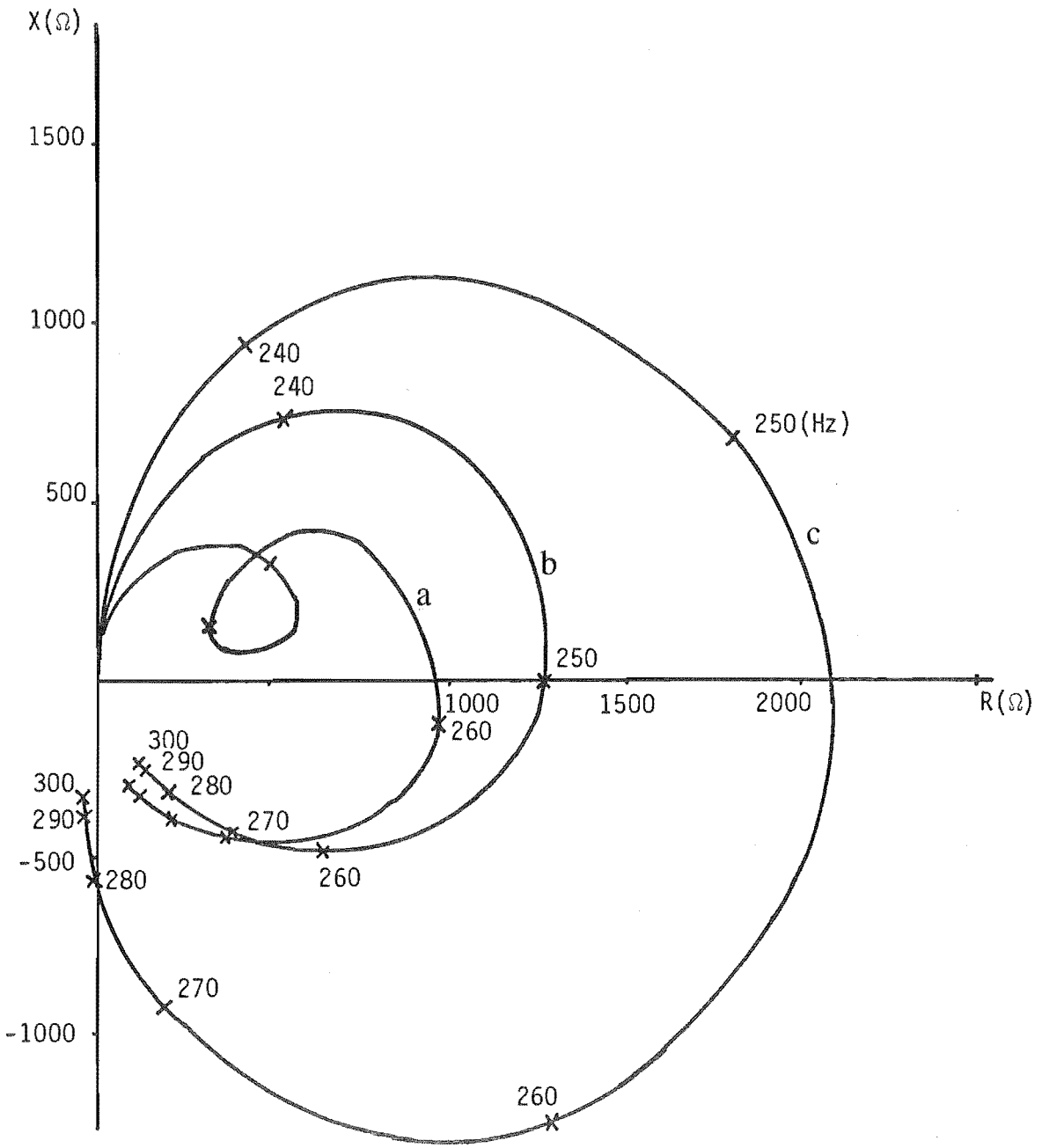

Figure 4.18 : Three Phase Impedance Loci

The effect of the filters is shown in figure 4.19. Similarly,

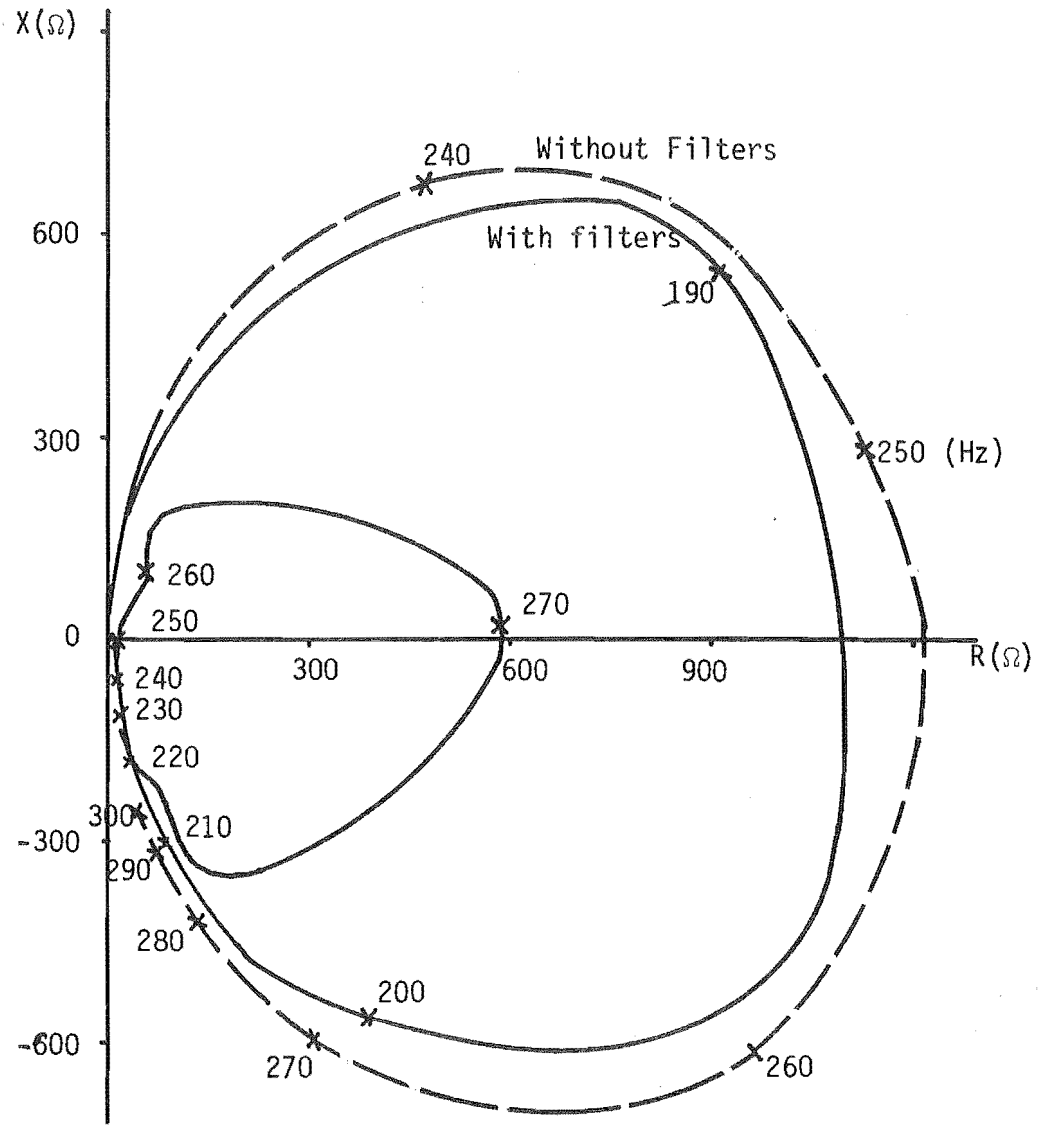

Figure 4.19 : The Effect of Filters on the Positive Sequence Impedance Loci

table 4.12 gives the system impedance magnitudes without and with the parallel filters for the first 10 harmonics.

Table 4.12 : The Effect of Harmonic Filters on System Impedance

Harmonic Order	System Impedance Magnitude (Ohms)	Parallel Combination Impedance Magnitude (Ohms)
2	51.1	46.3
3	96.6	143.6
4	212.8	687.4
5	1159.3	17.9
6	257.0	118.2
7	119.3	18.8
8	71.1	60.2
9	44.3	33.4
10	25.5	18.6

Of most importance to harmonic interaction and stability are the low order harmonics. From figure 4.19, a parallel resonance occurs between the fifth and sixth harmonics and a series resonance between the eleventh and twelfth harmonics.

As expected there is a dramatic reduction of the combined system impedance for the filtered fifth and seventh harmonics.

The effect of the filters at the non-filtered harmonic frequencies is also significant. At the second, sixth, eighth, ninth and tenth harmonics the parallel filters reduced the effect of the overall impedance. However, for the third and especially the fourth harmonics the system impedance increased substantially and it is therefore resonable to expect that there may be a problem at either of these two harmonics.

4.3.3 Initial Results of Iterative Algorithm

Using the test system described in section 4.3, the value of d.c. resistance was varied to give the required range of d.c. powers,

in MW. The number of iterations for cases of constant delay angle and equidistant firing control, without control filters, are given in table 4.13.

Table 4.13 : D.C. Power and Number of Iterations for Various D.C. Reistances

D.C. Resistance	Constant Delay Angle		Equidistant	
Kilo ohms	D.C. Power	No. Iterations	D.C. Power	No. Iterations
0.004650	238.86	5	238.68	4
0.004000	267.95	5	267.72	5
0.003500	295.18	6	294.93	5
0.003000	327.88	7	327.59	6
0.002800	342.74	9	342.46	6
0.002750	346.65	8	346.35	6
0.002740	347.46	8	347.14	6
0.002735	347.86	9	347.53	6
0.002730	348.25	x	347.93	6
0.002725	348.65	x	348.33	6
0.002700	350.65	x	350.32	6
0.002600	358.85	x	358.48	6
0.002325	382.97	x	382.59	7

An instability numerical or real, is evident with constant delay angle control when a d.c. power of 347.86 is exceeded. When the a.c. system admittance was diagonalized to its positive sequence value the instability shifted an insignificant amount to 348.25. The instability is consistent with the definition in section 4.2.1 as it appears to be independent of the unbalanced nature of the a.c. system.

The level of uncharacteristic third and fourth harmonic voltages for the stable runs with the constant delay angle control are given in table 4.14.

Table 4.14 : Level of Third and Fourth Harmonic Voltage (%) for Each Stable D.C. Power

D.C. Power	Third Harmonic			Fourth Harmonic		
MW	a	b	c	a	b	c
238.86	0.0432	0.0864	0.1290	0.0001	0.0002	0.0002
267.95	0.0491	0.1078	0.1560	0.0001	0.0001	0.0002
295.18	0.0507	0.1329	0.1822	0.0008	0.0004	0.0008
327.88	0.0413	0.1602	0.1998	0.0013	0.0011	0.0015
342.74	0.0415	0.1676	0.2068	0.0102	0.0090	0.0125
346.65	0.0414	0.1658	0.2049	0.0030	0.0023	0.0042
347.46	0.0409	0.1679	0.2065	0.0026	0.0028	0.0036
347.86	0.0409	0.1723	0.2106	0.0116	0.0093	0.0133

The level of third harmonic voltage is approximately linear with d.c. power. However, the level of fourth harmonic voltage, which is initially insignificant, increases in an erratic manner. This cannot be explained in terms of a simple harmonic magnification. The erratic nature of the fourth harmonic of the stable runs is due to an unstable fourth harmonic component which grows too slowly between successive iterations to be detected. This results in the premature convergence of the iterative algorithm.

4.3.4 Modifications to Avoid Premature Convergence of the Iterative Algorithm

The problem of premature convergence of the iterative algorithm can be rectified by either specifying a smaller convergence tolerance or introducing a disturbance to excite any potential instability.

4.3.4.1 Closer tolerance

There are two main disadvantages in simply reducing the convergence tolerance. Firstly, with the closer tolerance, stable runs would take an excessive number of iterations. Secondly, even

with a closer tolerance, marginally unstable cases may not be detected if the growth of the non-characteristic harmonic is sufficiently slow. Therefore the role of the convergence tolerance is in determining the degree of accuracy required and not in detecting instabilities.

4.3.4.2 Introducing a disturbance

The effect of introducing a disturbance into the algorithm was investigated by means of either an initial voltage distortion on the convertors terminal at the first iteration, a permanent background distortion or initial errors in the delay angles.

An initial voltage or permanent background distortion parallels the situation at an actual convertor which is exposed to such disturbances. The level of distortion should be large enough to excite any potential instability but not too large as to cause excessive iterations on a stable run. A level of about 0.1 percent would be reasonable as this approximates what may happen in reality.

Alternatively, a controller disturbance is also able to trigger an actual instability and is easily incorporated into the iterative algorithm. For example, at the end of the first iteration an initial error in each of the fourth, fifth and sixth delay angles was included and its effect on the a.c. current injection waveforms is shown in figure 4.20.

In figure 4.20 it has been assumed that the shape of the commutations has been unaffected by the disturbance. As a result of the initial disturbance, phases two and three have a d.c. component while all three phases will have all the even harmonics introduced. Following the first iterations the errors are removed. If an instability exists it will quickly develop and, if the solution is stable, the extra harmonics generated by the disturbance will reduce in size.

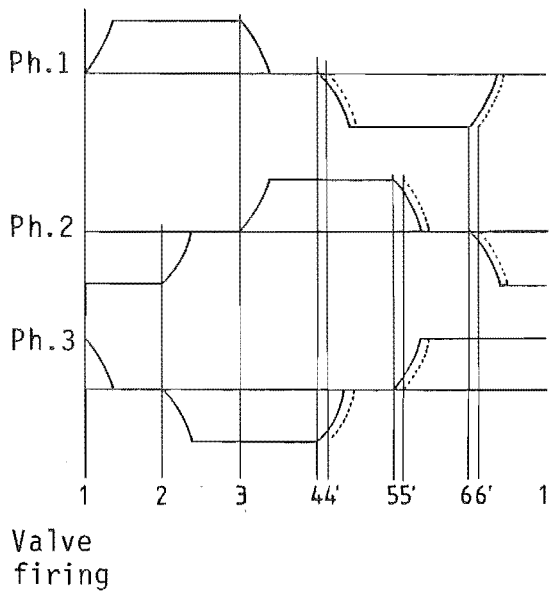

Figure 4.20 : The Effect of the Fourth, Fifth and Sixth Delay Angle Errors on the A.C. Current Injections.

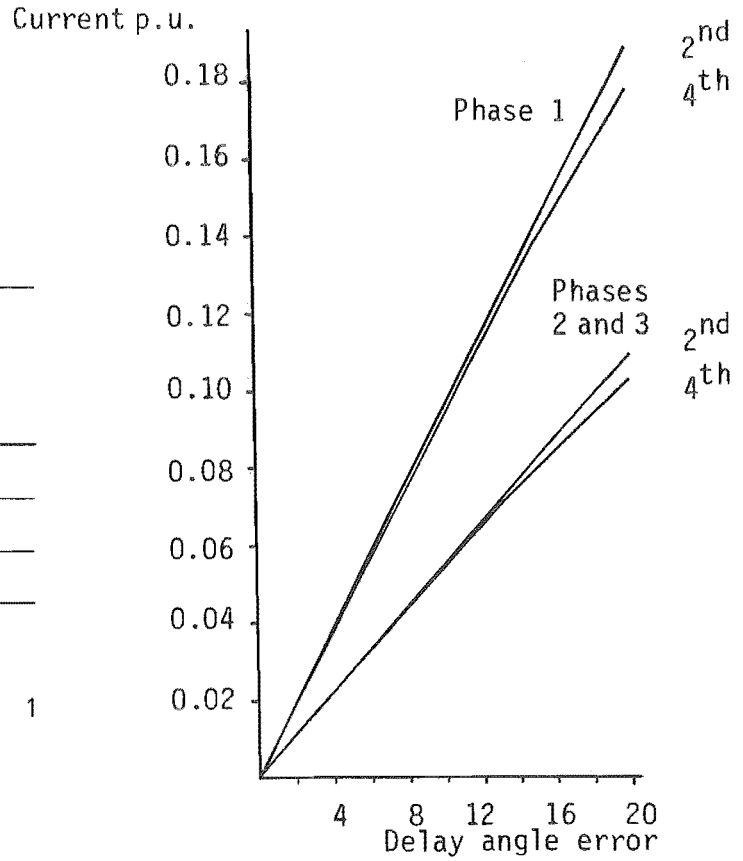

Figure 4.21 : The Magnitude of the Second and Fourth Harmonic Currents Against Delay Angle Error.

The level of the various harmonics generated depend on the size of the delay angle error introduced. Figure 4.21 shows the magnitude of the second and fourth harmonic currents in each of the phases for a d.c. current of 1.0 p.u. and zero commutation angles. The variation in magnitude of the second and fourth harmonics with delay angle error is approximately linear and contains equal components of positive and negative sequence. The initial absence of the uncharacteristic odd harmonics is not a problem as in any actual system the finite level of system voltage and impedance unbalance will generate these harmonics. Also the presence of even harmonics on the convertor terminal will lead to a complete spectrum of harmonics

(Reeve et al 1969) which will become evident at the end of the second iteration. Finally, minor reductions in the magnitudes of the characteristic harmonics may occur but this will have no effect on the stability.

An alternative approach of introducing the errors to the delay angles of the evenly numbered valves would, if adopted, generate no uncharacteristic odd harmonics, as for the previous case, and only produce uncharacteristic even harmonics on one sequence. That is, positive sequence for orders of $6k + 4$ and nagative sequence for orders $6k + 2$, where k is an integer. Because harmonic instabilities can exist either because of a positive or a negative sequence uncharacteristic harmonic voltage (Ainsworth 1967), this type of disturbance was not used.

4.3.5 The Effect of Control Disturbance

When a control disturbance is introduced at the end of the first iteration of the iterative algorithm, several program runs previously thought to be stable diverged. Table 4.15 shows the d.c. power and the number of iterations for the case of a constant delay angle controller for a disturbance of 0.1 radians to the fourth, fifth and sixth delay angles.

Instead of the previous maximum d.c. power before divergence (347.86 MW), the inclusion of controller disturbance has reduced the d.c. power limit to 151.83 MW.

The stable 85.59 MW d.c. power case was examined with a varying sized initial disturbance. With an initial error of 0.0025 radians the algorithm converged to a stable solution in seven iterations. This was increased to thirteen iterations with an initial disturbance of 0.1 radians. Similarly, the 225.53 MW d.c. power case, previously thought to be stable, was examined more fully.

Table 4.15 : D.C. Power and Number of Iterations for An Introduced Controller Disturbance

D.C. Resistance Kilo ohms	D.C. Power	No. Iterations	
0.02000	65.15	8	
0.01500	85.59	10	
0.01200	105.33	12	
0.01100	114.12	15	
0.01050	119.02	17	
0.01000	124.40	19	
0.00800	151.83	221	
0.00775	156.11	232	diverged
0.00750	160.71	81	diverged
0.00700	170.55	49	diverged
0.00600	194.34	19	diverged
0.00500	225.53	11	diverged

When the disturbance was equal to or less than 0.000126 radians the solution converged in five iterations. For slightly larger disturbances divergence of the solution was found, being detected by the presence multiple zero crossings of the commutating voltages, in 23 iterations and in only seven iterations for a disturbance of 0.1 radians.

Ideally, for a stable case, a small if not zero disturbance is desirable for rapid convergence. However, for an unstable case a large disturbance is required to detect an instability quickly. Therefore as it is not known before the iterative algorithm is run whether convergence or divergence will occur, a compromise is needed. About 3.0 degrees or about 0.05 radians would be a good size of disturbance as this would be a typical value for controller errors (Reeve and Krishnayya 1968). Also, from the results in this section,

a disturbance of this size would be large enough to trigger a potential instability.

4.3.6 Harmonic Voltage Distortion of the Simplified Test System with Increased Filter Capacity

The reactive power rating of the filters was increased from previous value of 46.9 MVar to 66 MVar. This was achieved in the algorithm by increasing the voltage base on the filters from 33 kV to 39 kV. This had the effect of reducing the a.c. system impedance at fourth harmonic and increasing the system impedance at third harmonic. Also the equidistant controller was modified to produce firing instants which are independent of the terminal voltage distortion, instead of the previous strategy described in chapter 3 of fixing the delay angle of valve one and adjusting the other delay angle to maintain equidistant firing pulses.

Figures 4.22 to 4.26 show the level of third harmonic voltage on the convertor terminal, as a function of the d.c. power, for various combinations of control strategy and system conditions.

The need for an iterative algorithm is clearly demonstrated by comparing figures 4.22 and 4.23.

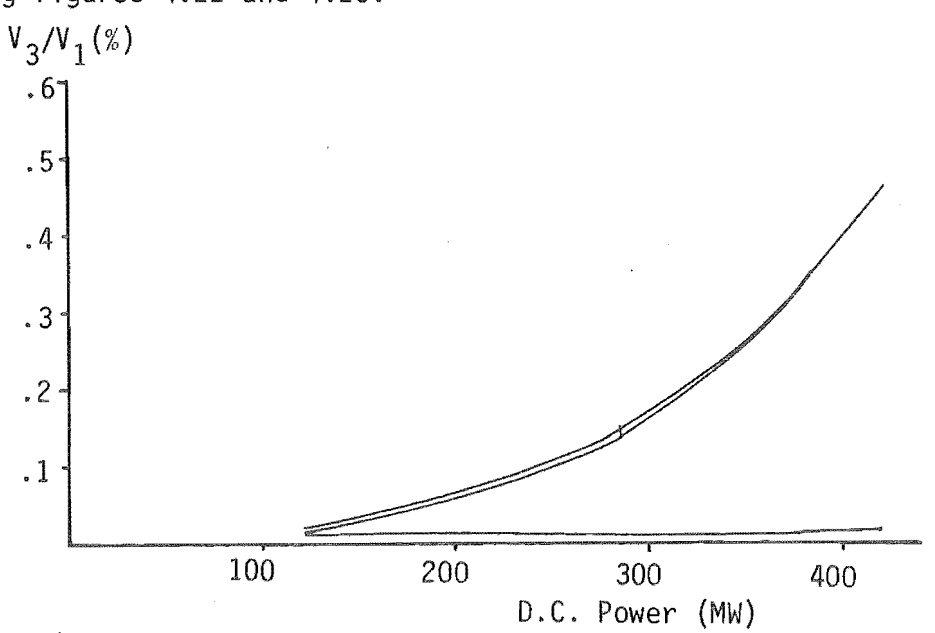

Figure 4.22 : Third Harmonic Voltage in the Three Phases of the Convertor Terminal with Equidistant Control and Perfectly Flat D.C. Current : Without Iterations

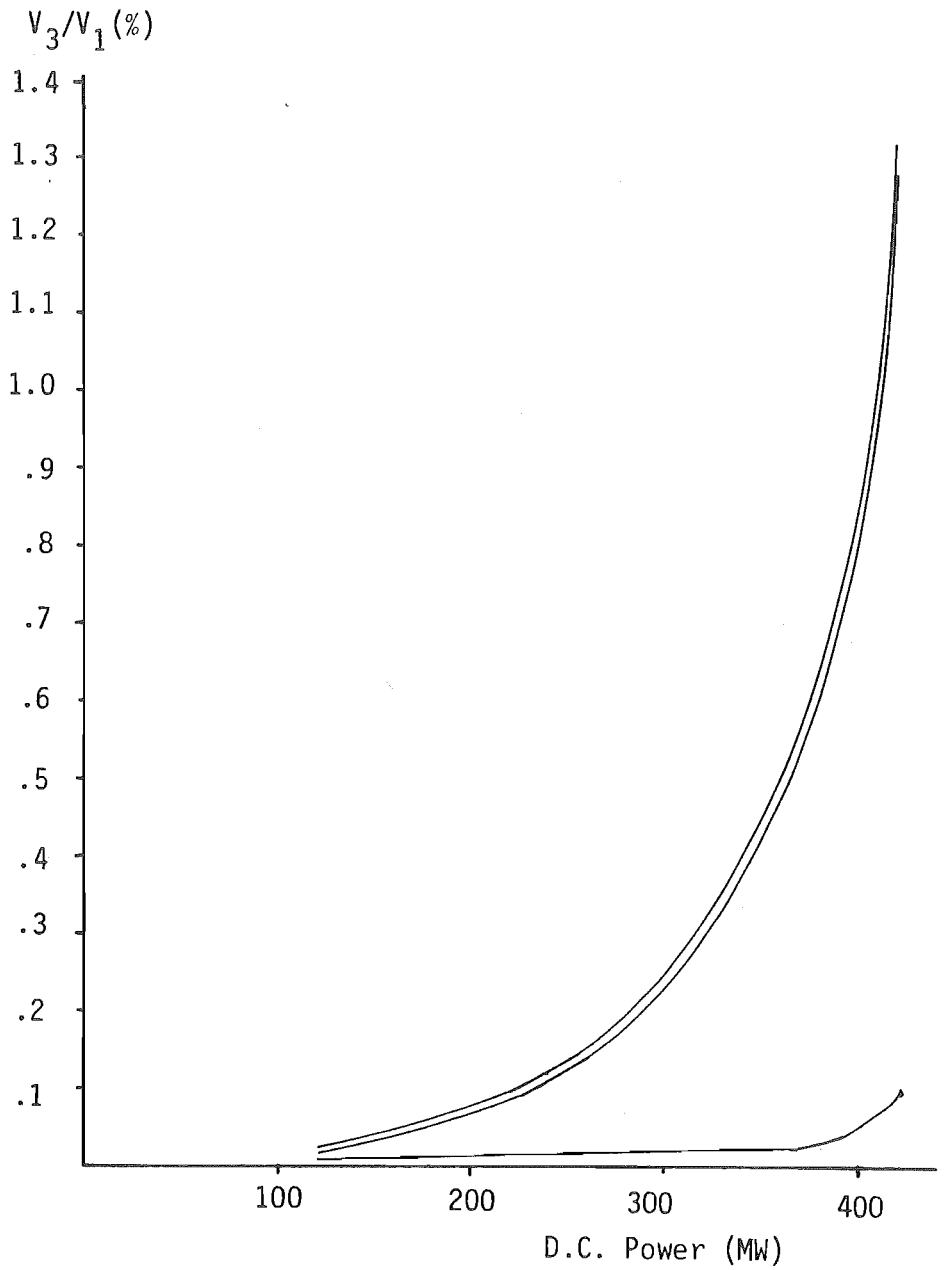

Figure 4.23 : Third Harmonic Voltage in the Three Phases of the Convertor Terminal with Equidistant Control and Perfectly Flat D.C. Current : With Iterations

In both cases an equidistant controller is specified, the d.c. current is assumed to be perfectly flat and the d.c. power varied. Figure 4.22 illustrates the voltage distortion without iterations, that is the a.c. current is due to the fundamental component of the terminal voltage only, while figure 4.23 shows the voltage distortion at the end of the iterative process. The iterative solution greatly changes the level of the uncharacteristic third harmonic.

The effect of the type of controller is illustrated in figures 4.23 (equidistant control) and 4.24 (constant delay angle control).

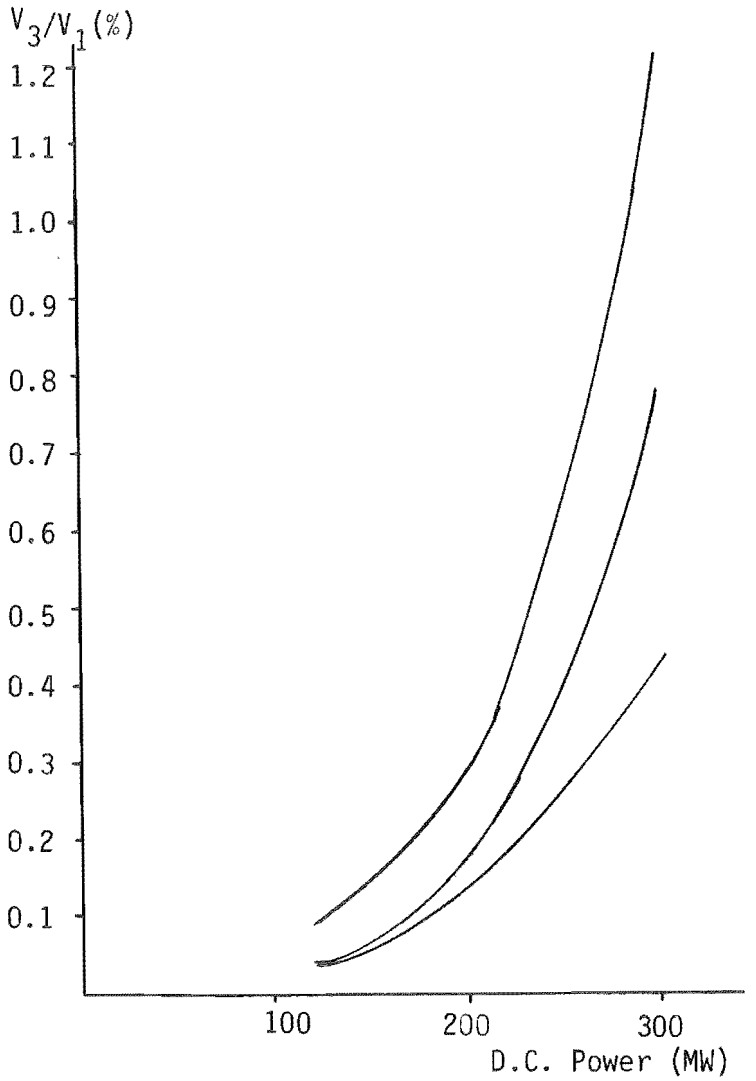

Figure 4.24 : Third Harmonic Voltage in the Three Phases of the Convertor Terminal with Constant Delay Control and Perfectly Flat D.C. Current

As expected (Ainsworth 1967) the levels of third harmonic distortion for the same d.c. power are seen to be much larger in the case of phase angle control.

If the size of the filters is further increased the characteristic harmonics are reduced due to the lower filter impedance. However, such an increase results in larger capacitance at lower order harmonics, in particular the third. The results of figure 4.25 are for the case when the filters have been increased from 66 MVar to 83 MVar which produces an a.c. system impedance closer

to resonance at the third harmonic.

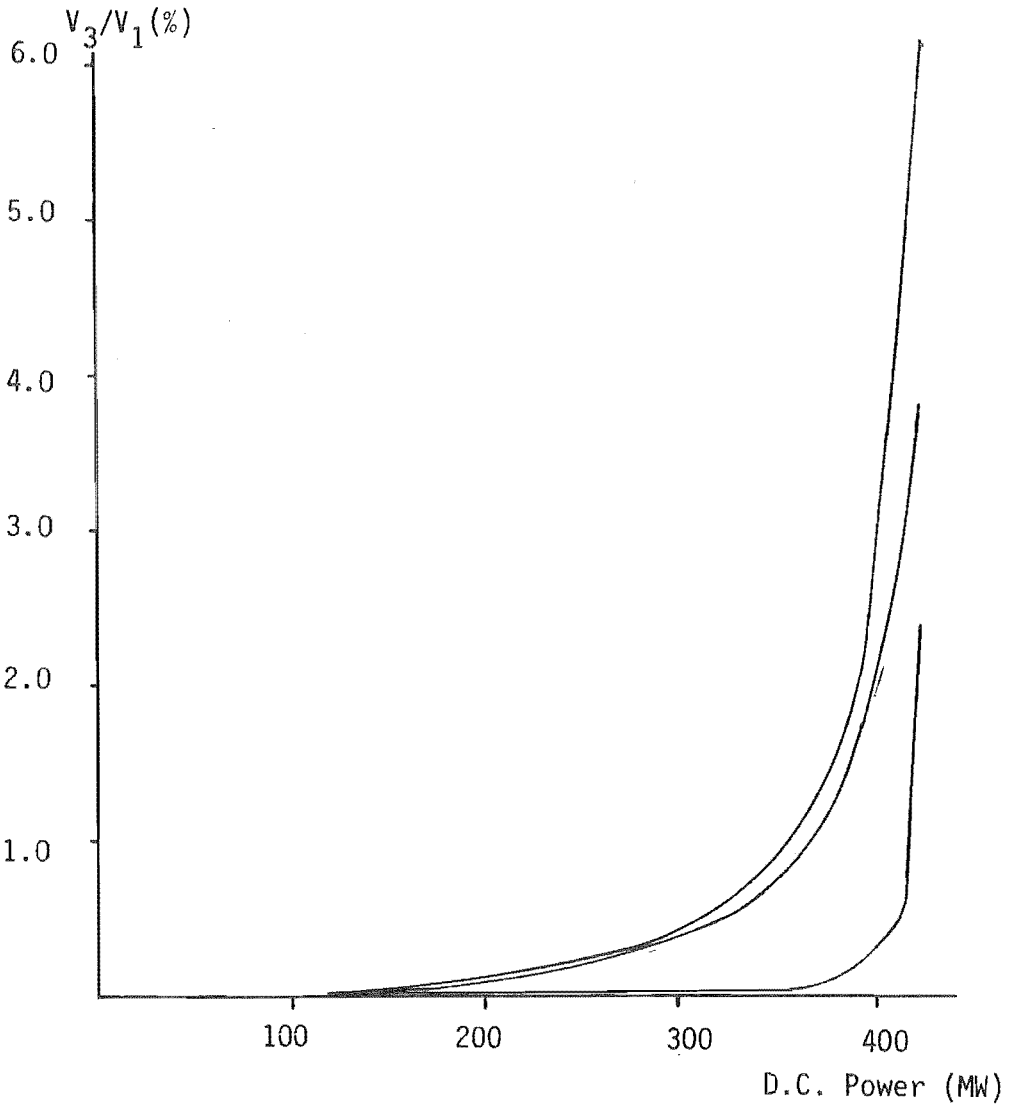

Figure 4.25 : Third Harmonic Voltage in the Three Phases of the Converter Terminal with Increased Filter Rating

When these last results are compared to those in figure 4.23 the greatly increased distortion clearly shows the need to accurately model the filters and the a.c. system, especially near resonance.

4.3.7 The Inclusion of the Non-infinite D.C. System

The test system of figure 4.17 was modified to include a more realistic d.c. system consisting of a 600 km d.c. transmission line with 0.8 H smoothing inductors at each end and in each pole with 0.32 ohms resistance per inductor. The results for a case with 66 MVar rated filters are shown in figure 4.26.

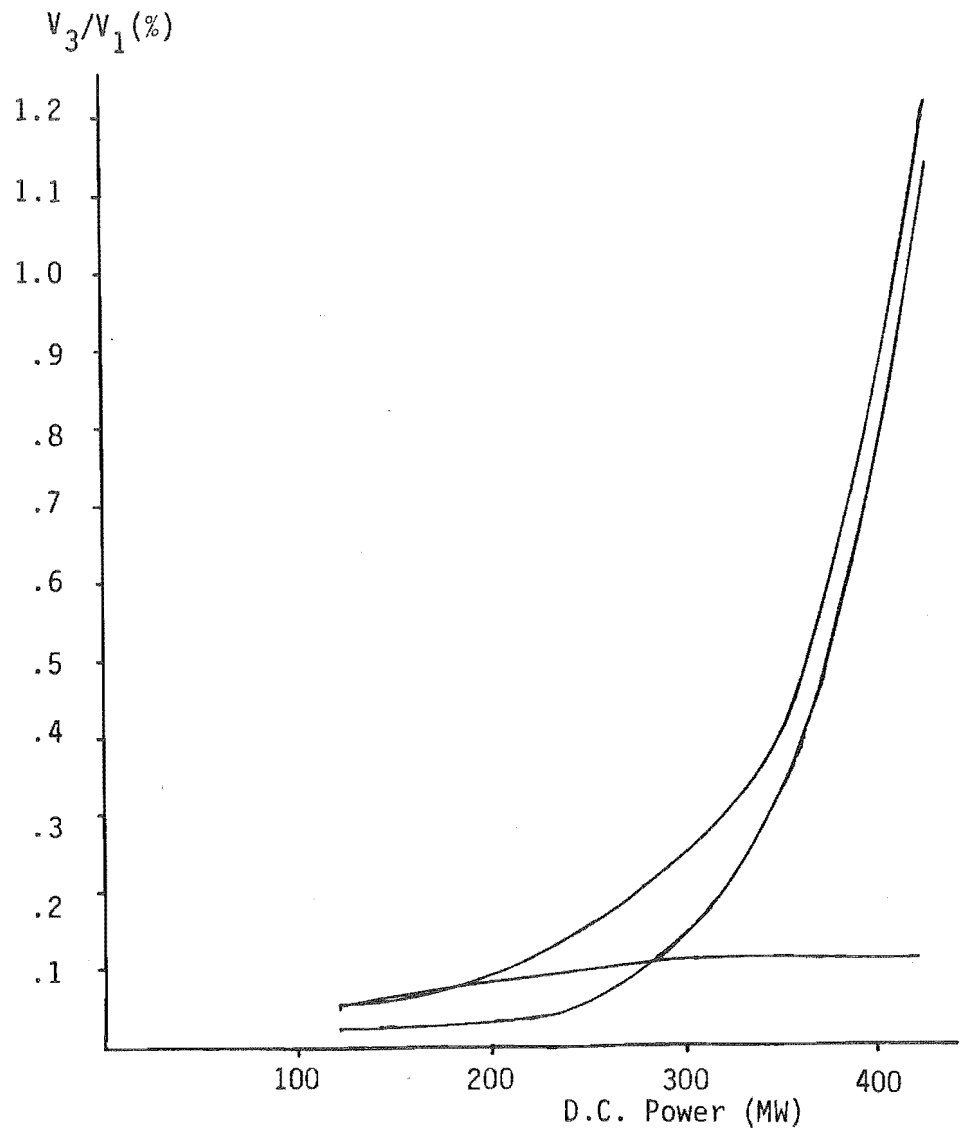

Figure 4.26 : Effect of D.C. Current Ripple on the Third Harmonic Voltage at the Convertor Terminal

When compared to figure 4.23, with no d.c. ripple, the differences are small indicating that normally there is no need to accurately model the d.c. system. However, under some conditions (Ainsworth 1977 and Yacamini and de Oliveira 1980b) the ripple on the d.c. side has been shown to increase greatly the uncharacteristic a.c. system voltage harmonics and even produce a harmonic instability.

4.3.8 Conclusions

The analysis of harmonic interactions and instabilities using the simplified test system of figure 4.17 shows a similar pattern to that of section 4.2.

As in section 4.2.2.2, diagonalizing the a.c. system produced no significant change in the stability of the solution. Also the filter system combination appears to be the primary cause of the instability as this causes a resonance which weakens the system to harmonics by increasing the magnitude of the system impedance seen by the convertor.

Premature convergence of the iterative algorithm has been exposed as a possible problem. However, this can be overcome by the inclusion of a controller disturbance as described in section 4.3.4.2. The results of section 4.3.5 show that this is a successful technique of exciting potentially unstable harmonics. Also when a controller disturbance is applied to a stable case the solution did not diverge indicating that the final answer is independent of the path of the solution, as in conclusions of section 4.2.

4.4 VERIFICATION OF THE ITERATIVE ALGORITHM

4.4.1 Introduction

The use of an iterative algorithm introduces the possibility of false solutions and numerical instability. Therefore, the accuracy and reliability of such an algorithm needs to be established, especially when a divergent solution is detected.

In order to test the iterative algorithm it is neccessary to compare the results with those obtained from a credible alternative method. In our department two possible alternatives exist. These are a physical simulator (Graham 1984) and a Transient Convertor Simulator (TCS) computer program (Heffernan 1980). The TCS program was used because the convertor transformers of the physical simulator are inherently non-linear. This effect is not yet included into the iterative algorithm but is an area of research in the department.

If the same problem is solved using both the iterative algorithm and TCS (without the application of a fault), the two sets of results can be compared. In the cases of the TCS results, the computer run must be long enough for the intial transients to decrease to a negligible level. The harmonic content of the waveforms is then evaluated using an FFT.

A divergent run of the iterative algorithm could be compared to the dynamic solution of TCS. As TCS mimics the operation of the convertor in the time domain, any harmonic instability will develop in the same way as in an actual convertor, and will be free of the potential numerical instability problems of the iterative algorithm.

4.4.2 TCS Comparison Without A.C. Filters

A simple system that can be used to compare the iterative algorithm with TCS is a single-bridge convertor connected to a purely inductive system with no filters on the a.c. side and to a large smoothing inductor on the d.c. side (i.e., a perfectly flat d.c. current). This is described in figure 4.27.

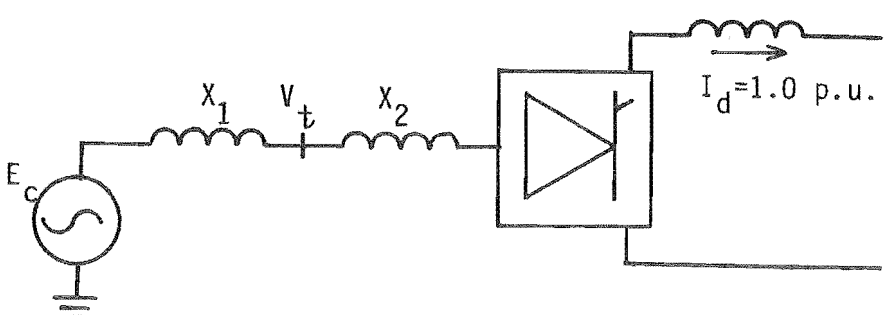

Figure 4.27 : Test System Without Filters

Traditionally the commutating voltage is defined as the sinusoidal voltage Ec which drives the commutation current (Arrillaga 1983), with the commutating reactance being the sum of X_1 and X_2. The delay angle is measured from the zero crossings of the E_c phase to

THE LIBRARY
UNIVERSITY OF CANTERBURY
CHRISTCHURCH, N.Z.

phase voltages and is set to 20° for the test example.

Analytically (Arrillaga 1983)

$$\frac{\sqrt{2}\ X_c I_d}{V_c} = \cos\alpha - \cos(\alpha+\mu)$$

with $V_c = \sqrt{3}$ p.u., $X_c = 0.2$ p.u., $I_d = 1.0$ p.u. and $\alpha = 20°$, the commutation angle is 19.07°

The a.c. system current injections and the V_t voltage distortion for the system of figure 4.27 were solved using the three following methods.

1. In the time domain using the TCS algorithm.

2. Using the iterative algorithm with E_c as the commutating voltage and a commutating reactance of 0.2 p.u.

3. Using the iterative algorithm, but with V_t as the commutating voltage, an a.c. system of 0.1 p.u. inductance and a commutating reactance of 0.1 p.u.

For the third method the initial value of the voltage V_t is specified as the fundamental voltage at that busbar. This can be found either using TCS or a simple power flow.

Using the TCS algorithm gives the current injections and terminal voltage V_t waveforms with reference to a $1\angle 0°$ cosine voltage on phase 'a' of E_c. However, the harmonic interaction algorithm uses a $1\angle 0°$ sinewave as reference. Also the a.c. currents are treated as injections in the harmonic interaction algorithm. Therefore, to compare the results the TCS reference needs to be advanced by 1/4 of a cycle and the FFT performed. This gives a set of phasors with an exponential or cosine series. To convert this to a sine series 90° is added to the phase of each phasor, at each harmonic.

The convertor currents in phase 'a', calculated by the three methods, are given in table 4.16 for the first five characteristic

harmonics. Non-characteristic harmonics are not generated because E_c is balanced.

Table 4.16 : Comparison of Phase 'a' Harmonic Currents

Harmonic	Method 1		Method 2		Method 3	
Order	Mag.	Phase	Mag.	Phase	Mag.	Phase
1	0.7666	149.3	0.7762	149.5	0.7658	149.6
5	0.1384	-152.9	0.1392	-152.6	0.1374	-152.3
7	0.0874	145.8	0.0887	146.1	0.0876	146.4
11	0.0381	-159.3	0.0386	-158.3	0.0383	-157.8
13	0.0246	137.9	0.0244	137.7	0.0243	138.2

Similarly, the phase 'a' harmonic voltages at V_t are compared in table 4.17. Because the case of the iterative algorithm with an infinite a.c. system source does not explicitly solve for V_t the results are not given.

Table 4.17 : Comparison of Phase 'a' Harmonic Voltages

Harmonic	Method 1		Method 3	
Order	Mag.	Phase	Mag.	Phase
1	0.96319	-4.1	0.96300	-4.1
5	0.06907	-63.2	0.06949	-62.3
7	0.06099	-124.1	0.06191	-123.6
11	0.04213	-69.0	0.04218	-67.9
13	0.03218	-132.5	0.03134	-131.9

The results of tables 4.16 and 4.17 for the phase 'a' harmonic currents and voltages show a close agreement. The magnitude of the harmonic currents also agree with those expected (Arrillaga 1983).

The comparison in this section verifies the formulation of both the iterative algorithm and TCS software.

4.4.3 TCS Comparison With A.C. Filters and a Non-Infinite D.C. System

Because a harmonic instability generally occurs when the a.c. system is near to resonance at a low order harmonic and the short circuit ratio is small, the a.c. system was chosen to have a parallel resonance between the filters and the a.c. system near the third harmonic. For simplicity, the a.c. system was a series inductor resistor combination and the filters the fifth, seventh, eleventh and thirteenth harmonic tuned branches of table 4.2. The a.c. system inductance was tuned to resonate near the third harmonic (140 Hz) with the equivalent capacitance of the filters (calculated at the third harmonic). For the iterative algorithm the d.c. current was made perfectly smooth. This was not possible for the TCS algorithm so the smoothing inductor was made sufficiently large to give an insignificant d.c. current ripple. The convertor transformer was specified as a star-g/star connection with a 0.05 p.u. leakage reactance per phase. The system configuration is described in figure 4.28.

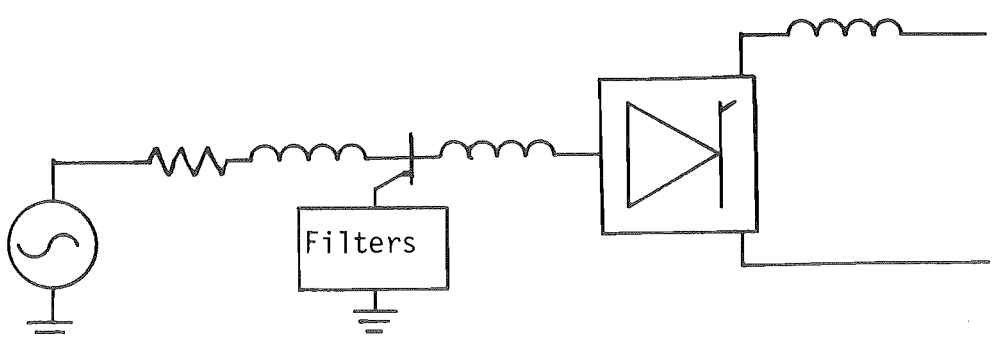

Figure 4.28 : Test System With Filters

The convertor was operated with an equidistant firing control strategy, a nominal delay angle of 5° and a d.c. current level of 1.0417 p.u. The a.c. system phase 'a' current and terminal voltage distortions are compared in tables 4.18 and 4.19 respectively.

Table 4.18 : Harmonic Current Comparison for the Case With Filters

Harmonic	TCS		Iterative Algorithm	
Order	Mag.	Phase	Mag.	Phase
1	0.8111	167.2	0.8102	167.8
5	0.1585	-64.1	0.1530	-61.2
7	0.0984	-86.1	0.1031	-85.9
11	0.0549	40.9	0.0546	44.2
13	0.0402	16.3	0.0407	18.6

Table 4.19 : Harmonic Voltage Comparison for the Case With Filters

Harmonic	TCS		Iterative Algorithm	
Order	Mag.	Phase	Mag.	Phase
1	0.91969	0.0	0.92026	0.0
5	0.00590	-66.8	0.00577	-66.7
7	0.00408	-94.2	0.00435	-97.1
11	0.00128	33.5	0.00125	35.4
13	0.00123	46.2	0.00116	43.1

In each case the phase of harmonic currents and voltages were referred to that of the fundamental component in the phase 'a' terminal voltage.

The results of tables 4.18 and 4.19 show close agreement, indicating the usefulness of the iterative algorithm. The minor discrepancies are caused by the difficulty in matching the fundamental conditions and the delay angle, due to the different per unit systems.

4.4.4 Unstable Case

The test of section 4.4.3 was repeated with the same system configuration, a delay angle of 5°, and a d.c. current of 3.94 p.u. As before, the TCS algorithm settled down to a steady state solution

but the iterative algorithm did not converge.

4.4.5 Conclusions

The test comparisons made between the iterative harmonic interaction and TCS algorithms illustrate both the positive and negative aspects of the iteration algorithm.

The iterative algorithm has been shown to be accurate as it produces results which are in close agreement with those produced by the TCS algorithm. Also, the case of a purely inductive system without filters, which can be solved analytically, shows the accuracy of both the iterative and TCS algorithms.

During the course of the comparisons it was observed that the iterative algorithm required less complex data preparation and generally less CPU time to reach a solution.

However, the iterative algorithm may diverge even when stable operation exists in the time domain. In this case the convertor's steady state operation needs to be solved using the TCS algorithm.

4.5 FUTURE WORK WITH THE ITERATIVE ALGORITHM

4.5.1 Multiple Sources

In many transmission systems there are several sources of harmonics. For instance, in the South Island of New Zealand system there is an h.v.d.c. link and an aluminium smelter, both of which are relatively large. The operation of each source depends on the distortion from the other sources and therefore the sources should not be treated separately.

The iterative algorithm of chapter 3 can be used to model multiple sources. The a.c. current injections and the d.c. voltage waveforms of each convertor are solved for at the beginning of each iteration. With each of the convertors operation updated, the a.c.

voltage distortion and d.c. current ripple on each convertor are evaluated together. However, while this is simple, it may not be the most computationally efficient method.

Most of the computational effort is needed to solve the operation of the convertor and relatively little needed to solve the a.c. and d.c. systems. Therefore, each convertor could be solved individually with the complete a.c. and d.c. systems updated before the next convertor is solved. As in the Gauss-Seidel method for solving simultaneous sparse linear equations (Kreyzig 1979), this would provide the convertor with the most accurate information possible when it is solved and would probably accelerate the solution.

In the case where one or more convertors is a twelve pulse configuration, both bridges should be solved before the a.c. and d.c. systems to prevent the unnecessary generation of harmonics that would otherwise cancel due to the connection of the converter transformers.

To assess the effect of a second source on an existing convertor, a test system containing two convertors should be derived. With one convertor turned off, the iterative algorithm could be run and the system solved. Then the power of the second convertor could be gradually increased and the operation of the first convertor examined for any change.

4.5.2 Inclusion of the Harmonic Effects in the Three Phase Power Flow

The three phase power flow algorithm assumes that the voltage distortion on the convertor terminal is zero. As the results of this chapter show, the terminal busbar voltage is not purely sinusoidal and this may result in the fundamental current injections being altered. This may affect the solution of the power flow which may require further interactions to reach the improved solution.

This would not be a major effect in case of adequate filtering, but may have an effect in the case of negative sequence terminal voltage which causes uncharacteristic odd harmonic orders which are generally unfiltered. As the magnitude of the fundamental convertor currents is reasonably independent of the delay angles, and hence commutation angles (Harker 1980), the major effect of voltage distortion is expected to be on the current angles and hence the system real power flows.

4.5.3 Harmonic Instability

Further work may be warranted to assess when the iterative algorithm diverges and TCS is needed. Similarly, further comparisons between the iterative algorithm and TCS should be performed to check an unbalanced case. However, because a detailed harmonic system admittance matrix is used for both the a.c. and d.c. systems in the iterative algorithm, a comparison with TCS for a real system with an unbalanced impedance loci will require an equally detailed time domain equivalents for these systems. This is an area of current work in the department (Watson et al 1985).

CHAPTER 5

HARMONIC MODELLING OF SINGLE PHASE FEEDER AND CONVERTOR SYSTEMS

Of particular interest in New Zealand is the fact that part of the main trunk line in the North Island is being electrified. A 25/50 kV single phase feeder system is to be used to supply power to the locomotive's d.c. drives via single phase a.c./d.c. convertors. The use of convertors will result in harmonic currents entering the feeder system. The harmonic modelling of the operation of the traction system can be divided into the modelling of the a.c. feeder system and the harmonic interaction of the locomotive's single phase convertors with their associated a.c. and d.c. systems. These are discussed in sections 5.1 and 5.2 respectively.

It should be noted that in this chapter single phase refers to an actual single phase system, rather than balanced three phase which is often termed single phase.

5.1 HARMONIC MODELLING OF THE NEW ZEALAND RAILWAY FEEDER SYSTEM

To help assess the effect of a.c. current distortion from the locomotives on local communication circuits and the three phase transmission system supplying the railway substations, a single phase harmonic penetration study was performed. Harmonic models of the feeder and contact wires, the rails, the lines terminations, the locomotive and substations' transformers and the three phases transmission system were collated. At each frequency of interest the models were formed into an admittance matrix.

Proposed filters at the substation and line terminations were assessed by calculating the harmonic voltages and the current flows throughout the feeder system. This involved the use of the harmonic

admittance matrix and fixed current injections into the secondary (convertor side) of the locomotive's transformer.

5.1.1 Component Models

5.1.1.1 Feeder wires

The cross section of the proposed towers is in figure 5.1.

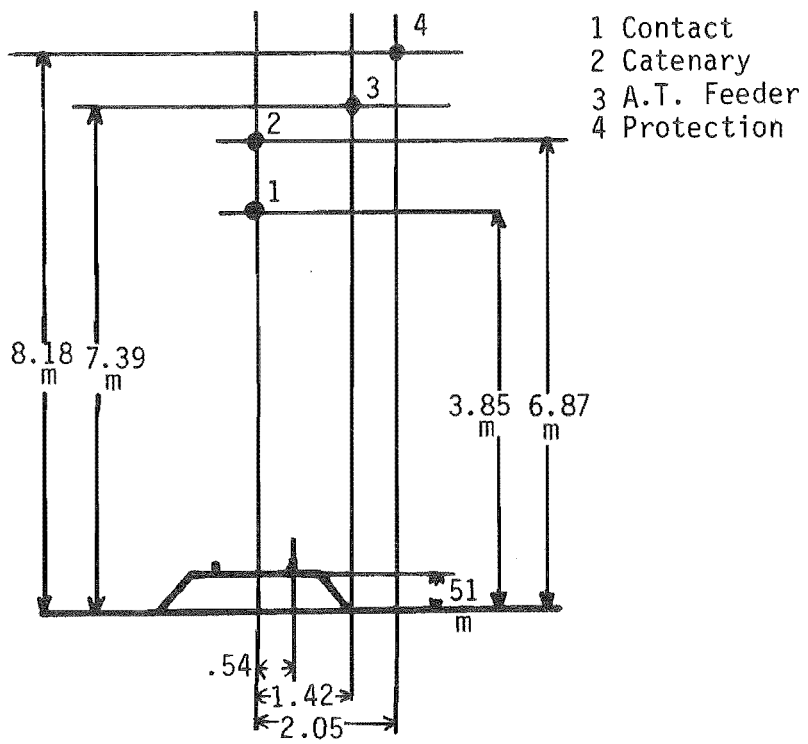

Figure 5.1 : Cross Section of the Feeder System Towers

In the absence of specific data the following assumptions were made.

1. Data for the protection wire is identical to that used for the protection wire in the New Zealand d.c. link.

2. The rails consisted of solid circular conductors of 100 mm diameter.

3. The catenary wire and contact wire are assumed to be identical.

4. All conductors are flat between towers and, therefore, of constant cross section.

This gives the conductor data of table 5.1.

Table 5.1 : Conductor Data

	Contact	Catenary	Feeder	Protection	Rails
Resistance (Ohms/km)	.4372	.4372	.3183	3.1	.2490
Diameter (mm)	5.836	5.836	5.642	11.0	100.0

The rails were assumed to be earthed. This is a reasonable assumption as they are bonded to the protection wire every 7.5 km or sixteenth of a wavelength at the fiftieth harmonic. Similarly, there are auto transformers every 15 km to extract the locomotive's current out of the rail and into the feeder wire, as described in figure 5.2.

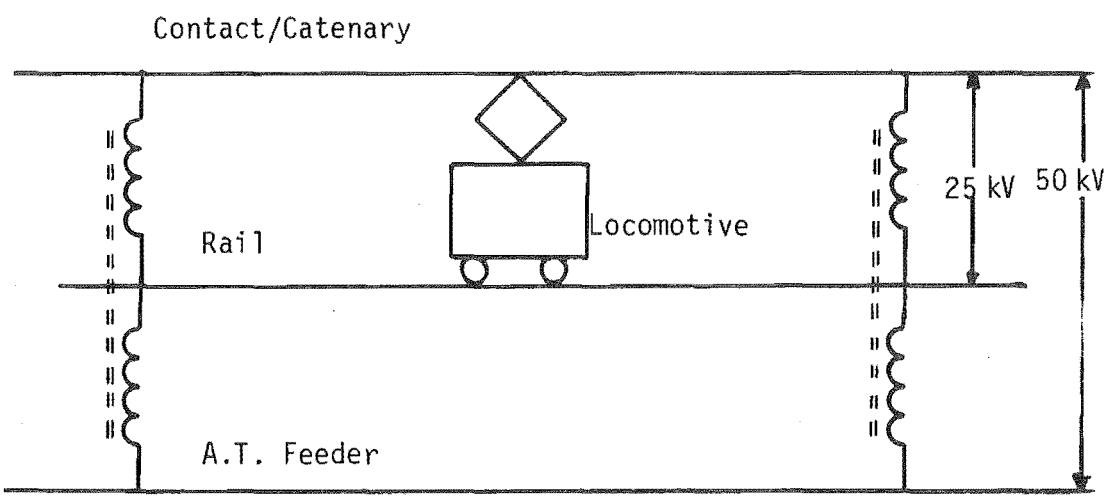

Figure 5.2 : The Auto Transformer Position

With the above assumptions the feeder system can be approximated by an equivalent positive sequence system. Therefore, the current only flows in the feeder, contact and catenary wires and not in the rails.

As for the modelling of the d.c. lines (described in Appendix A3) the feeder and contact wire's per unit length impedance and admittance were calculated using a line constants program (Dommel 1980). Using the positive sequence parameters at each harmonic, an

equivalent-π model can be derived for each section which takes into account the transmission line effects.

5.1.1.2 Locomotive, including power factor correction

The proposed locomotives have four convertors with power factor correction on each of the convertor transformer's secondary windings. For the analysis the four convertor secondary windings were reduced to a single equivalent transformer. As the leakage of each transformer is 0.0985 p.u. on a 1043 KVA base, the equivalent reactance of the single group becomes 0.0236 p.u. on a 1 MVA base.

Similarly, the four sets of 2.1 mH series inductors and the 1.5 mF capacitors, at a 0.570 kV voltage base, are combined to single equivalent reactances of 0.5076 p.u. and 1.6 p.u. at fundamental frequency, respectively.

5.1.1.3 The substation and locomotive transformer model

The harmonic model chosen for the transformer was a parallel combination of the leakage reactance and a resistance 80 times the leakage at fundamental (Harker 1980 and Densem 1983). The leakage reactance of the locomotive transformer is 0.0236 p.u., as in section 5.1.1.2, and that of the substation transformer 0.013 p.u.

5.1.1.4 The line terminations

The line terminations consist of a series connection of a 600 ohms resistor and a 6366 ohms (at 50 Hz) capacitor. These are connected between the feeder wire and the protection wire and, similarly, between the contact wire and the protection wire. They are included to terminate the feeder system in its characteristic impedance.

5.1.1.5 The three phase transmission system

An equivalent impedance looking into the three phase transmission system from the substation is required. Owing to the lack of data it was assumed that the transmission system is sufficiently strong to be regarded as a short circuit to harmonics. The transmission system

impedance would generally be of little significance as the substation transformer impedance is in series with it.

5.1.1.6 The harmonic filters

The harmonic filters proposed for the substation were single tuned shunt branches for the third and fifth harmonics. They have a Q of 50 and supply a total of 5.0 MVAr reactive power compensation, with the third and fifth harmonic filter were specified to give 3.0 MVAr and 2.0 MVAr compensation respectively.

5.1.2 Forming the Admittance Matrix for the Feeder System

With all of the individual system component models defined at harmonic frequencies, an overall admittance matrix can be formed for the feeder system at each harmonic. The example of a single locomotive on the left of the substation is given in figure 5.3.

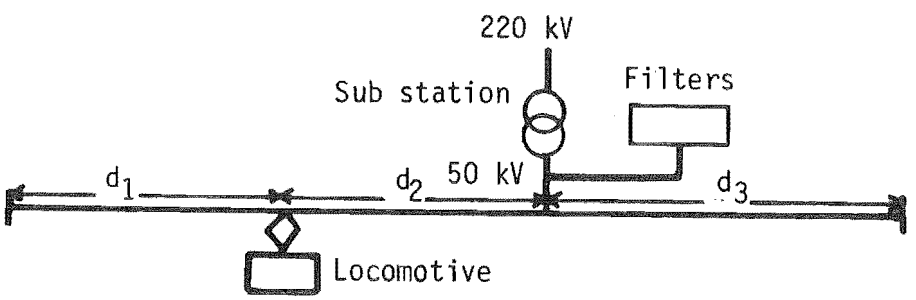

Figure 5.3 : A Single Locomotive Left of the Substation

To describe the feeder system 2Nt + 4 busbars are required, where Nt is the number of locomotives. Table 5.2 shows the numbering convention of the busbars chosen.

Table 5.2 : Busbar Numbering Convention

Busbar	Description
1	substation at the feeder voltage (50 kV)
2	substation at the transmission voltage (220 kV)
3 to Nt +2	locomotive's equivalent secondary winding
Nt + 3	line's left hand termination
Nt + 4 to 2Nt + 3	locomotive's pantograph
2Nt + 4	line's right hand termination

The example of figure 5.3 can be described by the circuit of figure 5.4.

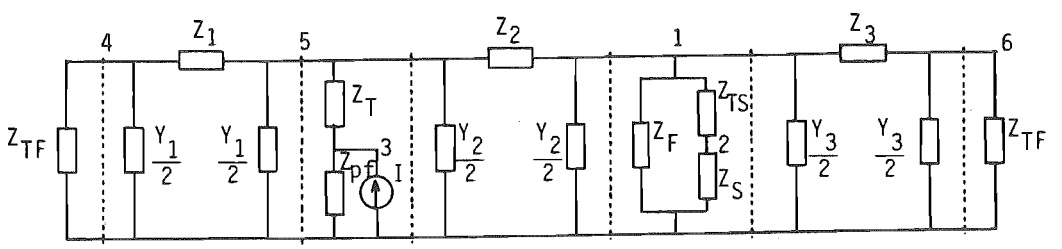

Figure 5.4 : Circuit Diagram for a Single Locomotive

where Z_1, Z_2 and Z_3 are the series impedances of the lines

Y_1, Y_2 and Y_3 are the shunt admittances on the lines

Z_t locomotive's transformer impedance

Z_{ts} substation's transformer impedance

Z_{tf} terminal filter impedance

Z_{pf} impedance of the power factor capacitor and choke

Z_f filter impedance

Z_s transmission system impedance.

For the case of a single locomotive, the feeder system admittance matrix, $[Y_{feeder}]$, is

$$\begin{bmatrix} Y_{11} & Y_{12} & 0 & 0 & Y_{15} & Y_{16} \\ Y_{21} & Y_{22} & 0 & 0 & 0 & 0 \\ 0 & 0 & Y_{33} & 0 & Y_{53} & 0 \\ 0 & 0 & 0 & Y_{44} & Y_{54} & 0 \\ Y_{51} & 0 & Y_{53} & Y_{54} & Y_{55} & 0 \\ Y_{61} & 0 & 0 & 0 & 0 & Y_{66} \end{bmatrix}$$

where $Y_{11} = 1/Z_2 + Y_2/2 + 1/Z_f + 1/Z_{ts} + 1/Z_3 + Y_3/2$

$Y_{12} = -1/Z_{ts}$

$Y_{15} = -1/Z_2$

$Y_{16} = -1/Z_3$

$Y_{22} = 1/Z_s + 1/Z_{ts}$

$Y_{33} = 1/Z_{pf} + 1/Z_t$

$Y_{35} = -1/Z_t$

$Y_{44} = 1/Z_{tf} + Y_1/2 + 1/Z_1$

$Y_{45} = -1/Z_1$

$Y_{55} = 1/Z_1 + Y_1/2 + 1/Z_t + Y_2/2 + 1/Z_2$

$Y_{66} = 1/Z_3 + Y_3/2 + 1/Z_{tf}$

With j being the number of trains to the left of the substation, the admittance matrix for a multi locomotive system can be defined.

At the substation,

$$Y_{11} = 1/Z_{j+1} + \frac{Y_{j+1}}{2} + \frac{1}{Z_{j+2}} + \frac{Y_{j+2}}{2} + 1/Z_f + 1/Z_{ts}$$

$Y_{12} = -1/z_{ts}$

$Y_{22} = 1/Z_s + 1/Z_{ts}$

At the locomotive's transformer secondary busbar, i = 3 to Nt + 2

$Y_{i,i} = 1/Z_t + 1/Z_{pf}$

$Y_{i,i+Nt+1} = -1/Z_t$

At the left termination, i = Nt + 3

$$Y_{i,i} = 1/Z_{tf} + Y_1/2 + 1/Z_1$$

At the right termination, i = 2Nt + 4

$$Y_{i,i} = 1/Z_{tf} + \frac{Y_{2+Nt}}{2} + \frac{1}{Z_{2+Nt}}$$

At the contact wire, i = Nt + 4 to 2Nt + 3

$$\text{left to substation } Y_{i,i} = 1/Z_k + Y_k/2 + 1/Z_t + Y_{k+1}/2 + 1/Z_{k+1}$$

$$\text{right to substation } Y_{i,i} = 1/Z_{k+1} + Y_{k+1}/2 + 1/Z_t + Y_{k+2}/2 + 1/Z_{k+2}$$

where k is the number of the train, i.e., k = 1 to Nt. The mutual admittances along the line are

$$Y_{Nt+2+m,Nt+3+m} = -1/Z_m \quad m = 1, j \text{ (if } j > 0)$$

$$Y_{1,Nt+2+m} = -1/Z_m \quad m = j + 1$$

$$Y1_{,Nt+2+m} = -1/Z_m \quad m = j + 2$$

$$Y_{Nt+1+m,Nt+2+m} = -1/Z_m \quad m = j + 2, Nt + 2 \text{ (if } j < Nt)$$

5.1.3 The Response of the Feeder System to Harmonics

With a harmonic admittance matrix calculated at each harmonic, the response of the feeder system to harmonic injections at the locomotive can be assessed. In the absence of more realistic data, the case of one locomotive was examined with the harmonic currents injected at the locomotive's transformer secondary busbar, such that,

$$\begin{bmatrix} 0 \\ 0 \\ I \\ 0 \\ 0 \\ 0 \end{bmatrix} = [Y_{feeder}] \begin{bmatrix} V_1 \\ V_2 \\ V_3 \\ V_4 \\ V_5 \\ V_6 \end{bmatrix} \qquad 5.1$$

Equation 5.1 is solved for the voltages throughout the feeder system by Gaussian elimination.

The two values of I in equation 5.1 of interest are a fixed 1.0 p.u. injection for each harmonic and the set of maximum expected injections supplied by the manufacturer, and given in table 5.3

Table 5.3 : The Set of Maximum Expected Injections

Harmonic Order	Value (amps)	Percentage of Fundamental
1	142.281	---
3	32.998	23.19
5	19.251	13.53
7	12.769	8.97
9	8.030	5.64
11	5.425	3.81
13	4.309	3.03
15	3.088	2.17
17	2.354	1.65
19	2.602	1.83
21	2.538	1.78
23	2.293	1.61
25	2.445	1.72
27	2.442	1.72
29	2.096	1.47
31	1.905	1.34
33	1.891	1.33
35	1.630	1.15
37	1.386	0.97
39	1.426	1.00
41	1.383	0.97
43	1.246	0.88
45	1.318	0.93
47	1.374	0.97
49	1.281	0.90

Of most interest are the voltages at the locomotive's pantograph and the currents into the harmonic filters and transmission system.

5.1.4 Evaluating the Currents in the Individual System Components

As the equivalent harmonic model represents the individual feeder system components, once the harmonic voltages are known the currents in each of the individual system components can be found.

Current in the harmonic filters	$I_f = Y_f V_1$	
" " " termination left filter	$I_{lt} = Y_{tf} V_{Nt+3}$	
" " " termination right filter	$I_{rt} = Y_{tf} V_{2Nt+4}$	
" " " substation transformer	$I_{ts} = Y_{ts} (V_1 - V_2)$	
" " " locomotive transformer	$I_{ti} = Y_t (V_{2+i} - V_{3+Nt+1})$	i=1,Nt
" " " locomotive p.f. circuit	$I_{pfi} = Y_{pf} V_{2+i}$	i=1,Nt

For the calculation of the line currents, sending was defined as towards to the substation (i.e., sending into the system) and receiving as towards the line terminations.

$$I_{send} = V_{send} (Y_i/2 + 1/Z_i) - V_{rec} (1/Z_i)$$

$$I_{rec} = V_{rec} (Y_i/2 + 1/Z_i) - V_{send} (1/Z_i)$$

where i refers to the section number on the line. The V_{send} and V_{rec} which correspond to a particular i depends on the number of locomotives left on the substation j.

Case	i	V_{send}	V_{rec}
j=0	1	V_{3+Nt}	V_1
	2	V_{4+Nt}	V_1
	i=3,Nt+1	V_{2+Nt+i}	V_{1+Nt+i}
	Nt+2	V_{2Nt+4}	V_{2Nt+3}

j=Nt	1	V_{3+Nt}	V_{4+Nt}	
	i=2,Nt	V_{2+Nt+i}	V_{3+Nt+i}	(j>1)
	Nt+1	V_{2Nt+3}	V_1	
	Nt+2	V_{2Nt+4}	V_1	
0<j<Nt	1	V_{3+Nt}	V_{4+Nt}	
	i=2,j	V_{2+Nt+i}	V_{3+Nt+i}	
	j+1	V_{3+Nt+i}	V_1	
	j+1	V_{4+Nt+i}	V_1	
	i=j+3,Nt+1	V_{2+Nt+i}	V_{1+Nt+i}	
	Nt+2	V_{2Nt+4}	V_1	

5.1.5 Results of a Test Section of Line

The test system chosen consists of a single locomotive on a 110 km section of line with the substation 70 km from the left line termination.

Figure 5.5 shows the transmission system harmonic currents for a 1.0 p.u. current injection into the secondary of the locomotive's transformer at various positions to the left of the substation. Similar results to these were found for a locomotive to the right of the substation. Similarly, figure 5.6 shows the transmission system currents for the locomotive current injections as listed in table 5.3

Figures 5.5 and 5.6 show that the harmonic currents entering the transmission system increase when the separation between the locomotive and the substation is larger.

To try and reduce the excessive current distortion expected in the transmission system, the third and fifth harmonic filters described in section 5.1.1.6 were proposed. Figure 5.7 shows the transmission system currents with the locomotive's injections and the proposed harmonic filters.

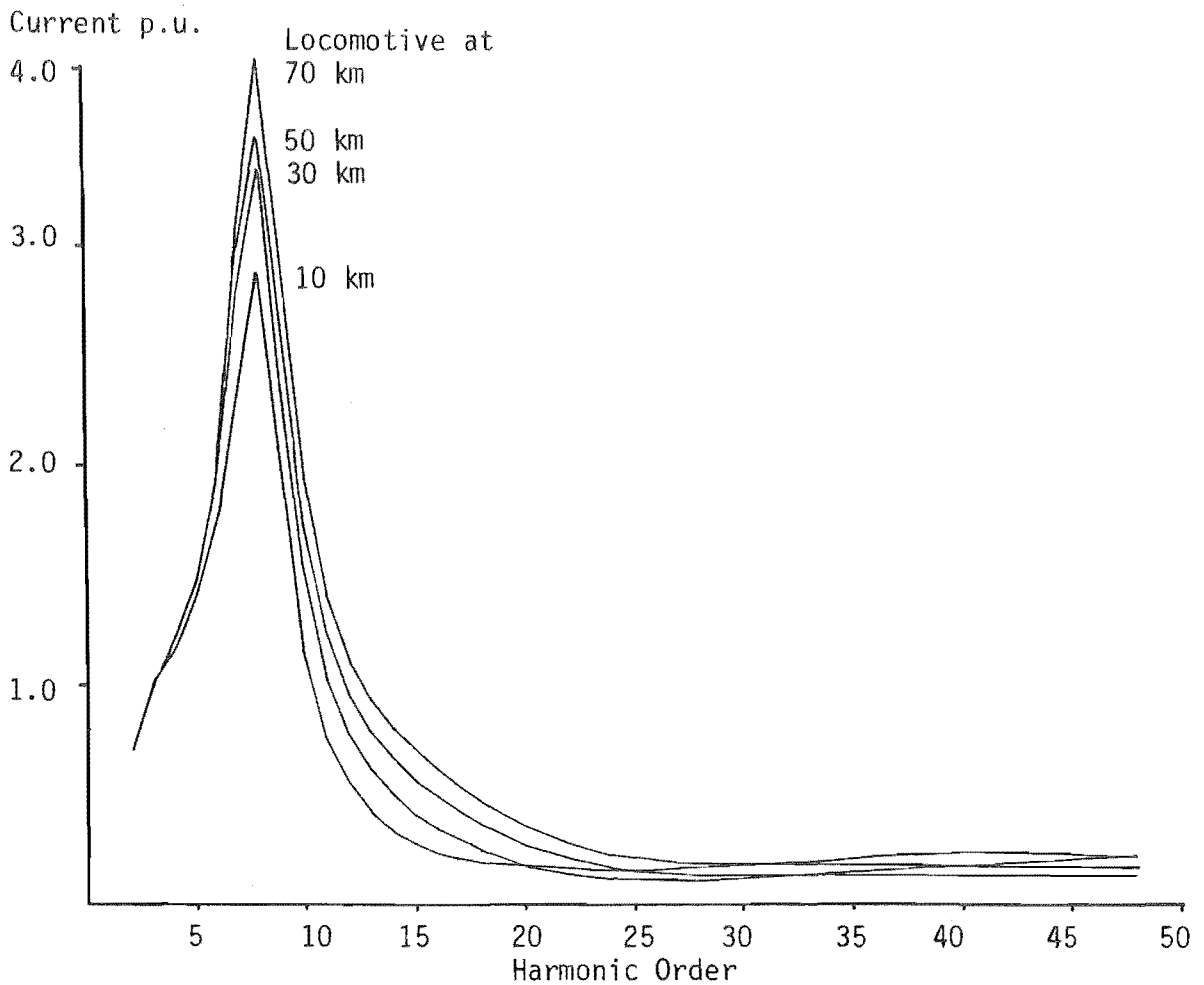

Figure 5.5 : Transmission System Currents for a 1.0 p.u. Injection (no filters).

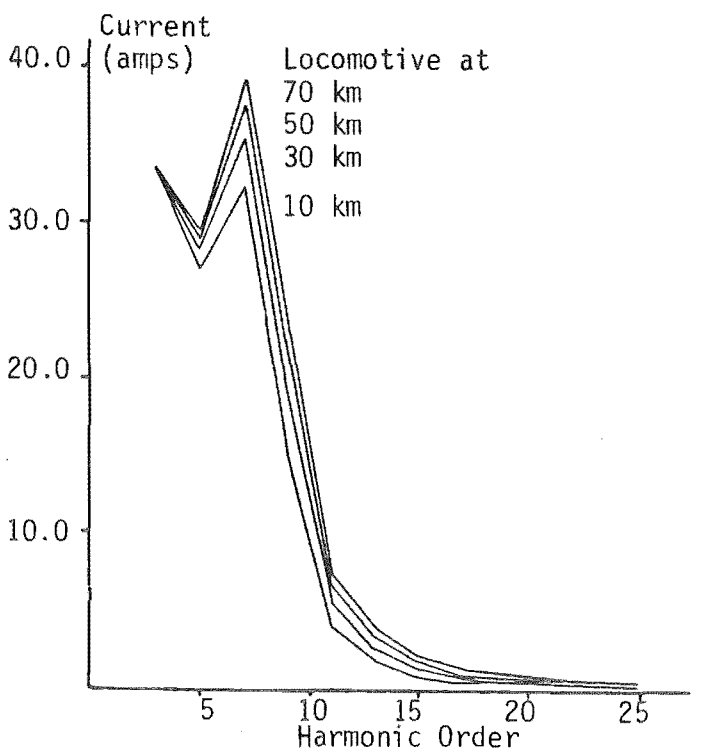

Figure 5.6 : Transmission System Currents for the Locomotive's Injections (no filters).

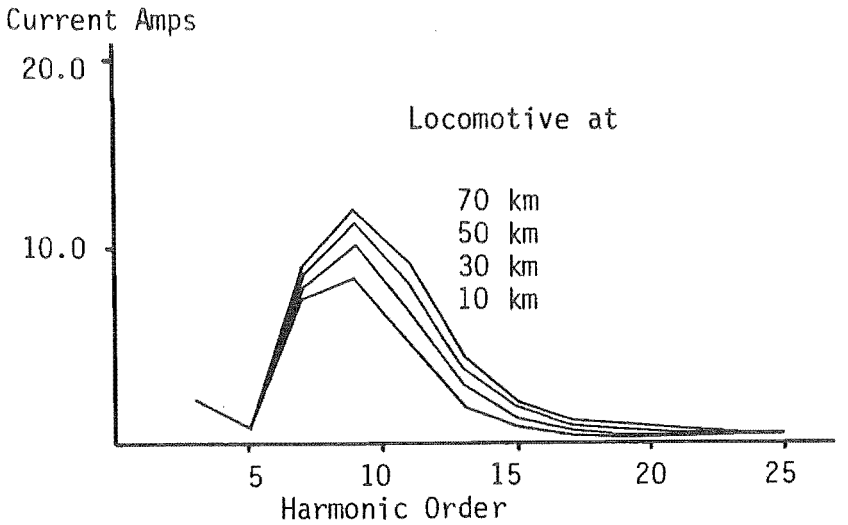

Figure 5.7 : Transmission System Currents for the Locomotive's Injections with the Proposed Harmonic Filters

A comparison of figures 5.6 and 5.7 illustrates the effect of the filters.

Because relatively large levels of seventh, ninth and eleventh harmonics still exist with the proposed filters, the effect of including a seventh harmonic filter was examined. To keep the total filtres rating of 5 MVar reactive power compensation, the third, fifth and seventh harmonic filters were rated at 2.333, 1.667 and 1.0 MVar respectively.

For the case of a locomotive 50 km to the left of the substation, figure 5.8 shows:

(1) the currents injected by the locomotive,

(2) the currents entering the transmission system for the case without filters,

(3) the currents entering the transmission system in the presence of third and fifth harmonic filters,

(4) the currents entering the transmission system for the case of third, fifth and seventh harmonic filters.

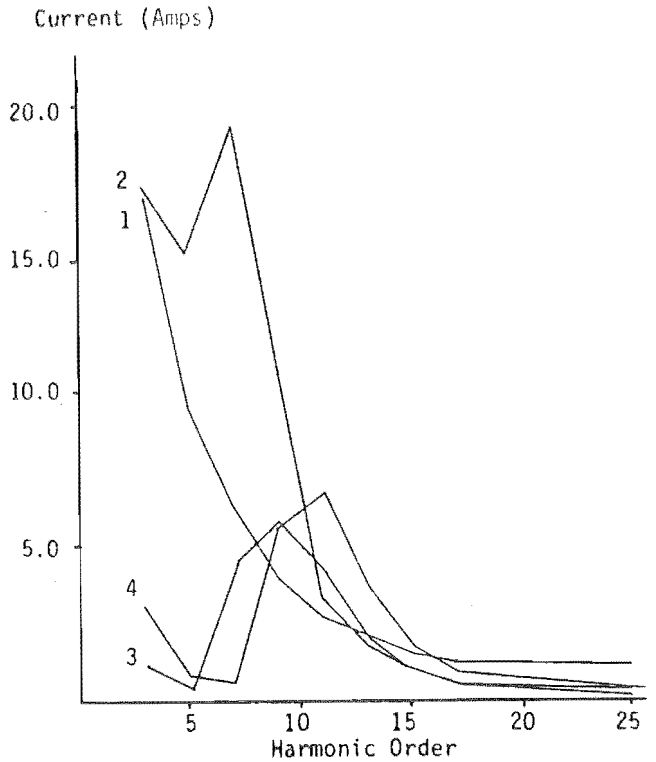

Figure 5.8 : Comparing the Transmission System Currents for the Various Filter Configurations

Similarly, the voltage distortion on the locomotive's pantograph for the same cases as figure 5.8 is given in figure 5.9.

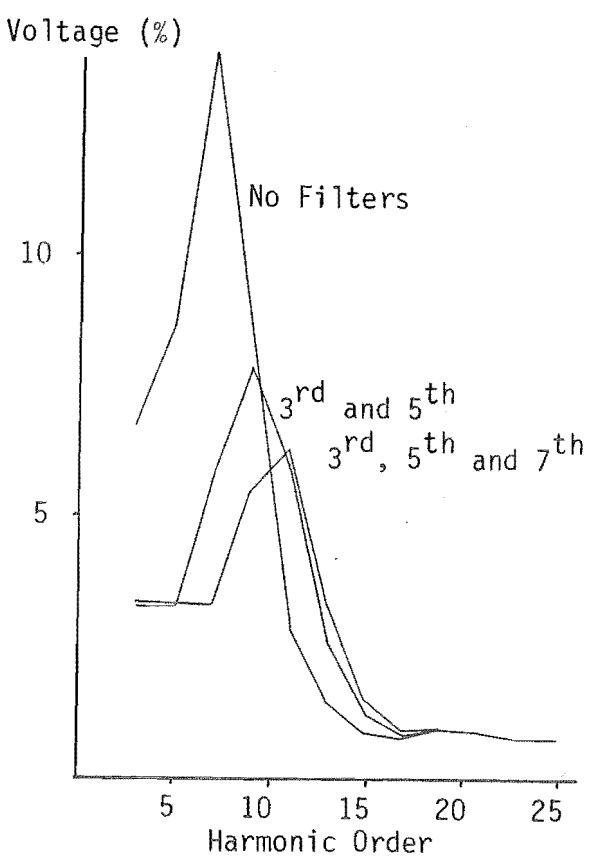

Figure 5.9 : Comparing the Pantograph Voltage Distortions for the Various Filter Configurations.

5.1.6 Conclusions of the Single Phase Harmonic Penetration

As the final design of the line terminations, the positioning of the power factor correction components and harmonic filters is not known, any more detailed analysis is not warranted at this stage. However, only minor changes to the existing algorithm would be needed to include any likely system changes.

5.2 MODELLING SINGLE PHASE SYSTEMS

The basic problem of modelling the harmonic interaction between single phase convertors and their associated a.c. and d.c. systems is similar to that of three phase convertors. The main differences are in the sampling routine and the need to model half controlled convertors which are common in single phase applications. Also the associated a.c. system is single phase.

Figure 5.10 consists of a single phase convertor bridge with its commutating voltage V_t and inductance L_t.

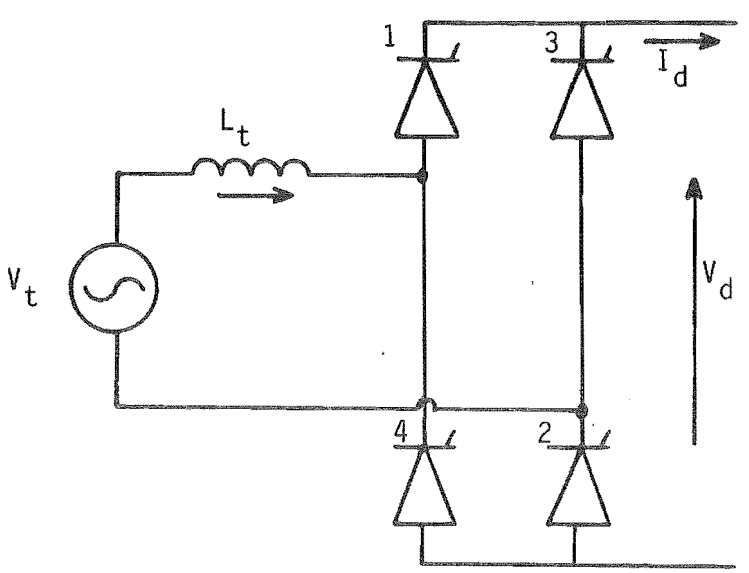

Figure 5.10 : Single Phase Convertor Bridge

5.2.1 Calculating the Commutation Current

The commutation circuit of figure 5.10 is assumed to be purely inductive. Therefore, during a commutation

$$V_t = L_t dI_t/dt \qquad 5.2$$

or

$$I_t = 1/L_t \int_0^t V_t \, dt + C \qquad 5.3$$

With

$$V_t(t) = \sum_{h=1}^{NHARM} \hat{V}_h \sin(\phi_h + h\theta_p + h\omega t) \qquad 5.4$$

where

$\hat{V}_h$ is the magnitude of the h^{th} harmonic of V_t

ϕ_h is the phase of the h^{th} harmonic of V_t

θ_p is the firing instant of the p^{th} valve

t is referred to θ_p.

Therefore

$$I_t(t) = C - \frac{1}{\omega L} \sum_h \frac{\hat{V}_h}{h} \cos(\phi_h + h\theta_p + h\omega t) \qquad 5.5$$

To simplify

$$\begin{aligned} \hat{V}_h \cos(\phi_h + h\theta_p + h\omega t) &= \hat{V}_j \cos(\phi_h + h\theta_p)\cos(h\omega t) \\ &\quad - \hat{V}_h \sin(\phi_h + h\theta_p)\sin(h\omega t) \\ &= A_{ph} \cos(h\omega t) - B_{ph} \sin(h\omega t) \end{aligned} \qquad 5.6$$

where

$$A_{ph} = \hat{V}_h \cos(\phi_h + h\theta_p) \qquad 5.7$$

$$B_{ph} = \hat{V}_h \sin(\phi_h + h\theta_p) \qquad 5.8$$

This makes equation 5.5 become

$$I_t(t) = C - \frac{1}{\omega L} \sum_h \frac{1}{h} (A_{ph} \cos(h\omega t) + B_{ph} \sin(h\omega t)) \qquad 5.9$$

The integration constant C can be found by setting t to zero, i.e.,

$$C = I_t(0) + \frac{1}{\omega L} \sum_h \frac{1}{h} A_{ph} \qquad 5.10$$

where $I_t(0)$ is the current at the beginning of the commutation.

5.2.2 Calculating the D.C. Voltage

With valves 1 and 2 conducting $V_d = V_t$. Similarly, when valves 3 and 4 are conducting $V_d = - V_t$. Otherwise $V_d = 0$. At any instant

$$V_t(t) = \sum_h \hat{V}_h \sin(\phi_h + h\theta_1 + h\omega t) \qquad 5.11$$

$$= \sum_h A_{1h} \sin(h\omega t) + B_{1h} \cos(h\omega t) \qquad 5.12$$

where t is referenced to θ_1 and A_{1h} and B_{1h} are calculated using equations 5.7 and 5.8.

5.2.3 Calculating the A.C. Current and D.C. Voltage Samples

For fully controlled convertors the valves are fired in pairs, being delayed by an angle alpha after the zero crossing. This is described in figure 5.11.

During the commutation process the d.c. voltage drops to zero and the a.c. current injection, I_t, reverses direction. Two commutations per cycle occur in a fully controlled convertor. Table 5.4 shows a complete cycle of the a.c. current injections and d.c. voltage waveforms for a fully controlled convertor.

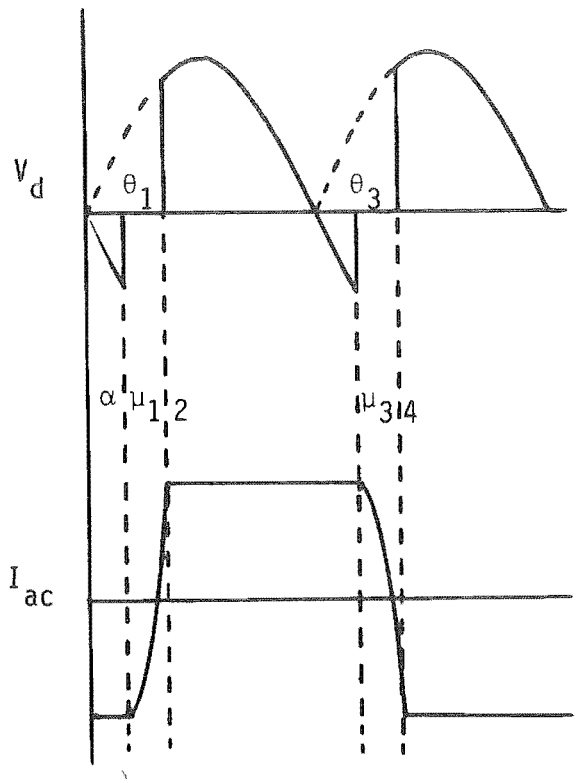

Figure 5.11 : Fully Controlled A.C. Current and D.C. Voltage Waveforms

Table 5.4 : A.C. Current and D.C. Voltage Waveforms for a Fully Controlled Convertor

Section	I_{ac}	V_{dc}	Limits, reference to 01		
1	I_c	0	0	$< \omega t <$	μ_{12}
2	I_d	V_t	μ_{12}	$< \omega t <$	$\theta_3 - \theta_1$
3	I_c	0	$\theta_3 - \theta_1$	$< \omega t <$	$\theta_3 - \theta_1 + \mu_{34}$
4	$-I_d$	$-V_t$	$\theta_3 - \theta_1 + \mu_{34}$	$< \omega t <$	2π

Half control is achieved by setting the delay angles for valves 1 and 3 equal to zero, effectively making them into diodes. Valves 2 and 4 are fired in the usual way after the specified delay angle. Thus, if valve 1 and 2 are conducting, valve 3 will commutate on when it becomes forward biased, causing valve 1 to turn off. This

gives rise to four commutations per cycle, as described in figure 5.12.

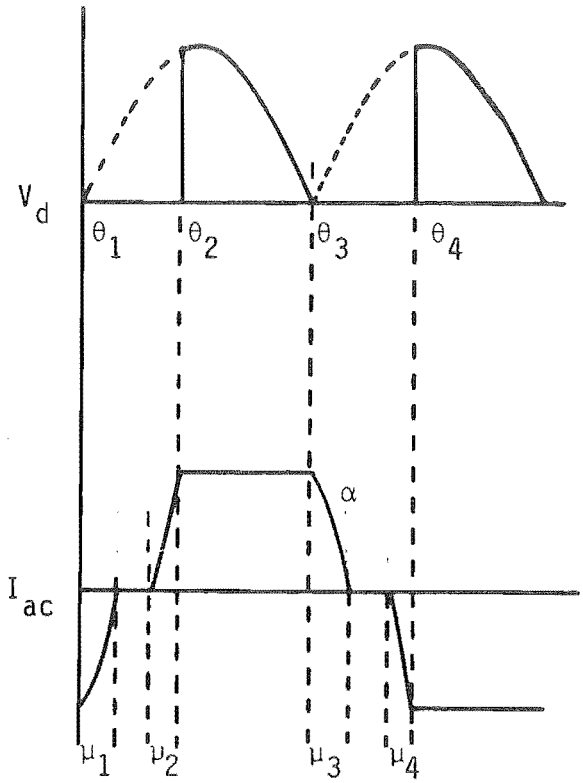

Figure 5.12 : Half Controlled A.C. Current and D.C. Voltage Waveforms

Table 5.5 shows a complete cycle of the a.c. current injections and d.c. voltage waveforms for a half controlled convertor.

Table 5.5 : A.C. Current and D.C. Voltage Waveforms for a Half Controlled Convertor

Section	I_{ac}	V_{dc}	Limits, reference to θ_1		
1	I_c	0	0	$< \omega t <$	μ_1
2	0	0	μ_1	$< \omega t <$	α
3	I_c	0	α	$< \omega t <$	$\alpha + \mu_2$
4	I_d	V_t	$\alpha + \mu_2$	$< \omega t <$	$\theta_3 - \theta_1$
5	I_c	0	$\theta_3 - \theta_1$	$< \omega t <$	$\theta_3 - \theta_1 + \mu_3$
6	0	0	$\theta_3 - \theta_1 + \mu_3$	$< \omega t <$	$\theta_3 - \theta_1 + \alpha$
7	I_c	0	$\theta_3 - \theta_1 + \alpha$	$< \omega t <$	$\theta_3 - \theta_1 + \alpha + \mu_4$
8	$-I_d$	$-V_t$	$\theta_3 - \theta_1 + \alpha + \mu_4$	$< \omega t <$	2π

However, if the delay angle is sufficiently small with half control, the first and second, and similarly, the third and fourth, commutations merge to give the same waveforms as a fully controlled convertor operating on a zero delay angle. If the delay angle is close to 180° then no commutation is complete and the d.c. voltage is zero for a complete cycle. This situation is ignored as this is not a practical operating state.

5.2.4 Results and Conclusions of Modelling Single Phase Convertors

The iterative algorithm of chapter 3 was modified and used by a final year project student, C.D. Callaghan. A summary of his results and conclusions are given in Appendix A7.

5.3 FUTURE WORK

The development of a detailed positive sequence admittance matrix representation of the feeder system has been discussed in section 5.1. Similarly, section 5.2 has given a detailed description of the operation of the locomotive's convertors.

For the analysis of the interaction between single phase convertors and their associated a.c. and d.c. systems, the a.c. system has been modelled either as a pure inductance or with data obtained from a three phase industrial busbar. This was for simplicity and because of a lack of data for a traction feeder system. However the a.c. system representation can be improved considerably by evaluating the impedance looking into the feeder system at the pantograph using a similar admittance matrix to that formed in section 5.1.

Because the locomotive transformer is already included into the a.c. system of the single phase iterative algorithm, this should

be removed from the feeder system admittance matrix before calculating its impedance. Similarly, if power factor correction is included on the secondary of the locomotive transformer, this should also be included in the a.c. system admittance matrix within the iterative algorithm. This leaves the locomotive pantographs, the left and right line terminations and the two substation busbars.

The inclusion of the power factor correction components on the secondary of the locomotive transformer may also affect the calculation of the commutation currents in the iterative algorithm. However, because the power factor series inductor/capacitor combination is tuned at about 90 Hz, their effect on the commutation process can be ignored.

Because not all the necessary convertor data and controller information was available, the operation of the proposed locomotives and feeder system could not be modelled. However, if more data is made available for both the locomotive and the feeder system, work in this area could continue.

CHAPTER 6

HARMONIC NORTON EQUIVALENT OF THE SYNCHRONOUS MACHINE FOR ANALYSIS IN THE HARMONIC SPACE

6.1 INTRODUCTION

The harmonic behaviour of the synchronous machine has not been given serious consideration in harmonic analysis (Densem et al 1984), even though it is well known that it converts negative sequence currents into third harmonic voltage (Clarke 1950), and, in general, acts as a harmonic convertor. This is probably because of the complexity of the problem and the fact that the conversion means coupling between harmonics that are otherwise considered separately. Therefore, synchronous machines are often represented by a single impedance, based on the subtransient reactances or the negative sequence reactance (Densem 1983).

Therefore, to a greater or lesser extent every synchronous machine acts as a harmonic source, as a harmonic impedance and a harmonic convertor.

The behaviour of the synchronous machine as a harmonic generator is well understood (Arrillaga et al 1985a) and the generated harmonic emf's are normally reduced to insignificant levels by appropriate machine design. In present harmonic flow analysis, or harmonic penetration studies, the synchronous machines are represented by inductor/resistor combinations derived empirically, i.e., the frequency conversion process is ignored. However, as part of any practical power system the synchronous machine is always subjected to some imbalance as well as imperfect external voltage and current waveforms that will excite the mechanism of harmonic conversion.

6.1.1 The Mechanism of Harmonic Conversion

When a positive sequence current of harmonic order h enters the stator of a perfectly non-salient synchronous machine a flux of harmonic order h-1 is set up in the rotor which, in turn, induces a stator voltage of the original harmonic order h and the same sequence. Similarly, a negative sequence current of order h produces a flux of order h+1 in the rotor which induces a negative sequence voltage of the original order h.

However, for a perfectly salient machine the rotor flux is concentrated along the direct axis of the rotor. This flux can be decomposed into two counter rotating fields and, therefore, induces two voltages components in the stator. For the case of a positive sequence current of harmonic order h entering the stator, the rotor flux consists of two counter rotating fields of order h-1, inducing a positive sequence voltage component of order h and a negative sequence voltage component of order h-2. Similarly a negative sequence current of order h produces counter rotating rotor fields of order h+1 which induces a negative sequence voltage component of order h and a positive sequence voltage component of order h+2. For the case of a fundamental positive sequence current entering the stator the d.c. rotor flux produced is stationary with respect to the rotor and, therefore, cannot be decomposed into two counter rotating components.

An actual synchronous machine is neither purely salient nor purely non salient. In the case of a turbo-generator the rotor is round and therefore not significantly salient. However, hydro-generators and most synchronous compensators do concentrate much of the flux along the direct axis and exhibit significant saliency.

6.1.2 The d-q Model of the Synchronous Machine

Data for synchronous machines is normally available in terms of the d-q axis and implicit in this information is the effect of the second harmonic terms of the inductances (Adkins and Harley 1975 and Anderson and Fouad 1977). Information on fourth order terms, absent from the d-q model, is not generally available and is ignored from this analysis.

Inherent in the d-q differential equations are the following assumptions (O'Kelly and Simmons 1968).

1. Magnetic saturation is neglected with the self and mutual inductances of all the machine windings being independent of the magnitude of the winding currents.

2. Air-gap m.m.f.s and fluxes are represented by the fundamental components of their spatial distributions.

3. Slotting effects are ignored. Distributed windings comprise finely spread conductors of negligible diameter.

4. Magnetic materials are free of eddy currents and hysterisis losses.

Assumption 1 is accurate for a machine which is not over excited. In the case of an over excited machine the incremental values of the machine's self and mutual inductances should be used at harmonic frequencies. Assumptions 2 and 3 hold for a large machine of good design. Throughout this analysis it will be assumed that assumption 4 holds for hydro-generators with the effects of eddy currents in round rotor machines treated in section 6.4.4.

The formation of the harmonic admittance of the synchronous machine is given in section 6.2. The effect of the excitation is included as a harmonic Norton current source, and, therefore, the field winding voltage is assumed to be zero during the formulation of the admittance matrix.

6.1.3 The Synchronous Machine Model in the Harmonic Space

The d-q model can be used to derive the time variation of the steady state current and voltage waveforms of the synchronous machine (Heffernan 1980) and their harmonic content can be obtained with the help of the FFT. However, difficulties in providing sufficient accuracy for the initial conditions, coupled with the very large time constants involved, mean extremely long computer runs are required to reach a particular steady state condition. Thus the derivation of voltage and current harmonics in the time domain is a very inefficient process and there is considerable incentive in developing alternative algorithms in the harmonic space.

Because of the significance of the sequences in the harmonic conversion process, the harmonic equivalent of the synchronous machine needs to be a full three phase representation, rather than simply a single phase. Also, because the coupling between the harmonics, the harmonic equivalent of the synchronous machine needs to be defined in the harmonic space. As discussed in section 2.6, each current and voltage in the harmonic space is described by a vector containing each phase, busbar and harmonic.

The synchronous machine, with the effect of the excitation removed, can be modelled by an admittance matrix $[Y_{abc}]$ such that

$$i = Y_{abc}\, v \qquad 6.1$$

where i, Y_{abc} and v are expressed in the harmonic space. Both odd and even harmonics are considered.

Equation 6.1 can be modified to include the excitation in the form of a Norton current source, I_o. This is described in figure 6.1(a)

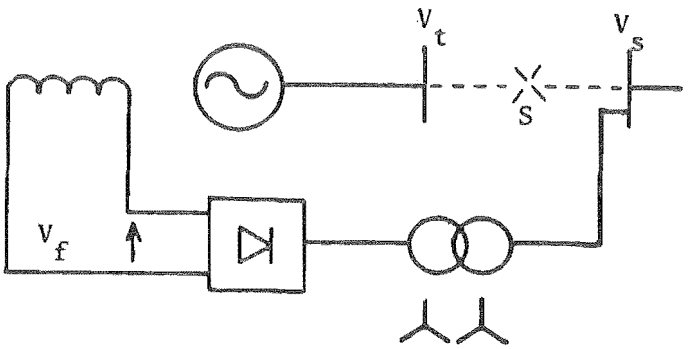

Figure 6.1(a) : Schematic diagram of exciter system

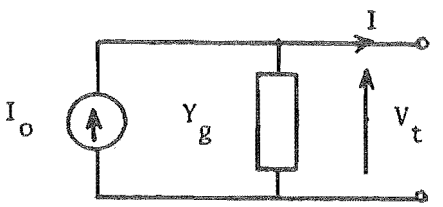

Figure 6.1(b) : Norton Equivalent of the Synchronous generator

with the current defined in the reverse direction. This gives the nodal equation

$$i = I_o - Y_{abc}\, v \qquad 6.2$$

The excitation of a synchronous machine can usually be assumed to be a purely flat d.c. voltage in the steady state. That is, any harmonic currents in the machine's windings have no effect on the field winding excitation voltage. The effect of ripple on the field voltage is examined in section 6.3.

6.1.4 Applications of the Harmonic Space Synchronous Machine Model

In this chapter the synchronous machine model derived in section 6.2 is analysed in isolation to the rest of the transmission system. Section 6.3 discusses the open circuit voltage distortion in the stator due to ripple in the field winding voltage. Similarly the characteristics of the synchronous machine model, as seen from the stator without any excitation, are discussed in section 6.4.

Chapter 7 discusses the use of the Norton harmonic equivalent model to analyse harmonic aspects of systems containing synchronous machines.

6.2 THE HARMONIC MODEL OF A SYNCHRONOUS MACHINE

6.2.1 Derivation of the Matrix Y_{dqh}

The synchronous machine admittance model is derived from the d,q-axis differential equations. Generally accepted conventions and notations are used (O'Kelly and Simmons 1968). With two damper windings in the rotor, s and t, the equations are:

$$\begin{aligned} v_d &= Ri_d + p(L_d i_d + M_{df} i_f + M_{ds} i_s) - \omega(L_q i_q + M_{qt} i_t) \\ v_q &= Ri_q + p(L_q i_q + M_{qt} i_t) + \omega(L_d i_d + M_{df} i_f + M_{ds} i_s) \end{aligned} \qquad 6.3'$$

$$\begin{aligned} v_f &= R_f i_f + p(L_f i_f + M_{df} i_d + M_{fs} i_s) = 0 \\ v_s &= R_s i_s + p(L_s i_s + M_{ds} i_d + M_{fs} i_f) = 0 \\ v_t &= R_t i_t + p(L_t i_t + M_{qt} i_q) = 0 \end{aligned} \qquad 6.3''$$

In equations 6.3, V_f has been set to zero for the calculation of the synchronous machine admittance matrix because the field voltage will be considered in the Norton current source.

All variables are phasors of harmonic h:

$$w_h = \mathrm{Re}\left\{W_h\, e^{jh\omega t}\right\} = W'_h \cos(h\omega t) - W''_h \sin(h\omega t) \qquad 6.4'$$

where

$$W_h = W'_h + j\, W''_h \qquad 6.4''$$

denotes any phasor. With

$$p = jh\omega \qquad 6.5$$

equations 6.3 becomes algebraic equations in V_{dh}, V_{qh}, I_{dh}, I_{qh}, I_{fh}, I_{sh} and I_{th}. The last three can be eliminated from 6.3', using 6.3'', so that

$$\begin{bmatrix} V_{dh} \\ V_{qh} \end{bmatrix} = \begin{bmatrix} Z_{1h} & Z_{2h} \\ Z_{3h} & Z_{4h} \end{bmatrix} \begin{bmatrix} I_{dh} \\ I_{qh} \end{bmatrix} \qquad 6.6$$

or, in a more compact form

$$V_{dqh} = Z_{dqh}\, i_{dqh} \qquad 6.7$$

and

$$i_{dqh} = Y_{dqh}\, v_{dqh}$$

For simplicity, the elements of the non-symmetric matrices Z_{dqh} or Y_{dqh} are denoted by

$$\begin{bmatrix} a_h & b_h \\ c_h & d_h \end{bmatrix} \qquad 6.8$$

A particular matrix Z_{dqh} of interest is for the rotor frequency h = 0. Then p becomes zero and equations 6.3 yield

$$Z_{dqo} = \begin{bmatrix} R & -\omega L_q \\ \omega L_d & R \end{bmatrix} \qquad 6.8'$$

6.2.2 Derivation of Connection Matrix C and of C^{-1}

The voltages in the d,q-axis can be transformed to the α,β-axis of two-phase stator coordinates by

$$\begin{bmatrix} v_{\alpha h'} \\ v_{\beta h'} \end{bmatrix} = \begin{bmatrix} \cos\omega t & -\sin\omega t \\ \sin\omega t & \cos\omega t \end{bmatrix} \begin{bmatrix} v_{dh} \\ v_{qh} \end{bmatrix} \qquad 6.9'$$

where h' denotes the resultant harmonics. The inverse transformation is

$$\begin{bmatrix} v_{dh'} \\ v_{qh'} \end{bmatrix} = \begin{bmatrix} \cos\omega t & \sin\omega t \\ -\sin\omega t & \cos\omega t \end{bmatrix} \begin{bmatrix} v_{\alpha h} \\ v_{\beta h} \end{bmatrix} \qquad 6.9''$$

An identical transformation applies for currents. If

$$v_{dh} = V'_{dh}\cosh\omega t - V''_{dh}\sinh\omega t \qquad 6.10'$$

$$v_{qh} = V'_{qh}\cosh\omega t - V''_{qh}\sinh\omega t \qquad 6.10''$$

and substitute 6.10 into 6.9′ we obtain expressions for $v_{\alpha h}$ and $v_{\beta h}$ in the form 6.4, with $h' = h \pm 1$:

$$\begin{aligned} V_{\alpha h} &= V'^{h}_{\alpha h-1} \cos(h-1)\omega t - V''^{h}_{\alpha h-1} \sin(h-1)\omega t \\ &+ V'_{\alpha h+1} \cos(h+1)\omega t - V''_{\alpha h+1} \sin(h+1)\omega t \end{aligned} \qquad 6.11'$$

$$\begin{aligned} V_{\beta h} &= V'^{h}_{\beta h-1} \cos(h-1)\omega t - V''^{h}_{\beta h-1} \sin(h-1)\omega t \\ &+ V'^{h}_{\beta h+1} \cos(h+1)\omega t - V''^{h}_{\beta h+1} \sin(h+1)\omega t \end{aligned} \qquad 6.11''$$

where

$$\begin{aligned} V'^{h}_{\alpha h-1} &= \tfrac{1}{2}(V'_{dh} + V''_{qh}) & V''^{h}_{\alpha h-1} &= \tfrac{1}{2}(V''_{dh} - V'_{qh}) \\ V'^{h}_{\alpha h+1} &= \tfrac{1}{2}(V'_{dh} - V''_{qh}) & V''^{h}_{\alpha h+1} &= \tfrac{1}{2}(V''_{dh} + V'_{qh}) \end{aligned} \qquad 6.12'$$

and

$$\begin{aligned} V'^{h}_{\beta h-1} &= \tfrac{1}{2}(-V''_{dh} + V'_{qh}) & V''^{h}_{h-1} &= \tfrac{1}{2}(V'_{dh} + V''_{qh}) \\ V''^{h}_{\beta h+1} &= \tfrac{1}{2}(V''_{dh} + V'_{qh}) & V''^{h}_{\beta h+1} &= \tfrac{1}{2}(-V'_{dh} + V''_{qh}) \end{aligned} \qquad 6.12''$$

These can be combined into phasors, as in 6.4″ yielding:

$$\begin{aligned} V^{h}_{\alpha h-1} &= \tfrac{1}{2}(V_{dh} - jV_{dh}) \\ V^{h}_{\alpha h+1} &= \tfrac{1}{2}(V_{dh} + jV_{qh}) \end{aligned} \qquad 6.13'$$

and

$$\begin{aligned} V^{h}_{\beta h-1} &= \tfrac{1}{2}(jV_{dh} + V_{qh}) \\ V^{h}_{\beta h+1} &= \tfrac{1}{2}(-jV_{dh} + V_{qh}) \end{aligned} \qquad 6.13''$$

In equations 6.11, 6.12 and 6.13 the superscript h indicates the related d,q-axis harmonic for a component of order h±1 of a stator (α,β-axis) harmonic. When two such components of the same order (related to a lower and a higher order rotor harmonic) combine, the superscript is dropped; see the vector 6.16′.

Equations 6.13 should be written for all h. However, if h=0 or h-1=0 then $V_0 = V'_0$. If h=0 then we obtain directly from 6.9′

converted into phasor relations,

$$V_{\alpha 1} = V_{d0} + jV_{q0} \qquad 6.14'$$

$$V_{\beta 1} = jV_{d0} + V_{q0} \qquad 6.14''$$

By assembling equations 6.13 and taking 6.14 into account, we obtain

$$v_{\alpha\beta} = Cv_{dq} \qquad 6.15'$$

An identical transformation applies for currents:

$$i_{\alpha\beta} = Ci_{dq} \qquad 6.15''$$

In 6.15

$$v_{\alpha\beta} = [V_{\alpha 0}, V_{\beta 0}, V_{\alpha 1}, V_{\beta 1}, V_{\alpha 2}, V_{\beta 2}, \ldots V_{\alpha n}, V_{\beta n}]^T \qquad 6.16'$$

$$v_{dq} = [V_{d0}, V_{q0}, V_{d1}, V_{q1}, V_{d2}, V_{q2}, \ldots V_{dn}, V_{qn}]^T \qquad 6.16''$$

and

$$C = \frac{1}{2}\begin{bmatrix} N & & & & & & \\ 2M & N & & & & & \\ M & & N & & & & \\ & M & & & & & \\ & & & N & & & \\ & & & M & & N & \\ & & & & M & & \end{bmatrix} \qquad 6.17'$$

with

$$M = N^* = \begin{bmatrix} 1 & j \\ -j & 1 \end{bmatrix} \qquad 6.17''$$

where the asterisk denotes the conjugate and n the highest harmonic investigated.

The matrix C is singular because it contains two redundant variables, one at d.c. and the other at the maximum harmonic considered.

At d.c.

$$V^{0}_{\alpha 1} = V_{do} + jV_{90} = - jV^{0}_{\beta 1}$$

at h=n

$$V^{n}_{\alpha n-1} = \frac{1}{2}(V_{dn} - jV_{qn}) = jV^{n}_{\beta n-1}$$

Also at d.c.

$$V^{1}_{\beta 0} = \frac{1}{2}(jV_{d1} + V_{q1}) = jV^{1}_{\alpha 0}$$

similarly at h=n

$$V^{n-1}_{\beta n} = \frac{1}{2}(-jV_{dn-1} + V_{qn-1}) = -jV^{n-1}_{\alpha n}$$

This singularity of C could of course be removed by keeping only a reduced number of variables. It is preferable, however, to preserve the symmetry and simplicity of the full matrix C of 6.17. An inverse relationship to 6.15 can then be derived starting with equation 6.9 and performing calculations as in equations 6.10 to 6.14.

This gives

$$v_{dq} = C^{*}v_{\alpha\beta} \qquad 6.18'$$

$$i_{dq} = C^{*}i_{\alpha\beta} \qquad 6.18''$$

6.2.3 Derivation of Matrix $Y_{\alpha\beta}$

Equations 6.7″ are assembled for all h, into the relation

$$i_{dq} = Y_{dq}v_{dq} \qquad 6.19$$

where Y_{dq} is block diagonal with blocks of the form 6.8.

Equations 6.18′, 6.19 and 6.15″ can be combined to give

$$i_{\alpha\beta} = Y_{\alpha\beta}v_{\alpha\beta} \qquad 6.20$$

where

$$Y_{\alpha\beta} = CY_{dq}C^{*} \qquad 6.21$$

The non-symmetric matrix Y has the form

$$Y_{\alpha\beta} = \begin{bmatrix} A_0 & B''_1 & & & & & \\ & A_1 & B''_2 & & & & \\ B'_1 & & A_2 & & & & \\ & B'_2 & & & B''_h & & \\ & & & A_h & & & \\ & & B'_h & & & B''_{n-1} & \\ & & & & A_{n-1} & & \\ & & & B'_{n-1} & & A_n & \end{bmatrix} \qquad 6.22$$

where

$$\begin{aligned} A_0 &= NY_{dq1}N/2 \\ A_1 &= (2MY_{dq0}M + NY_{dq2}N)/4 \\ A_h &= (MY_{dqh-1}M + NY_{dqh+1}N)/4 \quad (\text{for } h=2,\ldots,n-1) \\ B'_1 &= MY_{dq1}N/2 \\ B'_h &= MY_{dqh}N/4 \quad (\text{for } h=2,\ldots,n-1) \\ B''_h &= NY_{dqh}M/4 \quad (\text{for } h=1,\ldots,n-1) \\ A_n &= MY_{dqn-1}M/4 \end{aligned} \qquad 6.23$$

These expressions can be calculated from:

$$\begin{aligned} MY_{dqi}M &= ((a_i+d_i) - j(b_i-c_i))M \\ NY_{dqi}N &= ((a_i+d_i) + j(b_i-c_i))N \\ MYd_{qi}N &= ((a_i-d_i) + j(b_i+c_i))P \\ NY_{dqi}M &= ((a_i-d_i) - j(b_i+c_i))Q \end{aligned} \qquad 6.24$$

where

$$P = \begin{bmatrix} 1 & -j \\ -j & -1 \end{bmatrix}, Q = \begin{bmatrix} 1 & j \\ j & -1 \end{bmatrix} \qquad 6.25$$

From equations 6.23 it can be seen that the self admittance A_h for the harmonic of order h depends only on the rotor frequencies of order h±1, and the mutuals B'_h and B''_h between harmonics h+1 and h-1

depend on the rotor frequency of order h. These results are consistent with the well known physical phenomena. An intuitive block diagram of the voltage and current harmonic relationships in the armature and rotor is shown in Figure 6.2.

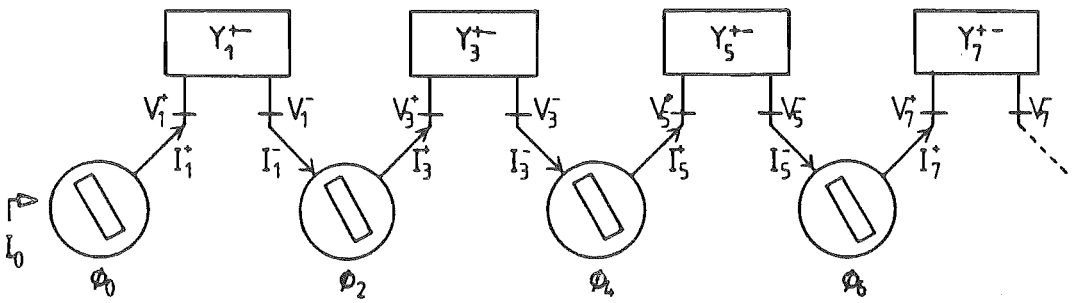

Figure 6.2 : Harmonic Interaction Between Synchronous Machine and the System

The matrix $Y_{\alpha\beta}$ has one non-zero block band on each side of the diagonal and a zero block separating band. Therefore, even and odd harmonics do not interact in the synchronous machine.

The impedance matrix $Z_{\alpha\beta}$ can be obtained similarly to 6.21:

$$Z_{\alpha\beta} = C\ Z_{dq}\ C^* \qquad 6.26$$

6.2.4 Derivation of Matrix Y_{abc}

Firstly, $Y_{\alpha\beta}$ is augmented by a zero sequence diagonal matrix, comprising all harmonics:

$$Y_{\alpha\beta 0} = \begin{bmatrix} Y_{\alpha\beta} & \\ & Y_0 \end{bmatrix} \qquad 6.27$$

It is generally assumed that zero sequence currents produce no significant resultant flux in the air-gap and accordingly equation 6.27 shows no coupling between the zero sequence and the α,β components. Jones (1967) discusses coupling with the zero sequence, but stresses that it is negligible and subsequently removes

the coupling from the analysis. Coupling between the zero sequence and the α and β components is inherently zero in the d-q synchonous machine equations 6.3.

For any harmonic

$$\begin{aligned} v_{\alpha\beta 0h} &= T_h v_{abch} \\ i_{\alpha\beta 0h} &= T_h i_{abch} \end{aligned} \qquad 6.28$$

where

$$T_h = \begin{bmatrix} 1 & -\frac{1}{2} & -\frac{1}{2} \\ 0 & \frac{\sqrt{3}}{2} & -\frac{\sqrt{3}}{2} \\ \frac{1}{3} & \frac{1}{3} & \frac{1}{3} \end{bmatrix} \qquad 6.29'$$

The inverse of T_h is

$$T_h^{-1} = \begin{bmatrix} \frac{2}{3} & 0 & 1 \\ -\frac{1}{3} & \frac{1}{\sqrt{3}} & 1 \\ -\frac{1}{3} & \frac{1}{\sqrt{3}} & 1 \end{bmatrix} \qquad 6.29''$$

Equations 6.27, 6.28 and 6.29 can be completed and combined to yield

$$\begin{aligned} v_{\alpha\beta 0} &= T v_{abc} \\ i_{\alpha\beta 0} &= Y_{\alpha\beta 0} v_{\alpha\beta 0} \\ i_{abc} &= T^{-1} i_{\alpha\beta 0} \end{aligned} \qquad 6.30$$

An admittance matrix

$$Y_{abc} = T^{-1} Y_{\alpha\beta 0} T \qquad 6.31'$$

is evaluated and of the same form as 6.1, with the subscripts abc having omitted from v and i. That is

$$i = Y_{abc} v \qquad 6.31''$$

6.2.5 Calculation of the Norton Current

In figure 6.1(a) V_{sys}, the system voltage, is applied to the exciter via a star/star transformer. From V_{sys} and the exciter bridge delay angle the harmonic content of the field voltage V_f can be calculated, including the d.c. component V_{fo}. The Norton current, I_o, is calculated in d-q quantities from the machine parameters and field voltage, then transformed into phase quantities and applied to the generator, as in figure 6.1(b).

The current injection I_o of the Norton equivalent of figure 6.1(b) consists of a specified fundamental frequency current, derived from the d.c. excitation to maintain a particular terminal voltage, and an unwanted harmonic contribution caused by the ripple content of the excitation voltage waveform.

The relative importance of the excitation voltage harmonics can be assessed with the generator isolated from the system, i.e., with switch S open in figure 6.1(a). Moreover, the presence of any practical harmonic distortion in the system voltage will have negligible effect on the rectified voltage waveform. V_{sys} is therefore assumed perfectly sinusoidal but provision is made to show the effect of voltage imbalance.

Appencix A8 gives the equations required for the calculation of V_f from V_{sys} and the specified delay angle.

A transfer function from field voltage harmonics to the dq axis Norton currents can be derived from the equations 6.3, presented in a simplified form in equation 6.32.

$$\begin{bmatrix} V_{dqf} \\ V_{st} \end{bmatrix} = \begin{bmatrix} M_1 & M_2 \\ M_3 & M_4 \end{bmatrix} \begin{bmatrix} I_{dqf} \\ I_{st} \end{bmatrix} \qquad 6.32$$

As the 2 damper circuits are shorted, $V_s = V_t = 0$, equation 6.32 can be reduced to

$$V_{dqf} = (M_1 - M_2 M_4^{-1} M_3)\, i_{dqf} \qquad 6.33$$

or

$$V_{dqf} = Z_h I_{dqf} \qquad 6.34$$

The direct and quadrature axis Norton currents, found by shorting the stator (i.e., $V_{term} = 0$ or $V_d = V_q = 0$), can be expressed as

$$I_{dNorton} = \sigma_f Y_{df} V_f \qquad 3.35$$

$$I_{qNorton} = \sigma_f Y_{qf} V_f \qquad 3.36$$

where σ_f is a constant to include the different voltage base and operating delay angle and is calculated to give the 1 p.u. terminal voltage at a specified delay angle.

The Norton current required is calculated in phase quantities from figure 6.1(b).

$$I_o = Y_{abc} V_+ \qquad 6.37$$

where V_+ is the specified positive sequence fundamental voltage. With d.c. in the rotor, and an open circuited stator, I_{qo} is negligible and the d.c. component of the direct axis Norton current can be approximated to

$$I_{doNorton} = 1.5|I_o| \qquad 6.38$$

where the 1.5 is due to the transformation from phase to dq quantities. The value of σ_f is calculated from equations 6.35 and 6.38, i.e.,

$$\sigma_f = \frac{I_{doNorton}}{Y_{dfo} V_{fo}} \qquad 6.39$$

With σ_f known and the values of V_f, Y_{df} and Y_{qf} derived for each frequency, the $I_{dNorton}$ and $I_{qNorton}$ spectra can be calculated

from equations 6.35 and 6.36. From these currents the I_o of figure 6.1(b) can be calculated in phase quantities, including the harmonic components due to the ripple in the field voltage.

Finally the terminal voltage can be found by solving

$$I_o = Y_{abc} V_{term} \qquad 3.40$$

which is similar to equation 6.37 except that I_o is specified and contains harmonics (as described above) and is solved for V_{term}.

6.3 OPEN CIRCUIT VOLTAGES

Equation 6.40 has been used to assess the levels of open circuit emf distortion caused by ripple of the rectified exciter voltage waveform on two typical generators. Data for the two machines is given in table 6.1.

Table 6.1 : Data for the Two Test Machines
(All data in p.u.)

(i) A 100 MVA hydro machine (Hwang 1969)

(ii) A 100 MVA turbo generator (Anderson and Fouad 1977)

	Hydro Machine	Round Rotor Machine
R	.005	.001096
R_f	.0005	.000742
R_s	.02	.0131
R_t	.02	.0540
L_d	1.2	1.70
L_q	0.8	1.64
L_f	1.2	1.65
L_s	1.0	1.605
L_t	0.831	1.526
M_{df}	1.0	1.55
M_{ds}	1.0	1.55
M_{qt}	0.6	1.49
M_{fs}	1.0	1.55
L''_d	0.2	0.185
L''_q	0.367	0.185

With a balanced system voltage and a firing angle of 85° the round rotor machine produced .023% and .031% harmonic emf's for the -5th and +7th harmonics respectively. For the same conditions the hydro generator only produced .002% levels of +5th and +7th harmonic emf's.

The addition of 4% imbalance (negative sequence) to the system voltage resulted in the appearance of some second harmonic on the field voltage, which then produced third harmonic positive sequence in the stator. The magnitude of the third harmonic with a delay angle of 75° was .148% for the round rotor machine and .028% for the hydro machine.

Thus the effect of excitation voltage ripple is small. Relatively large values of field resistance R_f or damper resistances R_s, R_t will increase the harmonic levels. However, such effect is not significant with large synchronous generators and the Norton equivalent current injection can in most cases be assumed to consist of purely fundamental frequency.

6.4 GENERATOR HARMONIC PARAMETERS

The response of the synchronous generator to the presence of individual current and voltage harmonics in the stator can be better understood with reference to a series of harmonic transfer relationships described in this section.

6.4.1 Parameters Derived from Harmonic Current Injections

With reference to the general matrix equations 6.22 and 6.31" the injection of 1 per unit current of harmonic order h into the machine stator causes harmonic voltages of the same sequence and order, i.e., V_h, and also of orders V_{h-2} or V_{h+2} depending on whether the current injection is of positive or negative sequence respectively.

The harmonic admittance matrix equation 6.31" can thus be reduced to the following two:

$$\begin{vmatrix} 0 \\ I_{+h} \end{vmatrix} = \begin{vmatrix} A_{h-2} & B''_{h-1} \\ B'_{h-1} & A_{gh} \end{vmatrix} \begin{vmatrix} V_{h-2} \\ V_h \end{vmatrix} \qquad 6.41$$

$$\begin{vmatrix} I_{-h} \\ 0 \end{vmatrix} = \begin{vmatrix} A_h & B''_{h+1} \\ B'_{h+1} & A_{h+2} \end{vmatrix} \begin{vmatrix} V_h \\ V_{h+2} \end{vmatrix} \qquad 6.42$$

Various empirical equivalent impedances have been proposed to represent synchronous generators in harmonic penetration studies. Ross and Smith (1948) used the subtransient reactance multiplied by the harmonic order and a constant power factor at all frequencies. Pesonen (1981) has suggested the use of a constant resistance in parallel, i.e., an increasing power factor with increasing frequency. Clarke (1973) has proposed a resistance proportional to frequency and a reactance varying as a 2nd order function of frequency and Northcote-Green (1973) a linear reactance and a resistance which is an unspecified function of frequency.

Equations 6.41 and 6.42 can be rearranged to give equations 6.43 and 6.44 when I_h is of positive sequence and 6.45 and 6.46 when I_h is of negative sequence.

$$V_{+h} = Z_{+h}^{+h} I_{+h} \qquad 6.43$$

$$V_{-(h-2)} = Z_{+h}^{-(h-2)} I_{+h} \qquad 6.44$$

$$V_{-h} = Z_{-h}^{-h} I_{-h} \qquad 6.45$$

$$V_{+h+2} = Z_{-h}^{h+2} I_{-h} \qquad 6.46$$

where

$$Z_{+h}^{+h} = [A_h - B'_{h-1} (A_{h-2})^{-1} B''_{h-1}]^{-1} \qquad 6.47$$

$$Z_{+h}^{-(h-2)} = [B'_{h-1} - A_h (B''_{h-1})^{-1} A_{h-2}]^{-1} \qquad 6.48$$

$$Z_{-h}^{-h} = [A_h - B''_{h+1} (A_{h+2})^{-1} B'_{h+1}]^{-1} \qquad 6.49$$

$$Z_{-h}^{+h+2} = [B''_{h+1} - A_h (B'_{h+1})^{-1} A_{h+2}]^{-1} \qquad 6.50$$

The subscripts of the impedances refer to the harmonic order of the current injection, the superscript to the harmonic order of the voltage produced and the sign of subscripts and superscripts refer to the sequence (i.e., + for positive sequence).

Z^{+h}_{+h} and Z^{-h}_{-h} are defined as the open circuit harmonic impedances while $Z^{-(h-2)}_{-h}$ and Z^{h+2}_{-h} are defined as the open circuit conversion impedances.

The variation in the magnitude of these impedances with frequency is illustrated in figure 6.3 for the hydro set described in table 6.1

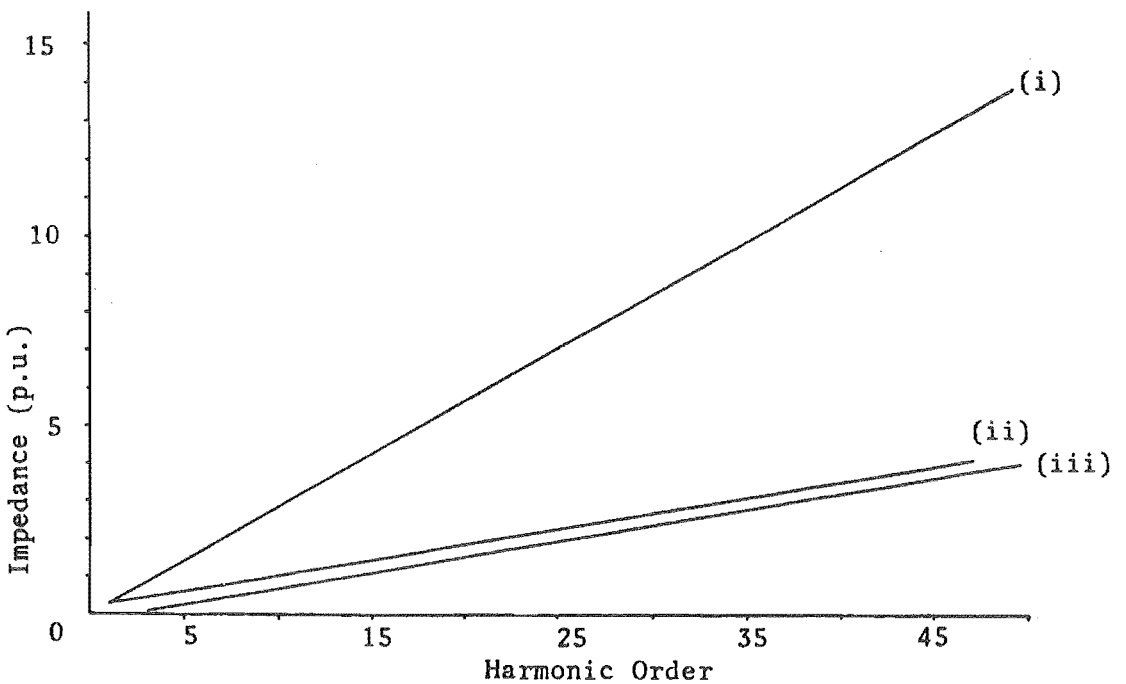

Figure 6.3 : Magnitude of the hydrogenerator harmonic impedances

(i) Z^{+h}_{+h} and Z^{-h}_{-h}

(ii) $Z^{+(h+2)}_{-h}$

(iii) $Z^{-(h-2)}_{+h}$

Figure 6.3 shows that the magnitude of the (self) harmonic inductance is very close to that of the established models (Adkins and Harley 1975), i.e.,

$$\frac{h}{2}\,(X''_d + X''_q)$$

However the magnitudes of the conversion impedances, neglected by the established models are significant. Figure 6.4 shows that the theoretical harmonic impedances are very inductive, i.e., their phase angles are higher than 87° at frequencies higher than the fundamental. However, experimental information obtained from negative sequence injection tests (Wright 1931) indicates that in practice the power factors are higher. The difference is expected to be largely due to the presence of eddy currents and the effect of these currents is added to the model for round rotor machines in section 6.4.3.

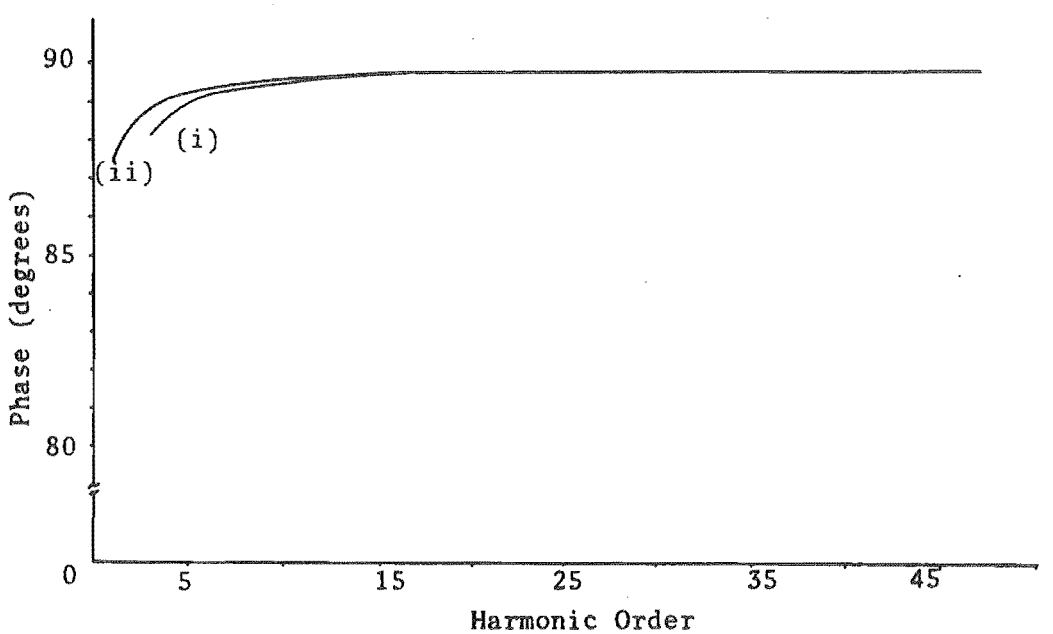

Figure 6.4 : Phase angle of the hydrogenerator harmonic impedance

(i) Phase of Z_{+h}^{+h}

(ii) Phase of Z_{-h}^{-h}

Other useful relationships are the open circuit voltage ratios, i.e.,

$$G_{-h}^{h+2} = \frac{V_{h+2}}{V_{-h}} \quad \text{for } I_{-h} \text{ negative sequence injection} \tag{6.51}$$

$$G_{+h}^{-(h-2)} = \frac{V_{-(h-2)}}{V_h} \quad \text{for } I_h \text{ positive sequence injection} \tag{6.52}$$

where

$$G_{-1}^{h+2} = A_{h+2}^{-1} B'_{h+1} \qquad 6.53$$

and

$$G_{+h}^{-(h-2)} = -A_{h-2}^{-1} B''_{h+1}$$

The variation of open circuit conversion voltage ratios (G) with frequency is shown in figure 6.5. Again the subscripts refer to sequence and harmonic order of the injected current and the superscript to the sequence and harmonic order of the resultant voltage.

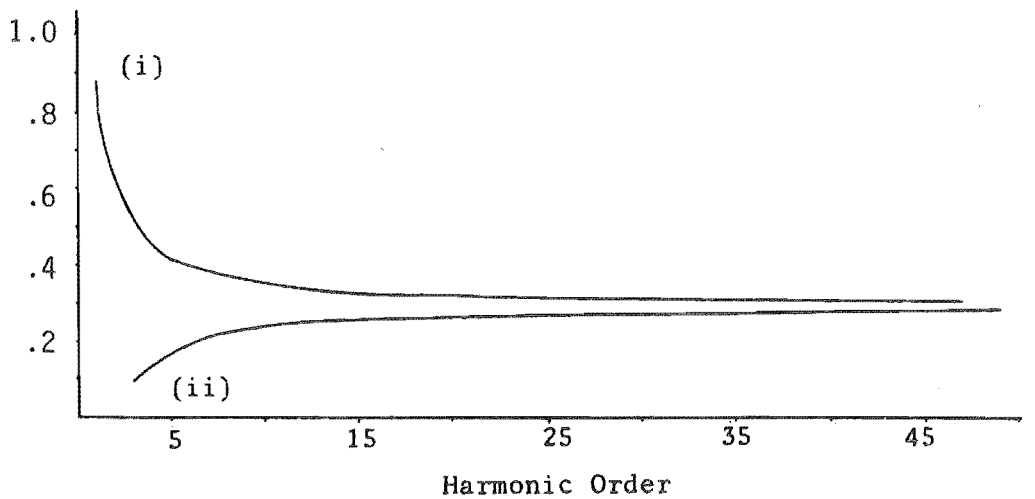

Figure 6.5 : Open circuit voltage ratios for the hydro generator

(i) G_{-h}^{h+2}

(ii) $G_{+h}^{-(h-2)}$

Corresponding results for the round rotor generator described in table 6.1 are shown in Figures 6.6 and 6.7. In this case the conversion impedances, and consequently the conversion ratios, were very small and have not been plotted in the figures.

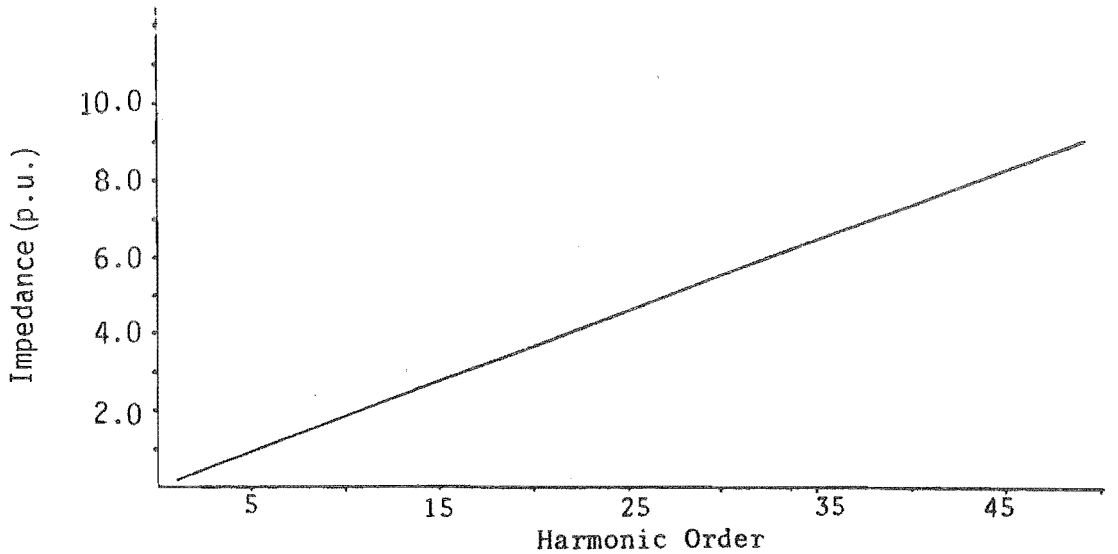

Figure 6.6 : Magnitude of the harmonic impedances of the round rotor generator (Z^{+h}_{+h} and Z^{-h}_{-h})

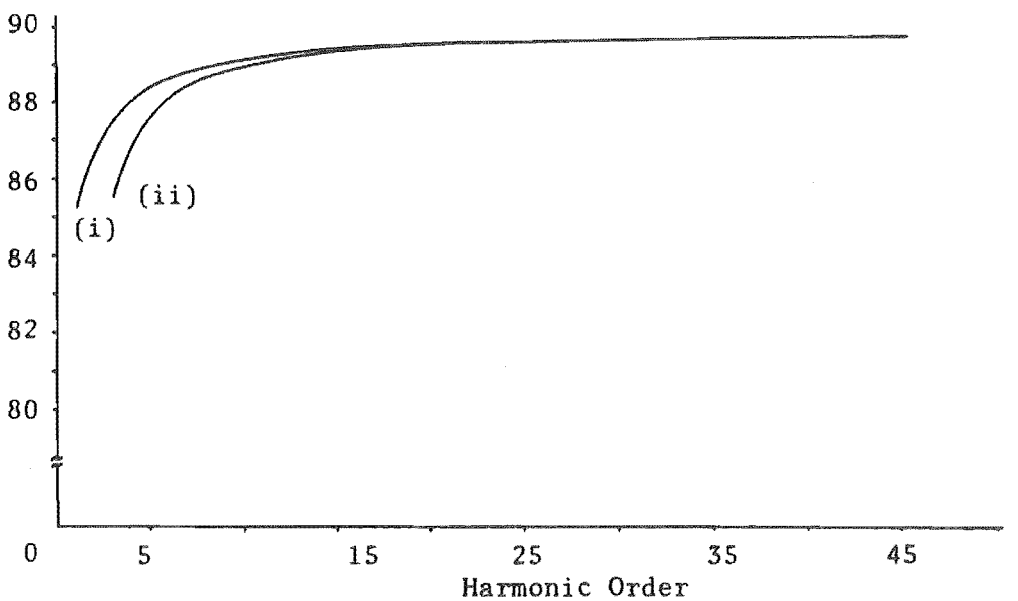

Figure 6.7 : Phase angle of the harmonic impedance of the round rotor generator

(i) Phase of Z^{+h}_{+h}

(ii) Phase of Z^{-h}_{-h}

6.4.2 Simplified Modelling

As the phase of the open circuit conversion impedances is close to -90° and that of the G^{h+2}_{-h} and $G^{-(h-2)}_{h}$ is about 180° the resistances can be neglected if desired and the following approximate harmonic conversion relationships result:

$$Z_{-h}^{h+2} = - j \frac{h+2}{2} (L''_q - L''_d) \qquad 6.55$$

$$Z_{+h}^{(h-2)} = - j \frac{h-2}{2} (L''_q - L''_d) \qquad 6.56$$

$$G_{-h}^{h+2} = - \frac{h+2}{h} \left(\frac{L''_q - L''_d}{L''_q + L''_d} \right) \qquad 6.57$$

$$G_{+h}^{-(h-2)} = - \frac{h-2}{h} \left(\frac{L''_q - L''_d}{L''_q + L''_d} \right) \qquad 6.58$$

The approximations of equations 6.55 to 6.58 agree well with the results of figures 6.3 to 6.7.

6.4.3 Parameters derived from harmonic voltage sources

If instead of the current injection of the machine stator is connected to a 1 per unit harmonic voltage source of either positive or negative sequence the harmonic matrix equations, i.e., 6.22 and 6.31" reduce to:

$$\begin{bmatrix} I_{h-2} \\ I_h \\ I_{h+2} \end{bmatrix} = \begin{bmatrix} A_{h-2} & B''_{h-1} & 0 \\ B'_{h-1} & A_h & B''_{h+1} \\ 0 & B'_{h+1} & A_{h+2} \end{bmatrix} \begin{bmatrix} 0 \\ V_h \\ 0 \end{bmatrix} \qquad 6.59$$

or

$$I_h = A_h V_h \qquad 6.60$$

$$I_{h-2} = B''_{h-1} V_h \text{ (when } I_h \text{ is of positive sequence)} \qquad 6.61$$

$$I_{h+2} = B'_{h+1} V_h \text{ (when } I_h \text{ is of negative sequence)} \qquad 6.62$$

An alternative harmonic impedance can then be derived from 6.60 such that

$$Z_h = A_h^{-1}$$

Figure 6.8 shows a comparison between Z_h and the previously calculated Z_h^h for the hydro machine. The difference is about 8% and therefore of significance. For the round rotor machine, however, the difference is negligible.

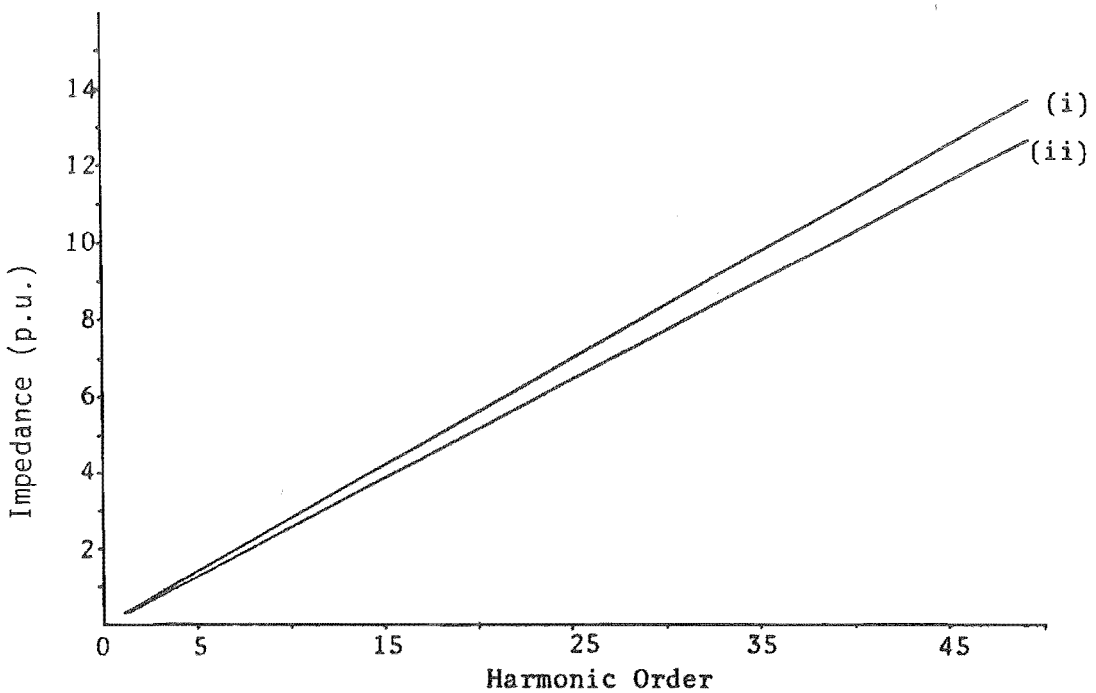

Figure 6.8 : Comparison of hydro generator impedances

(i) Derived from current injection (Z_{+h}^{+h} and Z_{-h}^{-h})

(ii) Derived from voltage application (Z_h)

Several authors (Kimbark 1956 and Adkins and Harley 1975) have used the following expression for the negative sequence reactance when the generator has a negative sequence voltage applied to it.

$$X_{-1} = \frac{2\ X''_d\ X''_q}{X''_d + X''_q} \qquad 6.63$$

At harmonic frequencies the corresponding expression would be:

$$Z_h = j\ h\ \frac{2\ X''_d\ X''_q}{X''_d + X''_q} \qquad 6.64$$

Equation (6.64) gives approximately equal results to those calculated and plotted in figure 6.8.

Similarly to the voltage ratios defined earlier the following short circuit relationships can be defined from equations 6.60, 6.61 and 6.62.

$$H_{-h}^{h+2} = I_{h+2}/I_{-h} = B'_{h+1}\, A_h^{-1} \qquad 6.65$$

$$H_{+h}^{-(h-2)} = I_{-(h-2)}/I_h = B''_{h-1}\, A_h^{-1} \qquad 6.66$$

Figure 6.9 shows that both H_{-h}^{h+2} and $H_{+h}^{-(h-2)}$ are approximately constant and equal to $\frac{X''_q - X''_d}{X''_q + X''_d}$ or .3 per unit in the test case.

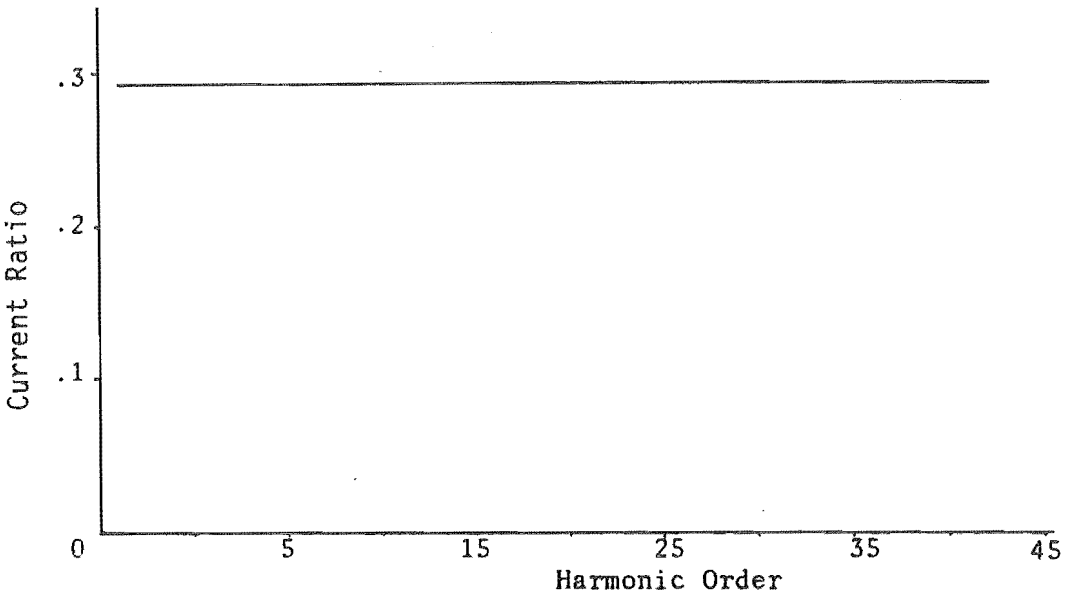

Figure 6.9 : Current ratios for the hydro generator ($H_h^{-(h-2)}$ and H_{-h}^{h+2})

6.4.4 Modification of the model to include the effect of eddy currents

The response of a solid rotor machine differs (Adkins and Harley 1975) from that predicted by equation 6.3. This is because the damper winding does not model the complicated nature of the eddy currents induced into the rotor by negative sequence and harmonic currents in the stator. Therefore the model of the round rotor generator must be modified.

In Bharali and Adkins (1963) the damper resistance and leakage reactance are replaced in each axis by sZ_{kd} where is the slip (or harmonic order in the rotor) and Z_{kd} is inversely proportional to $\sqrt{h}$ and of constant phase.

Thus the elements of the impedance matrix of equation (6.3″) are modified by

$$(R_s + jh\omega L_s) = \sqrt{h}(R_s + j\omega(L_s - M_{ds})) + jh\omega M_{ds} \qquad 6.67$$

$$(R_t + jh\omega L_s) = h(R_t + j\omega(L_t - M_{qt})) + jh\omega M_{qt} \qquad 6.68$$

This assumes that the frequencies are sufficiently high to make the resistance dominated by skin effect.

The effect of the improved model on the magnitude and phase of Z_{-h}^{-h} and Z_{+h}^{+h} is quite significant. Figure 6.10 shows that the magnitudes of Z_{+h}^{+h} (equal to the magnitude of Z_{-h}^{-h}) with the improved model and those of the basic model differ by about 15%. Figure 6.11, when compared to figure 6.7 also shows a decrease in the phases of Z_{+h}^{+h} and Z_{-h}^{-h}. Both these effects are consistent with the decrease in damper leakage reactance and increased damper resistance resulting from equations 6.67 and 6.68.

6.5 CONCLUSIONS

Existing harmonic equivalents are derived from experimental tests and the results vary considerably. Moreover, they tend to use the same expressions for the derivation of the harmonic impedances of hydro and solid rotor machines.

A general Norton equivalent circuit has been developed that represents the steady state behaviour of synchronous generators in the harmonic space. The open circuit harmonic impedances of the Norton equivalent are in reasonable agreement with the empirical harmonic impedances in current use, except for the resistive dampings which are lower in the theoretical model. Such differences have been reduced in the case of solid rotor machines by the addition of eddy current representation in the form of frequency dependent damper leakage and resistances.

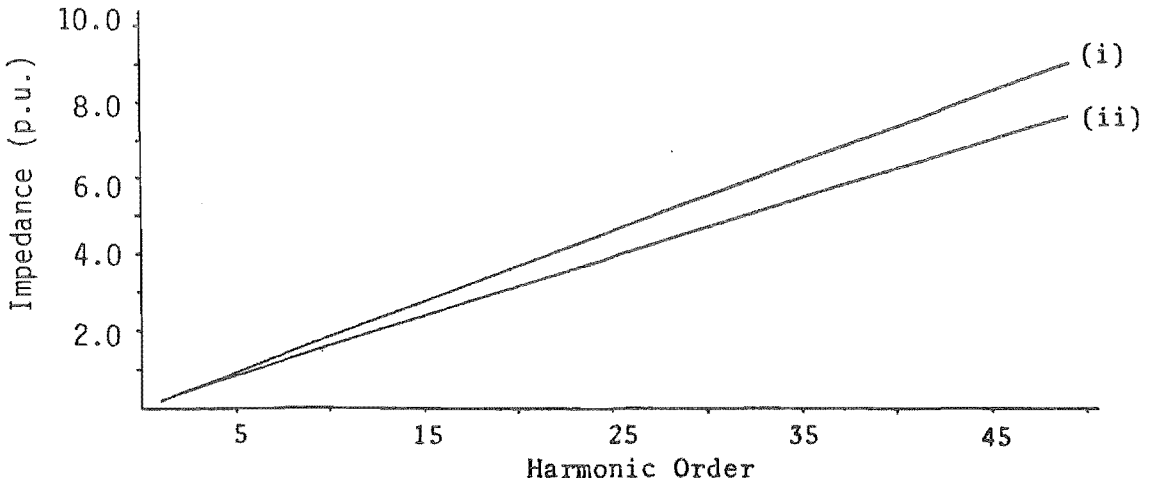

Figure 6.10 : Effect of eddy current representation on the magnitude of Z^{+h}_{+h}

(i) without eddy current

(ii) with eddy current

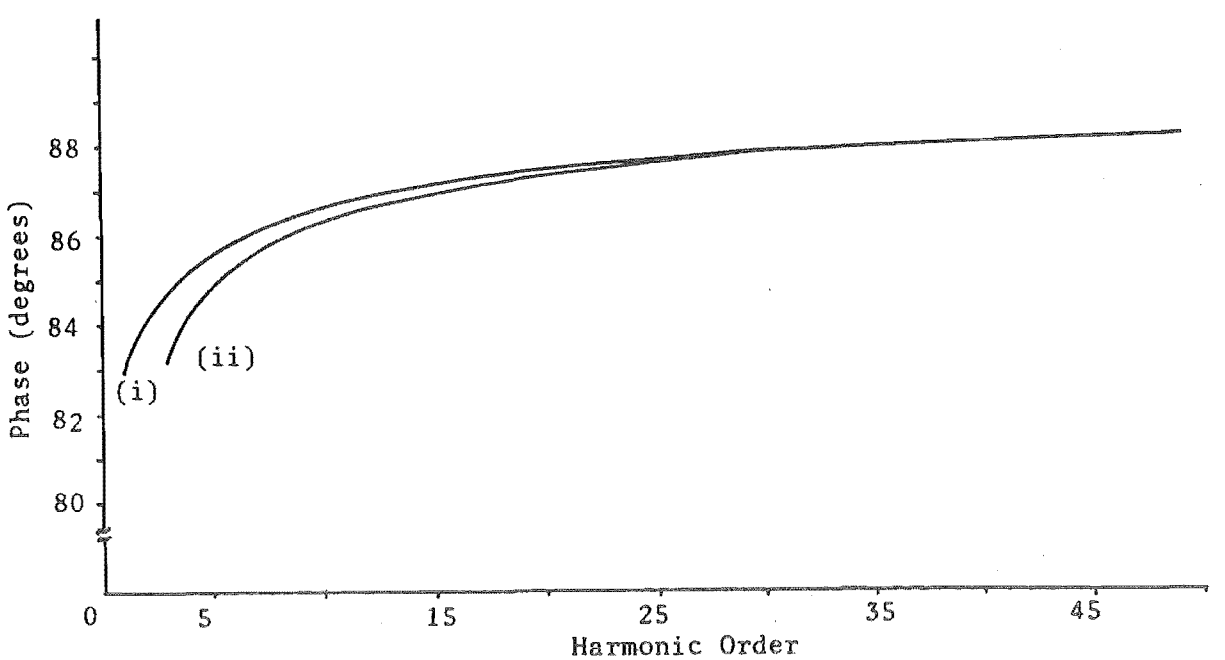

Figure 6.11 : Effect of eddy current representation on the phase of Z^{-h}_{-h} and Z^{+h}_{+h}

(i) phase of Z^{-h}_{-h}

(ii) phase of Z^{+h}_{+h}

The main contribution of the generalized model is the inclusion of the already observed but practically ignored effect of frequency conversion, which is considerable in the case of hydrogenerators. The model has also shown the existence of different harmonic impedances in the cases of voltage and current harmonic injections.

The effect of static excitation on the Norton current injection distortion has been shown to be negligible in most practical cases.

As a result of harmonic coupling the use of independent frequency harmonic flows is unrealistic. Instead, the harmonic Norton equivalent derived in this chapter should provide the means for a realistic direct solution in the harmonic space. This is discussed in chapter 7.

CHAPTER 7

APPLICATION OF THE HARMONIC NORTON EQUIVALENT OF THE SYNCHRONOUS MACHINE

7.1 INTRODUCTION

In section 6.4 the harmonic Norton equivalent of the salient poled synchronous machine, examined in isolation to any other system components, has been shown to have significant levels of coupling between frequencies. To examine the proposed synchronous machine equivalent in conjunction with other system components, and hence to show fully its potential impact on the solution of transmission system harmonic distortion, several system configurations are examined in this chapter.

As it is known that negative sequence stator currents of fundamental frequency lead to third harmonic voltage distortion, the synchronous machine model was tested with unbalanced loads. This is described in section 7.2.

In the presence of a current harmonic injection the harmonic current propagates into the system and a proportion of it will enter the stator of the machine. Due to harmonic conversion, other harmonic currents and voltages are then produced which in turn propagate throughout the system. This case is considered in section 7.3.

The largest sources of harmonic distortion in transmission systems are generally h.v.d.c. convertor stations. As many convertor stations include either generators or synchronous compensators, the effect of a synchronous machine model which includes harmonic conversion needs to be assessed. This is discussed in section 7.4.

The coupling between freaquencies, ignored in conventional harmonic flows, is discussed in section 7.5.

7.2 APPLICATION OF THE HARMONIC NORTON EQUIVALENT TO AN ASYMMETRICALLY LOADED GENERATOR

It has been shown by Clarke (1950) that under unbalanced fault conditions significant harmonic currents and voltages are produced due to harmonic conversion. In the steady state a generator is rarely unbalanced to such an extent, but under conditions of large unbalance or resonance, significant levels of distortion may arise. The presence of significant levels of third harmonic in the Souht Island of New Zealand (Hyland 1981) could be due in part to negative sequence currents entering the machine's stators.

The synchronous generator of table 6.1(1) is used as a test system with various unbalanced loads. The system, illustrated in Figure 7.1 consists of a single cirucit line of flat configuration corresponding to the Islington to Kikiwa 220 kV transmission line in the New Zealand system (Densem et al 1984). The transformer is star-g/star connected, and its rating is 100 MVA, 14 kV/220 kV, with a leakage reactance of 0.112 p.u.

Figure 7.1 : Test System

The Norton current, I_o, is a positive sequence fundamental current injection which maintains a constant (1 p.u.) positive sequence component of fundamental voltage at the generator terminals. Taking into account the sign convention indicated in figure 7.1 the generator current is

$$i = -Y_{gen}v + I_o \qquad 7.1$$

Because there is no coupling between odd and even harmonics, vectors i and v and the generator admittance matrix Y_{gen} contain only the odd harmonics of Y_{abc}.

The input impedance matrix of the system (Z_s), as seen from the generator bus, can be derived from existing programs (Arrillaga et al 1983b and Densem et al 1984), so that for each harmonic the following relationship applies

$$v_h = Z_{sh} i_h \qquad 7.2$$

and for all harmonics

$$v = Z_s i \qquad 7.3$$

where Z_s is a block diagonal matrix.

From equation 7.1

$$I_o = Y_{gen} v + i \qquad 7.4$$

However, when the excitation is perfectly smooth, I_o is only affected by positive sequence fundamental frequency current. Therefore equation 7.4 becomes

$$I_o = Y_{gen} v_+ + I_+ \qquad 7.5$$

where v_+ and i_+ are vectors in the phase frame of reference containing only the positive sequence fundamental components of v and i respectively. While v_+ is kept fixed at 1 p.u., i_+ is not known until the final solution. However i_+ can be expressed as a function of i using

$$i_+ = Ti \qquad 7.6$$

where

$$T = \frac{1}{3}$$

Fundamental			Harmonics	
1	α	α^2		
α^2	1	α	0	Fundamental
α	α^2	1		
0			0	Harmonics

7.7

Combining equations 7.1, 7.3, 7.5, 7.6 and 7.7 yields the following expression for the generator current

$$i = -Y_{gen}Z_s i + Y_{gen}v_+ + Ti \qquad 7.8$$

or

$$Ai = b \qquad 7.9$$

where

$$A = U + Y_{gen}Z_s - T$$

and

$$b = Y_{gen}v_+$$

Equation 7.9 is solved for i by Gaussian elimination and v_h is obtained from 7.2 for each harmonic.

The transmission line introduces resonance and standing wave effects which somewhat obscure the understainding of the generator harmonic contribution. Thus the problem is analyzed in three stages, i.e., with the generator connected to (i) an unbalanced resistive dummy load, (ii) an unbalanced tuned load and (iii) an untransposed transmission line via a transformer.

7.2.1 Unbalanced Resistive Load

The load is represented by the following admittance matrix

$$Y_{o+-} = \begin{bmatrix} Y_o & & \\ & Y_+ & KY_+ \\ & KY_+ & Y_+ \end{bmatrix} \qquad 7.10$$

where

Y_o is a zero sequence conductance

Y_+ is a positive (and negative) sequence conductance

K is a coupling coefficient between the positive and negative sequences.

Since the generator produces no zero sequence voltage, Y_o can be chosen arbitrarily. To prevent a singularity its value is made

equal to Y_+. Thus the three-phase admittance matrix becomes

$$Y_{abc} = Y_+ \begin{bmatrix} 1 + \frac{2K}{3} & -\frac{K}{3} & -\frac{K}{3} \\ -\frac{K}{3} & 1 - \frac{K}{3} & \frac{2K}{3} \\ -\frac{K}{3} & \frac{2K}{3} & 1 - \frac{K}{3} \end{bmatrix} \qquad 7.11$$

The matrix, although not physically realizable, can be used to examine the effect of generator loading and degrees of unbalance.

Figure 7.2 shows the effect of coupling and loading on the level of 3rd harmonic voltage distortion. The results indicate that for loads within the nominal rating (i.e. 1 p.u.) the 3rd harmonic voltage

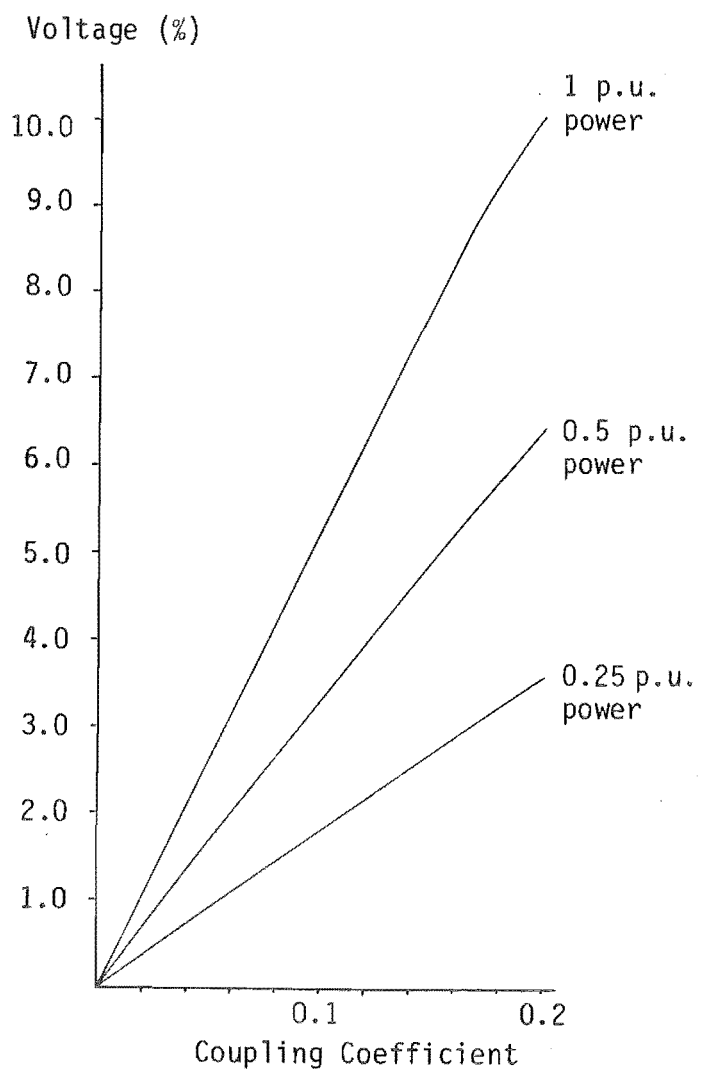

Figure 7.2 : Variation of Positive Sequence Third Harmonic Voltage with Coupling and Loading

is almost directly proportional to the load admittance, and hence to current or power. Also, the 3rd harmonic voltage is seen to be directly proportional to the level of coupling. The 5th harmonic voltage, not shown in the figure, varies approximately in proportion to K^2.

7.2.2 Effect of Saliency

It is apparent from chapter 6 that saliency is the main determining factor in the process of harmonic conversion. To examine the effect of saliency, the simplified equivalent circuits in figure 7.3 are used for the machine's direct and quadrature axes respectively. These circuits include only one winding in each axis of the rotor (i.e. $M_{ds} = M_{fs} = 0$). Further simplification is achieved by setting the direct axis magnetizing inductance M_{df} to 1 p.u. and making $L_d = L_f$, $L_q = L_t$ and $R_f = R_t$ and assuming equal leakage in both axes (i.e., $L_d - M_{df} = L_q - M_{qt}$). Finally saliency, defined as the ratio of quadrature to direct axis rotor fluxes, can be expressed by

$$S = 1 - \frac{M_{qt}}{M_{df}} \qquad 7.12$$

Thus from specified leakage, saliency and resistances R and R_f, the machine parameters of equation 7.1 can be calculated. While this model is not representative of an actual machine, it does prove a useful indication of the effect of saliency.

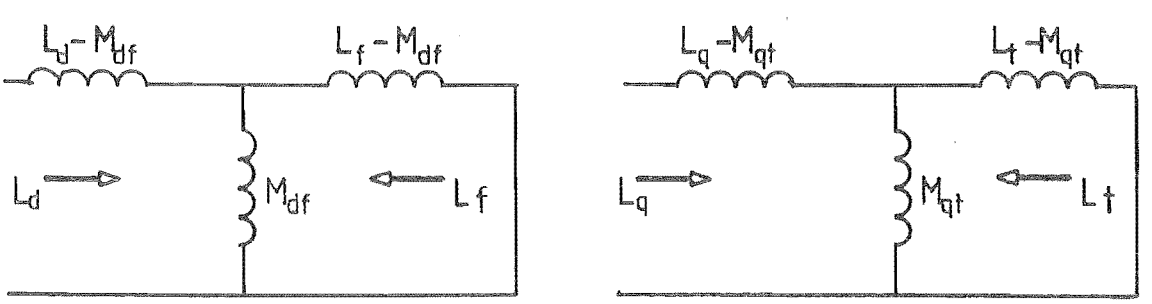

Figure 7.3 : Simplified Equivalent Circuit of the Machine
(a) Direct axis, (b) Quadrature axis

The effect of saliency has been tested on a purely resistive load of 484Ω (1 p.u.) with a coupling coefficient of 10%. Cases of perfect saliency (M_{qt} = 0) and zero saliency (M_{qt} = 1) produced no noticeable effect with perfect coupling (i.e. zero leakages). However, the addition of some leakage (0.2 p.u.) showed considerable difference in the resulting levels of harmonic voltage distortion, as shown in figure 7.4.

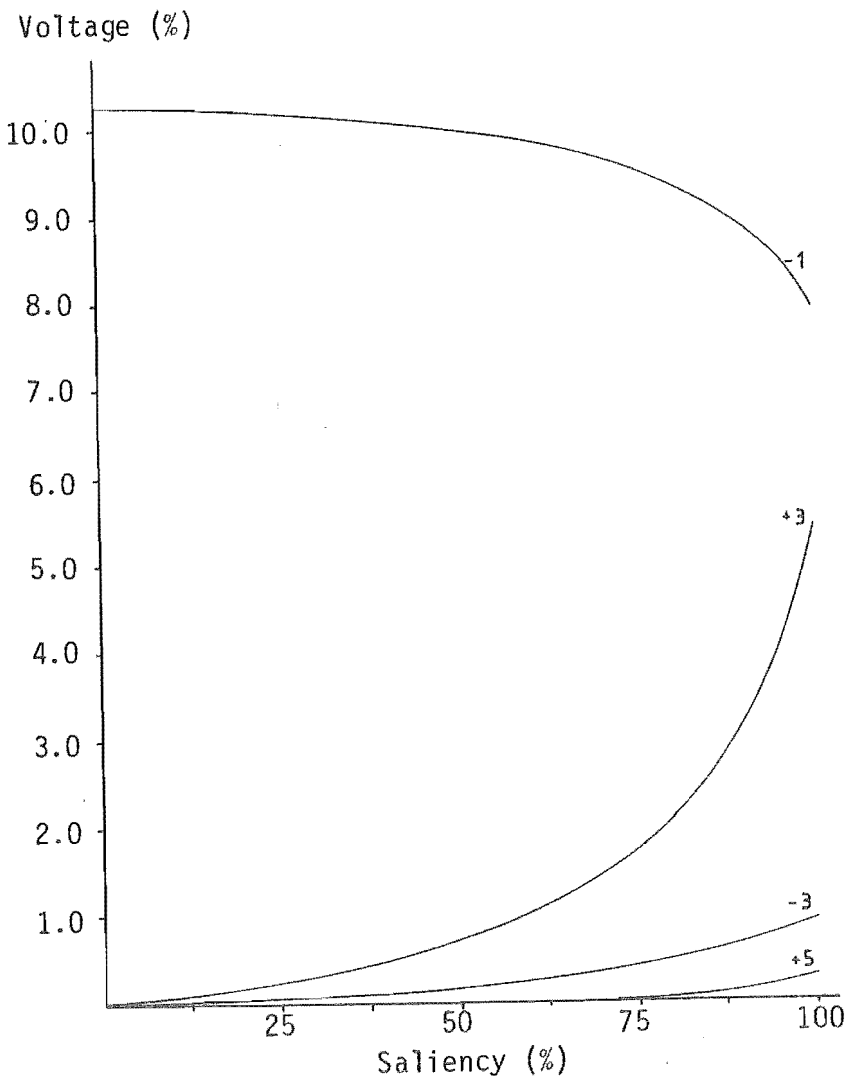

Figure 7.4 : Effect of Saliency on Generator Harmonic Voltages

7.2.3 Unbalanced Tuned Load

This case introduces the effect of resonance by replacing the resistive load with the delta connected circuit of figure 7.5. The resonance frequencies approximating those of the open circuited line

of the test system. The original machine data of table 6.1(a) was used.

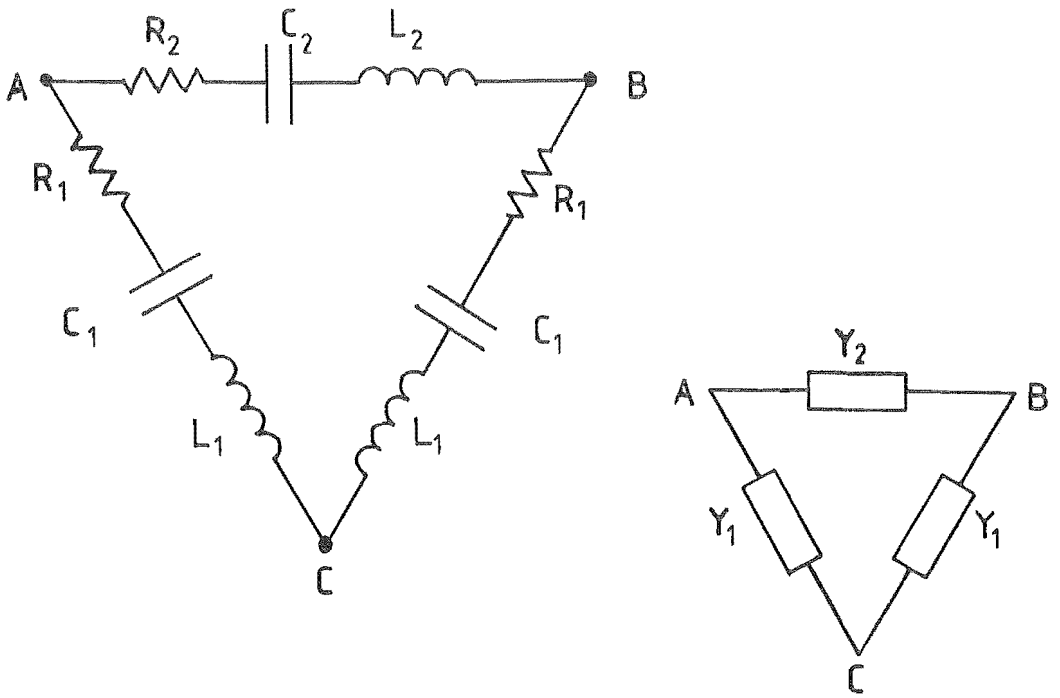

Figure 7.5 : Tuned Delta Load

The sequence components admittance matrix of the delta circuit is

$$Y_{o+-} = \begin{bmatrix} 0 & 0 & 0 \\ 0 & (3+\delta)Y_1 & -\delta a Y_1 \\ 0 & -\delta a^2 Y_1 & 3+\delta \end{bmatrix} \qquad 7.13$$

where

$$a = 1\angle 120°$$

$Y_2 = (1+\delta)Y_1$, valid at a particular frequency

and, using the previous definition of coupling coefficient,

$$|K| = \left|\frac{\delta}{3+\delta}\right| \qquad 7.14$$

The values of L_1, C_1, L_2 and C_2 are chosen to satisfy three conditions, namely to give the same positive sequence admittance at the fundamental frequency, to produce specified resonance frequencies f_{o1} and f_{o2} for Y_1 and Y_2 respectively, and to maintain a specified degree of unbalance (determined by the coupling coefficient) at fundamental frequency. The three resistances are assumed equal.

From the test system with a line length of 200 km, approximate values are derived for the delta branch parameters; at 50 Hz the reactance (mostly capacitive) and resistance are 1555 and 12 ohms, respectively.

In a real transmission line of flat construction the asymmetrical input impedance gives rise to two line modes which resonate at slightly different frequencies. This effect is simulated in the dummy load by maintaining a centre resonance frequency f_o and varying the actual resonant frequencies of Y_1 and Y_2 symmetrically on both sides of f_o. Figure 7.6 shows the variation of harmonic voltages with $f_{o1}-f_{o2}$ while keeping f_o constant at the third harmonic.

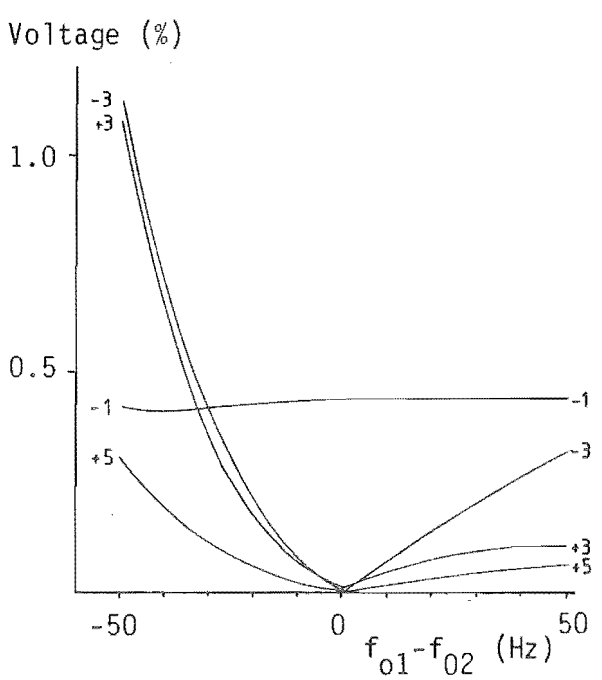

Figure 7.6 : Harmonic Voltage Distortion Versus $f_{o1}-f_{o2}$ with Centre Resonant Frequency f_o=150 Hz

By maintaining a constant unbalance, the amount of negative sequence voltage and current at fundamental frequency is approximately constant with varying $f_{o1}-f_{o2}$.

With $f_{o1}>f_{o2}$ Y_1 is capacitive and Y_2 inductive and vice versa with $f_{o2}>f_{o1}$. This results in a strong unbalance at 3rd harmonic, leading to increasing negative sequence 3rd harmonic voltage and current with $f_{o1}-f_{o2}$. This is followed by corresponding increases of 5th harmonic voltage and current. The ratio of 5th harmonic positive sequence to 3rd harmonic negative sequence is approximately constant.

7.2.4 Untransposed Open Circuit Line

In the test system of figure 7.1 the length of the untransposed line was varied from 50 to 800 km.

Figures 7.7(a) and (b) show the positive and negative sequence third harmonic voltages at the machine terminals. While the machine cannot generate harmonics directly, these appear as a result of the unbalance proproduced by the untransposed line and are therefore very dependent on the length of line.

In the range of line lengths between 165 to 200 km each harmonic voltage shows a double peak. These peaks correspond to the different resonant lengths of the α and β propagation modes present in a line of flat construction. The peaks occur at different lengths for the different harmonics (e.g. at 170 and 195 km for positive sequence third and at 175 and 190 km for negative sequence third). This effect is due to the impedances and degree of unbalance varying greatly near the resonances of the two modes.

The harmonic voltage levels in this range of distances are too large to be ignored, i.e., 6½% of positive sequence third and 4% of negative sequence third harmonics respectively. This clearly demonstrates the need for detailed generator representation as proposed

in chapter 6. The levels of distortion are also substantially higher than the levels calculated in the dummy loads, as a consequence of the standing wave effect of the line.

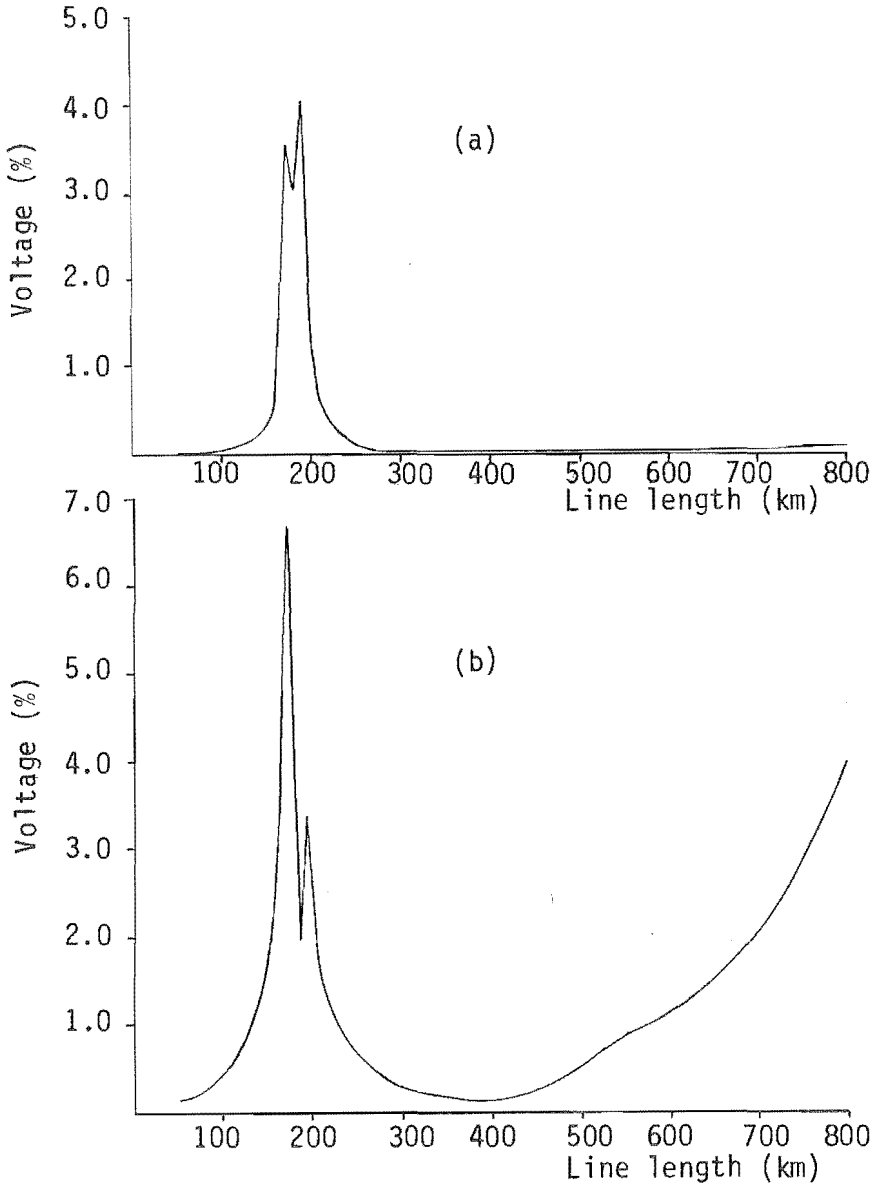

Figure 7.7 : Variation of third harmonic voltage with transmission line length
(a) Negative sequence (b) Positive sequence

A generalized steady state model of the synchronous machine has been developed which can take into account any assymmetry or distortion present in the armature voltages. The level of inter-harmonic coupling has proved to be partly load related (size and degree of unbalance) and partly generator related (saliency).

Such harmonic coupling cannot be detected with present harmonic models, where the generator is short-circuited behind the subtransient reactance.

Test results, with the machine connected to a dummy (asymmetrical) load and to an untransposed transmission line, have been obtained to corroborate the theory. They indicate that the harmonics generated by the machine may often exceed the levels prescribed by harmonic legislation and they need to be assessed accurately. The effect of two different resonant modes have been demonstrated, leading to a strong unbalance and thus high voltage distortion. The main harmonic contributions from the generator are positive and negative sequence third harmonic currents, which therefore cannot be eliminated by generator or transformer connections.

7.3 HARMONIC CURRENT INJECTION INTO A SYSTEM INCLUDING A SYNCHRONOUS MACHINE

Normally in any real power system the sources of harmonics are geographically separated from the synchronous machines in the system by one or more transmission lines. A typical example of this is in the South Island of New Zealand with the large smelter at Tiwai being supplied predominantly by the large hydro station at Manapouri (Densem 1983).

7.3.1 Simplified Test System

To simplify the system to a more manageable size, the same test system used in section 7.2 was chosen, i.e., figure 7.1, with the point of injection chosen to be the open circuited end of the transmission line, as described in figure 7.8. As the only busbars of interest are 1, to maintain the fundamental voltage at the synchronous

generators terminal, and 2, the point of injection, the system was reduced by eliminating busbar 3.

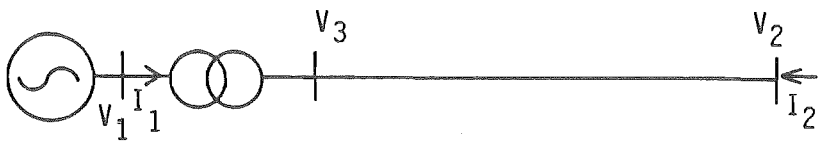

Figure 7.8 : Modified Test System

The system can then be described by the 2 x 2 matrix equations 7.14 and 7.15.

$$I_1 = Y_{11} V_1 + Y_{12} V_2 \qquad 7.14$$

$$I_2 = Y_{21} V_1 + Y_{22} V_2 \qquad 7.15$$

Combining equations 7.1, 7.5, 7.6 and 7.7, of section 7.2, gives

$$(U - T) I_1 = Y_{gen}(V_+ - V_1) \qquad 7.16$$

In this case Y_{gen} contains both even and odd harmonics, necessary if the current injection I_2 is an even harmonic. Therefore, combining equations 7.14 and 7.16 gives

$$(U - T)(Y_{11} V_1 + Y_{12} V_2) = Y_{gen}(V_+ - V_1) \qquad 7.17$$

or

$$Y_{gen} V_+ = (Y_{gen} + (U - T) Y_{11}) V_1 + (U-T) Y_{12} V_2 \qquad 7.18$$

Finally, combining equations 7.15 and 7.18 into matrix form gives

$$\begin{bmatrix} Y_{gen} V_+ \\ I_2 \end{bmatrix} = \begin{bmatrix} Y_{gen} + (U - T) Y_{11} & (U-T) Y_{12} \\ Y_{21} & Y_{22} \end{bmatrix} \begin{bmatrix} V_1 \\ V_2 \end{bmatrix} \qquad 7.19$$

or

$$[I] = [Y][V] \qquad 7.20$$

The matrix (U-T) has the following form

$$\left[\begin{array}{ccc|c} \frac{2}{3} & -\frac{1}{3}a & -\frac{1}{3}a^2 & \\ -\frac{1}{3}a^2 & \frac{2}{3} & -\frac{1}{3}a & 0 \\ \frac{1}{3}a & \frac{1}{3}a^2 & \frac{2}{3} & \\ \hline & 0 & & U_{N-3,N-3} \end{array}\right] \qquad 7.21$$

where N is three times the number of harmonics. Because T is zero at harmonics, only the fundamental values of Y_{11} and Y_{12} are changed in equation (7.19).

For consistency with existing software and with the definition of the harmonic space in section 2.6, I (and V) were rearranged to be of the form

$$I = \left[\begin{array}{l} I_1 \\ I_2 \end{array}\right] \} \text{ fundamental}$$
$$\left[\begin{array}{l} I_1 \\ I_2 \end{array}\right] \} \text{ 2nd harmonic} \qquad 7.22$$
$$\left[\begin{array}{l} I_1 \\ \cdot \\ \cdot \\ \cdot \end{array}\right]$$

Similarly, Y in equations 7.19 and 7.20 needs to be rearranged to

$$
\left[\begin{array}{cc|cc|cc}
A_1 + (U-T)Y'_{11} & (U-T)Y'_{12} & 0 & 0 & B''_2 & 0 \\
Y'_{21} & Y'_{22} & 0 & 0 & 0 & 0 \\
\hline
0 & 0 & A_2 + Y^2_{11} & Y^2_{12} & & \\
0 & 0 & Y^2_{21} & Y^2_{22} & & \\
\hline
B'_2 & 0 & 0 & 0 & A_3 + Y^3_{11} & Y^3_{12} \\
0 & 0 & 0 & 0 & Y^3_{21} & Y^3_{22}
\end{array}\right]
\begin{array}{l} \} \ 1^{st} \\ \} \ 2^{nd} \\ \} \ 3^{rd} \end{array}
\qquad 7.23
$$

where the superscripts of Y^i_{11}, Y^i_{12}, Y^i_{21} and Y^i_{22} refer to the i^{th} harmonic.

Equation 7.20 can be solved for V_1 and V_2 by Gaussian elimination. Equation 7.19 shows that the voltages V_1 and V_2 are made up of 2 components. One due to the harmonic current injection, I_2, which is considered in conventional harmonic penetraction studies, the second component being due to the asymmetrically loaded generator as analysed in section 7.2. Because equaiton 7.19 is linear, these two effects can be examined separately and combined using superposition.

7.3.2 The Effect of Excitation Alone

This is essentially the same problem described in section 7.2.4 with the exception that the solution includes the voltage at the unterminated end of the transmission line, V_2.

For the range of line lengths 50 to 800 km the negative and positive sequence third harmonic voltage components are given in figures 7.9(a) and (b) respectively.

For both the negative and positive sequences the generator terminal voltage (V_1) is identical to that previously calculated in section 7.2.4, i.e., figure 7.7. It can also be seen that the open circuit voltages are significantly larger than the generator terminal voltages.

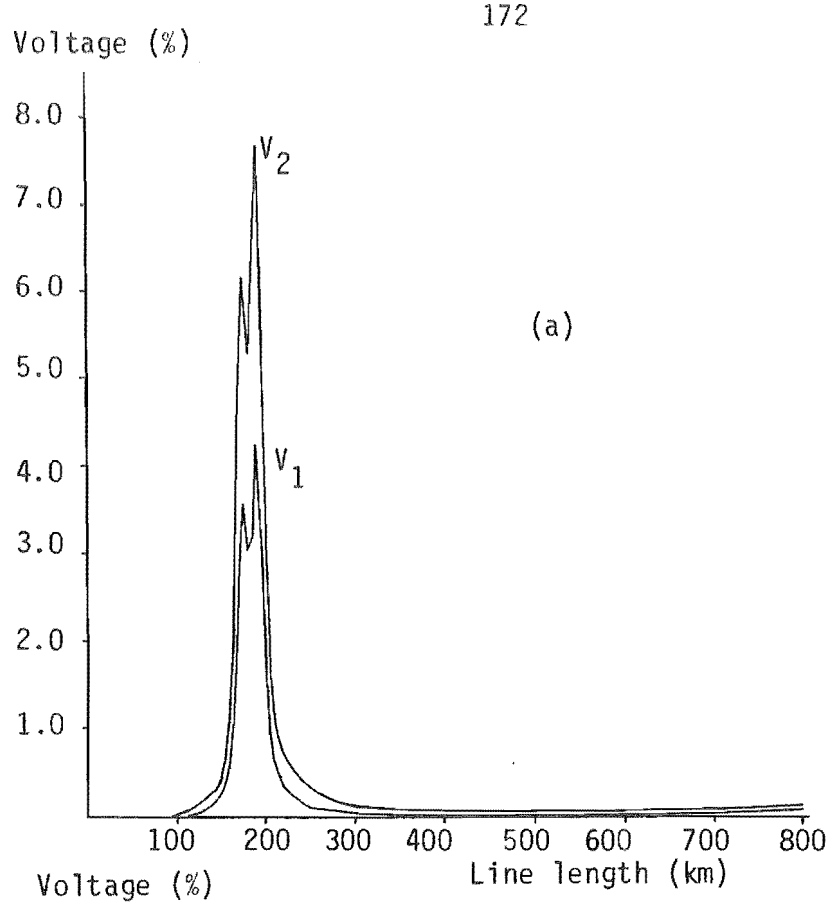

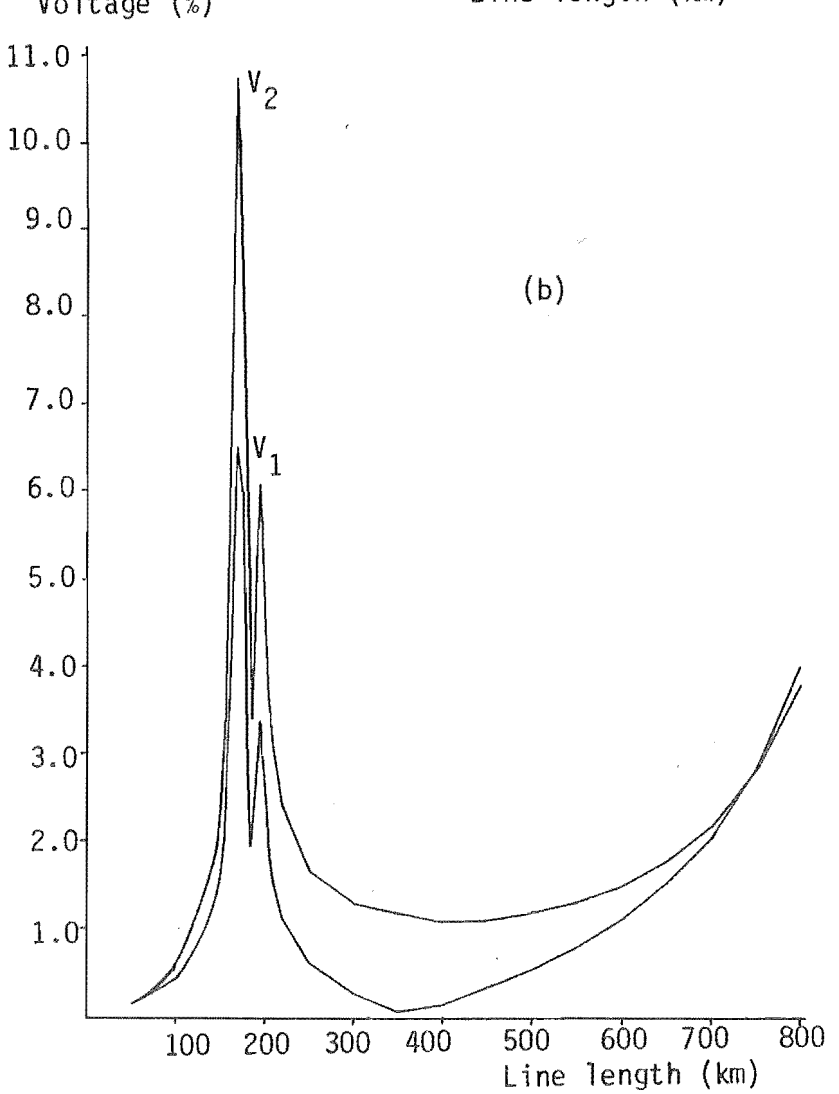

Figure 7.9 : Variation of Third Harmonic Voltage with V_2 included
(a) Negative sequence (b) Positive sequence

7.3.3 The Effect of a Current Injection

If the synchronous generator excitation is removed, by setting V_+ to zero in equation 7.19, the effect of an injected current into busbar 2 can be assessed. Because the test system of figure 7.1 was shown in section 7.2 to be close to third harmonic resonance for the range of line lengths 155 to 195 km, this range of line lengths was chosen. It is expected that when a 1.0 p.u. positive sequence fifth harmonic current is injected into busbar 2, significant levels of both negative and positive sequence third harmonic voltage will be produced due to the coupling between frequencies exhibited by the synchronous generator. As for section 7.2, the generator data is that of the hydro generator of table 6.1(1).

As discussed in sections 2.3.2 and 2.6, conventional harmonic penetration algorithms treat each frequency separately and would, therefore, not be able to predict voltage distortion at any other frequency except the injected fifth harmonic. The positive sequence fifth harmonic voltage predicted by a conventional harmonic penetration algorithm (Densem 1983) is given as a function of line length in curve (1) of figure 7.10. Note that while negative sequence fifth harmonic voltage will also be produced, it is not included in figure 7.10.

However when equation 7.19 is solved with 1.0 p.u. positive sequence fifth harmonic injection into busbar 2, significant levels of positive fifth, negative third, positive third and negative sequence fundamental harmonic voltage are produced. These are plotted as curves (2) to (5) in figure 7.10 respectively. As was the case previously in sections 7.2 and 7.3.2, the peaks in the negative and positive sequence third harmonic components do not occur at the same line length, being due to the different propagation modes of the system.

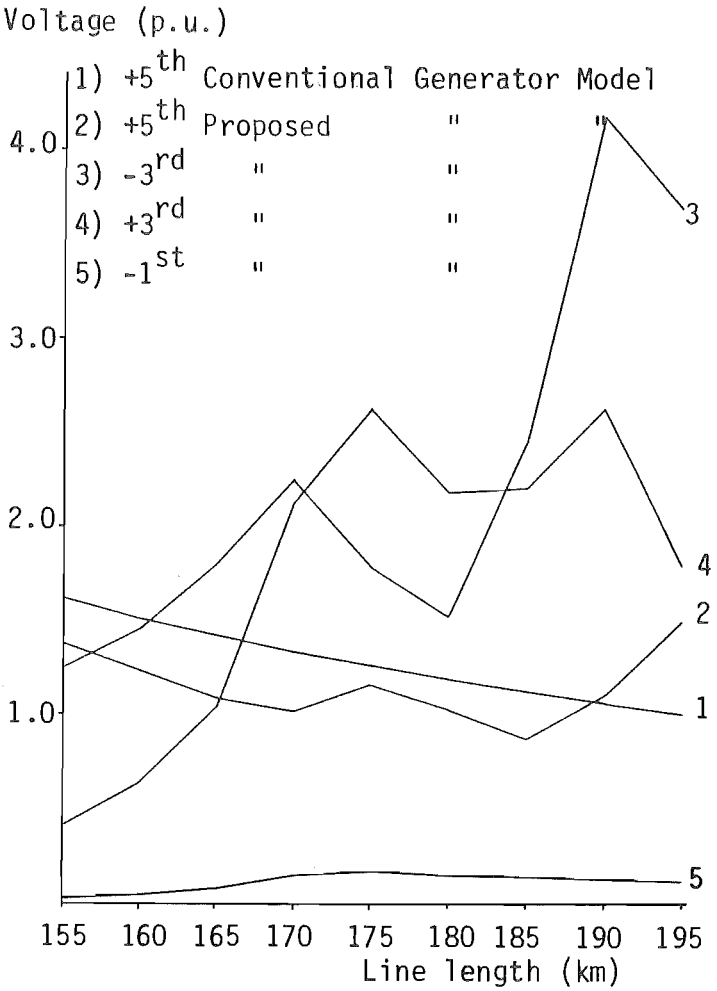

Figure 7.10 : Comparison of Conventional and Harmonic Space Penetration Studies

The relatively large levels of negative and positive sequence third harmonic magnitudes, 3.78 and 2.38 times the positive fifth harmonic voltage of 190 km respectively, show the importance of modelling the harmonic process of synchronous machine.

7.4 HARMONIC INTERACTION BETWEEN SYNCHRONOUS MACHINES AND H.V.D.C. CONVERTORS

7.4.1 Introduction

When assessing power system harmonics distortion, synchronous machines are currently modelled by their negative sequence reactance. As already shown, the synchronous machine acts as a frequency convertor and, if this property is not adequately represented, the harmonic

assessment will be in error.

Synchronous machines, either as generators or synchronous compensators, have found their place in many h.v.d.c. convertor schemes. Although the harmonic filters are generally located between the synchronous machines and the convertor, some harmonic currents enter the machines in the presence of imperfect filtering and uncharacteristic harmonics. Moreover, in some schemes the machines are placed between the convertor and the harmonic filters and they will attract a substantial proportion of the convertor harmonic current. With single generator-convertor units (Arrillaga 1983) all the convertor currents enter the machines. In all these cases the harmonic current entering the machines provides the source of harmonic conversion.

As many h.v.d.c. links are associated with remote hydro-generation and synchronous compensators, both of which are generally salient in nature, the use of a synchronous machine model which includes harmonic conversion is important when assessing the waveform distortion associated with h.v.d.c. convertors.

Harmonic conversion results from the off-diagonal B′ and B″ terms of Y_{gen} in equation 7.1. Therefore, a harmonic voltage V_h may produce harmonic currents I_{h-2}, I_h and I_{h+2} depending on the sequence of V_h. Similarly, a harmonic current may produce components of voltage V_{h-2}, V_h and V_{h+2}. In this section the harmonic space representation of the synchronous machine is used to provide a more accurate assessment of the harmonic interaction that takes place between h.v.d.c. convertors and local synchronous machines such as hydro-generators and synchronous compensators.

7.4.2 Approximate Direct Solution

The significance of the harmonic conversion of synchronous machines, when associated with h.v.d.c. convertors, is first examined

by modelling the convertor as a fixed injection of characteristic current harmonics. The simplest system for the phenomena under consideration is illustrated in figure 7.11 which consists of a single generator-transformer-convertor unit.

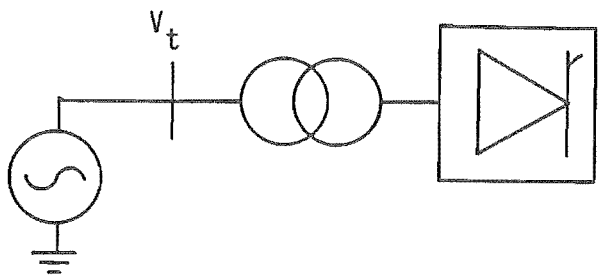

Figure 7.11 : Single Generator-Transformer-Generator Unit

Under idealized a.c. and d.c. conditions (Arrilliga 1983) the a.c. current is a perfectly rectangular waveform which contains only the characteristics (6Q+1) positive and (6Q-1) negative sequence harmonic orders, where Q is an integer.

In the time domain phase 'a' current has the form

$$i_a(t) = \frac{\sqrt{2}\sqrt{6}\ I_d}{\pi}\left[\cos(\omega t+\alpha) + \frac{1}{5}\cos(5\omega t +5\alpha +\pi) + \frac{1}{7}\cos(7\omega t + 7\alpha) + \frac{1}{11}\cos(11\omega t + 11\alpha + \pi)...\right] \qquad 7.24$$

where α is the delay angle. The magnitude of the h^{th} harmonic rms component is

$$I_h = \frac{\sqrt{6}}{h\pi}\ I_d \qquad 7.25$$

For conventional harmonic studies the generator impedance is $_j h(X''_d + X''_q)/2$ (Clarke 1950 and Ross and Smith 1948). When these impedances are multiplied by the corresponding frequency component of the phase current, equation 7.25, the resultant voltage distortion is

$$V_h = \frac{\sqrt{6}}{\pi} (X''_d + X''_q)/2 \qquad 7.26$$

For the hydro-generator described in table 6.1(1), but adjusted to a 500 MVA rating rather than the previous 100 MVA, equation 7.26 gives a value of $V_h = 0.0442$.

However, when the effect of harmonic conversion is included these currents cannot be treated separately for salient machines because the characteristic negative sequence (6Q-1) and positive sequence (6Q+1) harmonic current pairs produced by the convertor correspond to the same rotor harmonic Q. Each positive sequence (6Q+1) voltage is therefore made up of two components due to the corresponding positive sequence (6Q+1) and the negative sequence (6Q-1) respectively. Similarly, each negative sequence (6Q-1) voltage is made up of two components. This is demonstrated in equations 7.27 and 7.28 for the positive and negative sequence voltage respectively.

$$V_{6Q+1} = V^{6Q+1}_{6Q+1} + V^{6Q+1}_{-(6Q-1)} \qquad 7.27$$

$$V_{-(6Q-1)} = V^{-(6Q-1)}_{-(6Q-1)} + V^{-(6Q-1)}_{(6Q+1)} \qquad 7.28$$

where

$$V^{6Q+1}_{6Q+1} = Z^{6Q+1}_{6Q+1} \; I_{6Q+1} \qquad 7.29$$

$$V^{-(6Q-1)}_{-(6Q-1)} = Z^{-(6Q-1)}_{-(6Q-1)} \; I_{-(6Q-1)} \qquad 7.30$$

$$V^{6Q+1}_{-(6Q-1)} = Z^{6Q+1}_{-(6Q+1)} \; I_{-(6Q-1)} \qquad 7.31$$

$$V^{-(6Q-1)}_{6Q+1} = Z^{-(6Q-1)}_{6Q+1} \; I_{6Q+1} \qquad 7.32$$

where the Z are defined in section 6.4. Note the subscripts and superscripts indicate the harmonic order and sequence of the current injections and voltage distortions respectively.

It is clear that the relative phase between $I_{-(6Q-1)}$ and $I_{(6Q+1)}$ is important. As shown by equation 7.24, in the case of an

a.c./d.c. convertor the relative phase of these two current components vary with the delay angle. This effect was examined by injecting rectangular pulses of current into the test generator and varying the delay angle. Figure 7.12 shows the effect of varying the delay angle on the negative sequence fifth and positive sequence seventh harmonic voltage distortions. The dotted line indicates the value of V_h derived from equation 7.26.

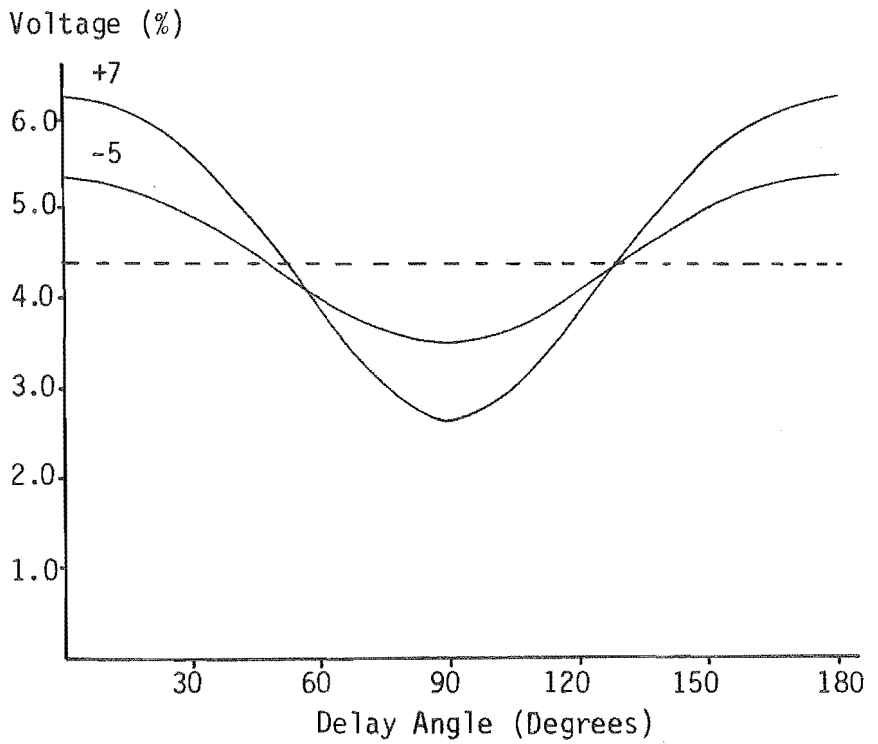

Figure 7.12 : Negative Sequence Fifth and Positive Sequence Seventh Versus Delay Angle

From equation 7.24 it can be seen that for a delay angle of zero degrees the relative phase of the fifth and seventh harmonic currents is 180°. From section 6.4 the phase of Z^{6Q+1}_{6Q+1} and $Z^{-(6Q-1)}_{-(6Q-1)}$ is approximately 90° while the phase of $Z^{6Q+1}_{-(6Q-1)}$ and $Z^{-(6Q-1)}_{6Q+1}$ is approximately -90°. Therefore, with zero delay angle the two components of voltage in equations 7.27 and 7.28 add in phase. However, as the delay angle increases the relative phase of the harmonics changes as the higher order harmonics are shifted by a larger amount.

With reference to equation 7.24, the phase difference between the 6Q+1 and 6Q-1 harmonic currents is $(\pi - 2\alpha)$ and, therefore, the sum of the resulting voltage components vary with α. Figure 7.13(a) demonstrates this effect for the negative sequence fifth harmonic and figure 7.13(b) for the positive sequence seventh harmonic voltage. The approximate values for the machines' impedances, derived from section 6.4, are as follows

$$Z_7^7 = j\,\frac{7}{2}(X''_d + X''_q) = j\ 0.3969 \text{ p.u.} \qquad 7.33$$

$$Z_{-5}^{-5} = j\,\frac{5}{2}(X''_d + X''_q) = j\ 0.2835 \text{ p.u.} \qquad 7.34$$

$$Z_{-5}^{7} = -j\,\frac{7}{2}(X''_q - X''_d) = -j\ 0.1169 \text{ p.u.} \qquad 7.35$$

$$Z_7^{-5} = -j\,\frac{5}{2}(X''_q - X''_d) = -j\ 0.0835 \text{ p.u.} \qquad 7.36$$

and the corresponding voltage magnitudes are

$$V_7^7 = V_{-5}^{-5} = 0.0442 \text{ p.u.}$$

$$V_{-5}^{7} = 0.0182 \text{ p.u.}$$

$$V_7^{-5} = 0.0093 \text{ p.u.}$$

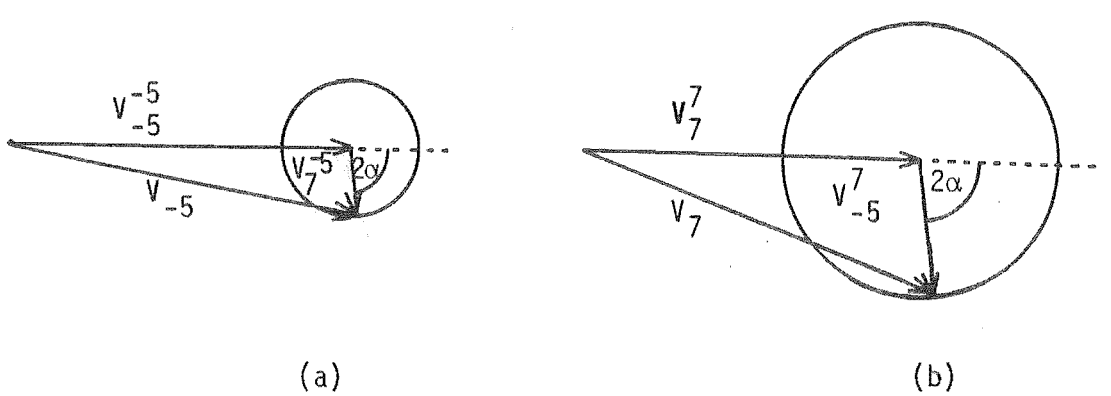

(a) (b)

Figure 7.13 : Graphical Derivation of the
a) Negative Fifth and
b) Positive Seventh Voltage Magnitudes

The magnitudes of the negative sequence fifth and positive seventh harmonic voltages, derived graphically in figures 7.13(a) and (b), agree with the values calculated from the full admittance matrix and plotted in figure 7.12.

7.4.3 Accurate Iterative Solution

Modelling the static convertor as a fixed source of current harmonics is unrealistic because convertor currents depend on the terminal voltage waveform. As described in chapter 3, the harmonic interaction between the convertor and the a.c. system requires an iterative algorithm with the convertor analysis in the time domain and the harmonic power flows in the frequency domain.

The a.c. system representation in chapter 3 does not represent harmonic coupling and, consequently, harmonic flows are carried out independently for each harmonic and their effect is finally superimposed to update the voltage distortion at the convertor terminals in order to derive the new harmonic current injections. However, with the inclusion of harmonic conversion into the generator model the individual harmonics are no longer independent and their effect must be considered together.

For a three-phase study involving many harmonics the system admittance matrix is extremely large. An efficient way of solving this problem is to replace the off diagonal terms of the generator admittance matrix by an equivalent current injection. From equation 6.22 and 6.31",

$$I_h = B'_{h-1} V_{h-2} + A_h V_h + B''_{h+1} V_{h+2} \qquad 7.37$$

This current can be divided into two components, as illustrated in figure 7.14, one due to the diagonal A_h term and the second due to the off diagonal B'_{h-1} and B''_{h+1} terms. That is

$$I_h + I_{gh} = A_h V_h \qquad 7.38$$

where

$$I_{gh} = -\left(B'_{h-1}\, V_{h-2} + B''_{h+1}\, V_{h+2}\right) \qquad 7.39$$

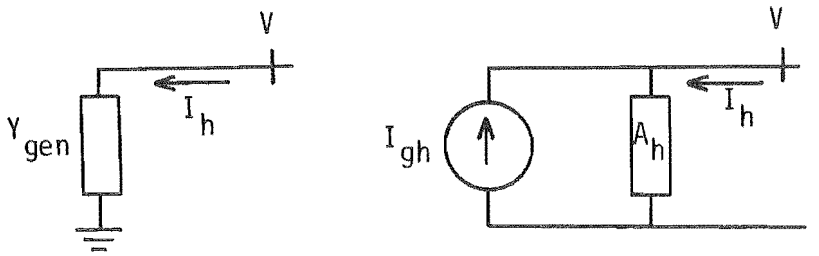

Figure 7.14 : Generator Representation
a) Conventional Admittance
b) Modified to Include Conversion

A simplified equivalent of a rectifier connected to a generator via the convertor transformer is illustrated in figure 7.15. Current injection I_1 represents the effect of the off diagonal terms while I_2 is the convertor current injection. V_1 is the generator, and convertor, terminal voltage.

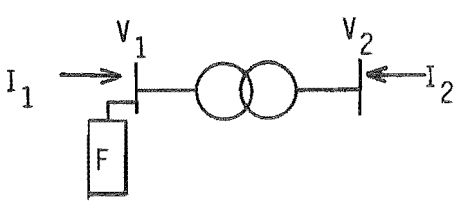

Figure 7.15 : Simplified Equivalent of a Single Generator Convertor Unit

As described in chapter 3, I_2 is calculated in the time domain from the terminal voltage at each iteration and then converted to the frequency domain using an FFT. For each harmonic in turn I_1 is calculated using equation 7.39 and, with I_2, the a.c. system is solved

for V_1. Because V_1 is updated at each harmonic, the most recent values of the terminal voltage are always used. Also an acceleration factor of 0.5 has been included to improve numerical stability, i.e.,

$$I_{gh}^{i+1} = 0.5(I_{gh}^{i+1} - I_{gh}^{i}) + I_{gh}^{i} \qquad 7.40$$

where i is the iteration number.

To verify the modified generator representation of figure 7.14(b) the earlier fixed injections of equation 7.24 were used and the results did not change from those of figure 7.12.

The modified generator model and a 6-pulse bridge with negligible commutating reactance were then solved iteratively. The solution took between four to eight iterations to reach a tolerance of 0.0001 radians for the convertor commutating voltage phase to phase zero-crossings.

Figures 7.16(a) and 7.16(b) show the levels of negative sequence fifth and positive sequence seventh harmonic voltage for the case of star-star and star-delta connected convertor transformers respectively. The results agree closely with those of figure 7.12. Note that the value of I_d is now 0.1 p.u. rather than the previous 1.0 p.u.

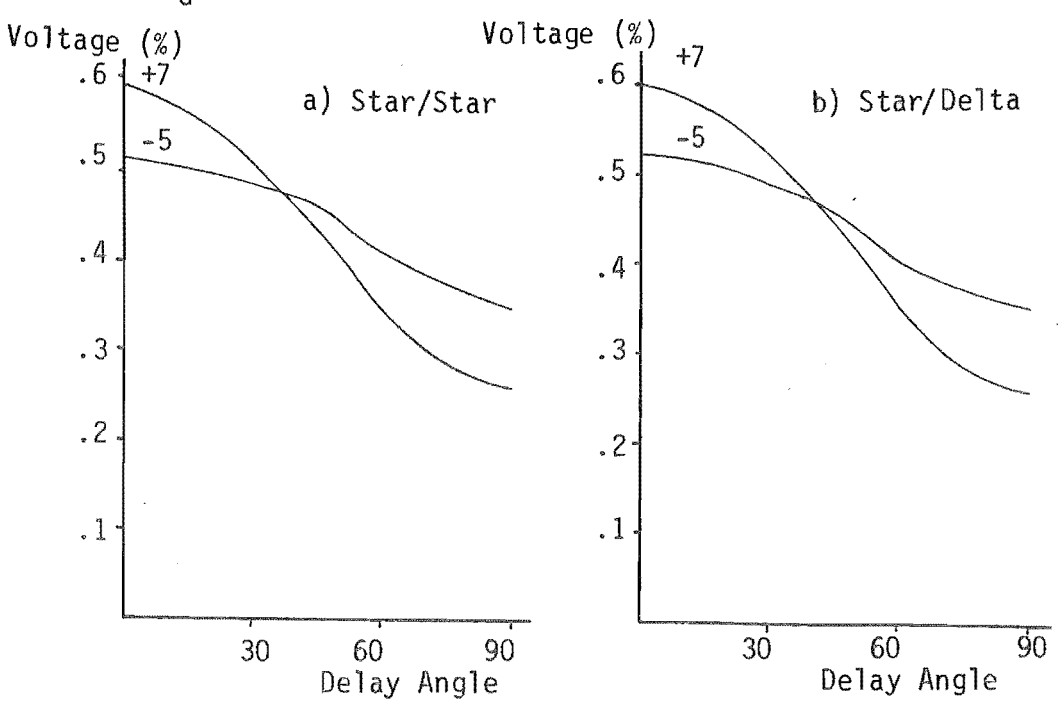

Figure 7.16 : Voltage Distortion Versus Delay Angle
(a) Star-g/Star Connection
(b) Star-g/Delta Connection

7.4.4 The Effect of Commutating Reactance

In a practical system the commutating reactance will reduce the magnitude of the harmonic current injections (Arrillaga 1983) and change their relative phase. The two effects are important when considering the voltage distortion at the generator terminal. The iterative algorithm described in section 7.4.3 was used to examine the effect of including the commutations.

Commutating reactances of 0.015, 0.03, 0.06 and 0.12 p.u. were used with nominal convèrtor fundamental terminal voltage and 1 p.u. d.c. current. Figure 7.17 shows the resulting commutation angles for the various commutating reactances for the range of delay angles 0 to 20 degrees.

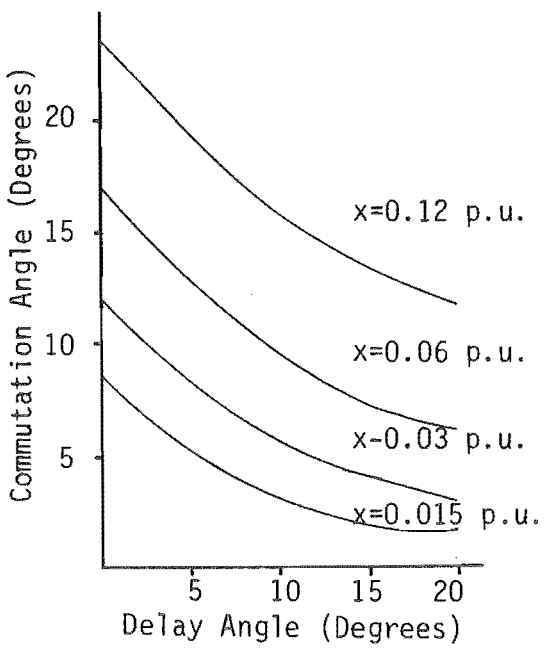

Figure 7.17 : Commutation Angle Versus Delay Angle for the Various Commutating Reactances

Figures 7.18(a) to (d) show the magnitude of all negative sequence fifth harmonic voltage for the conventional and proposed generator models, with commutating reactances at 0.015 to 0.12 p.u. respectively. Similarly, figures 7.19(a) to (d) show the magnitude of the positive sequence seventh harmonic voltage.

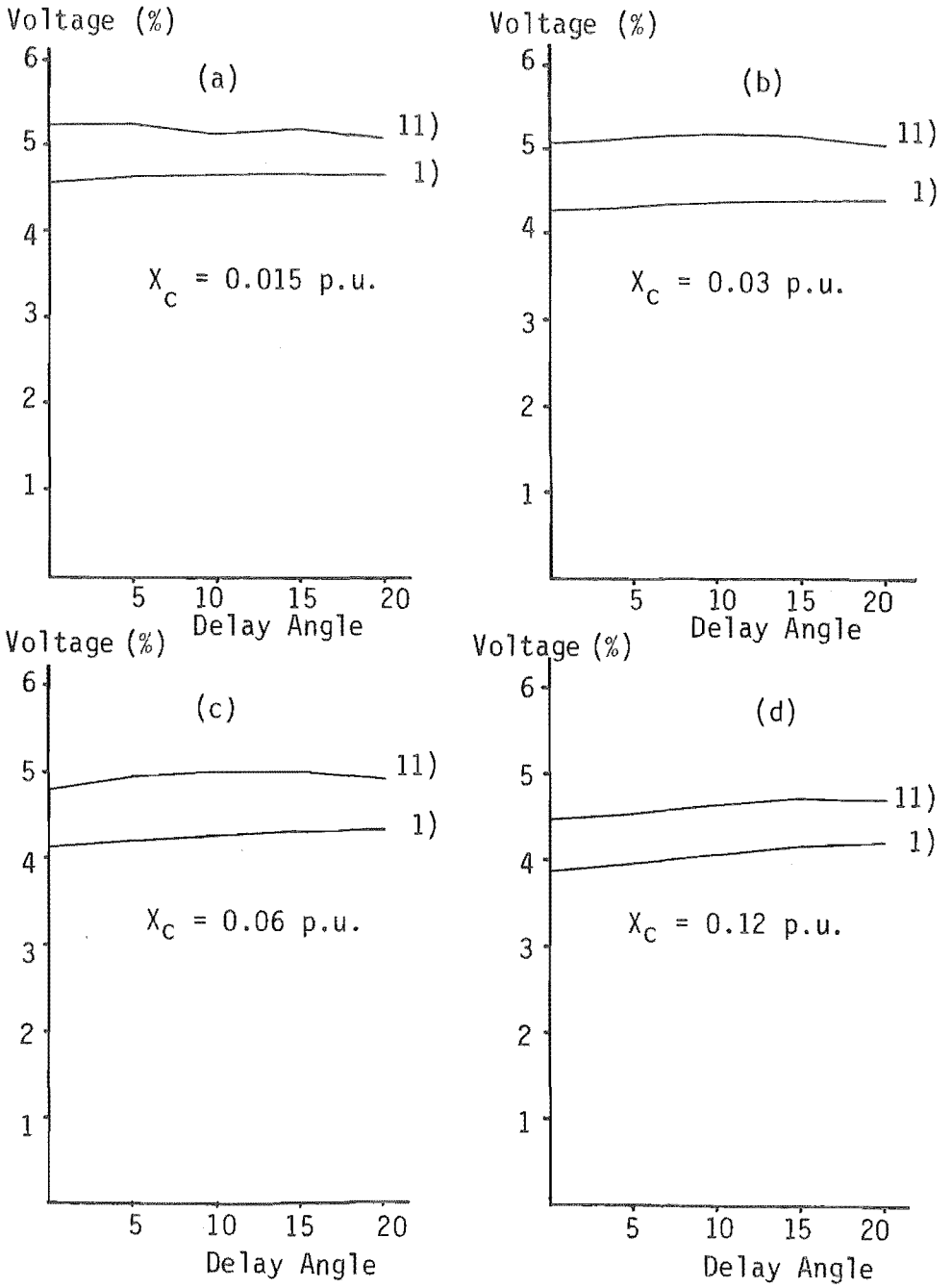

Figure 7.18 : Negative Sequence Fifth Harmonic Voltage Versus Delay Angle

a) X_c = 0.015 p.u.
b) X_c = 0.03 p.u.
c) X_c = 0.06 p.u.
d) X_c - 0.12 p.u.

In both figures 7.18 and 7.19 (1) refers to the conventional generator model results and (11) to the results of the proposed model.

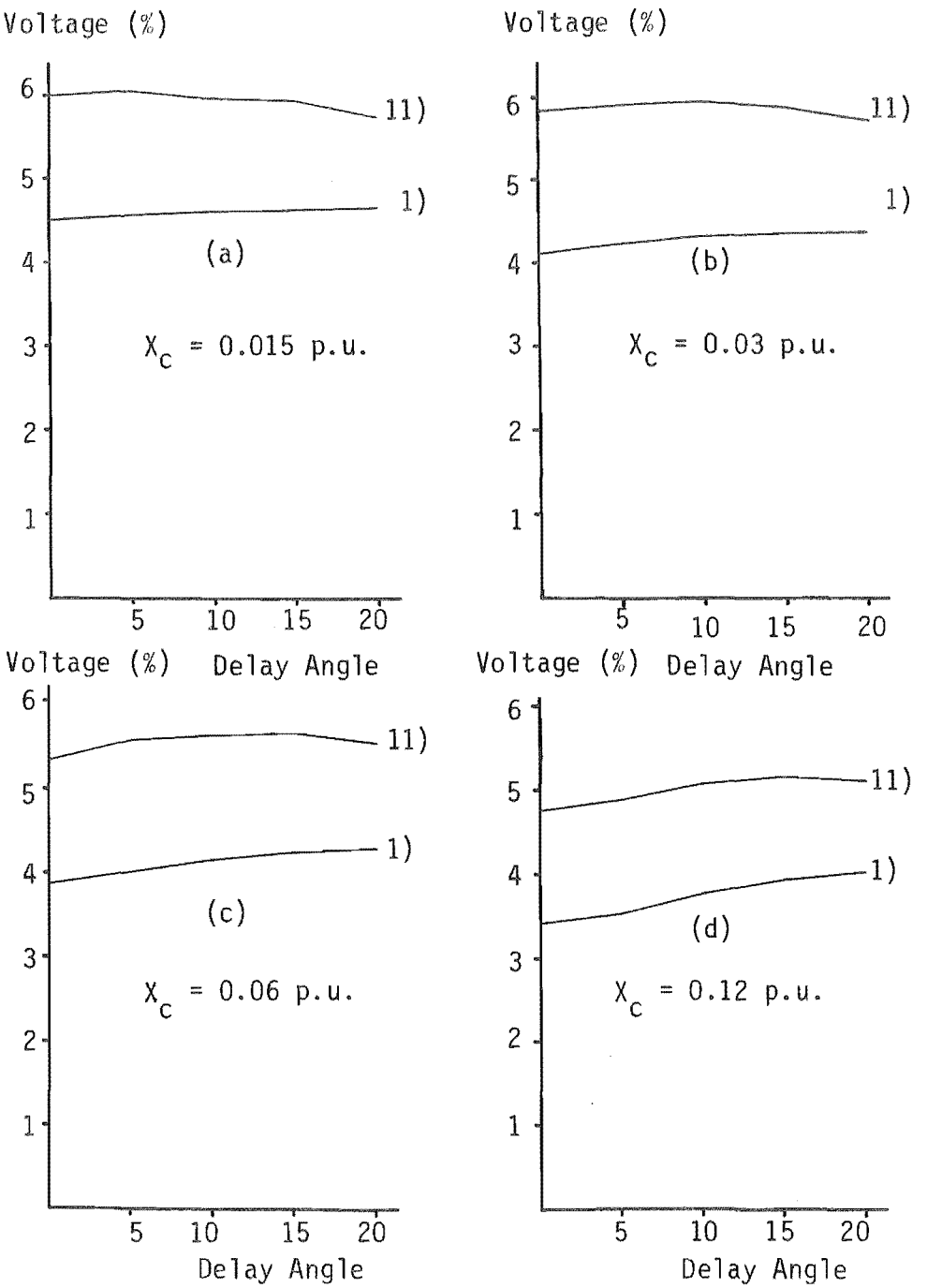

Figure 7.19 : Positive Sequence Seventh Harmonic Voltage Versus Delay Angle (Including Commutations)

a) X_c = 0.015 p.u.
b) X_c = 0.03 p.u.
c) X_c = 0.06 p.u.
d) X_c = 0.12 p.u.

As the delay angle is increased with the conventional generator model, and the commutation angle reduced, the level of harmonic distortion

increases. This effect is most pronounced with the larger commutating reactances. Reduced distortion at zero delay angle has been given as one of the advantages of diode generator units (Arrillaga 1983).

However, the results of figures 7.18 and 7.19 show that when the generator is represented by the proposed synchronous machine model of chapter 6, the voltage distortion is significantly greater than expected due to coupling between the harmonics and that, similarly to figure 7.12, the voltage distortion can even decrease at large delay angles.

7.4.5 Actual System Data

The proposed synchronous machine has been used to calculate the voltage distortion caused by one pole of the Benmore terminal of the New Zealand H.V.D.C. link. The relevant components attached to the terminal are shown in figure 7.20.

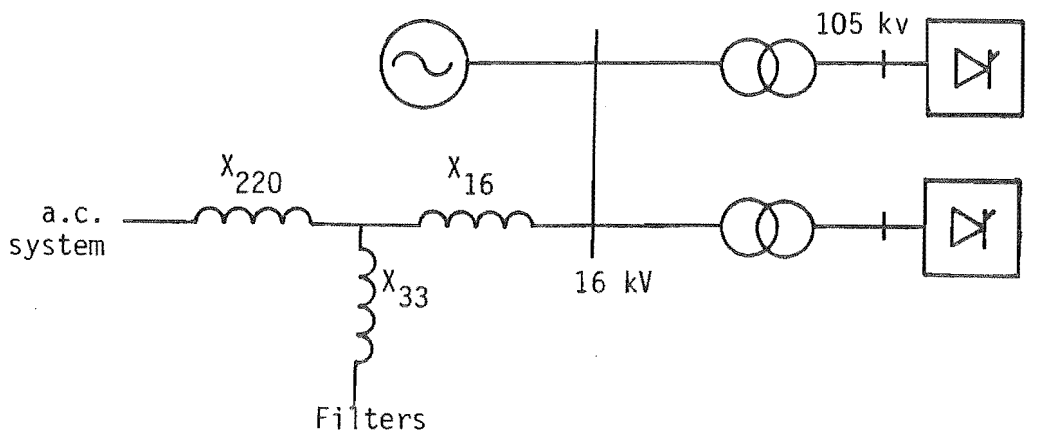

Figure 7.20 : Schematic Diagram of a Benmore Pole

To simplify the problem the filters, connected to the tertiary of the system transformer, are assumed to provide a perfect short circuit to harmonics and the d.c. current made perfectly smooth. The three winding transformer, the perfect filters and the a.c. system are

reduced to a single equivalent reactor X_{sys} at the 16 kV bus. Moreover, when the conventional generator is used a reactance $X_g = \frac{1}{2}(X''_d + X''_q)$ is added in parallel for the claculation of X_{sys}.

Relevant data for the test system is given in Appendix A9. Two system configurations, i.e., an open and short circuit at the 220 kV bus, are considered with both the conventional and new synchronous machine models.

With the conventional generator model the overall system reactance, including the generator, at the convertor terminal is

$$X_{sys} = (X_{16} + X_{33}) // X_g = 0.01254 \text{ p.u.} \qquad 7.41$$

for the open circuit case, and

$$X_{sys} = (X_{16} + X_{33} // X_{220}) // X_g = 0.01223 \text{ p.u.} \qquad 7.42$$

for the short circuit case.

With proposed synchronous machine model the generator is represented separately and the reactance of the system is

$$X_{sys} = (X_{16} + X_{33}) = 0.0161 \text{ p.u.} \qquad 7.43$$

for the open circuit case, and

$$X_{sys} = (X_{16} + X_{33} // X_{220}) = 0.0156 \text{ p.u.} \qquad 7.44$$

Table 7.1 shows the comparison between the conventional and proposed machine models for 6-pulse operation with a delay angle of 5°.

Table 7.1 : Comparison of Models for 6-Pulse Operation (α=5°)

	Open Circuit			Short Circuit		
	Conventional	Proposed	% Diff.	Conventional	Proposed	% Diff.
-5^{th} voltage (%)	2.007	2.0595	2.6	1.960	2.009	2.5
$+7^{th}$ voltage (%)	1.894	2.0402	7.7	1.855	1.986	7.1
-11^{th} voltage (%)	1.586	1.630	2.8	1.545	1.597	3.4
$+13^{th}$ voltage (%)	1.400	1.488	6.3	1.368	1.452	6.1

As expected from figure 7.12, the largest percentage difference occurs at the seventh harmonic. Also for the open circuit case a larger proportion of the convertor harmonics enter the stator and, therefore, produces a larger difference between the models.

7.4.6 Conclusions

It has been shown that in the presence of harmonic currents the effect of harmonic conversion inherent in salient pole synchronous machines is significant and should not be ignored when modelling synchronous machines at convertor stations. When the convertor terminal offers several paths to the harmonic currents, the proportion entering the synchronous machines reduce and the resulting harmonic conversion will be less significant.

The case of a single generator-convertor unit has shown considerable differences in the voltage distortion calculated with the conventional and detailed synchronous machine models. It has also been shown that the use of diode rectification does not necessarily result in lower voltage distortion because the delay angle affects the relative phase of the current harmonics, and hence the harmonic conversion process.

In general it is difficult to predict the level of harmonic distortion resulting from the interactions between the generator and

convertor. The extent to which the generator can affect the level of voltage distortion depends on the harmonic current paths at the convertor terminal, i.e. the proportion of the harmonic currents entering the machine. Therefore, each particular terminal configuration and operating condition needs to be modelled separately to determine the resulting distortion. Because the harmonic conversion process can made a significant difference to the distortion, the proposed synchronous machine model should be used when modelling hydro-generators or salient pole synchronous compensators.

7.5 Numerical Considerations of Solutions in the Harmonic Space

As discussed in section 2.6, the solution of a transmission system in the harmonic space requires a matrix [Y] of dimension 3nk x 3nk, where n is the number of busbars and k is the number of harmonics to be considered.

For the simple systems in section 7.2, only the synchronous machine's terminal busbar exists and the odd harmonics up to the 49^{th} considered. This means that the dimension of [Y] is 75 x 75 which is not too large to be explicitly formed. Similarly, for the system in section 7.3, two busbars were considered for 15 harmonics. Thus the dimension of [Y] is 90 x 90 and it was explicitly formed. However, for any real system containing several hundred busbars to be solved for the first 50 harmonics, to be consistent with the harmonic regulations (New Zealand Electricity 1983), the dimension of [Y] becomes too large to be represented explicitly.

Sparsity storage techniques are already used in power system computer modelling (Arrillaga et al 1983a). This is because in large power systems each busbar is generally connected to only a few other busbars.

Transmission systems described in the harmonic space would be more sparse than single frequency studies as nearly all system components produce no coupling between frequencies.

Synchronous machines only produce coupling between a particular harmonic and the components two harmonic orders either side, as described in equation 7.37.

Power transformers also produce harmonic conversion due to the magnetic non-linearity of their iron core. For a single valued magnetizing characteristic, odd harmonic voltages couple to all other odd orders of current and, similarly, even harmonic voltages couple to all other even orders. For a double valued magnetizing characteristic, i.e., including hysteresis, odd harmonic voltages will produce all harmonic orders of currents but even orders will produce all other orders. While the admittance matrix of each magnetizing branch of a transformer is not sparse, the overall admittance matrix [Y] is still very sparse, making sparsity storage techniques efficient.

The alternative to forming the matrix [Y] using sparsity storage techniques is to include the effect of harmonic conversion as an equivalent current injection, and solving each frequency separately using existing harmonic penetration techniques. However, since the exact voltage distortion at each frequency and therefore the current injection due to harmonic conversion are not known, this alternative requires the use of an iterative process which repetitively updates each harmonic (using the most up-to-date data available). This is essentially what occurred in section 7.4 when the harmonic conversion of a synchronous machine was included into the convertor interaction algorithm.

Forming the entire system admittance matrix in the harmonics space using sparsity storage techniques is immune to numerical instability, as the solution if found using row reduction techniques

as in the present harmonic penetration algorithms. Because the representation of harmonic conversion as an equivalent current injection requires an iterative process, it may be susceptible to numerical instability and not give reliable operation. This would be more probable in the case of a resonate system and a strong harmonic source.

However the effect of harmonic conversion was included as a current injection in section 7.4 because the operation of a convertor already required an iterative algortihm. In that case as the system contained no potential resonances, the numerical stability of the convertor interaction algorithm did not deteriorate.

From sections 7.2 and 7.3.2, where no external harmonic current injections exist, the sole excitation for the harmonic distortion is the positive sequence fundamental Norton current injection, I_o, with the primary cause being the fundamental negative sequence current entering the machine stator. Therefore any assessment of the harmonic distortion of a system should include the effect of the fundamental frequency power flows.

Three phase fundamental power flows must be used to solve for the fundamental voltages at the terminals of each system component which either generates or converts harmonics. This includes synchronous machines, a.c./d.c. convertors and transformer. With the fundamental conditions fixed, the harmonic voltages throughout the system can be solved using equaiton 2.4. Alternatively, the harmonic flows could be integrated into the fundamental power flow algorithm and solved together. This takes into account the effect that large harmonic distortion may have on the fundamental power flow.

When the system contains one or more convertors the solution becomes more complex as the solution of the harmonic interaction requires an iterative algorithm at each convertor. If the

fundamental conditions are fixed by an initial power flow, the solution of the convertors is the same as in chapter 3, but with the harmonic conversion of the synchronous machines and power transformers included as either current injections or an interharmonic mutual admittance, as seen from the convertor terminals.

However, the most general solution would be found by integrating the harmonic interactions of the convertors, synchronous machines and power transformers into a multiharmonic power flow. A similar algorithm (Xia and Heydt 1982) may be proposed, but only includes a single phase system representation of the system. This means that only characteristic harmonic orders can be considered. Moreover, the synchronous machine and transformer models do not represent harmonic conversion.

CHAPTER 8

CONCLUSIONS

As a complement to the propagation of harmonic currents in a transmission system, defined by Densem (1983), the aim of this thesis has been to model the major harmonic sources, especially those of relevance to the New Zealand system.

By far the largest harmonic source in a transmission system is the h.v.d.c. convertor. An iterative algorithm which evaluates the harmonic interaction at a.c./d.c. convertors has been developed which incorporates the best features of existing models and includes improvements as required. The iterative algorithm has been tested with several system configurations including a large 6-pulse convertor connected to a transmission system and a d.c. drive connected to an industrial busbar. In each case the results are consistent with the operation of a real convertor, although the algorithm appeared to be susceptible to numerical instability.

To verify the results produced by the iterative algorithm, and to investigate further the problem of divergence, a simple test system was devised and the iterative algorithm results were compared with those produced by a Transient Convertor Simulation program. The results of the two algorithms were in good agreement for cases where the iterative algorithm converged. However, with very large current ratings the iterative algorithm diverged whereas the TCS program produced stable solutions in the time domain. Despite this limitation the iterative algorithm is preferable as it requires less complex data preparation, uses less cpu time and is able to accurately model the frequency dependencies of the a.c. and d.c. systems.

However, the TCS algorithm must be used in cases of divergence of the iterative algorithm. A genuine case of harmonic instability would show up by divergence of both algorithms.

Of special interest at the moment in New Zealand is the harmonic distortion associated with single phase traction systems. Consequently, an admittance matrix model has been devised to evaluate the harmonic flows throughout the feeder system as well as the effectiveness of prospect harmonic filters.

Similarly to the three phase case, to solve for the current injections at the locomotive's convertor requires an iterative technique. Thus the three phase iterative algorithm has been adapted to model half and fully controlled single phase convertors. The results show the importance of detailed convertor and d.c. drive models, as compared to fixed injections.

Salient poled synchronous machines have also been shown to be a source of harmonics by converting power from one frequency to another, with the strongest coupling between the negative sequence fundamental and the positive sequence third harmonic. A harmonic Norton equivalent of the synchronous machine based on the d-q axes differential equations has been derived. Harmonic and conversion impedances have been defined and evaluated for typical machines.

The harmonic impedances have been shown to match those of conventional models. However, conventional machine models do not include the effect of harmonic conversion, which has been shown to be significant for salient poled machines. Also, the effect of eddy-currents, which is important for round rotor machines, has been added to the model.

The conditions under which the modelling of harmonic conversion is important have been determined. The saliency of the subtransient reactances plays an important part. Strong coupling

between frequencies is found where the machine is connected to an extremely unbalanced load, such as an open circuited transmission line, or a more balanced but larger load. A current injection at a particular frequency into a system containing a synchronous machine can produce larger voltage distortion at another (coupled) frequency if the system is near resonance at a sound frequency. Similarly, the effect of harmonic conversion in the synchronous machines at a convertor terminal modifies the harmonic current flows and voltage distortion.

Because synchronous machines (and power transformers) produce coupling between frequencies, conventional harmonic penetration techniques are not sufficient as each harmonic is solved separately. Therefore, the harmonic space has been defined to allow for this interharmonic coupling and some techniques discussed for the solution of larger systems.

In general the distortion produced by a harmonic source such as a convertor or synchronous machine depends greatly on the fundamental voltages in the system. At present a three phase power flow is used to evaluate the fundamental voltage at the terminals of the harmonic sources and the resulting distortion calculated using the techniques described in this thesis. However, because the presence of distortion modifies the operation of the harmonic sources, the fundamental currents, and hence the busbar voltages, are dependent on the harmonic interaction in the system. Therefore, a more accurate steady state algorithm should integrate the effects of the harmonic interaction of the harmonic sources into the three phase power flow solution.

REFERENCES

Adkins, B. and Harley, R.G. (1975). "The General Theory of Alternating Current Machines", Chapman and Hall, London.

Anderson, P.M. and Fouad, A.A. (1977). "Power System Control and Stability", The Iowa State University Press, Ames, Iowa, USA.

Ainsworth, J.D. (1967). "Harmonic Instability Between Controlled Static Convertors and A.C. Networks", Proc. IEE, Vol. 114, No. 7, pp 949-957.

Ainsworth, J.D. (1968). "The Phase Locked Oscillator - a New Control System for Controlled Static Convertors", IEEE Trans., PAS-87, pp 859-864.

Ainsworth, J.D. (1977). "Core Saturation Instability in the Kingsworth H.V.D.C. Link", paper to CIGRE Study Committee 14.

Ainsworth, J.D. (1981). "Harmonic Instabilities", paper presented at an international conference on Harmonics in Power Systems, UMIST, Manchester.

Arrillaga, J. (1983). "High Voltage Direct Current Transmission", Peter Peregrinus Ltd., London.

Arrillaga, J., Arnold, C.P. and Harker, B.J. (1983a). "Computer Modelling of Electrical Power Systems", John Wiley and Sons.

Arrillaga, J., Densem, T.J. and Harker, B.J. (1983b). "Zero Sequence Harmonic Current Generation in Transmission Lines Connected to Large Convertor Plant", IEEE Trans., PAS-102, No. 7, pp 2357-2363.

Arrillaga, J., Bradley, D.A. and Bodger, P.S. (1985a). "Power System Harmonics", John Wiley and Sons, London.

Arrillaga, J., Eggleston, J.F. and Watson, N.R. (1985b). "Analysis of the AC Voltage Distortion Produced by Convertor Feed DC Drives" IEEE Trans., IA-21 No. 6.

Baker, W.P. (1981). "The Measurement of the System Impedance at Harmonic Frequencies", paper presented at an international conference on Harmonics in Power Systems, UMIST, Manchester.

Bharali, P. and Adkins, B. (1963). "Operational Impedances of Turbogenerators with Solid Rotors", IEE Proc., Vol. 110, No. 12, pp 2185-2199.

Bowles, J.P. (1970). "A.C. System and Transformer Representation for H.V.D.C. Transmission Studies", IEEE Trans., PAS-89, No. 7, pp 1603-1609.

Breuer, G.D., Chow, J.A., Gentile, T.J., Lindh, C.B., Numrich, F.H., Lasseter, R.H., Addis, G. and Vithayathil, J.J. (1982). "HVDC-AC Harmonic Interaction, Parts I and II", IEEE Trans., PAS-101, No. 3 pp 701-718.

Chen, M.S. and Dillon, W.E. (1974). "Power System Modelling", IEEE Proc., Vol. 62, No. 7, pp 901-915.

Clarke, E. (1950). "Circuit Analysis of AC Power Systems", Vol. 2, John Wiley, New York.

Clarke, C.D. (1973). Discussion on Northcote-Green et al (1973), High Voltage DC and/or AC Power Transmission, IEE No. 107, pp 100.

Densem, T.J. (1983). "Three Phase Power System Harmonic Penetration", Ph.D. Thesis, University of Canterbury, New Zealand.

Densem, T.J., Bodger, P.S. and Arrillaga, J. (1984). "Three Phase Transmission System Modelling for Harmonic Penetration Studies", IEEE Trans., Vol. PAS-103, No. 2, pp 310-317.

de Oliveira, J.C. (1978). "Multiple Convertor Harmonic Calculations with Non-Ideal Conditions", Ph.D. Thesis, UMIST, Manchester, England.

Dobinson, L.G. (1975). "Closer Accord on Harmonics", Electronics and Power, Vol. 21, pp 567-572.

Dommel, H.W. (1980). "Line Constants Program Manual", part of the EMPT package.

Ewing, J.S. (1968). "Lumped Circuit Impedance Representation for D.C. Machines", IEEE Trans., PAS-87, No. 4, pp 1106-1110.

Giesner, D.B. and Arrillaga, J. (1972) "Behaviour of H.V.D.C. Links Under Unbalanced A.C. Fault Conditions", Proc. IEE, Vol. 119, No. 2, pp 209,215.

Graham, J. (1984). "Microprocessor Based Control and Protection for HVDC Convertors", Ph.D. Thesis, University of Canterbury, New Zealand.

Harker, B.J. and Arrillaga, J. (1979). "3-Phase A.C./D.C. Load Flow", Proc. IEE, Vol. 126, No. 12, pp 1275-1281.

Harker, B.J. (1980). "Steady State Analysis of Integrated A.C. and D.C. Systems", Ph.D. Thesis, University of Canterbury, New Zealand.

Heffernan, M.D. (1980) "Analysis of A.C./D.C. System Disturbances", Ph.D. Thesis, University of Canterbury, New Zealand.

Hingorani, N.G. and Burbury, M.P. (1970). "Simulation of A.C. System Impedance in H.V.D.C. System Studies", Trans. IEEE, PAS-89, No. 7, pp 820-828.

Holmborn, H. and Martensson, H. (1966). "Experience with A.C. Harmonics from H.V.D.C. Installations", IEE Conf. Publ. 22, pp 445-449.

Hwang, H.H. (1969). "Unbalanced Operations of Three-Phase Machines with Damper Circuits", IEEE Trans., Vol. PAS-88, No. 11, pp 1585-1593.

Hyland, P.R. (1981). "Report on Harmonics Tests Conducted on July 8, 1981", New Zealand Electricity.

IEEE (1983). "Power System Harmonics : An Overview", IEEE Working Group on Power System Harmonics IEE Trans., Vol. PAS-102, No. 8, pp 2455-2460.

IEEE (1984a). "DC Power Transmission", International Conference on DC Power Transmission, June 4-8, Montreal, Quebec, Canada.

IEEE (1984b) "Bibliography of Power System Harmonics", Parts I and II, Trans, IEEE, PAS-103, No. 9, pp 2460-2479.

Jones, C.V. (1967). "The Unified Theory of Electrical Machines", Butterworks, London.

Kauferle, J., Mey, R. and Rogowsky, Y. (1970). "HVDC Stations Connected to Weak AC Systems", IEEE Trans., PAS-89, No. 7, pp 1610-1617.

Kimbark, E.W. (1950). "Electrical Transmission of Power and Signals", John Wiley, New York.

Kimbark, E.W. (1956). "Power System Stability : Synchronous Machines", Dover Publications, New York.

Kimbark, E.W. (1971). "Direct Current Transmission, Vol. 1", Wiley-Interscience, New York.

Kitchen, R.H. (1981). "New Method for Digital-Computer Evaluation of Convertor Harmonics in Power Systems Using State-Variable Analysis", Proc. IEE, Vol. 128, Pt. C., No. 4, pp 196-207.

Kreyszig, E. (1979). "Advanced Engineering Mathematics", 4th edition, N.Y., Wiley.

Last, F.H., Jarrett, G.S.H., Huddart, K.W., Brewer, G.L. and Watson, W.G. (1966). "Isolated Generator-DC Link Feasibility Trails", IEE Conf. Publ. 22, pp 58-65.

Laurent, P.G., Gary, C. and Clade, J. (1962). "D.C. Interconnection Between France and Great Britain by Submarine Cables", CIGRE, Vol. III, Paper No. 331.

Natale, M., Lane, F.J. and Calverley, T. (1966). "The Sardinian-Italian Mainland H.V.D.C. Interconnection", IEE Conf. Publ. 22, pp 42-45.

New Zealand Electricity (1983). "Limitation of Harmonic Levels", Issue 2.

Northcote-Green, J.E.D., Baron, J.A. and Vilks, P. (1973). "The Computation of Impedance Frequency Loci and Harmonic Current Penetration for AC Systems Adjacent to HVDC Conversion Equipment", Conference on High Voltage DC and/or AC Power Transmission, IEE, No. 107, pp 97-102.

O'Kelly, D. and Simmons, S. (1968). "Introduction to Generalized Machine Theory", McGraw-Hill, London.

Pesonen, M.A. (1981). "Harmonics, Characteristic Parameters, Methods of Study, Estimates of Existing Values in the Newwork", ELECTRA, Vol. 77, pp 35-54.

Phadke, A.G. and Harlow, J.H. (1968). "Generation of Abnormal Harmonics in High Voltage ACDC Power Systems", IEEE Trans., PAS-87, No. 3, pp 873-882.

Read, J.C. (1945). "The Calculation of Rectifier and Inverter Performance Characteristics", JEEE 92, Pt. II, pp 495-509.

Reeve, J. and Krishnayya, P.C.S. (1968). "Unusual Current Harmonic Arising from High-Voltage DC Transmission", IEEE Trans., PAS-87, No. 3, pp 883-893.

Reeve, J., Baron, J.A. and Krishnayya, P.C.S. (1969). "A General Approach to Harmonic Current Generation by HVDC Concertors", IEEE Trans., PAS-88, No. 7, pp 989-995.

Reeve, J. and Baron, J.A. (1971). "Harmonic Interaction Between HVDC Convertors and AC Power Systems", IEEE Trans., PAS-90, No. 6, pp 2785-2791.

Reeve, J. and Subba Rao, T. (1974). "Dynamic Analysis of Harmonic Interaction Between A.C. and D.C. Systems", IEEE Trans., Vol. PAS-93, No. 2, pp 640-646.

Robinson, G.H. (1966a). "Harmonic Phenomena Associated with the Benmore-Haywards HVDC Scheme", New Zealand Engineering, 21(1) pp 16-29.

Robinson, G.H. (1966b). "Experience with Harmonics : New Zealand HVDC Scheme", IEE Conf. Publ. 22, pp 442-444.

Roper, R.D. and Leedham, P.J. (1974). "A Review of the Causes and Effects of Distribution System Three Phase Unbalance", Conference on Sources and Effects of Power System Disturbances, IEE Conf. No. 110, London, pp 83-92.

Ross, T.W. and Smith, R.M.A. (1948). "Centralized Ripple Control on High Voltage Networks", IEE Proc., Vol. 95, Part II, pp 470-479.

Ross, N.W. (1972). "Modelling a Ripple Control System", The New Zealand Electrical Journal, pp 116-123.

Stevenson, W.D. (1975). "Elements of Power System Analysis", 3rd Edition, McGraw-Hill International Student Edition.

Subbarao, T. and Reeve, J. (1976). "Harmonics Caused by Imbalanced Transformer Impedances and Imperfect Twelve-Pulse Operation in HVDC Conversion", IEEE Trans., PAS-95, No. 5, pp 1732-1737.

UMIST (1981). "Harmonic in Power Systems", An International Conference on Harmonics in Power Systems, UMIST, Manchester.

Watson, N.R. (1983). "Harmonic Distortion Caused by Convertor Fed DC Drives", Final year project, University of Canterbury, New Zealand.

Watson, N.R., Arrillaga, J. and Joosten, A.P.B. (1985). "AC System Equivalent for the Dynamic Simulation of HVDC Convertors", Fourth International Conference on AC and DC Power Transmission, IEE Conf. No. 255, pp 394-399.

Whitehead, S. and Radley, W.G. (1949). "Generation and Flow of Harmonics in Transmission Systems", Proc. IEE, Vol 96, pp 22-48.

Wintrop, D.A. (1983). "Planning for a Railway Traction Load on the New Zealand Power System", IPENZ Conference, paper No. 62.

Wright, S.H. (1931). "Determination of Synchronous Machine Constants by Tests : Reactances, Resistances and Time Constants", AIEE Trans., Vol. 50, pp 1331-51.

Xia, D. and Heydt, G.T. (1982). "Harmonic Power Flow Studies, Parts I and II", IEEE Trans., Vol. PAS-101, No. 6, pp 1257-1270.

Yacamini, R. and de Oliveira, J.C. (1978). "Harmonics Produced by Direct Current in Converter Transformers", Proc. IEE, Vol. 125, No. 9, pp 873-878.

Yacamini, R. and de Oliveira, J.C. (1980a). "Harmonics in Multiple Converter Systems : A Generalized Approach", Proc. IEE, Vol. 127, Pt. B., No. 2, pp 96-106.

Yacamini, R. and de Oliveira, J.C. (1980b). "Instability in H.V.D.C. Schemes at Low-Order Harmonics", Proc. IEE, Vol. 127, Pt. C., No. 3., pp 179-188.

Yacamini, R. and Smith W.C. (1983). "Third-Harmonic Current from Unbalanced AC/DC Convertors", Proc. Iee, Vol. 130, Pt. C., No. 3, pp 122-126.

APPENDIX A1

VARIATION OF THIRD HARMONIC WITH COMMUTATION ANGLE

There is a well established link between non-equal commutation angles and the production of non-characteristic harmonics, especially the third. A brief investigation was carried out to quantify the effect.

For simplicity, the shape of each commutation is assumed to be linear , with the resulting current waveform as given in figure A1.1.

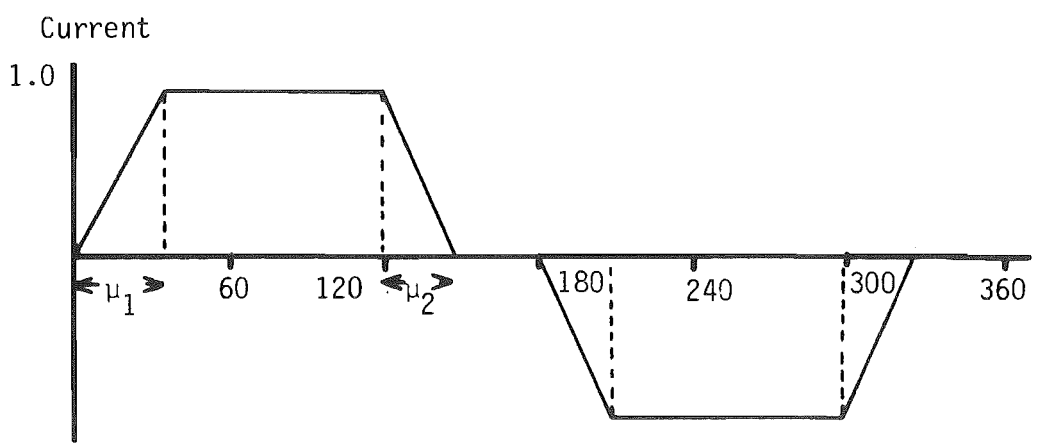

Figure A1.1 : The Current Waveform

average of the commutation angles = $(\mu_1 + \mu_2)/2$

difference of the commutation angles = $\mu_2 - \mu_1$

where μ_1 and μ_2 are the commutation angles.

For values of the average commutation angles of 10, 20, 30, 40 and 50 degrees, the difference between the two commutation angles was varied from -20 to 20 degrees. The resulting waveforms were sampled with 2048 samples per cycle and the FFT taken. The ratio of the magnitude of the third harmonic current component to the fundamental component was calculated and expressed as a percentage.

For a given average commutation angle, figure A1.2 shows that the percentage of third harmonic current is approximately linear with

the difference in the commutation angles. The results also show that when μ_2 is smaller than μ_1 more third harmonic current is produced than if μ_2 is greater than μ_1 by the same margin. Similarly an increase in the average commutation angle will result in a less third harmonic current for a given difference commutation angle.

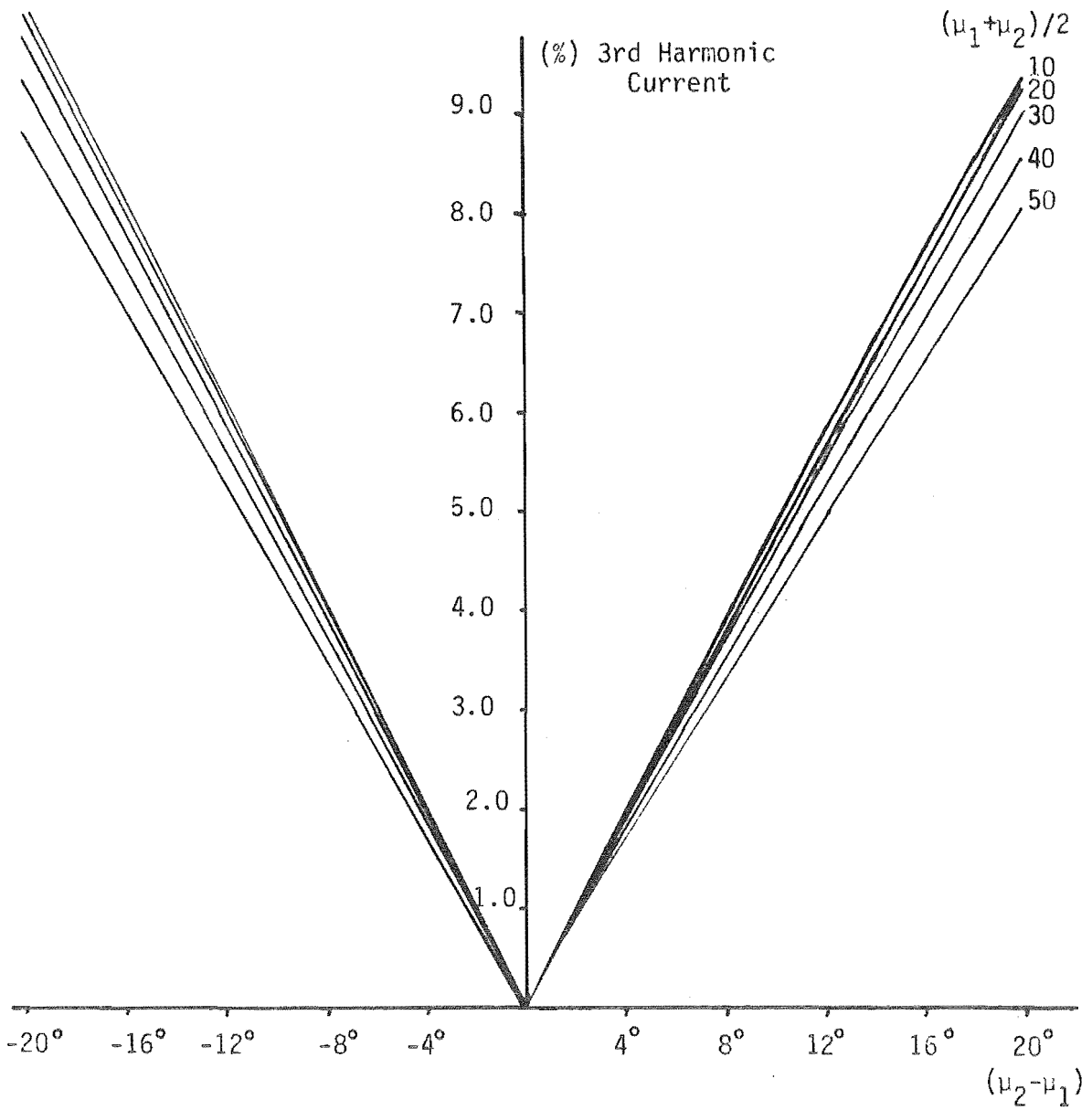

Figure A1.2 : The Percentage Third Harmonic Current Versus the Difference Between the Commutation Angles

APPENDIX 2

ERROR IN THE REPRESENTATION OF A STAR-g/DELTA TRANSFORMER BY AN EQUIVALENT ZIG-ZAG

Figure A2.1(a) shows the connection of a DY11 star-g/delta connected transformer while figure A2.1(b) shows its zig-zag equivalent.

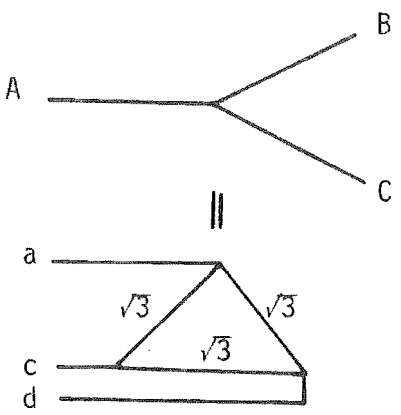

Figure A2.1(a) :
Star-g/Delta Connection

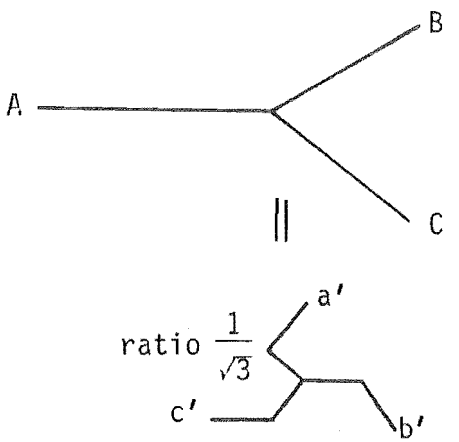

Figure A2.1(b) :
Equivalent Zig-zag Connection

The secondary phase to phase voltages for the star-g/delta and the equivalent zig-zag are

Actual star-g/delta	Equivalent zig-zag
$V_{ac} = \sqrt{3}\, V_B$	$V_{a'c'} = V_{a'} - V_{c'}$ $= 1/\sqrt{3}\,((V_B - V_C) - (V_A - V_C))$ $= \sqrt{3}\, V_B + 1/\sqrt{3}\,(V_A + V_B + V_C)$
$V_{cb} = \sqrt{3}\, V_A$	$V_{c'b'} = V_{c'} - V_{b'}$ $= 1/\sqrt{3}\,(V_A - V_B) - (V_C - V_A))$ $= \sqrt{3}\, V_A + 1/\sqrt{3}\,(V_A + V_B + V_C)$
$V_{ba} = \sqrt{3}\, V_C$	$V_{b'a'} = V_{b'} - V_{a'}$ $= 1/\sqrt{3}\,((V_C - V_A) - (V_B - V_C))$ $= \sqrt{3}\, V_C + 1/\sqrt{3}(V_A + V_B + V_C)$

Therefore $V_{ac} = V_{a'c'}$, $V_{cb} = V_{c'b'}$ and $V_{ba} = V_{b'a'}$ if, and only if, $V_a + V_b + V_c = 0$. A star-g/delta connected transformer acts like a short circuit to zero sequence currents and voltages. However, this short circuit has a finite impedance due to the leakage reactance of the transformer (Chen and Dillon 1974). Therefore, zero sequence currents in the a.c. system may cause some zero sequence voltage on the primary of the star-g/delta transformer. This means that, because $V_a + V_b + V_c$ will not be zero in practice, the equivalent zig-zag connection is not a valid representation of a star-g/delta transformer.

APPENDIX 3

THE FORMATION OF THE ADMITTANCE MATRIX OF A D.C. LINK

A d.c. link will in general be able to be divided into several sections which may include overhead lines and cables as well as smoothing inductors, surge capacitors and d.c. filters. These sections are numbered starting at the end of the link of most interest. For example the New Zealand d.c. link can be divided into six sections as described in figure A3.1.

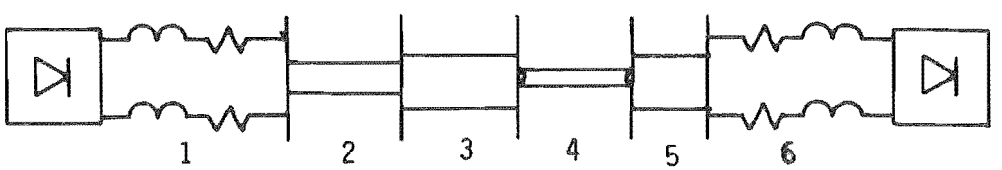

Figure A3.1 : The New Zealand D.C. Link Sections

Section 1 Benmore Inductors

Section 2 South Island Inland Section

Section 3 South Island Coastal Section

Section 4 Cook's Strait Submarine Cable

Section 5 North Island Coastal Section

Section 6 Haywards' Inductors

Because d.c. lines are balanced, of flat construction, the propagation modes are identical to the zero and positive sequences, shown in figure A3.2.

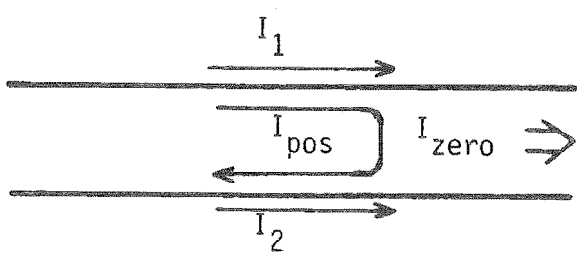

Figure A3.2 : The Zero and Positive Sequences of a D.C Line

Similarly submarine cables have propagation modes of the zero and positive sequence.

For each line the per unit length harmonic admittances and impedances, Y′ and Z′ respectively, are calculated in sequence components using the line constants program (Professor Dommel 1980). The geometry of the line sections is given in Appendix A4. Similarly, for each cable the per unit length harmonic admittances and impedances are calculated in sequence using the method described in Appendix A5. Then for each line and cable the series and shunt elements of the equivalent-π are calculated,

$$Z = Z' * \ell \ \frac{\sinh(\gamma \cdot \ell)}{\gamma \cdot \ell} \qquad \text{A3.1}$$

$$Y = Y' * \ell \ \frac{\tanh(\frac{\gamma \cdot \ell}{2})}{\frac{\gamma \cdot \ell}{2}} \qquad \text{A3.2}$$

where Z' is the impedance per unit length

Y' is the admittance per unit length

ℓ is the length of the section

γ is the complex square root of $Z'Y'$.

The next step is to convert these elements, plus the smoothing inductors and other series and shunt sections, to phase quantities, i.e.,

$$[Z_{phase}] = [C^{-1}] \, [Z_{sequence}] \, [C]$$

or

$$\begin{bmatrix} Z_s & Z_m \\ Z_m & Z_s \end{bmatrix} = \frac{1}{2} \begin{bmatrix} 1 & 1 \\ 1 & -1 \end{bmatrix} \begin{bmatrix} Z_o & 0 \\ 0 & Z_p \end{bmatrix} \begin{bmatrix} 1 & 1 \\ 1 & -1 \end{bmatrix}$$

Therefore

$$Z_s = (Z_o + Z_p)/2$$

$$Z_m = (Z_o - Z_p)/2$$

and similarly

$$Y_s = (Y_o + Y_p)/2$$
$$Y_m = (Y_o - Y_p)/2$$

For inductors $Z_s = R + jhwL$, $Z_m = Y_s = Y_m = 0$. Similarly for shunt branches $Y_s = Y_{shunt}$, $Y_m = Z_s = Z_m = 0$.

With the series impedance and shunt admittance known for each section, the ABCD parameters, as defined by Stevenson (1975), are formed for each section, i.e.,

$$[A_i] = [U] + 1/2[Y][Z]$$
$$[B_i] = [Z]$$
$$[C_i] = [Y] + 1/4[Z][Y]^2$$
$$[D_i] = [A_i]$$

where i is the i^{th} section, [u] is the identity matrix and each block is a 2 x 2 sub-matrix. The n sections of the link can be cascaded

$$\begin{bmatrix} [A] & [B] \\ [C] & [D] \end{bmatrix} = \begin{bmatrix} [A_1] & [B_1] \\ [C_1] & [D_1] \end{bmatrix} x\text{----}x \begin{bmatrix} [A_n] & [B_n] \\ [C_n] & [D_n] \end{bmatrix}$$

The ABCD parameter matrix above can be converted to a 4 x 4 admittance matrix for the 2 poles and two ends of the link.

$$Y = \begin{bmatrix} [D][B]^{-1}[C] - [D][B]^{-1}[A] \\ -[B]^{-1} \qquad [B]^{-1}[A] \end{bmatrix}$$

or expanded to

$$\begin{bmatrix} I_1 \\ I_2 \\ I_3 \\ I_4 \end{bmatrix} = \begin{bmatrix} Y_{11} & Y_{12} & Y_{13} & Y_{14} \\ Y_{21} & Y_{22} & Y_{23} & Y_{24} \\ Y_{31} & Y_{32} & Y_{33} & Y_{34} \\ Y_{41} & Y_{42} & Y_{43} & Y_{44} \end{bmatrix} \begin{bmatrix} V_1 \\ V_2 \\ V_3 \\ V_4 \end{bmatrix}$$

In practice the far end of the link can be regarded as a short to harmonics and, if the far end of the link is also earthed then $V_3 = V_4 = 0$. This assumption reduces the admittance matrix to

$$\begin{bmatrix} I_1 \\ I_2 \end{bmatrix} = \begin{bmatrix} Y_{11} & Y_{12} \\ Y_{21} & Y_{22} \end{bmatrix} \begin{bmatrix} V_1 \\ V_2 \end{bmatrix}$$

Finally, if only the positive sequence admittance is to be considered

$$Y_{pos} = (Y_{11} = Y_{12})/2$$
$$= (Y_{22} - Y_{21})/2$$

This corresponds to a voltage $2V_1$ across the terminals of the link causing a current of I_1 and $-I_1$ to flow in the positive and negative poles respectively.

APPENDIX 4

LINE GEOMETRY FOR THE A.C. AND D.C. TOWERS USED IN THIS THESIS

A4.1 The D.C. Overhead Line in New Zealand

Figure A4.1 shows a typical tower used in the South Island inland overhead line section of the New Zealand h.v.d.c. link.

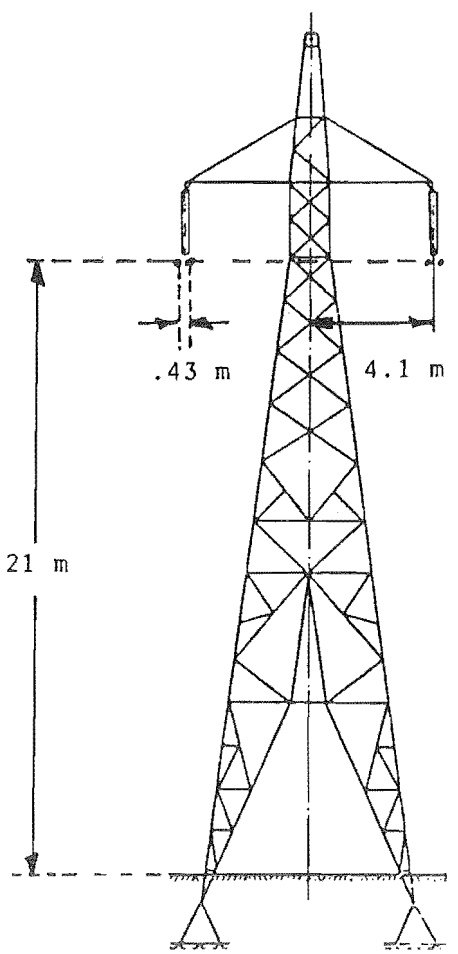

Figure A4.1 : Inland Overhead Line Tower

	Main conductors	Earth Wire
Resistance	.0351 Ohms/Km	3.1 Ohms/Km
Diameter	38.4 mm	11.5 mm
Skin ratio T/D	0.3849	0.5
Bundle Spacing	431.8 mm	---

Towers in the coastal sections are identical to those in figure A4.1 except the spacing between conductors is increased from 8.2 m to 12.8 m.

A4.2 The A.C. Overhead Lines

The a.c. line used in chapters 4 and 7 are the single and double circuit used by Densem (1983) with the length varied to suit as necessary. The tower of the single circuit line, shown in figure A4.2, is one from the Islington to Kikiwa line.

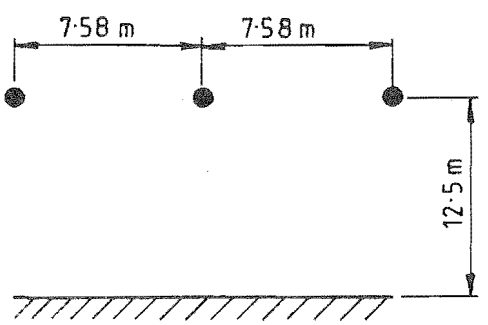

Conductor type Zebra (54/3.18 + 7/3.18)

Figure A4.2 : The Single Circuit Tower

Similarly, the double circuit tower, shown in figure A4.3, is one from the Makarewa to Manapouri line.

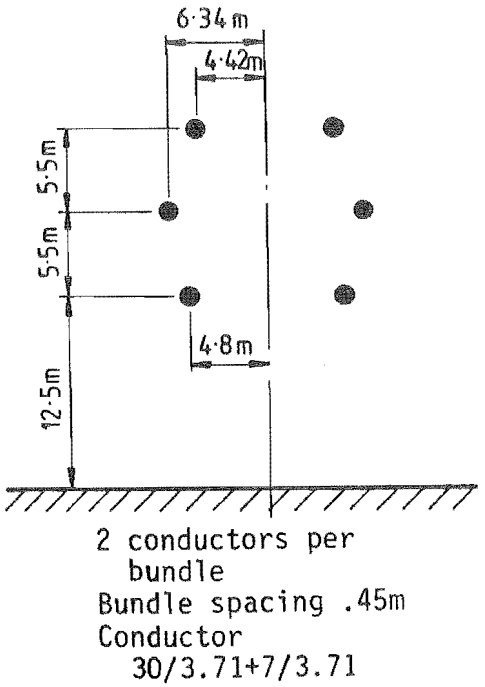

Figure A4.3 : The Double Circuit Tower

Full details of the line and conductor geometry can be obtained from Densem (1983). In every case the earth resistivity is 100 ohm-metres.

APPENDIX 5

THE METHOD OF CALCULATING THE PER UNIT LENGTH HARMONIC ADMITTANCES AND IMPEDANCES FOR A D.C. CABLE WITH THE NEW ZEALAND LINK AS AN EXAMPLE

In New Zealand there are three d.c. cables across Cook's Strait and only two are used at any one time. Because the cables are well separated the mutual effects between the cables can be ignored. This means that

$$Z_m = Y_m = \text{zero}$$

$$Z_s = Z_o = Z_p$$

and

$$Y_s = Y_o = Y_p$$

The actual cross section of the cable is very complex, but it can be simplified to the cross section of figure A5.1.

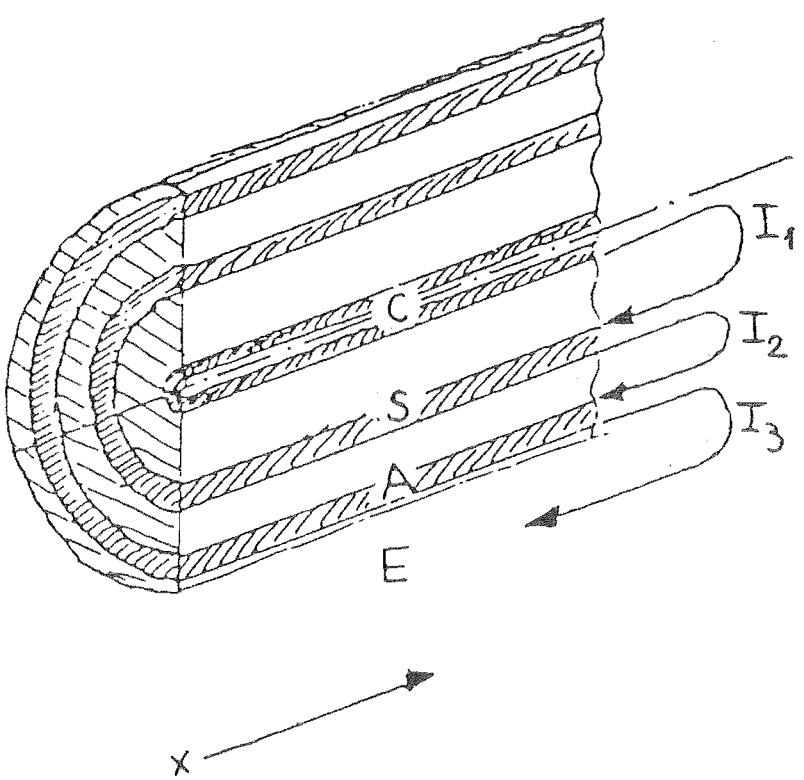

Figure A5.1 : Simplified Representation of the Cross Section

The series per unit length harmonic impedance for the cable is calculated by the following set of loop equations,

$$-\begin{bmatrix} dV_1/dx \\ dV_2/dx \\ dV_3/dx \end{bmatrix} = \begin{bmatrix} Z'_{11} & Z'_{12} & 0 \\ Z'_{21} & Z'_{22} & Z'_{23} \\ 0 & Z'_{32} & Z'_{33} \end{bmatrix} \begin{bmatrix} I_1 \\ I_2 \\ I_3 \end{bmatrix} \qquad \text{A5.1}$$

where

$$Z'_{11} = Z'_{\text{core-outside}} + Z'_{\text{core/sheath-insulation}} + Z'_{\text{sheath-inside}}$$

where $Z'_{\text{core-outside}}$ is the internal impedance of core with sheath return path,

$Z'_{\text{core/sheath insulation}}$ is the impedance of the insulation between core and sheath

$Z'_{\text{sheath-inside}}$ is the internal impedance of sheath with return path through the core.

Similarly,

$$Z'_{22} = Z'_{\text{sheath-outside}} + Z'_{\text{sheath/armour-insulation}} + Z'_{\text{armour-inside}}$$

$$Z'_{33} = Z'_{\text{armour-outside}} + Z'_{\text{armour/sea-insulation}} + Z'_{\text{sea-inside}}$$

$$Z'_{12} = Z'_{21} = Z'_{\text{mutual core-sheath}}$$

$$Z'_{23} = Z'_{32} = Z'_{\text{mutual sheath-armour}}$$

All the above impedances can be calculated using the TUBE subroutine (Dommel 1980), except for the insulation impedance which is given by

$$Z_{\text{insulation}} = j\omega\mu/2\pi \ \ln(R_{\text{out}}/R_{\text{in}})$$

where R_{out} and R_{in} are the outside and inside radii of the insulation.

With

$$V_1 = V_{core} - V_{sheath} \qquad I_1 = I_{core}$$

$$V_2 = V_{sheath} - V_{armour} \qquad I_2 = I_{core} + I_{sheath}$$

and $V_3 = V_{armour}$

equations A5.1 can be rewritten as

$$-\begin{bmatrix} dV_{core}/dx \\ dV_{sheath}/dx \\ dV_{armour}/dx \end{bmatrix} = \begin{bmatrix} Z'_{cc} & Z'_{cs} & Z'_{ca} \\ Z'_{sc} & Z'_{ss} & Z'_{sa} \\ Z'_{ac} & Z'_{as} & Z'_{aa} \end{bmatrix} \begin{bmatrix} I_{core} \\ I_{sheath} \\ I_{armour} \end{bmatrix} \qquad A5.2$$

where

$$Z'_{cc} = Z'_{11} + 2Z'_{12} + Z'_{22} + 2Z'_{23} + Z'_{33}$$

$$Z'_{cs} = Z'_{sc} = Z'_{12} + Z'_{22} + 2Z'_{23} + Z'_{33}$$

$$Z'_{ca} = Z'_{ac} = Z'_{sa} = Z'_{as} = Z'_{23} + Z'_{33}$$

$$Z'_{ss} = Z'_{22} + 2Z'_{23} + Z'_{33}$$

$$Z'_{aa} = Z'_{33}$$

Because a good approximation for many cables having bonding between the sheath and the armour and the armour is earthed to the sea is $V_{sheath} = V_{armour} = \text{zero}$, the system can be reduced to

$$-dV_{core}/dx = Z'I_{core} \qquad A5.3$$

where Z' is a reduction of the impedance matrix of equation A5.2.

Similarly, for each cable the per unit length harmonic admittance is calculated, i.e.,

$$-\begin{bmatrix} dI_1/dx \\ dI_2/dx \\ dI_3/dx \end{bmatrix} = \begin{bmatrix} jwC'_1 & 0 & 0 \\ 0 & jwC'_2 & 0 \\ 0 & 0 & jwC'_3 \end{bmatrix} \begin{bmatrix} V_1 \\ V_2 \\ V_3 \end{bmatrix} \qquad A5.4$$

where $C_i = 2\pi\varepsilon_o\varepsilon_r/\ln(R_{out}/R_{in})$. Therefore, when converted to core, sheath and armour quantities,

$$\begin{vmatrix} dI_{core}/dx \\ dI_{sheath}/dx \\ dI_{armour}/dx \end{vmatrix} = \begin{vmatrix} Y'_1 & -Y'_1 & 0 \\ -Y'_1 & Y'_1 + Y'_2 & -Y'_2 \\ 0 & -Y'_2 & Y'_2 + Y'_3 \end{vmatrix} \begin{vmatrix} V_{core} \\ V_{sheath} \\ V_{armour} \end{vmatrix} \quad \text{A5.5}$$

where $Y'_i = jwC_i$. If, as before, $V_{sheath} = V_{armour} =$ zero, equation A5.5 reduces to

$$-dI_{core}/dx = Y'_1 V_{core} \quad \text{A5.6}$$

Therefore, for frequency of interest, the cable, the per unit length harmonic impedance, Z', and admittance, Y', are calculated with both the zero and positive sequence values being equal to the Z' of equation A5.3 and the Y'_1 of equation A5.6 respectively.

Table A5.1 contains the geometry of the New Zealand submarine cable.

Table A5.1 : The Data for the New Zealand Cable System

Conductor	Inside Diameter	Outside Diameter	Resistance
core	13.462 mm	33.477 mm	.0331 Ohms/Km
sheath	63.242 mm	71.044 mm	.2865 Ohms/Km
armour	88.189 mm	98.958 mm	.1148 Ohms/Km
sea	110.896 mm	--	.21 Ohm-metres

A relative permittivity of 3.5 and a relative permeability of 1.0 for the insulation are also assumed.

APPENDIX A6

IA 11-01 8404171

ANALYSIS OF THE A.C. VOLTAGE DISTORTION PRODUCED BY CONVERTOR-FED D.C. DRIVES

J. Arrillaga (Sen. Mem.), J.F. Eggleston and N.R. Watson

Abstract

An iterative algorithm is presented for the analysis of the harmonic interaction between convertor-fed d.c. drives and a relatively weak a.c. distribution system. The individual effect of each of the main parameters influencing the level of voltage distortion is assessed, with reference to a typical large d.c. drive. Special attention is given to the analysis of the current waveform during commutations, without the restrictions normally used in such analysis, i.e. constant d.c. current and undistorted a.c. supply voltages.

The authors are with the Department of Electrical & Electronic Engineering, University of Canterbury, Christchurch, New Zealand.

INTRODUCTION

In the analysis of the harmonic currents produced by thyristor-controlled d.c. drives any distortion present on the supply voltage or created by the d.c. drive, is generally ignored. While this practice is perfectly reasonable for small and medium size drives, it is likely to yield unacceptable information in cases where either the d.c. drive is large and/or the supply system weak.

Moreover, as the numbers and ratings of power electronic devices increase there is a need for stricter harmonic regulations.

In the absence of accurate analytical models it is difficult to predict the levels of prospective distortion and to determine with certainty the liability of an alleged offender.

There is information in the literature on the harmonic behaviour of a.c. system impedances, d.c. motors, convertors and convertor transformers. However each publication tends to emphasixe only one aspect of the problem, e.g. the effect of the d.c. drive[2], the static convertor[3] or the a.c. system[4]. However these references do not consider the harmonic interaction between the drive, convertor and supply system. The solution of such problem requires a comprehensive computer model with flexibility to investigate the sensitivity of each particular scheme to variations in the representation of its individual components. Such a model, described in this paper, is essential in the prediction of harmonic current and voltage levels in the system. It also provides the basis for the optimization of filter design when required.

STRUCTURE OF THE PROGRAM

In the context of this paper harmonic interaction is the process by which any distortion present in the a.c. system voltage waveform can influence the harmonic currents generated by the convertor-fed d.c. drive and vice versa. A brief outline of the program structure developed to

investigate such harmonic interaction is illustrated in Figure 1.

The harmonic admittances for the a.c. and d.c. systems as well as the initial load flow conditions, are read-in prior to entering the iterative loop.

A load flow study is necessary to provide information of active power, reactive power and phase voltages at the convertor terminals as well as convertor firing delay angles for the particular operating condition. If a load flow program is unavailable the iterative program can start from information of the nominal voltage and operating conditions.

At each iteration the system can be considered to be constructed of three regions, each of which is solved in succession (Figure 2). For the first iteration it is assumed that the d.c. current is constant and the a.c. system voltages are sinusoidal. The sequence for each iteration is as follows:

Region 1: Using the a.c. system voltages and d.c. current waveform (from the previous iteration), the harmonic current injections and d.c. voltage waveform are found.

Region 2: From the harmonic currents injected into the a.c. system and its harmonic impedances, the a.c. system voltages are calculated.

Region 3: The d.c. voltage waveform (found when solving region 1) and d.c. system admittance at harmonic frequencies, are used to calculate the d.c. current waveform.

The terminating condition for the iterative loop is when the changes in voltage zero crossings between two successive iterations is smaller than a specified value. When this condition is met, one further iteration is performed.

A.C. System Representation

The degree to which the a.c. power system must be represented depends

on the purpose of the investigation. In general, the more simplifying assumptions made without invalidating the study the better. An obvious and simple representation often used is the short circuit impedance of the a.c. system at the busbar.

However, the variation of power system impedance with frequency is far from linear and can even change from inductive to capacitive in a spiral-like fashion when plotted in the impedance plane. At the utilization end of the scale, however, the impedance tends to be resistive-inductive as illustrated by the snap-shot information shown in Figure 3 which relates to an 11 kV supply to a mixed load system consisting of domestic, commercial and industrial customers[5].

Moreover, the harmonic impedances of the three phases are not exactly balanced. Transmission line geometry is such that some mutual impedance imbalance exists between phases. Also the imperfect distribution of single phase loadings contributes to the imbalance. Even when the system is reasonably balanced at fundamental frequency, the impedance imbalance may be considerable at harmonic frequencies. Due to the asymmetry inherent in all power systems, even if the harmonic currents injected into the a.c. system are balanced the harmonic voltages in the power system can be significantly unbalanced. So a realistic quantitative analysis of harmonic levels necessitates a detailed three phase model, which is capable of representing the coupling between circuits as well as the impedance imbalance between phases. A harmonic penetration model developed by one of the authors[6] provides such detail.

In harmonic penetration studies, the a.c. system components, other than those generating the harmonic injections, can be assumed to be linear and thus the voltage distorting effect of each harmonic can be considered separately.

Static Convertor Model

The conventional method of harmonic assessment for static convertors is to consider the harmonic currents injected into the a.c. system while the d.c. current is constant and the a.c. system voltages sinusoidal. Under such conditions the 6-pulse convertor produces only characteristic harmonics, i.e. those of order 6Q and 6Q±1, on the d.c. and a.c. sides respectively where Q is an integer. The characteristic harmonic current injections are then used to estimate the resultant harmonic voltage levels.

The real life situation is such that the d.c. current has some ripple, and the supply voltages are not perfectly sinusoidal and balanced. Therefore the characteristic harmonics are different from the ideal and small amounts of uncharacteristic harmonics are always present on both sides of the convertor. The convertor model used in the present study, while using the above assumptions as the initial condition, continues by reassessing the harmonic voltage levels using the most recently calculated harmonic information. This iterative method provides information of the interaction between the a.c. system voltage harmonics and injected harmonic currents. The formulation of the convertor voltages and currents and the derivation of the harmonic current injection is described in the Appendix.

D.C. Motor Representation

Early models represented the armature circuit as a series combination of resistance and inductance (Figure 4a), the inductance being a function of the shunt field current. However, the response of d.c. motors to harmonic frequencies deviates from those predicted by the simple R-L series circuit. The deviation is brought about by eddy currents generated in various parts of the windings and magnetic sections of the motor. The

eddy currents are due to the time-varying nature of the slot currents and the net effect is to reduce the effective inductance with frequency as well as to increase the apparent resistance. It is the increase of resistance that causes additional losses when operated on rectified power.

The equivalent circuit of Figure 4(b) has been proposed by Ewing[2] to improve the modelling of frequency dependence. In this model R_a represents the armature circuit resistance, $(L_a + L_c)$ the total armature circuit inductance and part of the inductance is shunted by a resistor R_c which represents the eddy current loss.

The use of lumped circuit parameter models in performance prediction is only practical when it is possible to obtain values for the circuit constants. For the model of Figure 4(b) this has been carried out by taking impedance measurements at a series of different frequencies.

It should be noted that if the various harmonic impedances of the motor were available the equivalent circuit would not be required as this information can be used to generate a data file to be used directly by the harmonic interaction program. However, at the planning stage the different motor options are not generally available as the manufacturers only supply two lumped constants, i.e. the overall armature resistance and inductance. The effect of the two alternative models is discussed in the next section.

TEST SYSTEM AND RESULTS

The characteristics of the drive and system selected to investigate the relative influence of the various parameters of the analytical model are as follows:

Motor rating: 950 kW

Back emf: 485 V

Armature current: 1900 A

Armature resistance: 0.0078Ω

Armature inductance: .41 mH

The d.c. motor is connected to the low voltage side of a 33 kV/415 V star-delta distribution transformer through a six-pulse SCR-controlled bridge rectifier.

The results presented in this section relate to a balanced a.c. system at the nominal voltage. However, the modelling of transformer and a.c. system impedances was varied in different studies.

Effect of Motor Representation

In order to assess the effect of the improved Ewing model, the armature inductance is divided in two parts, i.e. $L_a = 0.272$ mH and $L_c = 0.138$ mH, while a resistance ($R_c = 0.1495\Omega$) is connected in parallel with L_c.

The levels of 5th and 7th voltage harmonic distortion of the Ewing and series R-L models are plotted in Figure 5 versus a.c. system impedance. Although the difference is small for reasonably strong supply systems it can be substantial for weak systems. For instance the total harmonic distortion calculated by the conventional model exceeds the limit recommended by Engineering Recommendation G5/3[7] with a system inductance of 43.5 mH whereas that of the Ewing model is still within the limit.

The difference between the two models is more marked at large firing angles, i.e. when the d.c. side harmonic content increases. For example during motor start, under nominal d.c. current, the firing delay required is 86^{o} and the results of the two models with a system inductance of 43.5 mH are plotted in Figure 6. Under these conditions the Ewing model produces 7.5% extra 5th harmonic voltage but reduces the level of the 7th harmonic by 22%.

Effect of Commutating Reactance

The harmonics produced by a thyristor-controlled d.c. drive are largely affected by the leakage reactance of the convertor transformer

which is the main constituent of the commutation reactance. Figure 7 shows the comparison between two realistic extremes of transformer leakage reactance, i.e. X = 0.05 p.u. and X = 0.15 p.u., both in series with a 50 mH a.c. system inductance. In each case the delay angle was kept constant at 12.7^{o}, which in the case of the lower reactance was achieved by an off-nominal tap of +6.25% in the primary of the convertor transformer.

From Figure 7 it can be seen that the larger commutation reactance produces similar levels of 5th and 7th but considerably less 11th, 13th, 17th and 19th voltage harmonic distortion. However this advantage must be weighed against a reduced displacement factor, i.e. 0.9 compared to 0.95 for the case of the lower transformer reactance.

Effect of a.c. System Model

Throughout this section the d.c. motor is represented by the Ewing model and a transformer leakage reactance of 0.05 p.u. is used.

A simple representation often used for the a.c. system is a pure inductance corresponding to the short circuit impedance. When a series resistance is added, even up to 35% of the fundamental reactance, the harmonic distortion is practically identical to the case of pure inductance.

The addition of a resistance in parallel with the system short-circuit inductance provides an impedance of practically constant magnitude at higher frequencies, which is more typical of the behaviour of distribution systems. For the system under consideration the shunt resistance was calculated to give a cut-off frequency of 500 Hz.

If the information is available a separate system impedance should be used for each harmonic. The test impedances reported by Baker[5], and illustrated in Figure 3, are used as a reference to assess the

accuracy of the other models. To compensate for the different primary voltage, the a.c. system impedances had to be scaled from 11 to 33 kV.

Figure 8 indicates that considerable differences exist between the harmonic voltages obtained using the test impedances and those derived from the simpler parallel resistor/inductor or a pure inductance equivalents.

The comparison between studies using the pure inductance and the test impedances (Figure 8(a)) shows very little agreement. In particular the 5th harmonic level voltages of the test impedances is about double that of the pure inductance model, while those of the higher harmonics are only a half.

At frequencies above 500 Hz the magnitude of the test distribution a.c. system impedance appears to be reasonably constant[5] and thus the parallel inductance/resistance combination (Figure 8(b)) proves to be a reasonable approximation at higher frequencies. However the presence of a resonance near the 5th harmonic causes more voltage distortion than the short circuit impedance would have predicted.

As a rough approximation the distribution systems impedance in Figure 3 can be considered constant from about 250 Hz. Consequently the a.c. system was also modelled as a pure resistance, i.e. a constant impedance magnitude versus frequency. The results, compared to the case of the test impedances (Figure 8(c)), show very good agreement. Although there is some difficulty in choosing the value of the resistance, the magnitude of the system impedance of a typical distribution system appears to level off at about 500 Hz;[5] therefore the reactance of the short-circuit inductance at 500 Hz would thus prove to be a reasonable value.

CONCLUSIONS

The paper has described the structure of an iterative algorithm capable of assessing accurately the harmonic voltages produced by convertor-

controlled d.c. drives at the point of common coupling with other loads.

This algorithm provides a practical alternative to commonly used pessimistic models, which may suit the supply authority involved, but often results in an unnecessary expense to the industry.

The application of the algorithm in a practical situation has shown the importance of modelling the frequency dependence of the d.c. drive and the a.c. system wherever possible. The a.c. system can rarely be modelled with any degree of confidence and therefore a realistic worst case will often be a reasonable compromise; however, the use of the short-circuit impedance will in general produce unacceptable error.

The results have also highlighted the advantage of high transformer impedance in reducing the voltage distortion at the point of common coupling; this, however, worsens the power factor and may lead to excessive internal distortion when the same transformer feeds other plant components.

ACKNOWLEDGEMENTS

The authors wish to acknowledge the advice received from Dr. P.S. Bodger, Dr. B.J. Harker and Dr. T.J. Densem. They are also grateful to the New Zealand Energy Research and Development Corporation for the financial help towards this project and to Mr. W.P. Baker (Electricity Council Research Centre, Capenhurst) for the use of some of his experimental results.

APPENDIX: Formulation of Convertor Currents and Voltages

The Commutation Current Equation

In terms of the phase to neutral voltages of the incoming and outgoing phases the following general expression has been derived[3] for the commutation current:

$$i_n(t) = \sum_{j=1}^{50} (X_j e^{-t/T_{nm}} + S_j (j\omega t + \phi_j)) + Y(1-e^{-t/T_{nm}}) + C_{nm}$$

where $X_j = \frac{B_j}{L_{nm}} \frac{H_j - 1/T_{nm}}{j^2\omega^2 + 1/T_{nm}^2}$

$$S_j = \frac{B_j}{j\omega L_{nm}} \sqrt{\frac{H_j^2 + 1/T_{nm}^2}{j^2\omega^2 + 1/T_{nm}^2}}$$

$$Y = \frac{R_m I_d}{R_{nm}}$$

n is the incoming phase and m is the outgoing phase.

$$R_{nm} = R_n + R_m$$
$$L_{nm} = L_n + L_m$$
$$T_{nm} = L_{nm}/R_{nm}$$
$$A_j = \hat{V}_{jn} \cos(j\theta_n + \phi_{jn}) - \hat{V}_{jm} \cos(j\theta_n + \phi_{jm})$$
$$B_j = \hat{V}_{jn} \sin(j\theta_n + \phi_{jn}) - \hat{V}_{jm} \sin(j\theta_n + \phi_{jm})$$
$$H_j = j\omega A_j/B_j$$
$$\phi_j = \tan^{-1}(1/j\omega T_{nm}) - \tan^{-1}\left(\frac{H_j}{j\omega}\right)$$

$\hat{V}_{jn}$ and ϕ_{jn} are the magnitude and phase of the jth harmonic of the phase to neutral voltage of the incoming phase.

$\hat{V}_{jm}$ and ϕ_{jm} are as above for the outgoing phase.

C_{nm} is an integration constant such that $i_n(0) = 0$

However for a more general transformer model, capable of representing the star-delta connection in the presence of zero sequence voltage, the above equation needs to be rewritten in terms of the phase to phase voltages, i.e.

$$V_{nm} = \sum_{j=1}^{50} A_j \sin j\omega t + B_j \cos j\omega t$$

using as time reference θ_1 (the first firing angle).

For a star/star transformer

$$A_j = \hat{V}_{jn} \cos(j\theta_1 + \phi_{jn}) - \hat{V}_{jm} \cos(j\theta_1 + \phi_{jm})$$

$$B_j = \hat{V}_{jn} \sin(j\theta_1 + \phi_{jn}) - \hat{V}_{jm} \cos(j\theta_1 + \phi_{jm})$$

For a star-g/delta transformer (DY11), and a commutation from valve 1 to valve 3;

$$A_j = -\sqrt{3}\, V_1 \cos(j\theta_1 + \phi_{j1})$$

$$B_j = -\sqrt{3}\, V_1 \sin(j\theta_1 + \phi_{j1})$$

with equivalent equations for the other phase to phase pairs.

For the nth valve commutation the new A'_j and B'_j are calculated from the original A_j and B_j (with θ_1 as their reference), i.e.

$$A'_j = \hat{V}_{jn} \cos(j\theta_n + \phi_{jn}) - \hat{V}_{jm} \cos(j\theta_n + \phi_{jm})$$

$$= \hat{V}_{jn} \cos((j\theta_n - j\theta_1) + (j\theta_1 + \phi_{jm})) - \hat{V}_{jm} \cos((j\theta_n - j\theta_1) + (j\theta_1 + \phi_{jm}))$$

$$= A_j \cos(j\theta_n - j\theta_1) - B_j \sin(j\theta_n - j\theta_1)$$

similarly $B'_j = A_j \sin(j\theta_n - j\theta_1) + B_j \cos(j\theta_n - j\theta_1)$

A.C. Current Injections

The general expression for the d.c. current waveform is:

$$I_d = I_{do} + \sum_{j=1}^{50} I_{dj} \sin(j\omega t + \phi_{dj})$$

where I_{do} is the average d.c. current level and the I_{dj} coefficients are obtained from the previous iteration of the d.c. model, i.e.

$$[I_{dj}] = [Y_j]\,[V_{dj}]$$

where Y_j are the harmonic admittances of the d.c. drive.

When only two valves conduct, say 1 and 2, the instantaneous phase current injections are derived from the expression:

$$I = \begin{vmatrix} I_1 \\ I_2 \\ I_3 \end{vmatrix} = \begin{vmatrix} I_d \\ 0 \\ -I_d \end{vmatrix}$$

With reference to Figure 9 during the commutation from valve 1 to 3 the current injections are:

$$I = \begin{vmatrix} I_1 \\ I_2 \\ I_3 \end{vmatrix} = \begin{vmatrix} I_d - i_n \\ i_n \\ -I_d \end{vmatrix}$$

where i_n is the commutation current.

In order to calculate the current injections in the frequency domain the current waveforms are divided into 12 sections (Table A1), six of them with one conducting valve on each side of the bridge and the other six with one side of the bridge undergoing a commutation. Each of the three phases is sampled and a Fast Fourier Transform performed, to derive the harmonic content of the current injections.

Convertor d.c. Voltage

As with the current injections information of the commutating voltage, commutating impedance, the d.c. current waveform and the firing instants is needed. Because these are the same in both studies, and the same 12 sections are used, the current injections and the d.c. voltage can be sampled simultaneously.

The situation of one valve on each side of the bridge conducting is described in the previous section. With valves 1 and 2 conducting:

$$\begin{aligned} V_d &= V_1' - V_3' \\ &= (V_1 - L_1 \frac{dId}{dt} - R_1 I_d) - (V_3 + L_3 \frac{dId}{dt} + R_3 I_d) \\ &= V_1 - V_3 - (L_1 + L_3) \frac{dId}{dt} - (R_1 + R_3) I_d \end{aligned}$$

Yacamini and de Oliveira[3] used the approximation that $V_1' = V_1$ and $V_3' = V_3$ and hence $V_d = V_1 - V_3$, i.e. the voltage drop across the commutating

impedance is ignored.

However, during the commutation process the voltage drop across the commutating impedance is significant as the secondary of the transformer has two phases with a temporary short circuit. Figure 9, in the previous section, describes this situation. Valve 2 is conducting and there is a commutation from valves 1 to 3.

$$V_d = V_2' - V_3' \quad \text{and} \quad V_1' = V_2'$$

assume $V_3' = V_3 \qquad V_d = V_2 + V_x - V_3$

where $V_x = - L_2 \frac{di_2}{dt} - R_2 i_2$

and $$i_2 = \sum_{j=1}^{50} [X_j e^{-t/T_{nm}} + S_j \sin(j\omega t + \delta_j)] + Y[1 - e^{-t/T_{nm}}] + C_{nm}$$

the commutation current, with n=2 and m=1.

$$\text{Therefore } V_x = W e^{-t/T_{nm}} + \sum_{j=1}^{50} [M_j \cos(j\omega t) + N_j \sin(j\omega t)] + K_n .$$

where $M_j = -(j\omega L_n S_j \cos\delta_j + R_n S_j \sin\delta_j)$

$N_j = j\omega L_n S_j \sin\delta_j - R_n S_j \cos\delta_j$

$W = (\frac{L_n}{T_{nm}} - R_n) (\sum_{j=1}^{50} X_j - Y)$

$K_n = -R_n (Y + C_{nm})$

The equations applying to each of the 12 sections of the waveform are listed in Table A2.

TABLE A1. The 12 Sections of the line current waveforms.

Section	Equation line 1	line 2	line 3	Limit referenced to θ_1
0-1	i_c	$-I_d$	I_d-i_c	$0 \leq \theta \leq \mu_1$
1-2	I_d	$-I_d$	0	$\mu_1 \leq \theta \leq \theta_2-\theta_1$
2-3	I_d	$-I_d-i_c$	i_c	$\theta_2-\theta_1 \leq \theta \leq \theta_2-\theta_1+\mu_2$
3-4	I_d	0	$-I_d$	$\theta_2-\theta_1+\mu_2 \leq \theta \leq \theta_3-\theta_1$
4-5	I_d-i_c	i_c	$-I_d$	$\theta_3-\theta_1 \leq \theta \leq \theta_3-\theta_1+\mu_3$
5-6	0	I_d	$-I_d$	$\theta_3-\theta_1+\mu_3 \leq \theta \leq \theta_4-\theta_1$
6-7	i_c	I_d	$-I_d-i_c$	$\theta_4-\theta_1 \leq \theta \leq \theta_4-\theta_1+\mu_4$
7-8	$-I_d$	I_d	0	$\theta_4-\theta_1+\mu_4 \leq \theta \leq \theta_5-\theta_1$
8-9	$-I_d$	I_d-i_c	i_c	$\theta_5-\theta_1 \leq \theta \leq \theta_5-\theta_1+\mu_5$
9-10	$-I_d$	0	I_d	$\theta_5-\theta_1+\mu_5 \leq \theta \leq \theta_6-\theta_1$
10-11	$-I_d-i_c$	i_c	I_d	$\theta_6-\theta_1 \leq \theta \leq \theta_6-\theta_1+\mu_6$
11-12	0	$-I_d$	I_d	$\theta_6-\theta_1+\mu_6 \leq \theta \leq 2\pi$

where i_c is the commutating current in the incoming valve.

TABLE A2. The 12 Sections of the d.c. voltage waveform.

Section	Equation	Limits θ references to θ_1
0- 1	$V_d = V_1 - V_2 + V_x$	$0 \leq \theta \leq \mu_1$
1- 2	$V_d = V_1 - V_2$	$\mu_1 \leq \theta \leq \theta_2 - \theta_1$
2- 3	$V_d = V_1 - V_3 - V_x$	$\theta_2-\theta_1 \leq \theta \leq \theta_2-\theta_1 + \mu_2$
3- 4	$V_d = V_1 - V_3$	$\theta_2-\theta_1+\mu_1 \leq \theta \leq \theta_3 - \theta_1$
4- 5	$V_d = V_2 - V_3 + V_x$	$\theta_3-\theta_1 \leq \theta \leq \theta_3-\theta_1 + \mu_3$
5- 6	$V_d = V_2 - V_3$	$\theta_3-\theta_1+\mu_3 \leq \theta \leq \theta_4-\theta_1$
6- 7	$V_d = V_2 - V_1 - V_x$	$\theta_4-\theta_1 \leq \theta \leq \theta_4-\theta_1 + \mu_4$
7- 8	$V_d = V_2 - V_1$	$\theta_4-\theta_1+\mu_4 \leq \theta \leq \theta_5-\theta_1$
8- 9	$V_d = V_3 - V_1 + V_x$	$\theta_5-\theta_1 \leq \theta \leq \theta_5-\theta_1 + \mu_5$
9-10	$V_d = V_3 - V_1$	$\theta_5-\theta_1+\mu_5 \leq \theta \leq \theta_6-\theta_1$
10-11	$V_d = V_3 - V_2 - V_x$	$\theta_6-\theta_1 \leq \theta \leq \theta_6-\theta_1 + \mu_6$
11-12	$V_d = V_3 - V_2$	$\theta_6-\theta_1+\mu_6 \leq \theta \leq 2\pi$

REFERENCES

(1) Goldberg, G. 'The effect of voltage and current harmonics on electrical equipment', Der Electroniker, Vol. 14, No. 7, July 1975, pp. EL1-7.

(2) Ewing, J.S. 'Lumped circuit impedance representation for DC machines', Trans. IEEE, PAS-87, No. 4, 1968, pp. 1106-1110.

(3) Yacamini, R. and de Oliveira, J.C. 'Harmonics in multiple convertor systems: a generalised approach', Proc. IEE, Vol. 127, Pt. B, No. 2, 1980, pp. 96-106.

(4) Densem, T.J., Bodger, P.S. and Arrillaga, J. 'Three phase transmission system modelling for harmonic penetration studies', IEEE Power Engineering Society, Summer Meeting 1983, Los Angeles, paper 835M444-7.

(5) Baker, W.P. 'Measured impedances of power systems', International Conference on harmonics in Power Systems, University of Manchester Institute of Science and Technology, 1981, pp. 141-158.

(6) Arrillaga, J., Densem, T.J. and Harker, B.J. 'Zero sequence harmonic current generation in transmission lines connected to large convertor plant', Trans. IEEE, PAS-107, No. 7, 1983, pp. 2357-2363.

(7) Engineering Recommendation G5/3 (1976), 'Limits for harmonics in the United Kingdom Supply System', Electricity Council.

LIST OF FIGURES

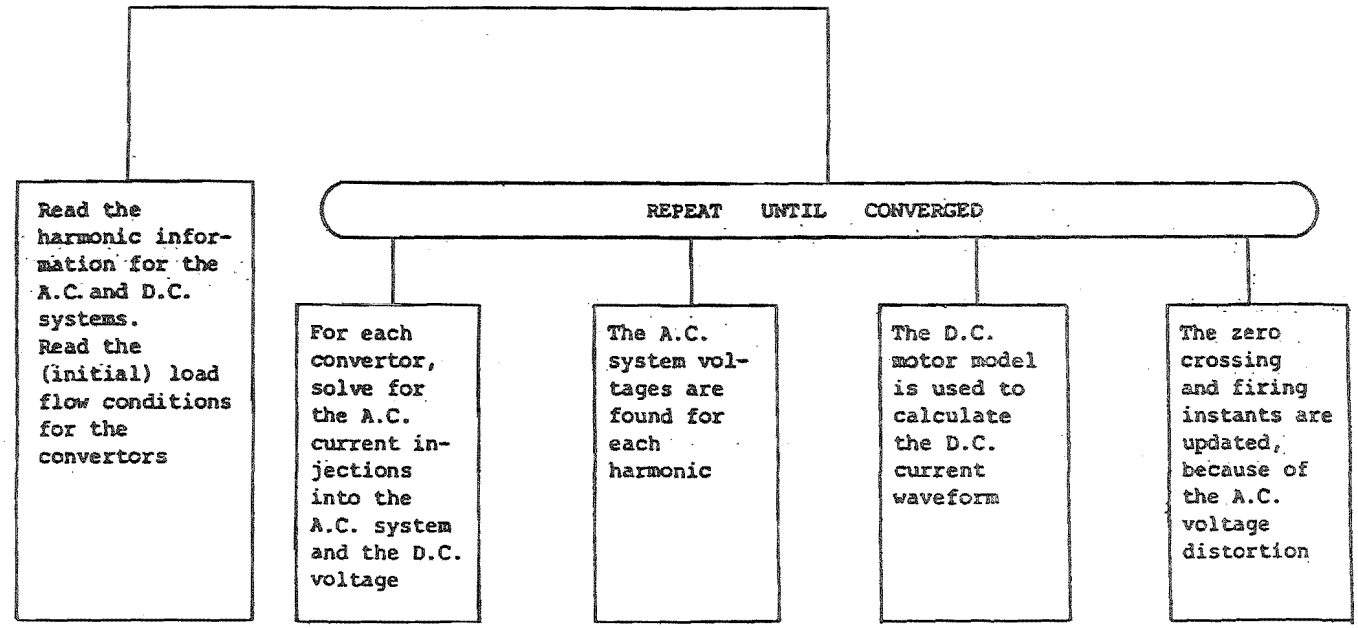

Fig. 1. Structure diagram showing the operation of the Harmonic Interaction Program.

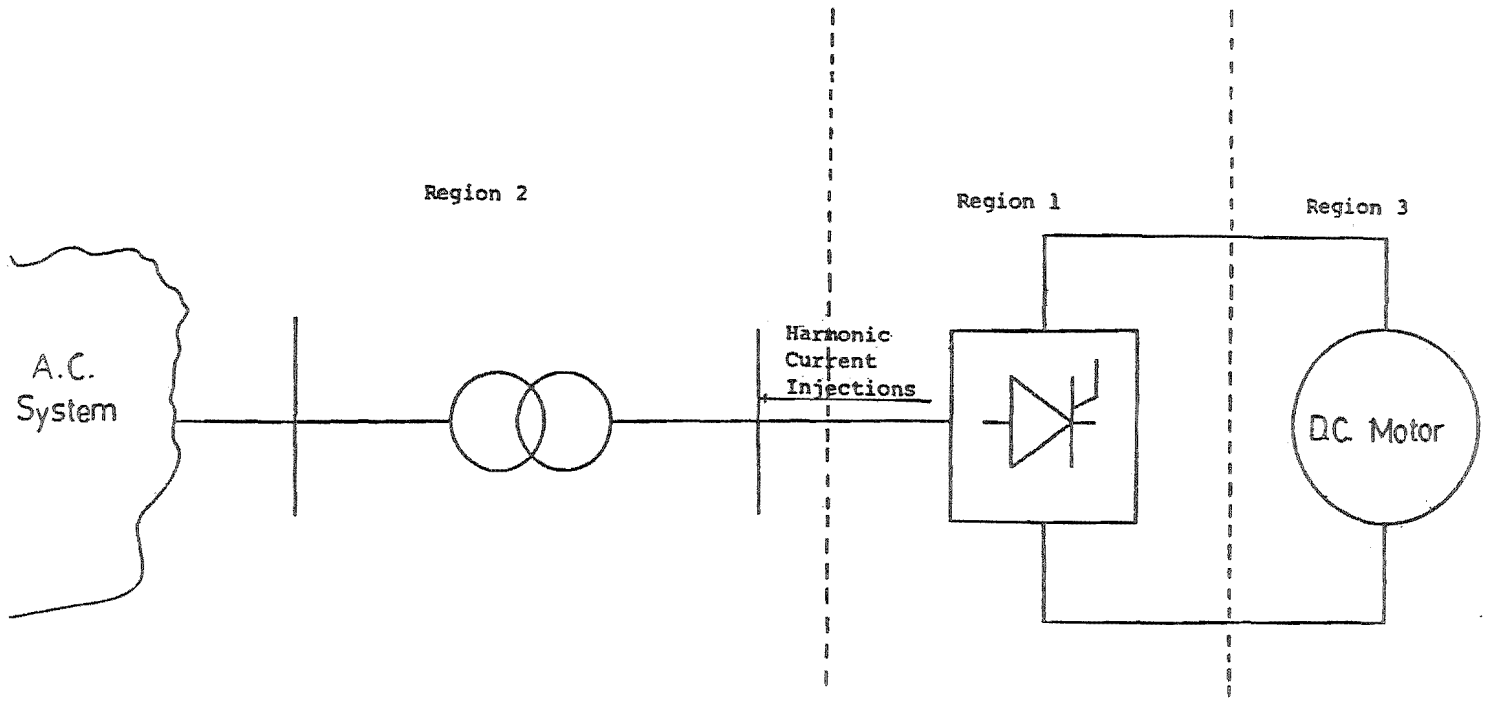

Fig. 2. The three regions of the system corresponding with the iteration sequence.

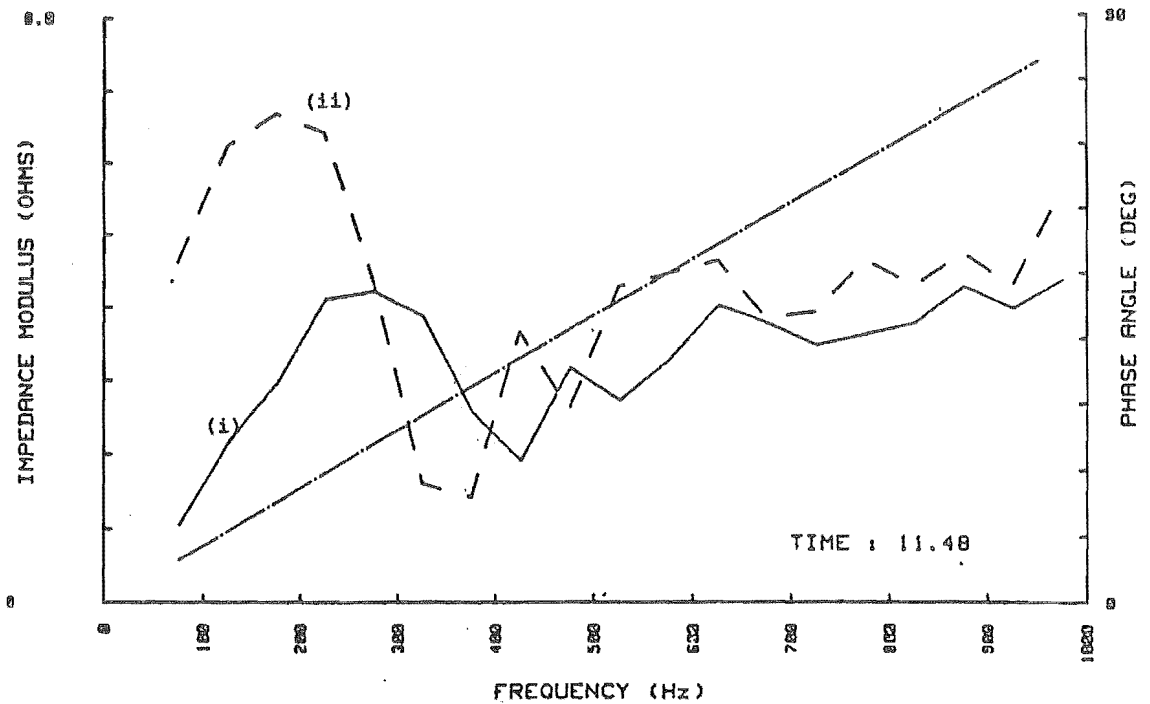
IMPEDANCE MODULUS (OHMS)
PHASE ANGLE (DEG)
FREQUENCY (Hz)
(i)
(ii)
TIME : 11.48

Fig. 3.

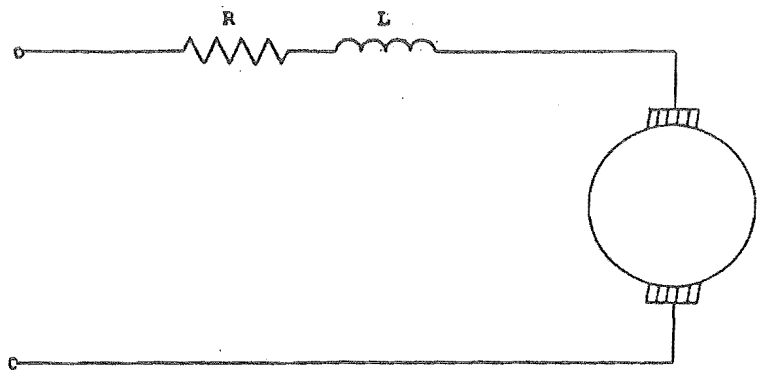

(a) R-L series model

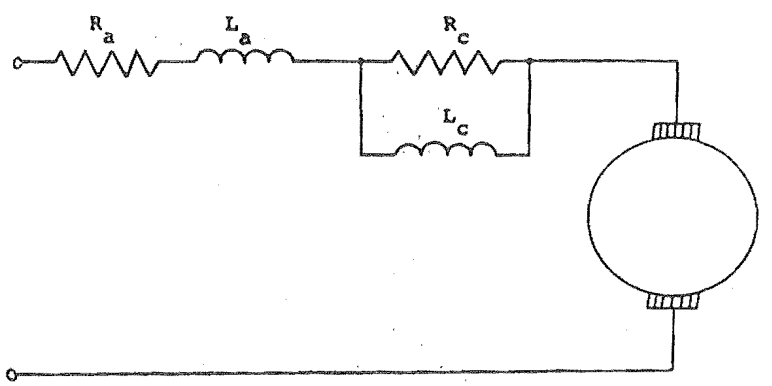

(b) Ewing model

Fig. 4. D.C. motor models.

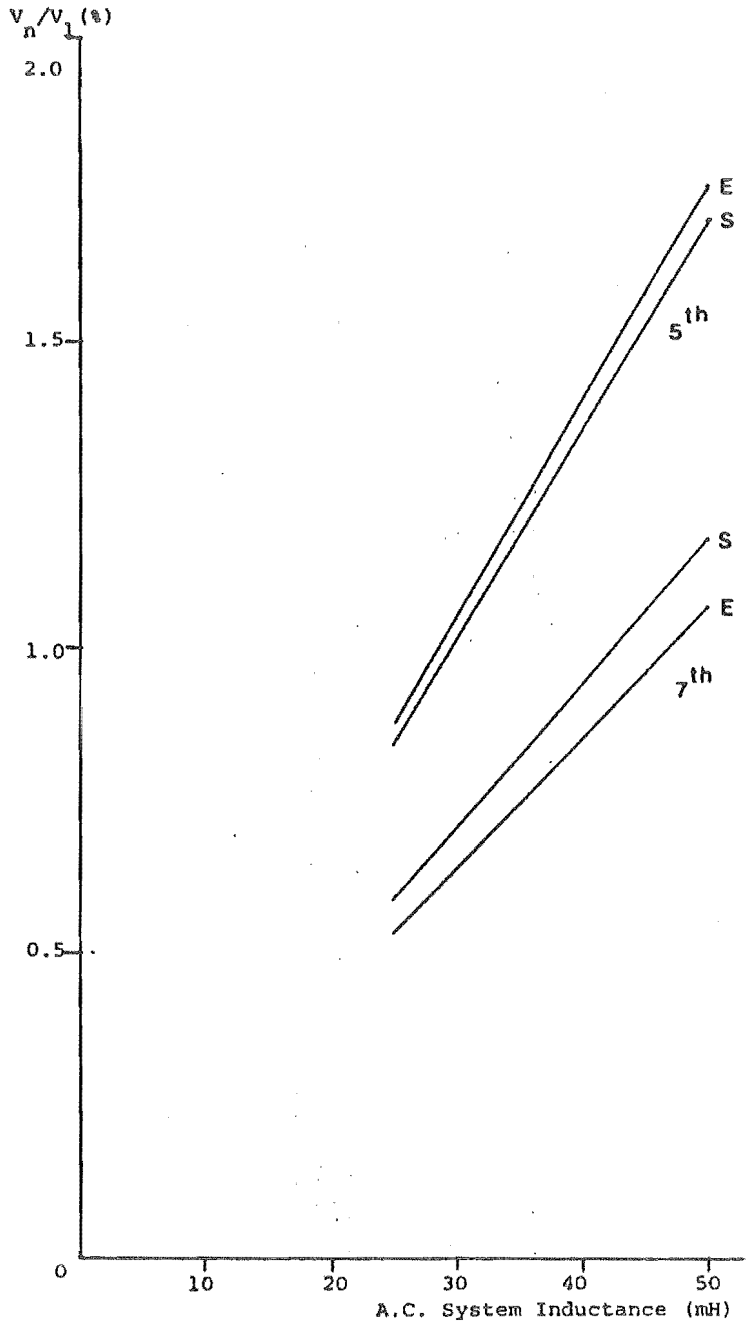

Fig. 5. Effect of d.c. drive model on the levels of 5th and 7th harmonic voltage distortion.

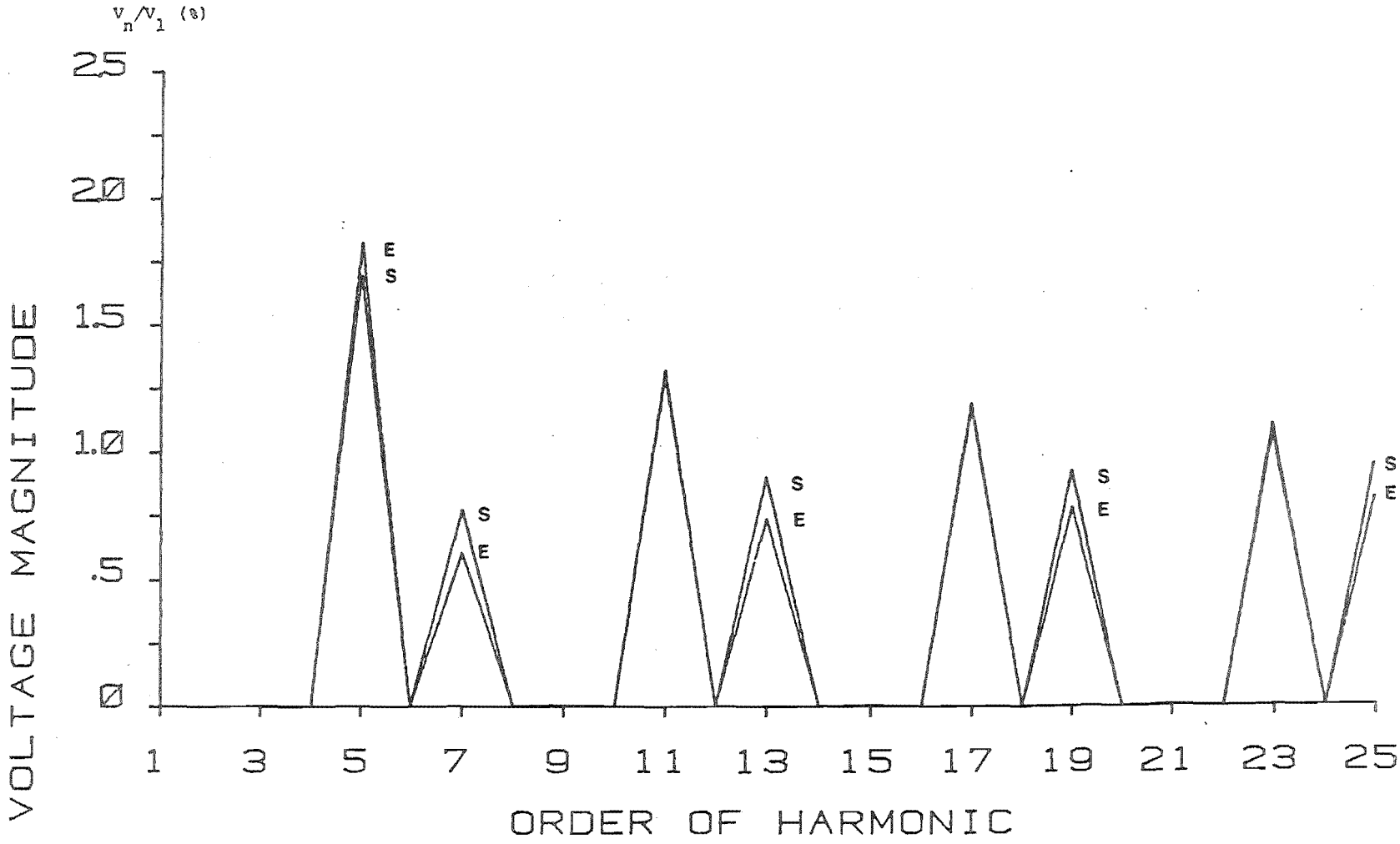

Fig. 6. Levels of harmonic distortion during starting.

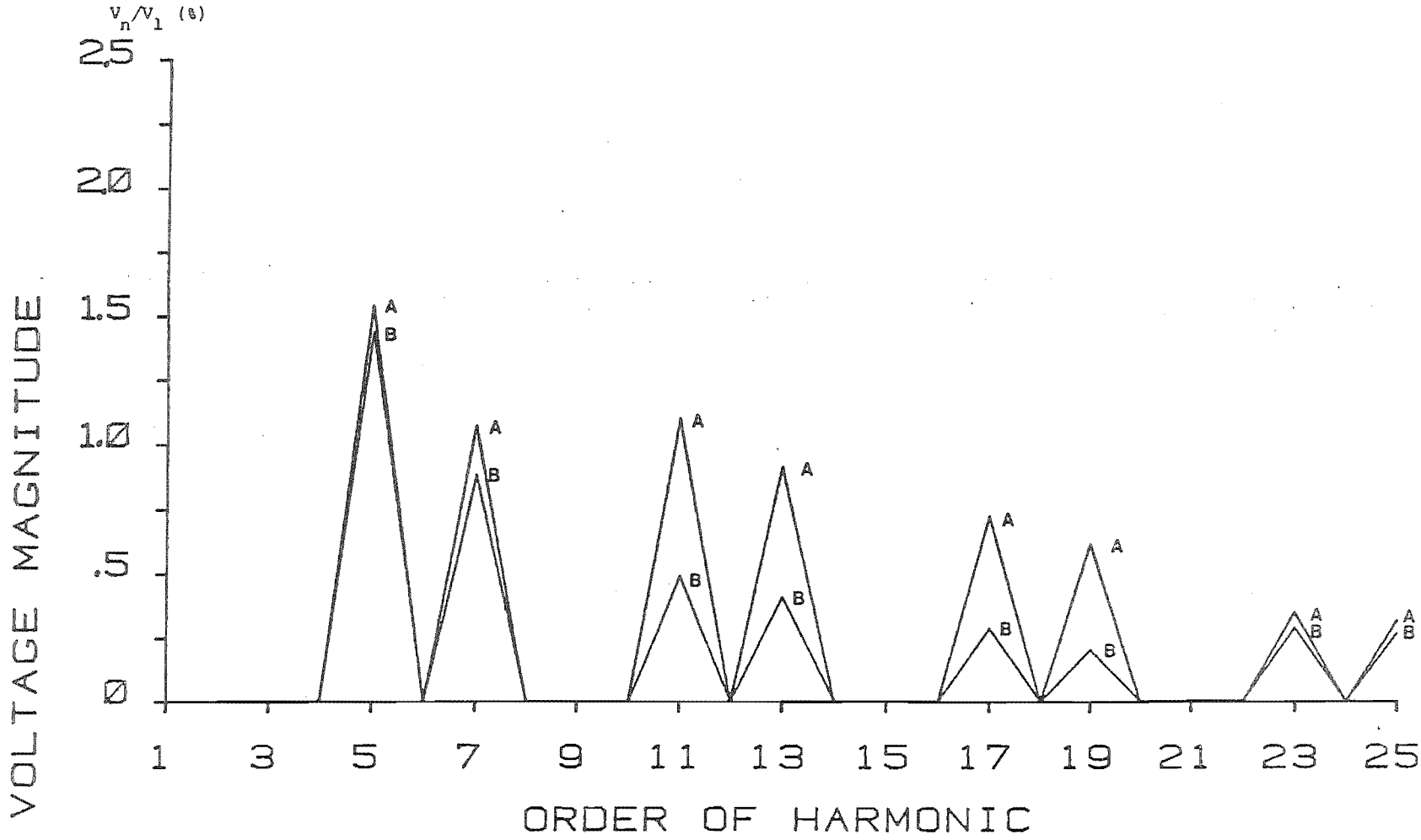

Fig. 7. Influence of the transformer reactance on the harmonic voltage distortion.

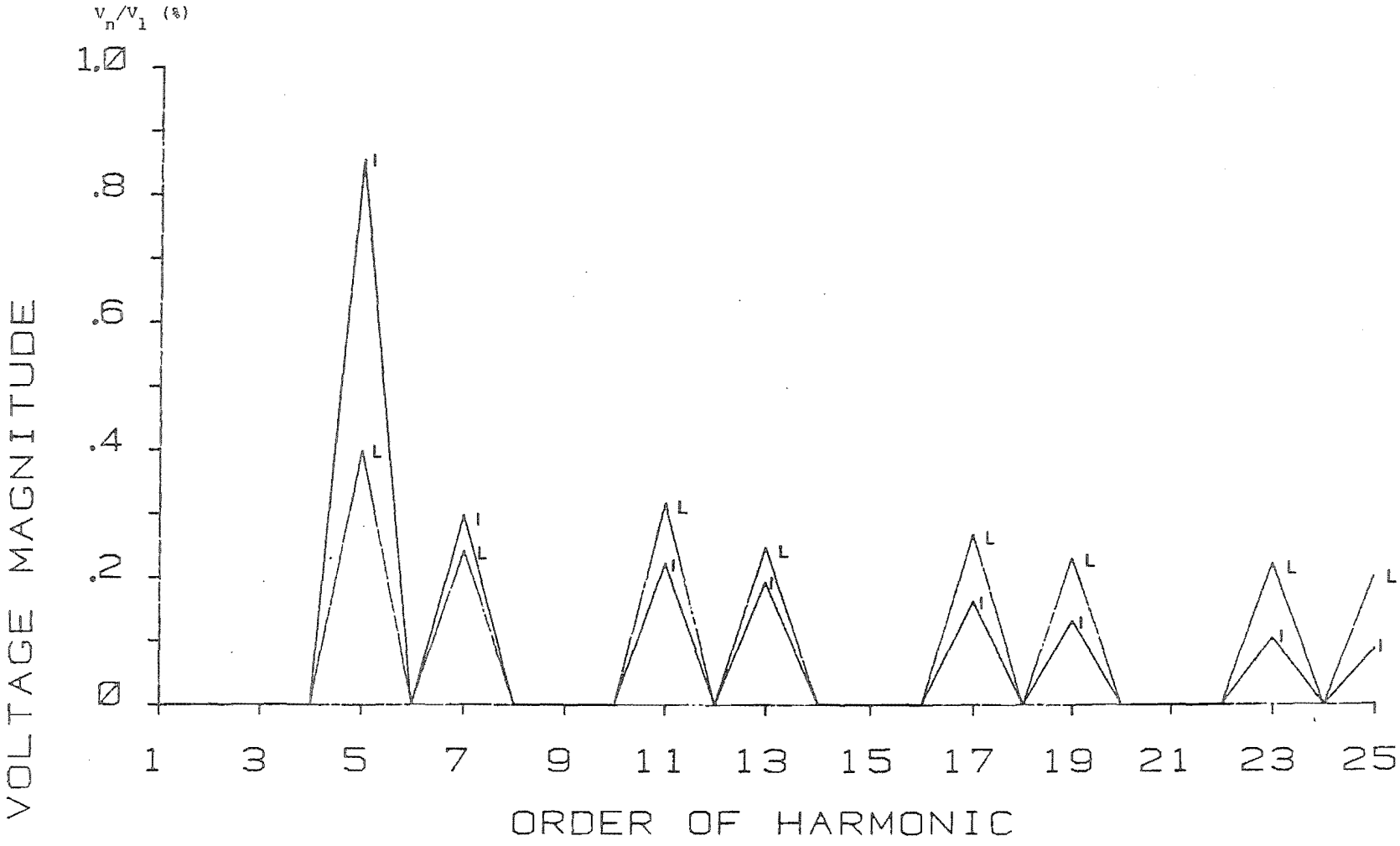

Fig. 8 a Effect of a.c. system representation.

Fig. 8(b) Test impedance and parallel RL models.

Fig. 8(c) Test impedance and resistance models.

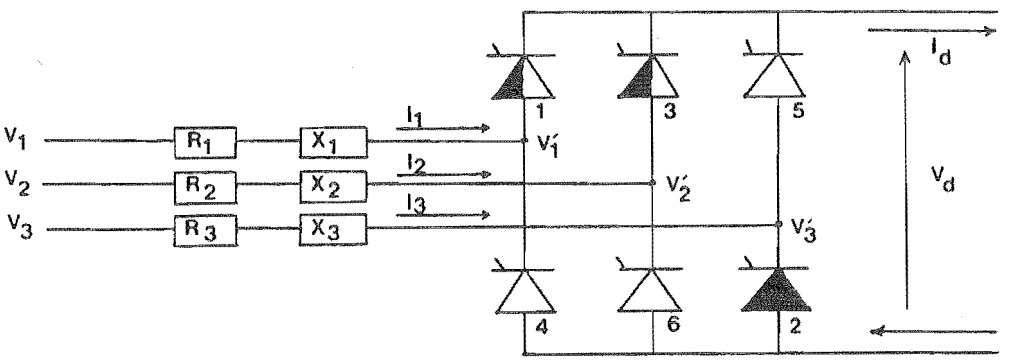

Fig. 9. Diagram showing the convertor during the commutation from valve 1 to valve 3.

APPENDIX A7

RESULTS OF SINGLE PHASE CONVERTOR MODELLING

A7.1 TEST SYSTEM

The test system was that previously used for three phase d.c. motor drives (Arrillaga et al 1985b) and included as Appendix A6.

The a.c. systems used in the study are a 10, 25 and 50 mH inductive system and an industrial busbar locus (Baker 1981), each at 33 kV. In each case the fundamental terminal busbar voltage was specified as 1.0 p.u.

A7.2 RESULTS OF FULLY CONTROLLED CONVERTORS

A7.2.1 Comparison of Motor Models

The R/L series and Ewing (1968) model injections were compared with a square pulse (classical solution) using a 10 mH system, a delay angle of 0.1 radians and a 1.0 p.u. d.c. current. Figure A7.1 shows the a.c. harmonic injections, as a fraction of the fundamental, for each case.

The Ewing model produced significantly smaller harmonic currents than the R/L series model, particularly at the higher order harmonics, while both the d.c. models give dramatically lower harmonic currents than those predicted using a square pulse. For the Ewing model, the inclusion of ripple on the d.c. current and a finite length of commutation results in 0.129 p.u. third harmonic current as compared to 0.333 p.u. expected using a rectangular a.c. current injection.

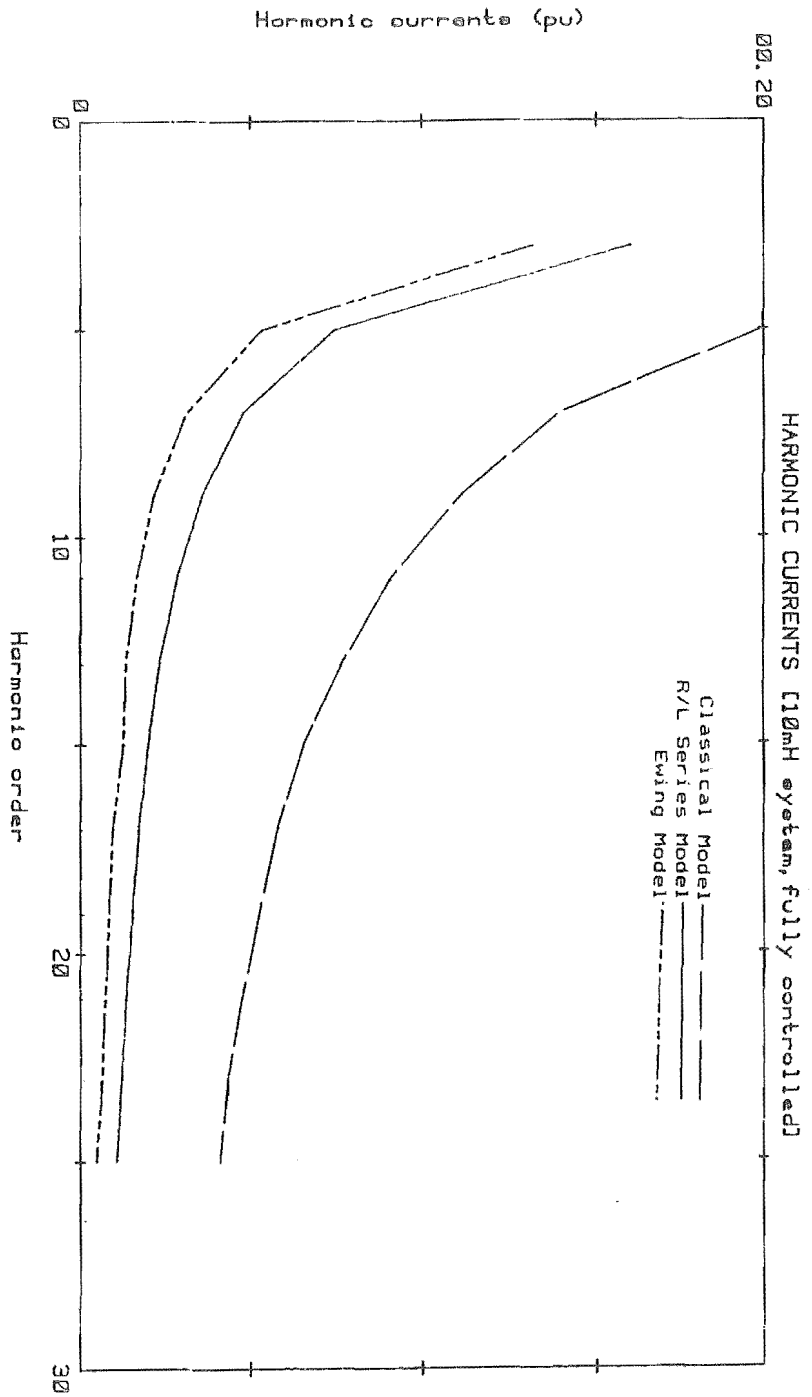

Figure A7.1 : Harmonic Currents [10 mH System, Fully Controlled]

A7.2.2 Comparison of A.C. Systems

The effect of the a.c. system representation on the levels of harmonic voltage distortion is illustrated in figure A7.2. The effect of the various a.c. systems on the harmonic current injections was minimal with the resulting voltage distortions approximately

proportional to the harmonic impedance of the system.

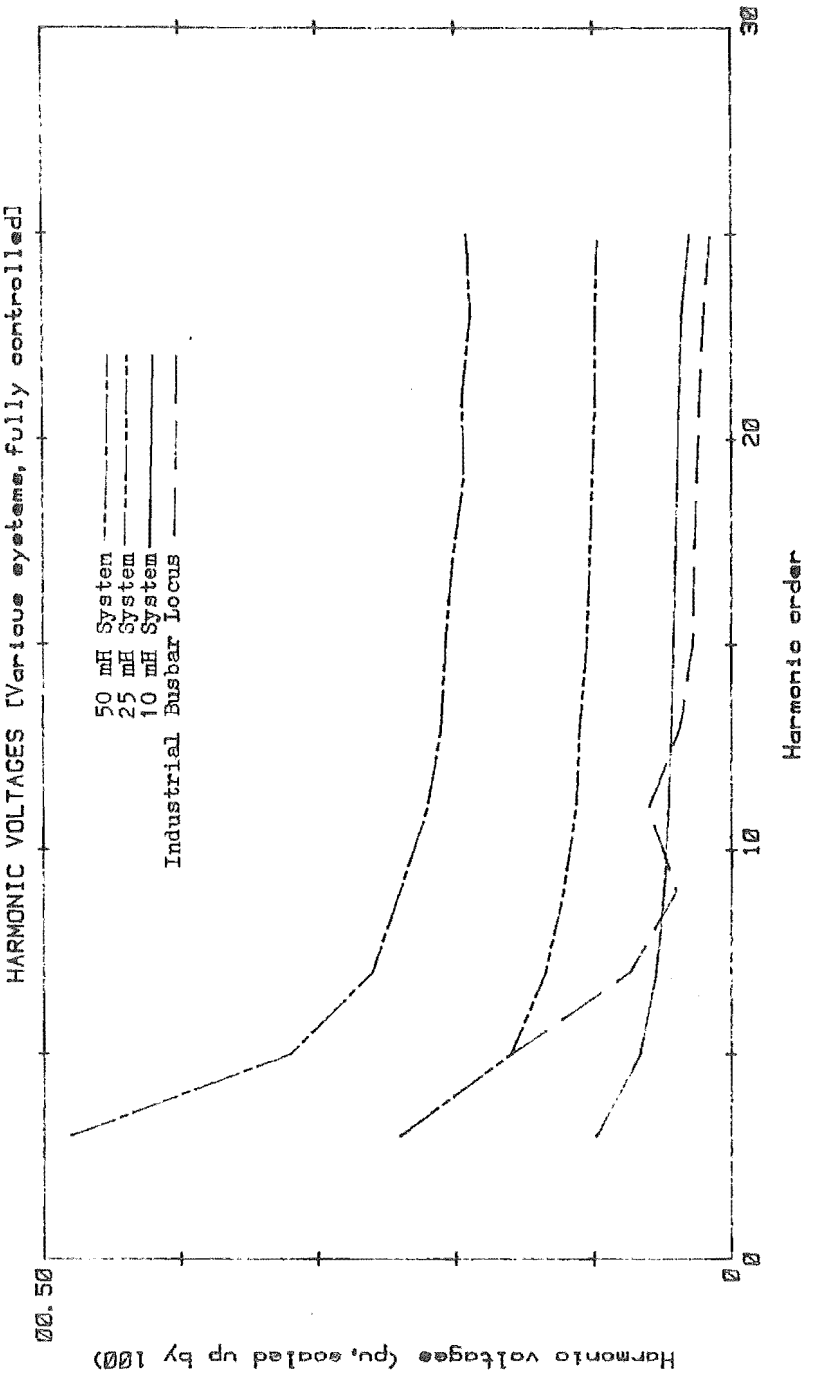

Figure A7.2 : Harmonic Voltages [Various Systems, Fully Controlled]

A7.2.3 Ripple Ratio Study

A simple theoretical study, which gives an indication as to the effect of d.c. current ripple on the a.c. system current injections, has been performed for three phase convertors (Dobinson 1975). In the absence of an equivalent study for single phase convertors, the following theoretical study was performed.

A7.2.3.1 Theoretical study

Assuming that the dominant ripple component is the second harmonic, the current waveform of figure A7.3 results.

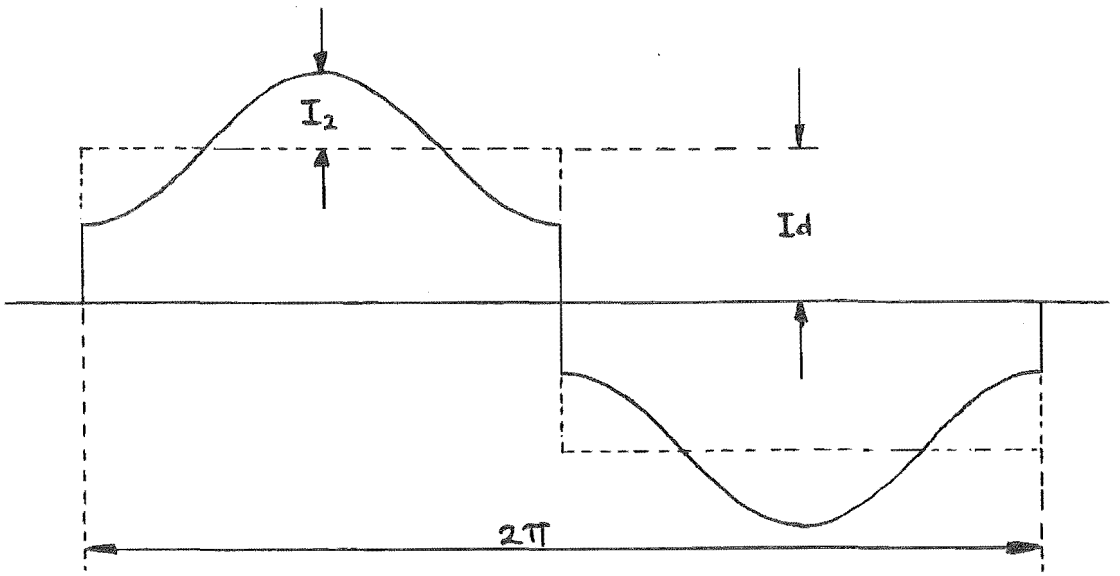

Figure A7.3 : Theoretical A.C. Current Waveform

Since the waveform is odd and contains half wave symmetry the Fourier series consists only of the odd B_n sin terms, such that

$$B_n = 2/\pi \int_0^{\pi} (I_d - I_2 \cos(2x))\sin(nx)dx$$

$$= \frac{4I_d}{n\pi} - \frac{I_2}{\pi(n^2-4)} \qquad \text{A7.1}$$

where

$$R = 2I_2/I_d \qquad \text{A7.2}$$

It can be seen that the fundamental component increases with increased ripple while the odd harmonics decrease.

A7.2.3.2 Test system for the study of D.C. current ripple

A series of runs were performed to investigate the effect of d.c. current ripple on the a.c. system current injections. The test system consisted of a resistor in series with a variable inductor, in

the range 0.4 mH to 2.0 mH, for the d.c. system, a 10 mH lumped inductance for the a.c. system, a 1.0 p.u. d.c. current and delay angles fo 0.1 and 1.0 radians. For simplicity the ripple ratio was defined as the ratio of the peak to peak second harmonic to the d.c. component.

A7.2.3.3 Results for the study of D.C. current ripple

The fundamental current injection as a function of the ripple ratio are given in figure A7.4 for the two delay angles in A7.2.3.2. Similarly, figures A7.5 and A7.6 show the third, fifth, seventh and ninth harmonic current injections, as a fraction of the fundamental, for the two delay angles respectively. The trends of these figures are similar to those predicted in the theoretical analysis of section A7.2.3.1, although this analysis does not take into account the commutation angles, which also affect the a.c. current injections.

A7.3 RESULTS FOR HALF-CONTROLLED CONVERTORS

A7.3.1 Classical Harmonic Behaviour of a Half-controlled Convertor

Assuming a perfectly flat d.c. current and zero commutation angles, the a.c. current waveform is that of figure A7.7.

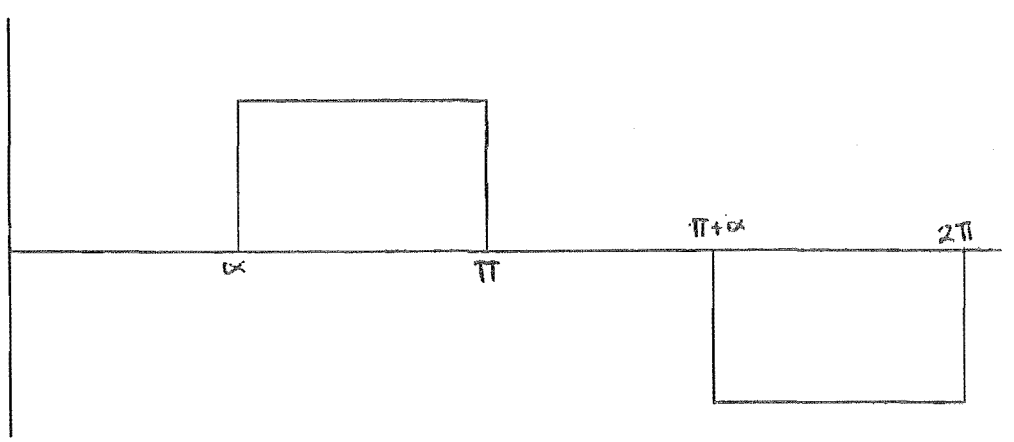

Figure A7.7 : Simplified Half-controlled A.C. Current Waveform

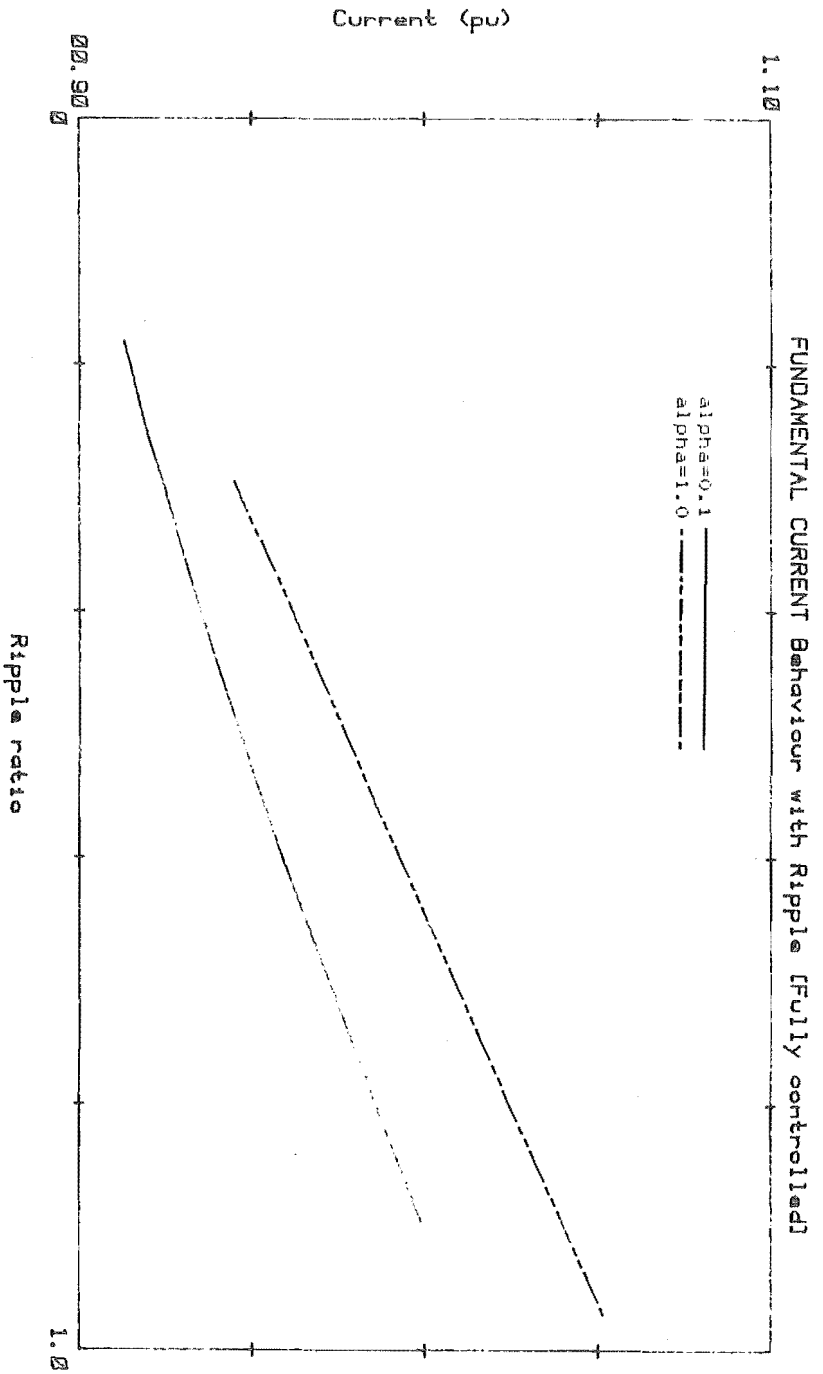

Figure A7.4 : Fundamental Current Behaviour with Ripple (Fully Controlled)

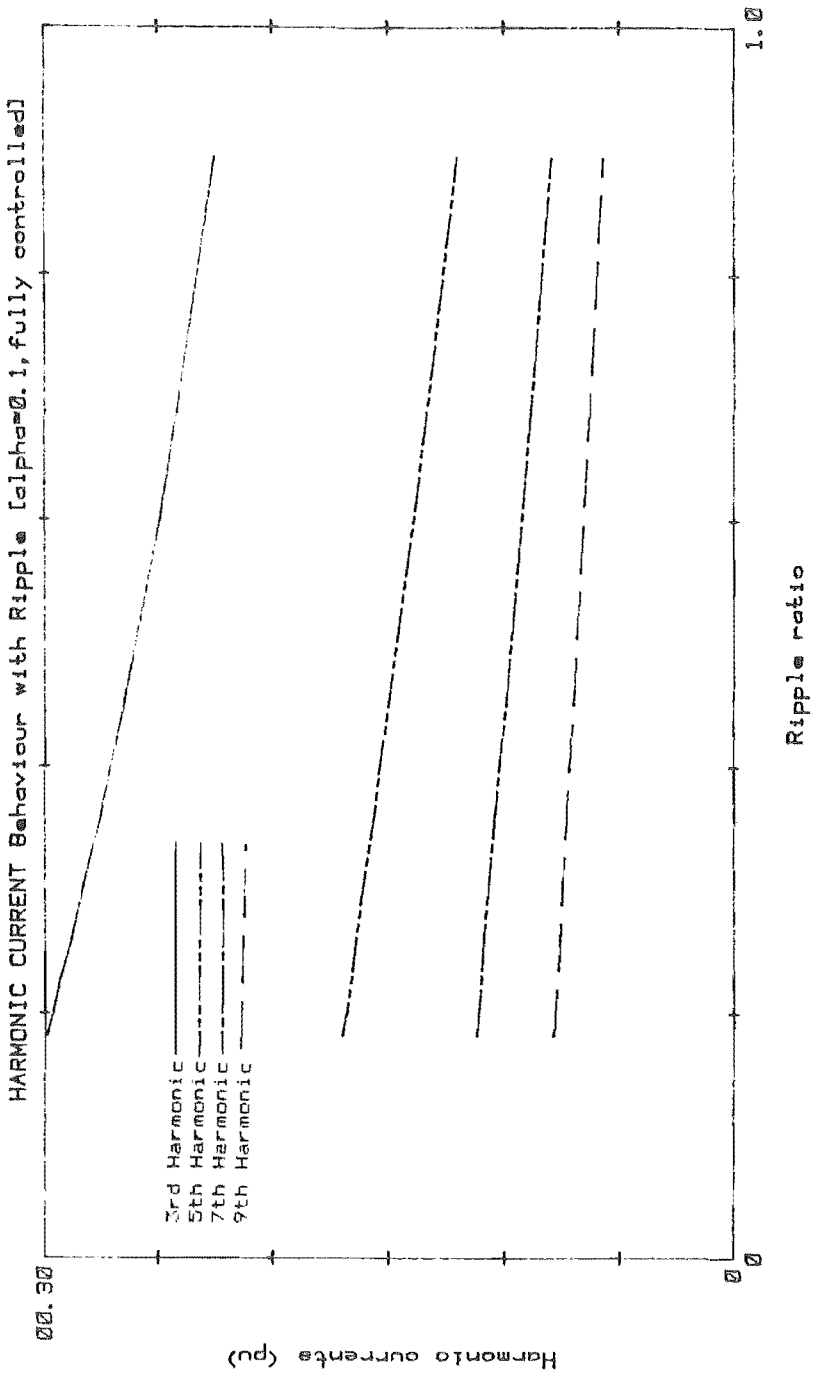

Figure A7.5 : Harmonic Current Behaviour with Ripple [Alpha=0.1]

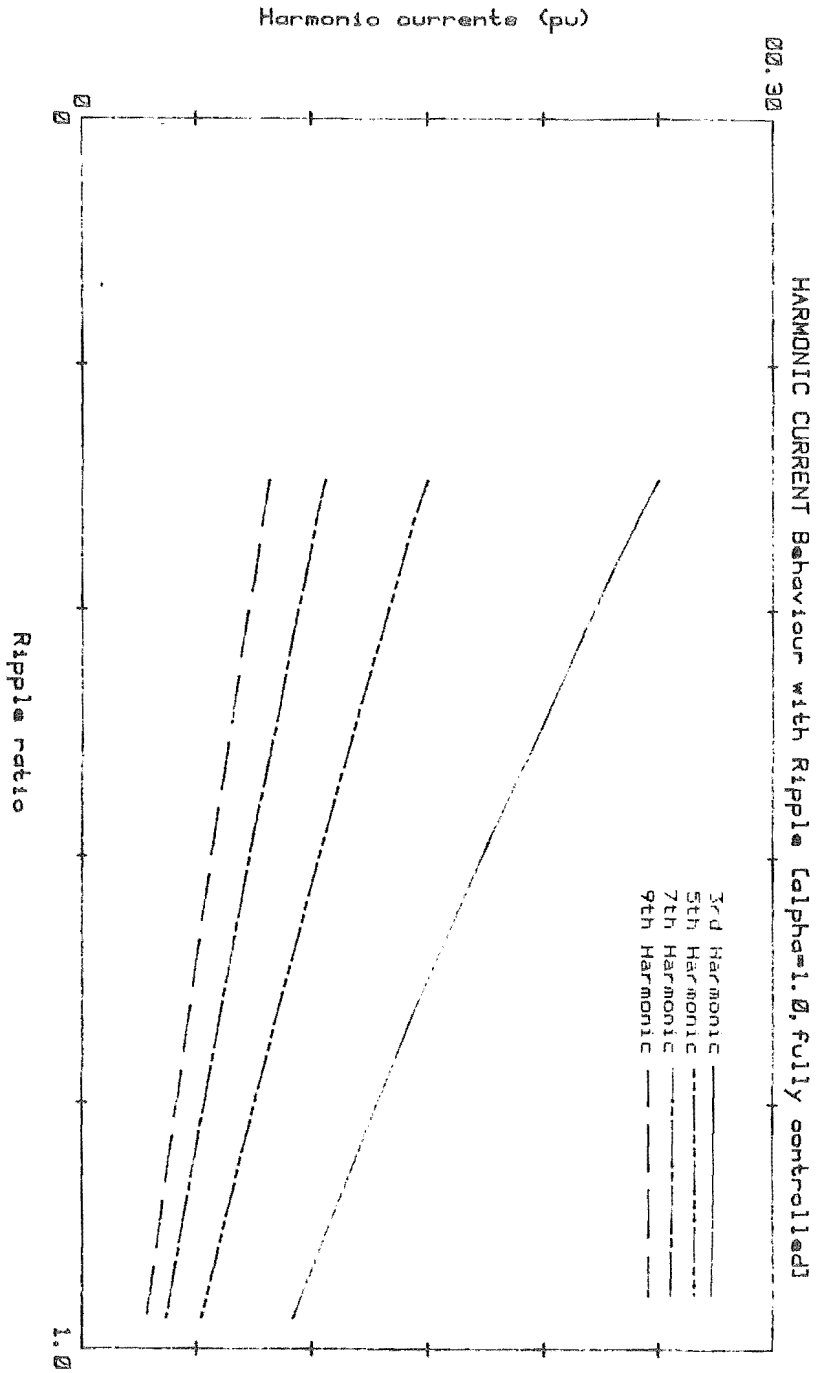

Figure A7.6 : Harmonic Current Behaviour with Ripple [Alpha=1.0]

By shifting the origin to make the waveform odd produces

$$B_n = \frac{2I_d}{n\pi}[\cos(\frac{n\alpha}{2}) - \cos(n(\pi - \frac{\alpha}{2}))] \qquad A7.3$$

where n=1,3,5...

A7.3.2 Comparison of Motor Models

The a.c. harmonic current injections, as a fraction of the fundamental, for the two motor models were compared with the classically predicted currents of equation A7.3 in figure A7.8, for a delay angle of 0.609 radians.

The injections of the two motor models show large deviations from the classical injections of section A7.3.1. Of particular note are the levels of third and fifth harmonics which differ by factors of 2.5 and 12 respectively. This clearly shows that a simple fixed current injection is not an adequate representation of the harmonic current injections of a single phase half-controlled convertor when connected to a d.c. drive.

A7.3.3 The Effect of Ripple Ratio with Half-controlled Rectification

A similar ripple ratio study to that used in section A7.2.3 was performed for the half-controlled case. As well as the 0.1 radians delay, a case of 0.302 radians was also investigated.

The fundamental current injections versus the ripple ratio, for delay angles of both 0.1 and 0.302 radians, are given in figure A7.9. Similarly, figures A7.10 and A7.11 show the third, fifth, seventh and ninth harmonic current injections, as fractions of the fundamental, for the two delay angles.

In contrast to the fully controlled case, the same d.c. conditions cover a much higher range of ripple. The tendency for

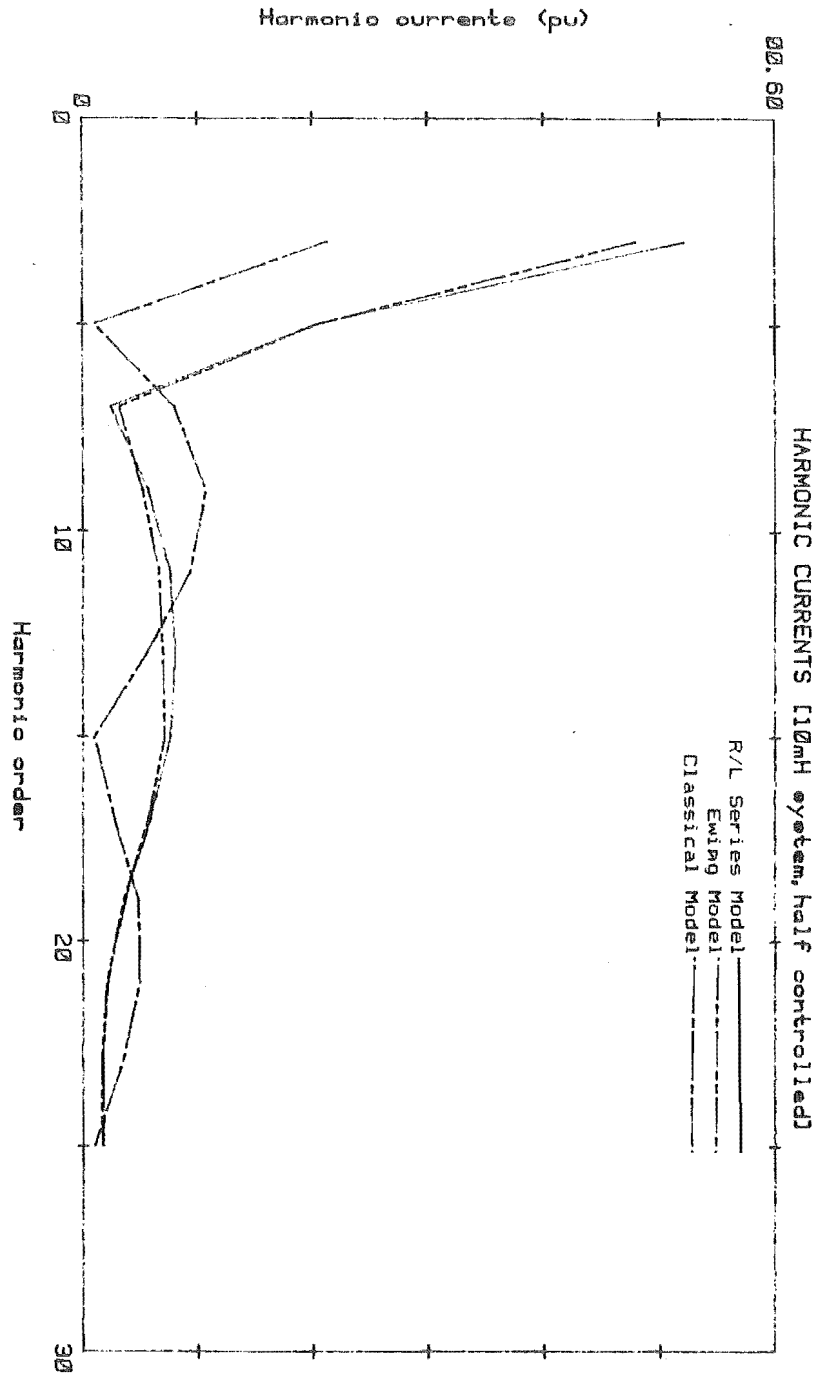

Figure A7.8 : Harmonic Currents [10 mH system, Half-Controlled]

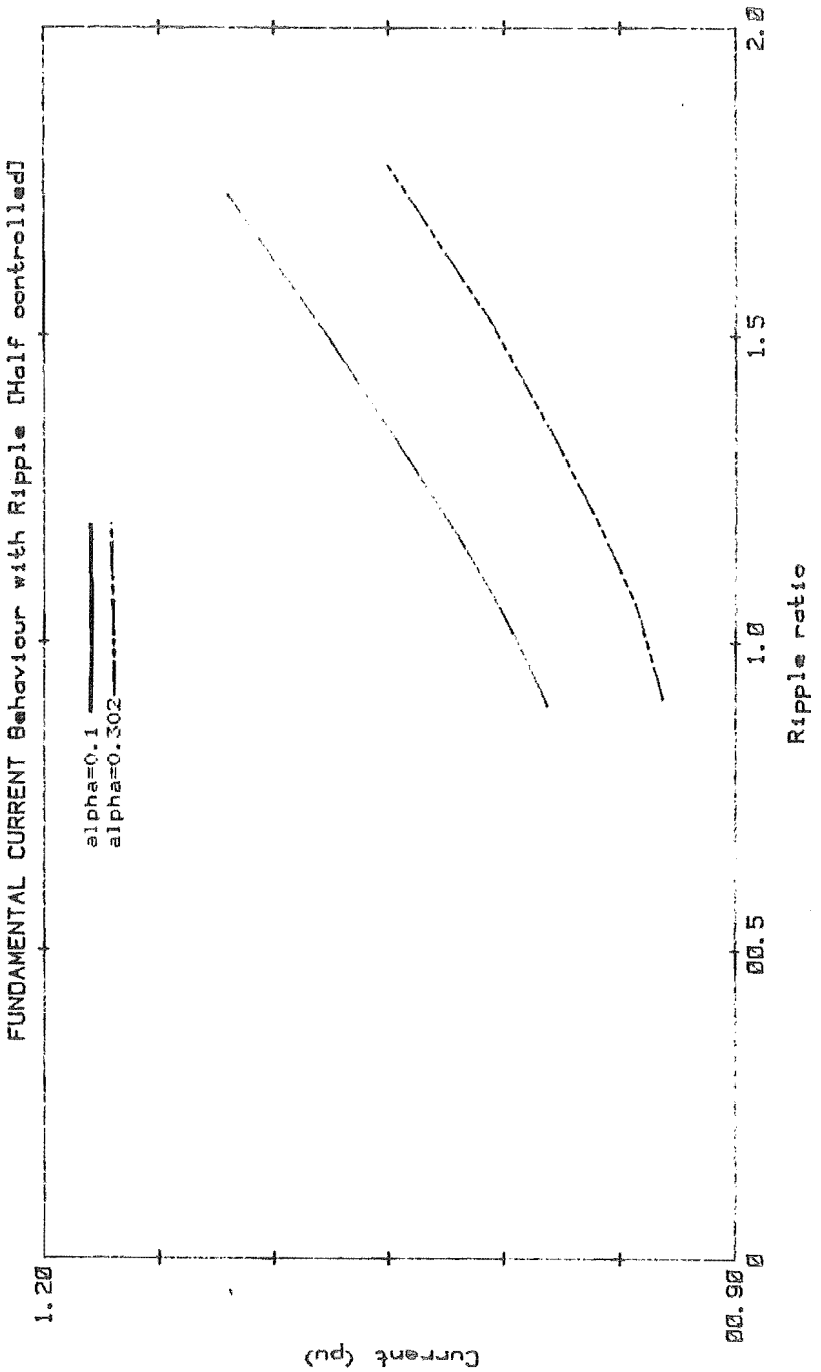

Figure A7.9 : Fundamental Current Behaviour with Ripple (Half-Controlled)

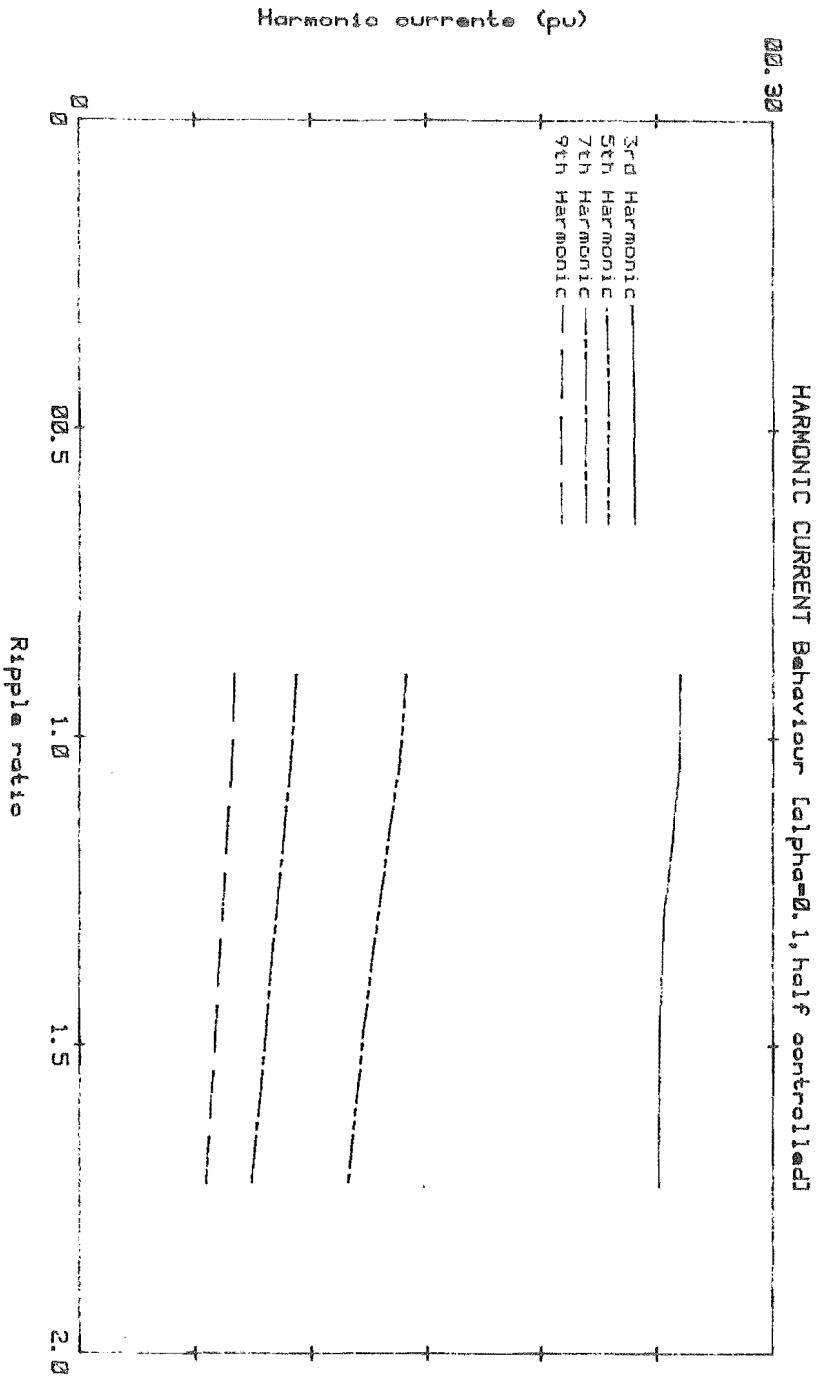

Figure A7.10 : Harmonic Current Behaviour with Ripple [Alpha=0.1]

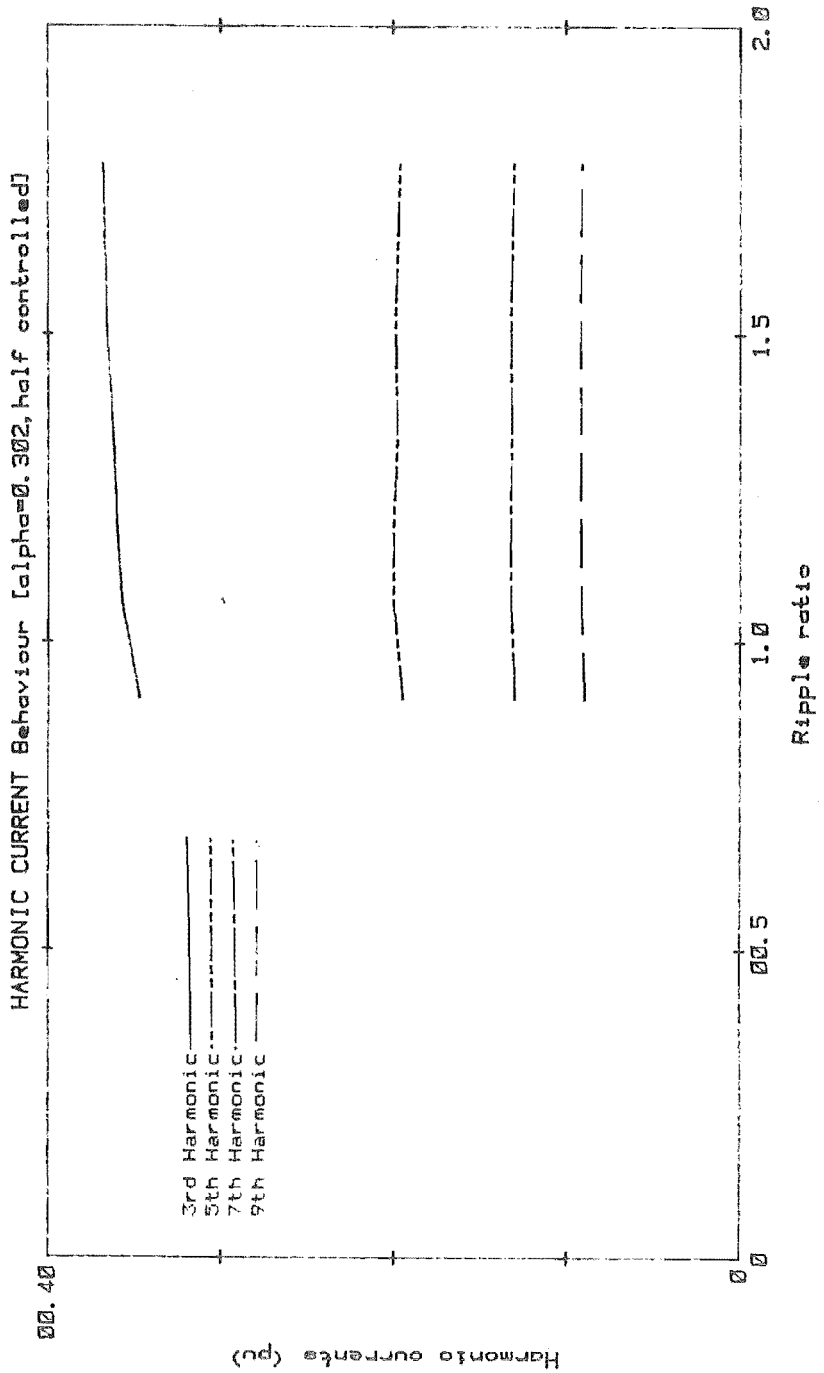

Figure A7.11 : Harmonic Current Behaviour with Ripple [Alpha=1.0]

harmonics to reduce with increasing ripple is not so apparent in this case. Because of difficulties in formulating a simple theory, there are no predicted results, as in section A7.2.3.1. This makes the interpretation of the results more difficult.

A7.4 CONCLUSIONS

The main result of this study is that classical methods of fixed current injections based on a flat d.c. current waveform are inadequate. This is especially true of the half-controlled case. The choice of d.c. motor representation is not so important, and in the absence of accurate information the R/L series model is adequate.

The a.c. system representation has little effect on the harmonic current injections, but should be accurate in order to assess the harmonic voltage distortions.

APPENDIX A8

THE HARMONIC SPECTRUM OF V_f

At any instant the field voltage is one of the phase to phase a.c. system voltages (assuming zero commutation angle). This is demonstrated in figure A8.1 where the phase voltages U_{13}, U_{23} and U_{21} have corresponding phases C_1, C_2 and C_3 (the zero crossings of the phase-neutral voltages).

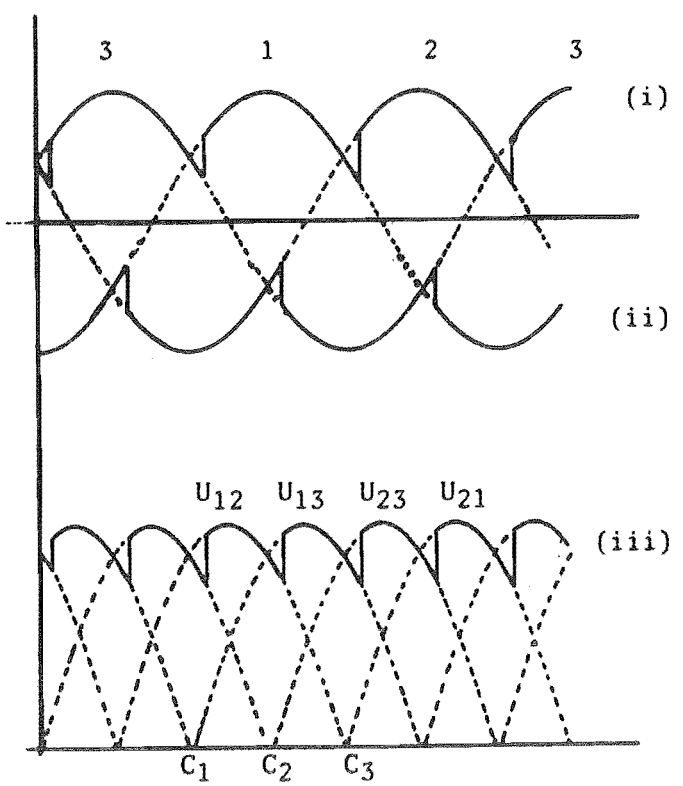

Figure A8.1 : Excitation Voltage Waveforms
(i) Common cathode potential
(ii) Common anode potential
(iii) Rectified voltage

Therefore the field voltage has the equation

$$V_f(t) = \sqrt{2}\, U_{21} \sin(\omega t - C_3 + \pi) \quad \text{for } C_1 + \alpha < \omega t < C_2 + \alpha$$
$$\sqrt{2}\, U_{13} \sin(\omega t - C_1) \qquad C_2 + \alpha < \omega t < C_3 + \alpha$$
$$\sqrt{2}\, U_{23} \sin(\omega t - C_2) \qquad C_3 + \alpha < \omega t < C_1 + \alpha + \pi$$

A8.1

where the waveform is repeated for the second half of the cycle, leading to only even harmonics h.

$V_f(t)$ can also be expressed in terms of a Fourier series

$$V_f(t) = 1/2\, a_o + \sum_{h=2}^{\infty} (a_h \cos h\omega t + b_h \sin h\omega t) \qquad \text{A8.2}$$

where

$$a_h = \frac{\sqrt{2}}{\pi(1+h)}\{U_{21}[\cos((1+h)(C_1+\alpha)-C_3+\pi) - \cos((1+h)(C_2+\alpha) - C_3+\pi)]$$
$$+ U_{13}[\cos((1+h)(C_2+\alpha) - C_1) - \cos((1+h)(C_3+\alpha) - C_1)]$$
$$+ U_{23}[\cos((1+h)(C_3+\alpha) - C_2) - \cos((1+h)(C_1+\alpha+\pi) - C_2)]\}$$
$$+ \frac{\sqrt{2}}{\pi(1-h)}\{U_{21}[\cos((1-h)(C_1+\alpha) - C_3+\pi) - \cos((1-h)(C_2+\alpha) - C_3+\pi)]$$
$$+ U_{13}[\cos((1-h)(C_2+\alpha) - C_1) - \cos((1-h)(C_3+\alpha) - C_1)]$$
$$+ U_{23}[\cos((1-h)(C_3+\alpha) - C_2) - \cos((1-h)(C_1+\alpha+\pi) - C_2)\}$$

A8.3

$$b_h = \frac{\sqrt{2}}{\pi(1-h)}\{U_{21}[\sin((1-h)(C_2+\alpha) - C_3+\pi) - \sin((1-h)(C_1+\alpha) - C_3+\pi)]$$
$$+ U_{13}[\sin((1-h)(C_3+\alpha) - C_1) - \sin((1-h)(C_2+\alpha) - C_1)]$$
$$+ U_{23}[\sin((1-h)(C_1+\alpha+\pi) - C_2) - \sin((1-h)(C_3+\alpha) - C_2)]\}$$
$$- \frac{\sqrt{2}}{\pi(1-h)}\{U_{21}[\sin((1-h)(C_2+\alpha) - C_3+\pi) - \sin((1-h)(C_1+\alpha) - C_3+\pi)]$$
$$+ U_{13}[\sin((1-h)(C_3+\alpha) - C_1) - \sin((1-h)(C_2+\alpha) - C_1)]$$
$$+ U_{23}[\sin((1-h)(C_1+\alpha+\pi) - C_2) - \sin((1-h)(C_3+\alpha) - C_2)]\}$$

A8.4

For each harmonic frequency a_h and b_h are combined to an equivalent rms harmonic phasor,

$$V_f = \frac{1}{\sqrt{2}}(a_h - jb_h) \qquad \text{A8.5}$$

APPENDIX 9

TEST DATA FOR BENMORE POLE

Transformer data:

X_{220} = .0460 p.u.

X_{16} = .0206 p.u.

X_{33} = -.0045 p.u.

X_c = .0308 p.u.

Equivalent Generator reactance:

X_g = .0567 p.u.

The operating condition for the pole was chosen to be the nominal values of 125 kV and 1200 amps per bridge.

D.C. System base:

D.C. power base	100 MVA
D.C. voltage base	105 kV (phase-phase) or 60.6 kV (phase-neutral)
D.C. current base	.55 kA

Therefore I_d = 2.18 p.u.

V_d = 2.062 p.u.